Coral Reefs in the Anthropocene Ocean: Novel Insights from Skeletal Proxies of Climate Change, Impacts, and Resilience

By

Nathaniel R. Mollica

B.S., Colorado School of Mines, 2014

Submitted to the Department of Earth, Atmospheric, and Planetary Sciences in partial fulfillment of the requirements for the degree of

Doctor of Philosophy

at the

MASSACHUSETTS INSTITUTE OF TECHNOLOGY
and the

WOODS HOLE OCEANOGRAPHIC INSTITUTION

February 2021

Signature of Author

_____

Nathaniel R. Mollica
Joint Program in Oceanography/Applied Ocean Science and Engineering
Massachusetts Institute of Technology
and Woods Hole Oceanographic Institution
December 31, 2020

Certified by

_____

Dr. Anne L. Cohen
Thesis Supervisor
Woods Hole Oceanographic Institution

Dr. Weifu Guo
Thesis Supervisor
Woods Hole Oceanographic Institution

Accepted by

_____

Dr. Oliver Jagoutz
Chair, Joint Committee for Marine Geology and Geophysics
Massachusetts Institute of Technology/
Woods Hole Oceanographic Institution

Coral Reefs in the Anthropocene Ocean: Novel Insights from Skeletal Proxies of Climate Change, Impacts, and Resilience

By Nathaniel Mollica

Submitted to the MIT-WHOI Joint Program in Oceanography and Applied Ocean Science and Engineering on December 31st, 2020 in partial fulfillment of the requirements for the degree of Doctor of Philosophy in Oceanography

Abstract

Anthropogenic emissions of greenhouse gases are driving rapid changes in ocean conditions. Shallow-water coral reefs are experiencing the brunt of these changes, including intensifying marine heatwaves (MHWs) and rapid ocean acidification (OA). Consequently, coral reefs are in broad-scale decline, threatening the livelihoods of hundreds of millions of people. Ensuring survival of coral reefs in the 21st century will thus require a new management approach that incorporates robust understanding of reef-scale climate change, the mechanisms by which these changes impact corals, and their potential for adaptation. In this thesis, I extract information from within coral skeletons to 1) Quantify the climate changes occurring on coral reefs and the effects on coral growth, 2) Identify differences in the sensitivity of coral reefs to these changes, and 3) Evaluate the adaptation potential of the keystone reef-building coral, *Porites*. First, I develop a mechanistic *Porites* growth model and reveal the physicochemical link between OA and skeletal formation. I show that the thickening (densification) of coral skeletal framework is most vulnerable to OA and that, under 21st century climate model projections, OA will reduce *Porites* skeletal density globally, with greatest impact in the Coral Triangle. Second, I develop an improved metric of thermal stress, and use a skeletal bleaching proxy to quantify coral responses to intensifying heatwaves in the central equatorial Pacific (CEP) since 1982. My work reveals a long history of bleaching in the CEP, and reef-specific differences in thermal tolerance linked to past heatwave exposure implying that, over time, reef communities have adapted to tolerate their unique thermal regimes. Third, I refine the Sr-U paleo-thermometer to enable monthly-resolved sea surface temperatures (SST) generation using laser ablation ICPMS. I show that laser Sr-U accurately captures CEP SST, including the frequency and amplitude of MHWs. Finally, I apply laser Sr-U to reconstruct the past 100 years of SST at Jarvis Island in the CEP, and evaluate my proxy record of bleaching severity in this context. I determine that *Porites* coral populations on Jarvis Island have not yet adapted to the pace of anthropogenic climate change.

Thesis Supervisors: Dr. Anne L. Cohen, Dr. Weifu Guo

Associate Scientists with Tenure, Woods Hole Oceanographic Institution

Table of Contents

Acknowledgments

The research presented here is the product of half a decade of hard work and struggle, building on strengths and overcoming weaknesses, and enduring a long road of victories and defeats. I could not have overcome these challenges without the invaluable help and support of the individuals I met along the way.

The first thanks are to my advisors, Weifu Guo and Anne Cohen. They took a chance on a kid from Colorado that had knew next to nothing about the ocean, let alone coral reefs. I will always remember the depth and care that Weifu devotes to his science – breaking every problem down to fundamental principles, and always searching for a mechanistic connection behind observations. I will keep the tools he taught me through the end of my career. Anne is a paragon of boldness and passion in science. Her love for coral and coral reef science has infected me, and her encouragement has instilled in me the confidence to take leaps.

The second thanks are to my committee, they have always been available with keen suggestions when I needed help. Together, their collective knowledge has been invaluable. I owe a special thanks to Andy Solow, who has helped me with statistical conundrums in all four of my projects. He has shown a level of interest and devotion to my research that truly goes above and beyond what could be expected.

The third thanks are to my colleagues, inside the Cohen Lab and out. Special thanks are owed to Hannah Barkley for taking me under her wing as a new first year student, and to Tom DeCarlo for laying so much foundational work for my studies and helping me establish an understanding of that work. Also, to Kathryn Pietro, Gretchen Swarr, Dan McCorckle, and David McGee for their contributions to generating the data herein.

And the last thanks are to my friends and family. Dad, you have been an unending well of positivity and support, and I am so grateful for that. Mom, I wish you could have shared in this accomplishment, and I miss you deeply.

This one is for you.

This research was supported by US National Science Foundation Awards OCE-1220529, ANT-1246387, OCE-1737311, OCE-1601365, OCE-1805618, OCE-1537338, OCE-2016133, and from the Woods Hole Oceanographic Institution through the Ocean Life Institute, the Ocean Ventures Fund, the Grassle Fellowship Fund, and the MIT-WHOI Academic Programs Office.

Additional funding was provided by the Taiwan MOST Grant 104-2628-M-001-007-MY3, the Robertson Foundation, the Leverhulme Trust in UK, the Atlantic Donor Advised Fund, The Prince Albert 2 of Monaco Foundation, the Akiko Shiraki Dynner Fund, the New England Aquarium, the Martin Family Society Fellowship for Sustainability, the Gates Millenium Scholarship, the Arthur Vining Davis Foundation, the NOAA Coral Reef Conservation Program, and from the Woods Hole Oceanographic Institution through Investment in Science Fund, the Early Career Award, and the Access to the Sea Award.

Chapter 1 – Introduction

Corals first appeared in the Cambrian, with Scleractinians, or stony corals, building the first reefs around 410 million years ago. Since then, corals have experienced five major extinction events, each associated with increased atmospheric CO_2 concentrations and rapid warming. During each extinction, corals and the vibrant diverse ecosystems they built disappeared from the fossil record for tens of millions of years. Present day shallow water coral reef ecosystems are similarly diverse and vibrant, and are home to an estimated 25% of all known species in the ocean. In addition to their vast benefits to marine life, modern reefs have also become of great importance to humankind. Covering less than 1% of the ocean floor, coral reefs now support an estimated 500 million people across the world, providing land on which to live and farm, providing food, supporting tourist economies and diverse cultures, and protecting thousands of kilometers of inhabited coastline from waves, storms and tsunamis (Spalding et al. 2001).

However, rising concentrations of CO_2 in Earth's atmosphere, caused by human activities, are driving large-scale changes in ocean conditions, and coral reefs once again, face extinction (Hoegh-Guldberg et al. 2007; Pandolfi et al. 2011; Hughes et al. 2017). As the ocean absorbs CO_2, the decline in pH and $CaCO_3$ saturation state (Ω_{arag}), known as ocean acidification, is slowing calcification and increasing the dissolution of reef organisms and sediments (Orr et al. 2005; Doney et al. 2009). Simultaneously, ocean warming and the increase in frequency and intensity of marine heat waves are causing coral bleaching and widespread mortality, and measurable reductions in live coral cover across the global tropics (Hoegh-Guldberg and Smith 1989; Hughes et al. 2017).

This thesis evaluates the potential for modern-day coral reefs to survive these changes by developing and applying novel tools that enable us to place recent observational data in a broader temporal and spatial context, to identify resilient reefs, and to understand the mechanisms underpinning resilience. Significant effort is currently invested in monitoring the impacts of marine heat waves and ocean acidification on reefs across the globe, simulating these effects in lab-based sensitivity experiments, and more recently, deciphering genetic markers associated with stress responses. Coral growth has been characterized under a variety of pH conditions in lab

experiments (numerous, summarized in Pandolfi et al. 2011; Chan and Connolly 2013) and field studies of naturally low pH reefs (Fabricius et al. 2011; Crook et al. 2013; Barkley et al. 2015; Enochs et al. 2015). Likewise, numerous coral bleaching experiments have been conducted (summarized in Brown 1997), and although transient in nature, natural bleaching events have been recorded opportunistically, with fairly extensive coverage in recent years (Van Hooidonk et al. 2014; Donner et al. 2017; Hughes et al. 2018). Although still emerging, current understanding of the genetic mechanisms around coral bleaching suggest a complex response, with heat stressed corals changing expression of hundreds of genes (Meyer et al. 2011; Barshis et al. 2013).

Nevertheless, a paucity of observational data across broad temporal and spatial scales leaves key areas of inquiry out of reach. We cannot yet answer questions such as: to what extent anthropogenic ocean acidification has and will impact coral growth, if and how corals are adapting to marine heat waves, and even whether 21st century heat waves are unprecedented in the lifetime of some corals. Here, I use information contained within the skeletons of massive long-lived corals to begin to fill these gaps in knowledge. Specifically, my thesis research aims to 1) Quantify the impacts of 20th century ocean acidification and warming on coral growth, 2) identify and explain differences in the vulnerabilities of coral reefs to these changes, and 3) evaluate the potential for these massive corals to adapt or acclimatize to rapid anthropogenic ocean warming.

1.1 Thesis objectives

The questions I address in this thesis cannot be answered with existing observational or experimental data alone. Therefore, a key component of the thesis is the development of a suite of forensic tools to uncover and interpret the information contained within the skeletons of corals that have lived through this period of ocean change. My research focuses on a keystone reef-building coral *Porites* spp. which is ubiquitous across the global tropics. Here I combine observational data and global climate model output with forensic information extracted using these tools. The most important results of my research are:

1. *Porites* skeletal growth is negatively affected by ocean acidification and the impacts are most significant in the density component of the growth processes. Reduction in skeletal density is directly related to the degree of acidification, and is consistent across all

populations in the study. Model projected 21st century ocean acidification, if realized, will reduce the skeletal density of coral on reefs globally, with strongest effects in the region of the coral triangle.

2. *Porites* skeletal records of bleaching reflect levels of coral community bleaching observed *in situ* during the corresponding bleaching event. Therefore, skeletal records can be a valuable tool for both reconstructing bleaching histories and comparing the thermal tolerances of different coral reefs. My data show that within the central equatorial Pacific alone, different reefs have distinct baseline thermal tolerances. Unlike the response of *Porites* to ocean acidification, which did not reveal different sensitivities based on pH regimes, these variations in thermal tolerance imply regional adaptation linked to the thermal regimes which these reefs they inhabit.

3. I developed a new approach to the coral-based Sr-U paleotemperature proxy, termed laser Sr-U, which addressed a major limitation of this promising new thermometer. Laser Sr-U, unlike traditional bulk Sr-U, exploits microscale variability in coral skeletal Element/Ca ratios to derive monthly-resolved Sr-U values. Laser Sr-U accurately reflected monthly resolved reef water temperatures as captured by the instrumental record, as well as the frequency and amplitude of marine heatwaves. Critically, Sr-U temperatures generated from three different *Porites* colonies yielded a single calibration equation, whereas the Sr/Ca-temperature data generated from the same corals did not.

4. I reconstructed a century long record of central equatorial Pacific temperatures and compared it with a record of coral bleaching over the same period which was also reconstructed using the tools developed in this thesis. The comparison reveals that populations of the keystone reef-building coral *Porites*, within a single reef system, have responded proportionately to levels of thermal stress over the past century, with no indications of adaptation or acclimatization. Although regional evidence suggests that this may not be the case on other equatorial Pacific reefs, this observation raises key questions about the nature of the selective pressure on *Porites* corals versus other Indo-Pacific taxa.

1.2 Chapter summaries

In Chapter 2, I develop a mechanistic model of *Porites* skeletal growth, and incorporate the environmental (temperature, pH, dissolved inorganic carbon (DIC)) and biological (extension, tissue thickness) controls on coral skeletal density. I applied the model to analyses of skeletal density profiles generated from corals collected across a range of pH environments. The output reveals a direct link between ocean pH and skeletal density after accounting for other factors. Using output from the CESM-BGC simulation, my model predicts an average 12.4 ± 5.8% (2σ) decline in *Porites* skeletal density globally by the end of the 21st century due to ocean acidification alone (Fig. 2). This decline results from the interplay between changes in seawater pH and DIC, with decreases in pH leading to an average decline in density of 16.8 ± 4.7%, mitigated by increasing DIC which drives a 6.4 ± 3.7% increase. The model predicts different rates of density decline among different reefs in concert with projected pH and DIC changes. Equatorial reefs are shown to be generally more impacted than higher latitude reefs. The largest decreases in skeletal density (11.4 to 20.3%) are projected for the Coral Triangle region driven by the largest projected pH declines (up to 0.35 units). In contrast, Caribbean and Arabian reefs are predicted to show insignificant declines in coral skeletal density because a relatively small pH decline (~0.29 units on average) will be balanced by the largest increases in DIC (~175 μmol/kg on average). Projected declines in skeletal density could increase the susceptibility of reef ecosystems to bioerosion, dissolution, and storm damage (Sammarco and Risk 1990; Madin et al. 2012; Woesik et al. 2013). However, GCM projections are based on global scale emissions and do not take local stressors such as land-based sources of pollution, which enhance rates of acidification, into account. These local stressors, when incorporated into the model, could very well overwhelm the projections made here and will be a critical focus of this work moving forward.

In Chapter 3, I develop and apply a skeletal stress band proxy to quantify the thermal thresholds of several central Pacific reefs. First, I built on the initial work by Barkley and Cohen (2016), expanding the Palau stress band-community bleaching calibration to include more Pacific reefs, and Caribbean reefs and species. I found the relationship between stress band proportion and observed bleaching severity held across all these sites. I then used the stress band calibration to construct the bleaching histories (1982 – present) of six central Pacific reef systems. I also developed a novel percentile-based method for quantifying thermal stress during bleaching events

based on the traditional NOAA degree heating week. Using this method in combination with the bleaching histories, I found that within the central Pacific, a wide range of thermal tolerance exists between reefs. Further, when comparing central Pacific reefs with data from Palau and the Great Barrier Reef, I found that the central Pacific thermal thresholds were universally higher, likely an adaptation or acclimation to their thermal regimes.

In Chapter 4 I developed a new method for deriving monthly water temperature data from coral skeletons in order to quantify the history of thermal stress exposure on coral reefs in the central Pacific. Sr-U is a new coral geochemical thermometer that corrects for vital effects but requires many paired Sr/Ca-U/Ca samples to yield a single derived temperature. Consequently, traditional Sr-U records have, at best, annual resolution. Laser ablation ICP-MS enables sampling of enough Sr/Ca and U/Ca measurements with sufficient variability within a single month of skeletal growth to calculate Sr-U (based on the regression of Sr/Ca versus U/Ca). Applying this method to two corals collected on atolls in the central equatorial Pacific, I generated 10 years of ~monthly Sr-U from each core, spanning the 2010 and the 2015 El Nino Southern Oscillation cycles. I compare the Sr-U records against satellite sea surface temperature (SST) and in-situ logged temperature data. In both cases, Sr-U captures the timing and amplitude of SST variability and trends to within ± 0.45 degrees (RMSE), including peak temperatures during both El Niño events. This dataset provides a calibration that will enable laser ablation Sr-U SST reconstructions with monthly resolution from corals that grew prior to the satellite era.

In Chapter 5, I utilize both the Sr-U paleo-temperature proxy and the stress band proxy of coral bleaching to reconstruct the history of both marine heat waves in the equatorial Pacific and the associated coral bleaching response over the last century. Using a logistic model to estimate region-wide bleaching severity, I show that bleaching has occurred coincident with strong El Niño events in the Niño 4 index for as far back as coral records allow. Prior to the 2015-2016 super El Niño, an event unprecedented in both heat stress and coral bleaching levels, there is no trend in the severity of region-wide bleaching. Using the Sr-U proxy I reconstruct SST at one of the reefs in the region (Jarvis island), and determine that thermal tolerance at Jarvis has not significantly increased over the last century, although region wide evidence suggests possible adaptation at other islands.

1.3 References

Barkley HC, Cohen AL (2016) Skeletal records of community-level bleaching in Porites corals from Palau. Coral Reefs 35:1407–1417

Barkley HC, Cohen AL, Golbuu Y, Starczak VR, Decarlo TM, Shamberger KEF (2015) Changes in coral reef communities across a natural gradient in seawater pH. Sci Adv 1–7

Barshis DJ, Ladner JT, Oliver TA, Seneca FO, Traylor-Knowles N, Palumbi SR (2013) Genomic basis for coral resilience to climate change. Proc Natl Acad Sci 110:1387–1392

Brown BE (1997) Coral bleaching: Causes and consequences. Coral Reefs 16:129–138

Chan NCS, Connolly SR (2013) Sensitivity of coral calcification to ocean acidification: A meta-analysis. Glob Chang Biol 19:282–290

Crook ED, Cohen AL, Rebolledo-Vieyra M, Hernandez L, Paytan A (2013) Reduced calcification and lack of acclimatization by coral colonies growing in areas of persistent natural acidification. Proc Natl Acad Sci U S A 110:11044–9

Doney SC, Fabry VJ, Feely RA, Kleypas JA (2009) Ocean Acidification: The Other CO2 Problem. Ann Rev Mar Sci 1:169–192

Donner SD, Rickbeil GJM, Heron SF (2017) A new, high-resolution global mass coral bleaching database. PLoS One 12:1–17

Enochs IC, Manzello DP, Donham EM, Kolodziej G, Okano R, Johnston L, Young C, Iguel J, Edwards CB, Fox MD, Valentino L, Johnson S, Benavente D, Clark SJ, Carlton R, Burton T, Eynaud Y, Price NN (2015) Shift from coral to macroalgae dominance on a volcanically acidified reef. Nat Clim Chang 5:1–9

Fabricius KE, Langdon C, Uthicke S, Humphrey C, Noonan S, De ’ath G, Okazaki R, Muehllehner N, Glas MS, Lough JM (2011) Losers and winners in coral reefs acclimatized to elevated carbon dioxide concentrations. Nat Clim Chang 1:165–169

Hoegh-Guldberg O, Mumby PJ, Hooten AJ, Steneck RS, Greenfield P, Gomez E, Harvell CD, Sale PF, Edwards a J, Caldeira K, Knowlton N, Eakin CM (2007) Coral Reefs Under Rapid Climate Change and Ocean Acidification. Science (80-) 318:1737–1742

Hoegh-Guldberg O, Smith GJ (1989) The effect of sudden changes in temperature, light and salinity on the population density and export of zooxanthellae from the reef corals *Stylophora pistillata* Esper and *Seriatopora hystrix* Dana. J Exp Mar Bio Ecol 129:279–303

Van Hooidonk R, Maynard JA, Manzello DP, Planes S (2014) Opposite latitudinal gradients in projected ocean acidification and bleaching impacts on coral reefs. Glob Chang Biol 20:103–112

Hughes TP, Anderson KD, Connolly SR, Heron SF, Kerry JT, Lough JM, Baird AH, Baum JK, Berumen ML, Bridge TC, Claar DC (2018) Spatial and temporal patterns of mass bleaching of corals in the Anthropocene. Science (80-) 359:80–83

Hughes TP, Kerry JT, Álvarez-Noriega M, Álvarez-Romero JG, Anderson KD, Baird AH, Babcock RC, Beger M, Bellwood DR, Berkelmans R, Bridge TC, Butler IR, Byrne M, Cantin NE, Comeau S, Connolly SR, Cumming GS, Dalton SJ, Diaz-Pulido G, Eakin CM, Figueira WF, Gilmour JP, Harrison HB, Heron SF, Hoey AS, Hobbs J-PA, Hoogenboom MO, Kennedy E V., Kuo C, Lough JM, Lowe RJ, Liu G, McCulloch MT, Malcolm HA, McWilliam MJ, Pandolfi JM, Pears RJ, Pratchett MS, Schoepf V, Simpson T, Skirving WJ, Sommer B, Torda G, Wachenfeld DR, Willis BL, Wilson SK (2017) Global warming and recurrent mass bleaching of corals. Nature 543:373–377

Madin JS, Hughes TP, Connolly SR (2012) Calcification, Storm Damage and Population Resilience of Tabular Corals under Climate Change. PLoS One 7:1–10

Meyer E, Aglyamova G V., Matz M V. (2011) Profiling gene expression responses of coral larvae (Acropora millepora) to elevated temperature and settlement inducers using a novel RNA-Seq procedure. Mol Ecol 20:3599–3616

Orr JC, Fabry VJ, Aumont O, Bopp L, Doney SC, Feely RA, Gnanadesikan A, Gruber N, Ishida A, Joos F, Key RM, Lindsay K, Maier-Reimer E, Matear R, Monfray P, Mouchet A, Najjar RG, Plattner G-K, Rodgers KB, Sabine CL, Sarmiento JL, Schlitzer R, Slater RD, Totterdell IJ, Weirig M-F, Yamanaka Y, Yool A (2005) Anthropogenic ocean acidification over the twenty-first century and its impact on calcifying organisms. Nature 437:681–6

Pandolfi JM, Connolly SR, Marshall DJ, Cohen AL (2011) Projecting Coral Reef Futures Under

Global Warming and Ocean Acidification. Science (80-) 333:418–422

Sammarco P, Risk M (1990) Large-scale patterns in internal bioerosion of Porites: cross continental shelf trends on the Great Barrier Reef. Mar Ecol Prog Ser 59:145–156

Spalding MD, Ravilious C, Green E. (2001) World Atlas of Coral Reefs. UNEP-WCMC,

Woesik R Van, Woesik K Van, Woesik L Van (2013) Effects of ocean acidification on the dissolution rates of reef-coral skeletons. PeerJ 1–15

Chapter 2 – Ocean Acidification Affects Coral Growth by Reducing Skeletal Density

Nathaniel R. Mollica, Weifu Guo, Anne L. Cohen, Kuo-Fang Huang, Gavin L. Foster, Hannah K. Donald, Andrew R. Solow

Published in PNAS February 20th, 2018

2.1 Introduction

Coral reefs are among the most diverse ecosystems on Earth, with enormous cultural, ecological, and economic value. The calcium carbonate (aragonite) skeletons of stony corals are the main building blocks of the reef structure, and provide food, shelter and substrate for a myriad of other organisms. However, corals are vulnerable to environmental changes, including ocean acidification, which reduces the concentration of carbonate ions ($[CO_3^{2-}]$) that corals need to build their skeletons (Kleypas 1999; Doney et al. 2009). Under the "business as usual" emissions scenario, seawater $[CO_3^{2-}]$ is projected to decline across the global tropics by ~100 µmol/kg by 2100 (Hoegh-Guldberg et al. 2007; Doney et al. 2009; Meissner et al. 2012), almost halving preindustrial concentration. Predictions based on abiogenic precipitation experiments imply an associated decrease in the precipitation rate of aragonite of ~48% (Burton and Walter 1987). Such predictions raise concerns that many coral reefs will shift from a state of net carbonate accretion to net dissolution (Hoegh-Guldberg et al. 2007). Nevertheless, both laboratory manipulation experiments rearing corals under high pCO_2 conditions and field studies of naturally low-pH reefs that are designed to explore the impact of ocean acidification on coral calcification, have yielded inconsistent results (Langdon et al. 2000; Fabricius et al. 2011; Pandolfi et al. 2011; Chan and Connolly 2013; Crook et al. 2013; Comeau et al. 2014; Barkley et al. 2015; Tambutté et al. 2015). Field based measurements of calcification rates of corals inhabiting naturally low pH reefs today vary widely from sharp decreases in calcification rate with decreasing pH to no significant response. For example, a non-linear response of *Porites astreoides* to declines in seawater aragonite saturation state (Ω_{sw}) was observed in the Yucatan Ojos, with no change in calcification

rate at $\Omega_{sw} > 1$ and a sharp decline in calcification when conditions become undersaturated (Crook et al. 2013). At CO_2 vent sites on the volcanic island Maug (Northern Mariana Islands), a significant decline in *Porites* calcification rate was observed between ambient and mid Ω_{sw} conditions (3.9 and 3.6 respectively), yet no change between the mid and low (Ω_{sw} = 3.4) conditions (Enochs et al. 2015). On other reefs, calcification rates are constant across the Ω_{sw} range. For example, *Porites* calcification at Milne Bay (Papua New Guinea) CO_2 vents showed no significant change between Ω_{sw} of 3.5 and 2.9 (Fabricius et al. 2011), and on Palau, no change in calcification rate of two massive genera of coral (*Porites* and *Favia*) was observed across an Ω_{sw} gradient of 3.7 to 2.4 (Barkley et al. 2015).

These results have raised questions about the potential for adaptation, acclimation and/or the role of non-pH factors in modulating the influence of ocean acidification in natural systems, confounding efforts to predict reef calcification responses to 21st century ocean acidification (Pandolfi et al. 2011). The reefs in the studies discussed above are very different both compositionally and environmentally, and in each case the low Ω_{sw} is a result of different factors (e.g. CO_2 vents vs. freshwater seeps). However, one commonality among these studies is that calcification rates are reported for massive species by measuring linear extension and skeletal density in cores extracted from living colonies. The product of annual linear extension and mean skeletal density is used to estimate the annual calcification rate (Lough 2008). While this measure provides an accurate estimate of the annual amount of $CaCO_3$ produced by the coral, it does not account for the possibility that density and extension could be influenced by different factors (e.g. seawater chemistry, light exposure, nutrient level). Here we combine measurements of seawater saturation state, skeletal growth of *Porites*, and constraints on the coral's calcifying fluid composition to examine the impact of ocean acidification on each skeletal growth parameter separately.

2.2 Results and Discussion

2.2.1 *Porites* skeletal density but not extension is sensitive to ocean acidification.

Extension, density, and calcification rates were quantified in nine *Porites* skeletal cores from four Pacific reefs (Palau, Donghsa Atoll, Green Island, and Saboga) representing average

Ω_{sw} ranging from ~2.4 to ~ 3.9, (Fig. 1). We observed no correlation between annual calcification rates and Ω_{sw} either within or between reef sites. However, coral calcification does not take place directly from ambient seawater but within an extracellular calcifying fluid or medium (ECM) that is located between the coral skeleton and its calicoblastic cell membrane (Constantz 1986; Cohen and McConnaughey 2003; Allemand et al. 2011). The carbonate chemistry of the ECM is strongly regulated by corals and can differ significantly from ambient seawater (Gattuso et al. 1999; Tambutté et al. 2007). Most notably, pH of the ECM is elevated above ambient seawater by up to 1 unit (Hönisch et al. 2004; Tambutté et al. 2011; Trotter et al. 2011; Venn et al. 2011; McCulloch et al. 2012). Geochemical proxy data suggest that dissolved inorganic carbon (DIC) concentrations in *Porites* ECM are also elevated relative to the seawater, (e.g. by a factor of ~1.4 or ~2.6) (Allison et al. 2014; Mcculloch et al. 2017), although in vivo microelectrode measurements of other coral species imply a DIC concentration in the ECM similar to seawater (Cai et al. 2016). A combination of elevated pH and DIC leads to higher aragonite saturation state in the ECM (Ω_{ECM}), which exerts direct control on the rate of aragonite precipitation by the coral.

To estimate Ω_{ECM} of our coral cores, we first reconstructed the pH of coral ECM based on their boron isotope compositions and then combined these pH estimates with *in situ* measurements of seawater temperature, salinity, and DIC concentration. An elevation factor (α) of 2 is adopted to account for the elevation of DIC concentration within the ECM relative to seawater values (See appendix A2). Our estimated Ω_{ECM} for these cores vary from 11.6 ± 0.9 to 17.8 ± 2.0, ~3.5-4.6 times higher than the Ω_{sw} in which the corals grew. Nevertheless, we do not observe any correlation between coral calcification rates and Ω_{ECM} (Fig. 1b). Instead, when we deconvolve calcification into skeletal extension and skeletal density, a significant correlation is observed between coral skeletal density and Ω_{ECM} and also, skeletal density and Ω_{sw} (Fig. 1c-d). Skeletal extension, however, does not show a statistically significant correlation with Ω_{ECM} or Ω_{sw} (Fig. 1e-f). Correlations between skeletal density and Ω_{sw}, similar to what observed in our data, have also been reported in other field studies (Fabricius et al. 2011; Crook et al. 2013; Barkley et al. 2015; Fantazzini et al. 2015), including at some of the key ocean acidification study sites (e.g., CO_2 vents in Italy, Papua New Guinea, and the Caribbean Ojos) (Fabricius et al. 2011; Crook et al. 2013; Fantazzini et al. 2015), but not all (Manzello et al. 2014; Enochs et al. 2015) (Fig. A2.1).

These observations, although counter-intuitive, are consistent with the two-step model of coral calcification, in which coral skeleton is accreted in two distinct phases (Barnes and Lough 1993): vertical upward growth (i.e. extension) creating new skeletal elements and lateral thickening of existing elements in contact with living tissue. These two components of coral growth are fundamentally different processes. Skeletal extension is driven by the accretion of successive, elongated early mineralization zones (EMZs; also referred to as centers of calcification and the immediately associated fibers) in a continuous or semi-continuous column parallel to the upward growth axis of the skeleton (Wells 1956; Cohen and McConnaughey 2003; Northdruft and Webb 2007). Conversely, skeletal thickening occurs via growth of bundles of mature, *c*-axis aligned aragonite fibers at an angle that is perpendicular or semi-perpendicular to the EMZ and upward growth axis of the coral. This thickening affects the bulk density of the skeleton because the more the fiber bundles thicken or lengthen, the lower the skeletal porosity (Fig. A2.2) (Cohen and McConnaughey 2003; Stolarski 2003; Northdruft and Webb 2007). Our data reveal the strong sensitivity of skeletal density to ECM carbonate chemistry and ocean acidification (Fig. 1). Conversely, skeletal extension appears less sensitive or insensitive to ECM carbonate chemistry. One explanation for this finding is that the EMZs, which contain a relatively high concentration of organic material (Cuif et al. 2003; Stolarski 2003; Shirai et al. 2012), are under stronger biological control (Clode and Marshall 2002, 2003; Van de Locht et al. 2013) and are thus shielded from changes in calcifying fluid pH and external seawater pH. Conversely, weaker biological control of fiber bundle growth would render skeletal density more exposed to physicochemical influences and thus, more sensitive to changes in both calcifying fluid pH and ocean acidification.

Results of experimental studies support this hypothesis. Laboratory experiments showed no decline in the extension rate of *Stylophora Pistillata* over a year of growth in low-Ω_{sw} seawater (1.1-3.2) (Tambutté et al. 2015). Similarly, most field studies, except one (Enochs et al. 2015), have found no significant effect of ocean acidification on coral skeletal extension over pH ranges expected in the 21st century (Fabricius et al. 2011; Crook et al. 2013; Barkley et al. 2015; Fantazzini et al. 2015). Instead, the extension is believed to be controlled by other environmental factors, such as irradiance, temperature, and nutrient environment (Lough and Cooper 2011). For example, studies show that coral extension rates decline exponentially with water depth over a range of ~40 m after light attenuation (Dustan 1975; Michael Huston 1985; Al-Rousan 2012) but increase with mean annual sea surface temperature (SST) until an optimum thermal threshold (Cooper et al.

2008; Cantin et al. 2010). In addition, sediment influx and nutrient loading have also been suggested to influence extension rates in a nonlinear fashion, with minor increases in nutrient availability promoting growth and more severe nutrient loading leading to abrupt declines (Tomascik and Sander 1985). We, however, observe none of these correlations in our coral cores, presumably due to the small depth and temperature ranges that they cover (i.e., 1 to 6 m and 26.4 to 30.3 ^{o}C) (Table A2.1).

Our observation that skeletal density but not extension is affected by seawater chemistry may explain the large variability in response of coral calcification to ocean acidification, as calcification is calculated as the product of linear extension and mean skeletal density. Our findings are consistent with previous suggestions that the accretion of EMZ during coral calcification is under stronger biological control (Cohen and McConnaughey 2003; Cuif et al. 2003; Stolarski 2003; Shirai et al. 2012), presumably through the organic matrix (Allemand et al. 1998; Watanabe et al. 2003; Euw et al. 2017), and also with previous reports of the sensitivity of skeletal porosity to ocean acidification (Fantazzini et al. 2015; Tambutté et al. 2015). Furthermore, because density is a critical component of the coral growth process, our results support laboratory and field-based studies that report negative impacts of ocean acidification on coral calcification and consequently, the health of coral reef ecosystems (Chan and Connolly 2013).

2.2.2 A numerical model of *Porites* skeletal growth.

Within the two-step model of coral calcification, coral skeletal density is strongly controlled by the rate of skeletal thickening, which is expected to vary as a function of Ω_{ECM}:

$$R_{ECM} = k(\Omega_{ECM} - 1)^n \quad (2.1)$$

where R_{ECM} is the expected aragonite precipitation rate in the ECM, and k and n are the rate constant and reaction order for aragonite precipitation, respectively (Burton and Walter 1987). This is confirmed by the significant correlation between skeletal density and expected aragonite precipitation rate in our cores on both annual and seasonal scales, providing a mechanistic link

between skeletal density and seawater chemistry subsequent to its modulation in the ECM (Fig. 2).

To quantitatively evaluate the sensitivity of skeletal density to ocean acidification, we construct a numerical model of *Porites* skeletal growth that builds on previous modeling studies (e.g., ref. 50) (Fig. 3a, also see Appendix A2). In this model, the coral calyx is approximated as a ring in which coral growth proceeds in two consecutive steps: vertical construction of new skeletal framework representing daily extension of EMZs (E) followed by lateral aragonite precipitation around the interior of the ring representing thickening. Thickening of the skeletal elements, which we prescribe an initial ring wall thickness of w_o, occurs throughout the tissue layer – most prominently at the polyp surface and diminishing with depth (Barnes and Lough 1993; Gagan et al. 2012):

$$R(z) = R_{ECM} \times e^{-\frac{\lambda \times z}{T_d}} \tag{2.2}$$

where $R(z)$ is the aragonite precipitation rate at depth z, λ is the decay constant, and T_d is the thickness of the coral tissue layer. In our model T_d is stretched daily coincident with skeletal extension, and reset at monthly intervals to simulate dissepiment formation and subsequent vertical migration of polyps (Sorauf 1970; Buddemeier et al. 1974). The final density of coral skeleton when exiting the tissue layer is then calculated as the fraction of filled calyx:

$$\rho_{coral} = \rho_{arag}\left(1 - \frac{r_f^2}{r_o^2}\right) \tag{2.3}$$

where ρ_{arag} is the density of aragonite, r_f and r_o represent the inner and outer radii of the calyx respectively (Fig. 3a).

Within this model framework, five key factors control the density of coral skeleton: initial calyx size (r_o), thickness of the new skeletal framework (w_o), aragonite precipitation rate in the ECM (R_{ECM}), decline of thickening rate from the surface to the depth of the tissue layer (λ), and the time a skeletal element spends within the tissue layer ($t = T_d/E$). R_{ECM} is calculated based on seawater physicochemical parameters, pH of the ECM, and the DIC elevation factor (i.e. α) in the ECM, and assumes the sensitivity of coral aragonite formation to the ECM carbonate chemistry is the same as that determined in abiotic precipitation experiments (See section 2.3 and Eq. 2.1)

(Wells 1956; Clode and Marshall 2002; Comeau et al. 2014). Most of these model parameters, e.g. r_o, T_d, E, can be accurately determined via computed tomography (CT) imaging and inspection of each coral core. But there are limited experimental constraints on the other parameters, including w_o, λ, and α. We assume these three parameters are the same for all *Porites* corals and optimize their values to reproduce the measured skeletal density of our cores via a Bayesian statistical method (See Appendix A2). Our estimated α value ($2.05\ ^{+0.39}_{-0.38}$, 2σ) is similar to the experimentally estimated DIC elevation factor for *Porites* [e.g. 1.4 ± 0.1 (Allison et al. 2014) or 2.6 ± 0.6 (Mcculloch et al. 2017)]. However, the optimized value of w_o ($59\ ^{+23}_{-24}$ μm), which translates to 37-49% of the total skeleton, is approximately twice that estimated from visual observation of the early mineralization zones in SEM images and petrographic thin-sections (e.g. Fig A2.2). This difference likely reflects the stacking of different skeletal elements in the simplified ring geometry assumed in our model and the normalization of the whole sensitivity spectrum of different skeletal components to ECM carbonate chemistry into two simplified groups in our model: not-sensitive (i.e. 'initial framework) and highly sensitive (i.e. 'thickening'). The exact sensitivity prescribed to the highly sensitive group (Eq. 2.1) also affects the estimated w_o value. Our analysis also provides the first quantitative estimates of λ ($12.8\ ^{+11.9}_{-6.2}$), suggesting 50% decrease in skeletal thickening rate at a depth of 4 to 12% into the tissue layer. With these estimated parameters, our model can quantitatively predict *Porites* skeletal densities under different seawater conditions.

To evaluate the performance of our model, we employ it to predict the skeletal densities of *Porites* corals at five tropical reefs and compare our model-predicted densities with the experimentally measured densities reported in previous studies (Fig. 3b and Fig. A2.6) (Lough and Barnes 2000; Poulsen et al. 2006; Tanzil et al. 2009, 2013; Crook et al. 2013; Manzello et al. 2014). These studies were selected because they report not only coral skeletal density but also extension and at least one of the following factors needed for our model prediction: r_o, T_d, or in situ seawater carbonate chemistry. This minimizes the uncertainty in our model prediction propagated from estimations of unmeasured parameters (See section 2.3). Corals in these studies consist of six different *Porites* species, and represent a wide range of reef environments across the Atlantic, Pacific, and Indian Ocean basins (21.7° S to 22.6° N), with large variations in annual SST (22.3 to 29.5 °C), pH (7.20 to 8.24), DIC (1780 to 3170 μmol kg^{-1}) and coral skeletal density (0.9 to 1.6 g cm^{-3}).

Our model predictions quantitatively reproduce the experimentally measured coral densities and explain a large amount of the variance in the measured densities (Fig. 3b) [Root-mean-square error (RMSE) = 0.15, $r^2 = 0.494$, $p < 0.0001$]. The exact agreements between modeled and measured densities vary between studies, and are related to the uncertainties in the unmeasured parameters in each study. Among these parameters, r_o has the strongest effect on the model predicted density, producing about -1% change in density for every 1% change in r_o. The model is less sensitive to R_{ECM} and T_d, yielding about 0.54% and 0.28% changes in density for every 1% change in each parameter respectively (Fig. A2.5). Three parameters, w_o, λ, and α, were held constant in the simulations for all studies. However, only two of the six species examined in these studies (i.e. *Porites lobata*, *Porites Lutea*) were included in our estimation of these three parameters, which could introduce additional uncertainties in our model predictions. Accordingly, we observe better agreements between model predicted density and measured density for studies in which skeletal and physiochemical parameters are well constrained and which are dominated by the same species as this study, (e.g. the Arabian Gulf and Great Barrier Reef studies) (Fig. A2.6). In contrast, locations with poor constraints on r_o, T_d and R_{ECM}, (e.g. the Andaman Sea and the Caribbean region) yield less satisfactory agreements.

Other than the parameters discussed above, the rate of skeletal extension which was measured in all these studies also affects coral skeletal density, as it influences the amount of time that each skeletal element spends inside the coral tissue layer subject to thickening ($t=T_d/E$). Although we do not observe significant correlations between skeletal density and extension rate in our *Porites* cores on either annual or seasonal scales, as were observed in some previous studies (Lough and Barnes 2000; DeCarlo and Cohen 2017), two of the six studies included in our model-data comparison show apparent correlations between annual density and extension (Fig. A2.7). When examined as a whole, skeletal data from most of these studies also show an apparent correlation between the two parameters across the large range of extension (0.2 ~ 2.3 cm yr^{-1}; Fig. A2.7), yielding a sensitivity of -0.20% change in density for every 1% change in extension. This observed correlation is consistent with our model predicted sensitivity of skeletal density to extension [i.e. -0.30% change in density for 1% change in extension (Fig. A2.5)] and contributes to the agreement between our model-predicted density and experimentally measured density.

2.2.3 Projecting the impact of ocean acidification on *Porites* skeletal density.

Our model takes into account the different factors that can influence *Porites* coral skeletal growth (e.g. seawater conditions, extension, polyp geometry), and enables us to isolate and evaluate the influence of each factor. Here, we use it to evaluate the response of *Porites* coral skeletal density to ocean acidification by forcing our model with outputs from the Community Earth System Model Biogeochemical run (CESM-BGC) in the RCP 8.5 projection (i.e. the 'business as usual' emission scenario). Among global reef sites, the CESM-BGC run predicts 0.25 to 0.35 units decrease in seawater pH, a -50 to 250 μmol/kg change in DIC, and a 1.7 to 3 ^{o}C increase in SSTs by the end of the 21st century. These translate to 0.85 to 1.95 decrease in seawater aragonite saturation states. There remain large uncertainties in how rising SSTs will affect coral calcification via its effects on zooxanthellae photosynthesis and coral bleaching (Coles and Jokiel 1977; Warner et al. 1996; Hooidonk et al. 2016). Thus, we focus solely on the impact of ocean acidification on coral skeletal density and do not include the effects of temperature on the reaction kinetics of aragonite precipitation in the following model simulations (See Appendix A2). For the similar reasons, all model parameters (i.e. r_o, T_d, E, λ, w_o, and α) were held constant in these simulations.

Our simulations predict an average 12.4 ± 5.8% (2σ) decline in *Porites* skeletal density across global reef sites by the end of the 21st century due to ocean acidification alone (Fig. 4). This decline results from the interplay between changes in seawater pH and DIC, with decreases in pH leading to an average decline in density of 16.8 ± 4.7%, mitigated by increasing DIC which drives a 6.4 ± 3.7% increase in density. Our model predicted density declines vary among different reefs, with equatorial reefs generally more impacted than higher-latitude reefs. For example, our model predicts the largest decreases in skeletal density (11.4 to 20.3%) in the coral triangle region driven by the largest pH decreases projected for this region (up to 0.35 units). In contrast, reefs in the Carribean and Arabian Gulf are predicted to experience no significant decline in coral skeletal density. In these regions, the effect of relatively small projected pH decrease (~0.29 units on average) is balanced by the largest increases in DIC (~175 μmol/kg on average). The model-predicted density changes also vary across reef systems. For example, up to 13% density decline is predicted in the northern Great Barrier Reef, while no significant change is predicted in the southern edges.

Our results suggest that ocean acidification alone would lead to declines in *Porites* coral skeletal density over the 21st century. Such declines in skeletal density could increase the susceptibility of reef ecosystems to bioerosion, dissolution, and storm damage (Sammarco and Risk 1990; Madin et al. 2012; Woesik et al. 2013). It is important to note that, in addition to ocean acidification, coral reefs today face many other environmental stressors, including changes in temperature, nutrient concentration, and sea level (Lough and Cooper 2011). Our model enables us to isolate the impact of ocean acidification on coral skeletal growth. With accurate incorporation of the impacts of these other stressors, future models of this kind will be able to quantitatively project the fate of reef ecosystems under 21st century climate change.

2.3 Methods

2.3.1 Coral samples and reef sites.

Nine 3-cm-diameter *Porites* cores were collected from reefs in Palau (six cores from four different sites), Dongsha Atoll (one core), Green Island (one core), and Isla Saboga (one core). For Palau sites, seawater salinity and carbonate chemistry parameters were acquired from four years of discrete sampling at each site (Barkley et al. 2015), and seawater temperatures were derived from the NOAA Optimum Interpolation SST (oiSST) data set after correcting for any mean and variance bias during overlapping periods of in situ logger temperatures (Reynolds et al. 2007). At other reef sites, seawater salinity and carbonate chemistry parameters were either determined based on discrete samples of seawater collected during coring and on subsequent visits to the respective reefs, or compiled from reported values in the literature (Table A2.1). Seawater temperatures for these sites were derived from the oiSST dataset, and were assumed to be representative of in situ reef conditions since no temperature loggers were deployed and satellite SST agreed reasonably with literature values. Total alkalinity (TA) and dissolved inorganic carbon (DIC) of all seawater samples were measured on a Versatile Instrument for Determination of Total inorganic Carbon (VINDTA) at Woods Hole Oceanographic Institution, with open cell potentiometric and coulometric titration method. Seawater pH and aragonite saturation states were then calculated using the CO2SYS program (Pierrot et al. 2006).

2.3.2 Determination of coral skeletal growth parameters.

Coral cores were imaged with a Siemens Volume Zoom Spiral Computerized Tomography scanner to determine skeletal density and to identify annual density bands. Annual extension rates, skeletal density and calcification rates were then determined based on these CT images, along polyp growth axes (DeCarlo and Cohen 2016, Table A2.1). Specifically, annual extension rate (E_A) was calculated as the average length of corallite traces between consecutive low-density band surfaces, and annual density ($\bar{\rho}_A$) was measured along each continuous corallite trace and averaged across corallites to avoid density anomalies from bioerosion or secondary crystallization. Annual calcification rates (C_A) were taken as the product of annual extension rate and density $C_A = E_A \times \bar{\rho}_A$. Average corallite areas were also calculated by identifying local density minima in each image, which correspond to porous calix centers, and assigning each nearby voxel to the closest density minimum. Because our skeletal growth model approximates corallite geometry as a ring, radii of each corallite were calculated assuming a circular geometry.

2.3.3 Boron Isotope Measurements.

Each core was sampled at ~1mm intervals for boron isotope measurements over at least one annual density band couplet, resulting in 6-10 measurements in each annual band (Table A2.1). The isotope measurements were conducted at Thermo Scientific Neptune multicollector ICP-MS either at Academia Sinica (Taiwan) or at National Oceanography Centre Southampton (Foster et al. 2008). The pH of the ECM was then estimated based on the measured $\delta^{11}B$ values:

$$pH_{ECM} = pK_B^* - \log\left(-\frac{\delta^{11}B_{SW} - \delta^{11}B_{coral}}{\delta^{11}B_{SW} - \alpha_B\delta^{11}B_{coral} - ([\alpha_B - 1] * 1000)}\right)$$

where pK_B^* is the equilibrium constant for the dissociation reaction of boric acid to borate estimated at respective seawater temperature and salinity (Dickson 1990), and the $\delta^{11}B$ of seawater was taken to be 39.61 ‰ (Foster et al. 2010). The boron isotope fractionation factor , α_B, is assumed to be 1.0272 (Klochko et al. 2006).

2.3.4 Estimation of aragonite precipitation rate in ECM.

Aragonite precipitation rate in the ECM **(**R_{ECM}**)** was calculated from aragonite saturation state in the ECM (Ω_{ECM}) (see Equation.2.1), based on the precipitation rate constants and rate orders determined by Burton and Walter (1987), fit by McCulloch et al. (2012):

$$k = -0.0177T^2 + 1.47T + 14.9, n = 0.0628T + 0.0985$$

Aragonite saturation state in the ECM was estimated as:

$$\Omega_{ECM} = \frac{[Ca^{2+}]_{ECM} \times [CO_3^{2-}]_{ECM}}{K_{sp}}$$

where K_{sp} is the solubility product of aragonite in seawater at the corresponding temperature and salinity (Mehrbach et al. 1973), and $[CO_3^{2-}]_{ECM}$ and $[Ca^{2+}]_{ECM}$ are the calcium and carbonate ion concentrations in the ECM, respectively. $[Ca^{2+}]_{ECM}$ was assumed to be the same as seawater which was estimated from seawater salinity (Krumgalz 1982). $[CO_3^{2-}]_{ECM}$ was calculated based on the pH_{ECM} derived from boron isotope measurements, and seawater temperature, salinity, and DIC with an elevation factor of α = 2, using CO2SYS program (Pierrot et al. 2006) using the carbonate equilibrium constants determined in Mehrbach et al. (1973) and refit by Dickson and Millero (1987).

2.3.5 Estimation of model parameters with Bayesian methods.

Three parameters in our coral skeletal growth model were estimated with a Bayesian inference method (See Appendix A2). These are the thickness of each new skeletal framework (w_o), the decline of thickening rate with depth within the tissue layer (λ), and the DIC elevation factor in the ECM (α). Prior distributions for each parameter were constructed based on constraints from existing studies, and were combined to form a joint prior distribution. The likelihood of each combination of parameters was then evaluated by comparing measured densities in our cores to the associated model predictions. The prior distribution was updated using the likelihood function via Bayes' Theorem to form a posterior distribution, from which the most likely values for each parameter were acquired.

2.3.6 Comparison of model prediction with existing studies.

Porites corals from five reefs reported in six previous studies were used to evaluate the accuracy of our skeletal growth model in predicting coral skeletal density. These corals were collected from reefs in the Galapagos, the Andaman Sea, the Great Barrier Reef, the Caribbean, and the Arabian Gulf (Lough and Barnes 2000; Poulsen et al. 2006; Tanzil et al. 2009, 2013; Crook et al. 2013; Manzello et al. 2014). Besides three parameters estimated above with Bayesian methods, other parameters required for our model prediction include E, r_o, T_d, seawater temperature, salinity and carbonate chemistry (from which R_{ECM} is calculated). Among these, only E was reported in all the studies. When not reported, r_o and T_d values were estimated from either studies conducted at nearby reef sites or from taxonomic averages for each species (See Appendix A2). In situ measurements of seawater carbonate chemistry, sea surface temperature and salinity, whenever available, were used to calculate R_{ECM}; when not available, pH, DIC, salinity, and temperature outputs from the CESM-BGC run were averaged over the time period skeletal growth parameters were measured and used to estimate R_{ECM}. As none of these studies determined carbonate chemistry of the coral ECM, we estimated the coral pH_{ECM} based on the $pH_{ECM} \sim pH_{SW}$ correlation observed in laboratory Porites manipulation experiments (Trotter et al. 2011) which cover a pHsw range similar to these studies (i.e. 7.19 to 8.09 v.s. 7.23 to 8.15).

2.3.7 Projection of future skeletal density changes for global reefs.

Changes in skeletal density on different reefs were predicted based on output from the CESM-BGC RCP 8.5 21st century prediction run. Monthly projections of DIC, pH, T, and S from the first ten (2006-2015) and last ten (2090-2099) years of the run were extracted from the 1^o x 1^o model and averaged to represent the current and end of century seawater conditions at different reef sites around the globe. Reef site locations are provided by ReefBase database of reef sites (McManus and Ablan 1996). Skeletal growth parameters, E (annual extension rate), T_d (tissue thickness), and r_o (polyp radii), were prescribed at 1.0 cm yr^{-1}, 0.56 cm, and 0.063 cm respectively (the average values observed in our cores), and were held constant for predictions over the 21th century. The effect of temperature on the reaction kinetics of aragonite precipitation was not considered in the model projection. A detailed analysis of the effects of the rising 21st century temperature on model predictions is presented in Appendix A2.

2.4 Figures

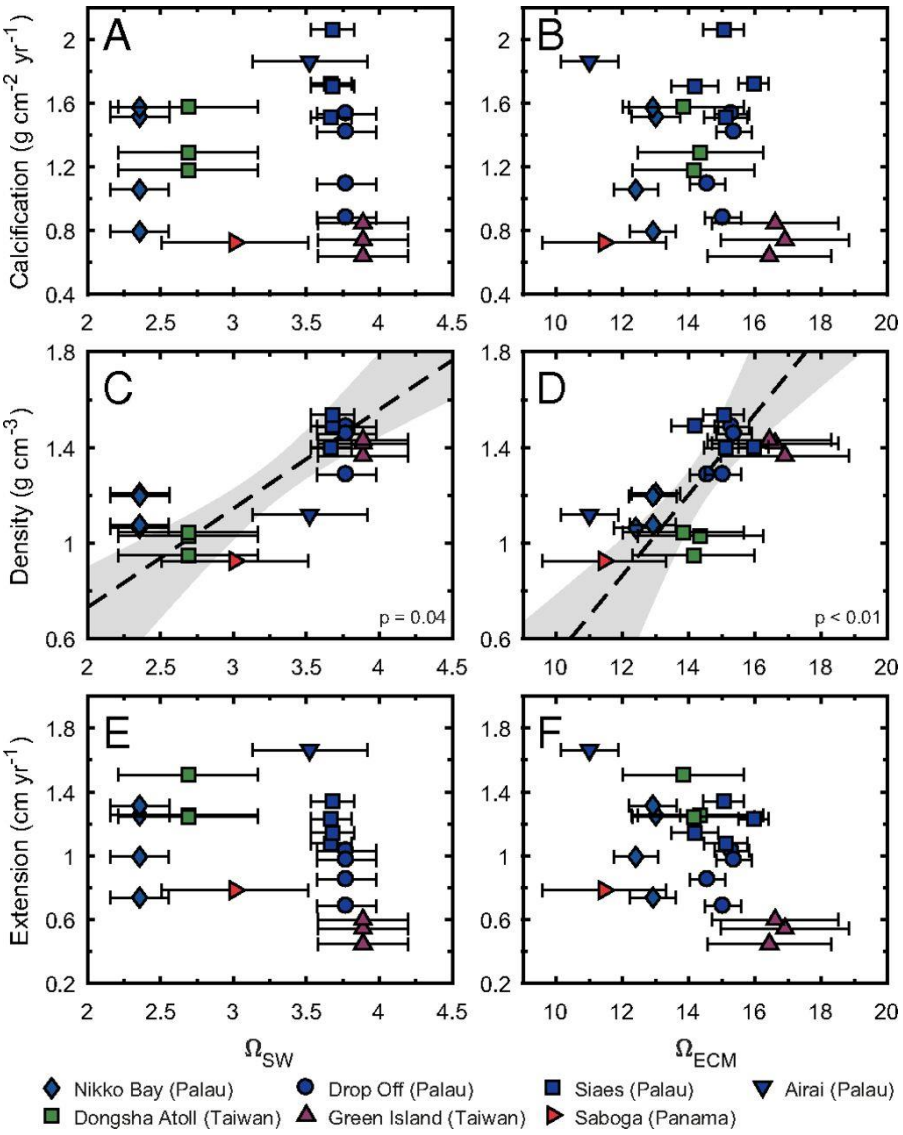

Figure 2.1. Coral skeletal parameters measured in representative *Porites* cores from four reefs across the Pacific. Coral calcification rates do not correlate with either Ω_{sw} or Ω_{ECM} (*A* and *B*). Instead, skeletal density exhibits a significant positive correlation with both Ω_{sw} and Ω_{ECM} (*C* and *D*), but extension does not (*E* and *F*; $P = 0.14$ and $P = 0.09$, respectively). Individual points represent annual averages of skeletal growth. Error bars denote 1 SD of Ω propagated from seasonal variability in seawater physicochemical parameters (for Ω_{sw} and Ω_{ECM}) and in boron isotope compositions of coral skeletons (for Ω_{ECM}).

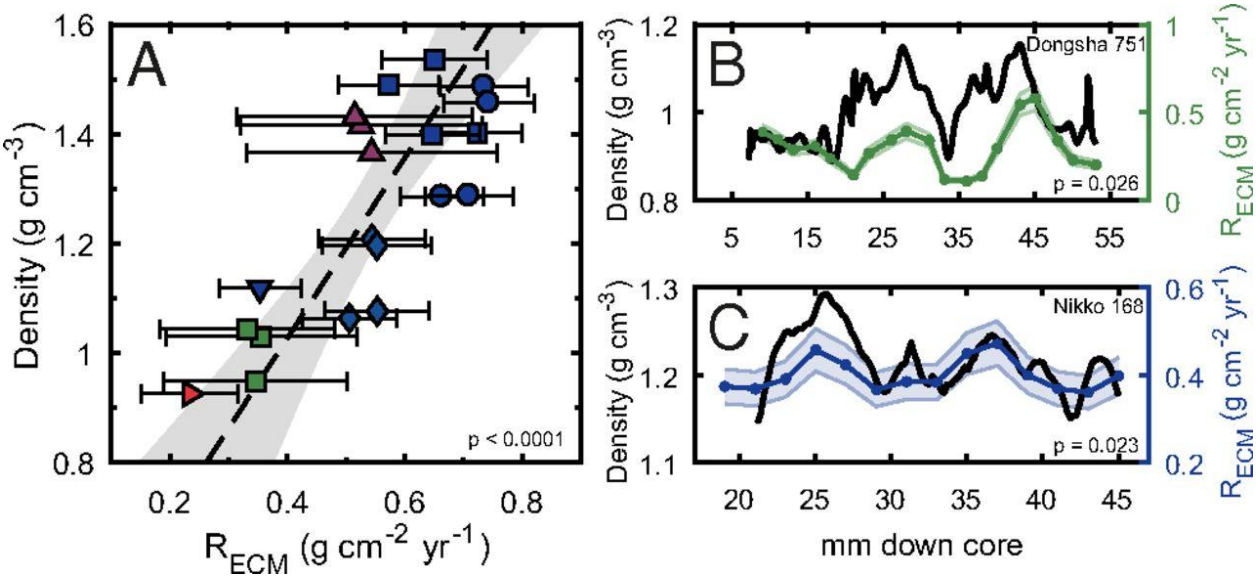

Figure 2.2. Correlation between coral skeletal density and expected aragonite precipitation rate in the coral ECM (R_{ECM}) on both the annual (*A*) and seasonal (*B* and *C*) scales. Data in *A* represent the same cores as in Fig. 1. Error bars (*A*) and shaded areas (*B* and *C*) denote 1 SD in R_{ECM} as propagated from uncertainties in seawater parameters and in boron isotope measurements. Seasonal density profiles were retrieved parallel to the sampling track for boron isotope measurements.

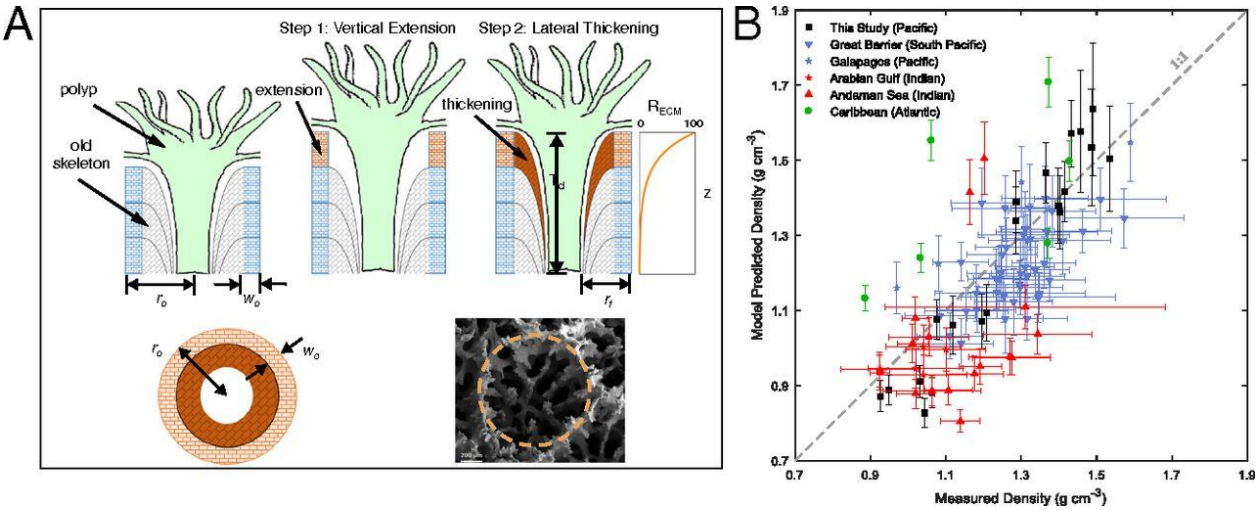

Figure 2.3. Schematic representation of our *Porites* skeletal growth model (*A*) and comparison between model-predicted skeletal density and measured density (*B*). Also shown in *A* are a cross-section view of our model polyp geometry and a representative SEM image of a *Porites* calyx (orange dashed line). *Porites* cores in *B* were collected from reefs in the Pacific, Atlantic, and Indian Oceans reported in previous studies (9, 30, 54–57). Data points from this study, the Caribbean, and the Andaman Sea represent densities of individual cores; data points from the Galapagos, the Great Barrier Reef, and the Andaman Sea represent site average densities for which error bars denote 2σ uncertainties. Vertical error bars represent uncertainties in model prediction propagated from uncertainties in model parameters α, λ, and w_o as well as measurements of in situ seawater conditions where available. Where seawater conditions were not reported, outputs from the CESM-BGC historical run were adopted.

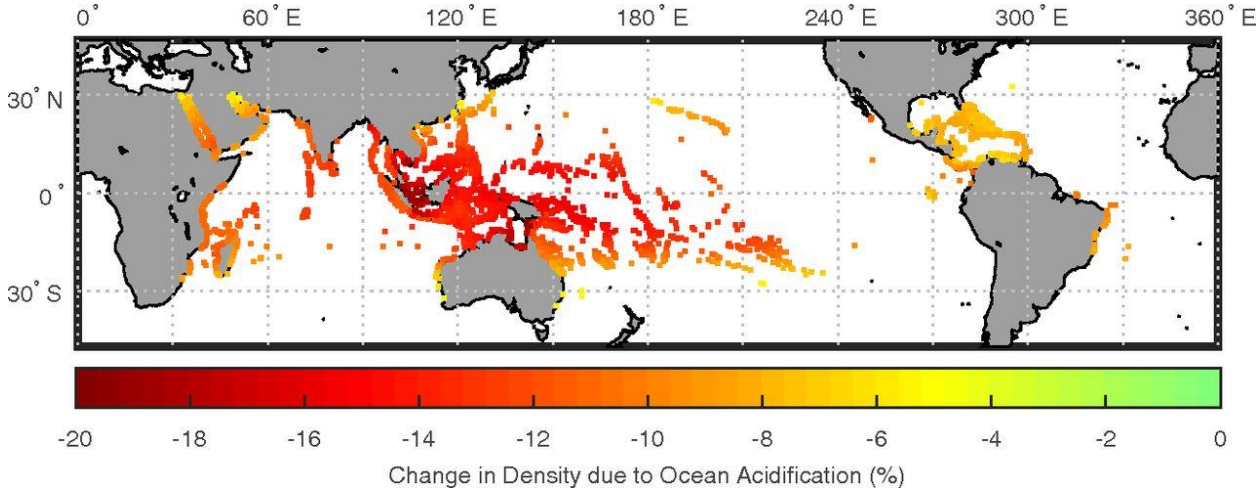

Figure 2.4. Model-predicted decline in *Porites* skeletal density over the 21st century due to ocean acidification. Our model predicts an average 12.4 ± 5.8% (2σ) decline in density across global reef sites, with the largest decline in the western tropical Pacific coral triangle region (an average of ~14% and a maximum of 20.3%) and the least in the Caribbean (~6%). Simulations were conducted based on outputs from the CESM-BGC RCP 8.5 run for the years 2006–2015 and 2090–2099 (See section 2.3). Skeletal extension, initial radius, and tissue thickness were held constant in these simulations. Error represents only that propagated from estimation of model parameters.

2.5 References

Al-Rousan S (2012) Skeletal extension rate of the reef building coral Porites species from Aqaba and their environmental variables. Nat Sci 4:

Allemand D, Tambutte E, Girard J, Jaubert J, Tambutté E, Girard J, Jaubert J (1998) Organic matrix synthesis in the scleractinian coral *Stylophora pistillata*: role in biomineralization and potential target of the organotin tributyltin. J Exp Biol 201:2001–9

Allemand D, Tambutté É, Zoccola D, Tambutté S (2011) Coral Calcification , Cells to Reefs.

Allison N, Cohen I, Finch AA, Erez J, Tudhope AW, Facility EIM (2014) Corals concentrate dissolved inorganic carbon to facilitate calcification. Nat Commun 5:5741

Barkley HC, Cohen AL, Golbuu Y, Starczak VR, Decarlo TM, Shamberger KEF (2015) Changes in coral reef communities across a natural gradient in seawater pH. Sci Adv 1–7

Barnes DJ, Lough JM (1993) On the nature and causes of density banding in massive coral skeletons. J Exp Mar Bio Ecol 167:91–108

Buddemeier RW, Maragos JE, Knutson DW (1974) Radiographic studies of reef coral exoskeletons: Rates and patterns of coral growth. J Exp Mar Bio Ecol 14:179–199

Burton EA, Walter LM (1987) Relative precipitation rates of aragonite and Mg calcite from seawater: temperature or carbonate ion control? Geology 15:111–114

Cai W, Ma Y, Hopkinson BM, Grottoli G, Warner ME, Ding Q, Hu X, Yuan X, Schoepf V, Xu H, Han C, Melman TF, Hoadley KD, Pettay DT, Matsui Y, Baumann JH, Levas S, Ying Y, Wang Y (2016) Microelectrode characterization of coral daytime interior pH and carbonate chemistry. Nat Commun 1–8

Cantin NE, Cohen AL, Karnauskas KB, Tarrant AM, McCorkle DC (2010) Ocean Warming Slows Coral Growth in the Central Red Sea. 329:322–325

Chan NCS, Connolly SR (2013) Sensitivity of coral calcification to ocean acidification: A meta-analysis. Glob Chang Biol 19:282–290

Clode PL, Marshall AT (2002) Low temperature FESEM of the calcifying interface of a scleractinian coral. Tissue Cell 34:187–198

Clode PL, Marshall AT (2003) Calcium associated with a fibrillar organic matrix in the scleractinian coral Galaxea fascicularis. Protoplasma 220:153–161

Cohen AL, McConnaughey TA (2003) Geochemical Perspectives on Coral Mineralization. Rev Mineral Geochemistry 54:151–187

Coles SL, Jokiel PL (1977) Effects of temperature on photosynthesis and respiration in hermatypic corals. Mar Biol 43:209–216

Comeau S, Edmunds PJ, Spindel NB, Carpenter RC (2014) Fast coral reef calcifiers are more sensitive to ocean acidification in short-term laboratory incubations. Limnol Ocean 59:1081–1091

Constantz BR (1986) Coral Skeleton Construction : A Physiochemically Dominated Process. Palaios 1:152–157

Cooper TF, De'ath G, Fabricius KE, Lough JM (2008) Declining coral calcification in massive Porites in two nearshore regions of the northern Great Barrier Reef. Glob Chang Biol 14:529–538

Crook ED, Cohen AL, Rebolledo-Vieyra M, Hernandez L, Paytan A (2013) Reduced calcification and lack of acclimatization by coral colonies growing in areas of persistent natural acidification. Proc Natl Acad Sci U S A 110:11044–9

Cuif JP, Dauphin YY, Doucet J, Salome M, Susini J (2003) XANES mapping of organic sulfate in three scleractinian coral skeletons. Geochim Cosmochim Acta 67:75–83

DeCarlo TM, Cohen AL (2016) coralCT: software tool to analyze computerized tomography (CT) scans of coral skeletal cores for calcification and bioerosion rates.

DeCarlo TM, Cohen AL (2017) Dissepiments, density bands, and signatures of thermal stress in Porites skeletons. Coral Reefs 1–13

Dickson AG (1990) Thermodynamics of the dissociation of boric acid in synthetic seawater from 273.15 to 318.15 K. Deep Sea Res Part A, Oceanogr Res Pap 37:755–766

Dickson AG, Millero FJ (1987) A comparison of the equilibrium constants for the dissociation of carbonic acid in seawater media. Deep Sea Res Part A, Oceanogr Res Pap 34:1733–1743

Doney SC, Fabry VJ, Feely RA, Kleypas JA (2009) Ocean Acidification: The Other CO2 Problem. Ann Rev Mar Sci 1:169–192

Dustan P (1975) Growth and Form in the Reef-Building Coral Montastrea annularis. Mar Biol 33:101–107

Enochs IC, Manzello DP, Donham EM, Kolodziej G, Okano R, Johnston L, Young C, Iguel J, Edwards CB, Fox MD, Valentino L, Johnson S, Benavente D, Clark SJ, Carlton R, Burton T, Eynaud Y, Price NN (2015) Shift from coral to macroalgae dominance on a volcanically acidified reef. Nat Clim Chang 5:1–9

Euw S Von, Zhang Q, Manichev V, Murali N, Gross J, Feldman LC, Gustafsson T, Flach C, Mendelsohn R, Falkowski PG (2017) Biological control of aragonite formation in stony corals. 938:933–938

Fabricius KE, Langdon C, Uthicke S, Humphrey C, Noonan S, De 'ath G, Okazaki R, Muehllehner N, Glas MS, Lough JM (2011) Losers and winners in coral reefs acclimatized to elevated carbon dioxide concentrations. Nat Clim Chang 1:165–169

Fantazzini P, Mengoli S, Pasquini L, Bortolotti V, Brizi L, Mariani M, Giosia M Di, Fermani S, Capaccioni B, Caroselli E, Prada F, Zaccanti F, Levy O, Dubinsky Z, Kaandorp JA, Konglerd P, Cuif J, Weaver JC, Fabricius KE, Wagermaier W, Fratzl P, Falini G, Goffredo S (2015) Gains and losses of coral skeletal porosity changes with ocean acidification acclimation. Nat Commun

Foster GL, Pogge Von Strandmann PAE, Rae JWB (2010) Boron and magnesium isotopic composition of seawater. Geochemistry, Geophys Geosystems 11:1–10

Foster GL, Rae J, Elliot T (2008) Boron isotope measurements of marine carbonate using MC-ICPMS. Geochim Cosmochim Acta 72:279

Gagan MK, Dunbar GB, Suzuki A (2012) The effect of skeletal mass accumulation in Porites on coral Sr/Ca and ??^{18}O paleothermometry. Paleoceanography 27:1–16

Gattuso J-P, Allemand D, Frankignoulle M (1999) Photosynthesis and Calcification at Cellular, Organismal and Community Levels in Coral Reefs: A Review on Interactions and Control by Carbonate Chemistry. Am Zool 39:160–183

Hoegh-Guldberg O, Mumby PJ, Hooten AJ, Steneck RS, Greenfield P, Gomez E, Harvell CD, Sale PF, Edwards a J, Caldeira K, Knowlton N, Eakin CM (2007) Coral Reefs Under Rapid Climate Change and Ocean Acidification. Science (80-) 318:1737–1742

Hönisch B, Hemming NG, Grottoli AG, Amat A, Hanson GN, Bijma J (2004) Assessing scleractinian corals as recorders for paleo-pH: Empirical calibration and vital effects. Geochim Cosmochim Acta 68:3675–3685

Hooidonk R Van, Maynard J, Tamelander J, Gove J (2016) Local-scale projections of coral reef futures and implications of the Paris Agreement. Nat Publ Gr 1–8

Kleypas J (1999) Geochemical Consequences of Increased Atmospheric Carbon Dioxide on Coral Reefs. Science (80-) 284:118–120

Klochko K, Kaufman AJ, Yao W, Byrne RH, Tossell JA (2006) Experimental measurement of boron isotope fractionation in seawater. Earth Planet Sci Lett 248:261–270

Krumgalz BS (1982) Calcium distribution in the world ocean waters. Oceanol Acta 5:121–128

Langdon C, Takahashi T, Marubini F, Atkinson M, Sweeney C, Aceves H, Barnett H, Chipman D, Goddard J (2000) Effect of calcium carbonate saturation state on the rate of calcification of an experimental coral reef. Global Biogeochem Cycles 14(2):639–654

Van de Locht R, Verch A, Saunders M, Dissard D, Rixen T, Moya A, Kroger R (2013) Microstructural evolution and nanoscale crystallography in scleractinian coral spherulites. J Struct Biol 183:57–65

Lough JM (2008) Coral calcification from skeletal records revisited. Mar Ecol Prog Ser 373:257–264

Lough JM, Barnes DJ (2000) Environmental controls on growth of the massive coral Porites. J Exp Mar Bio Ecol 245:225–243

Lough JM, Cooper TF (2011) New insights from coral growth band studies in an era of rapid environmental change. Earth-Science Rev 108:170–184

Madin JS, Hughes TP, Connolly SR (2012) Calcification, Storm Damage and Population Resilience of Tabular Corals under Climate Change. PLoS One 7:1–10

Manzello DP, Enochs IC, Bruckner A, Renaud PG, Kolodziej G, Budd DA, Carlton R, Glynn PW (2014) Galapagos coral reef persistence after ENSO warming across an acidification gradient. Geophys Res Lett 41:9001–9008

McCulloch M, Falter J, Trotter J, Montagna P (2012) Coral resilience to ocean acidification and global warming through pH up-regulation. Nat Clim Chang 2:623–627

Mcculloch MT, Olivo JPD, Falter J, Holcomb M, Trotter JA (2017) Coral calcification in a changing World and the interactive dynamics of pH and DIC upregulation. 1–8

McManus JM, Ablan MC (1996) ReefBase: a global database on coral reefs and their resources.

Mehrbach C, Culberson CH, Hawley JE, Pytkowicz RM (1973) Measurement of the apparent dissociation constants of carbonic acid in seawater at atmospheric pressure. Limnol Oceanogr 18:897–907

Meissner KJ, Lippmann T, Gupta A Sen (2012) Large-scale stress factors affecting coral reefs: Open ocean sea surface temperature and surface seawater aragonite saturation over the next 400 years. Coral Reefs 31:309–319

Michael Huston (1985) Variation in coral growth rates with depth at Discovery Bay, Jamaica. Coral Reefs 4:19–25

Northdruft LD, Webb GE (2007) Microstructure of common reef-building coral genera Acropora, Pocillopora, Goniastrea and Porites: constraints on spatial resolution in geochemical sampling. Facies - Carbonate Sedimentol Paleoecol 53:1–26

Pandolfi JM, Connolly SR, Marshall DJ, Cohen AL (2011) Projecting Coral Reef Futures Under Global Warming and Ocean Acidification. Science (80-) 333:418–422

Pierrot, Lewis DE, Wallace DWR (2006) MS Excel Program Developed for CO2 System Calculations. ORNL/CDIAC-105a

Poulsen A, Burns K, Lough J, Brinkman D, Delean S (2006) Trace analysis of hydrocarbons in coral cores from Saudi Arabia. Org Geochem 37:1913–1930

Reynolds RW, Smith TM, Liu C, Chelton DB, Casey KS, Schlax MG (2007) Daily high-resolution-blended analyses for sea surface temperature. J Clim 20:5473–5496

Sammarco P, Risk M (1990) Large-scale patterns in internal bioerosion of Porites: cross continental shelf trends on the Great Barrier Reef. Mar Ecol Prog Ser 59:145–156

Shirai K, Sowa K, Watanabe T, Sano Y, Nakamura T, Clode P (2012) Visualization of sub-daily skeletal growth patterns in massive Porites corals grown in Sr-enriched seawater. J Struct Biol 180:47–56

Sorauf J (1970) Microstructure and formation of dissepiments in the skeleton of the recent scleractinia (hexacorals). Biomineralization 2:1–22

Stolarski J (2003) Three-dimensional micro- and nanostructural characteristics of the scleractinian coral skeleton: A biocalcification proxy. Acta Palaeontol Pol 48:497–530

Tambutté E, Venn AA, Holcomb M, Segonds N, Techer N, Zoccola D, Allemand D, Tambutté S (2015) Morphological plasticity of the coral skeleton under CO2-driven seawater acidification. Nat Commun 6:7368

Tambutté S, Holcomb M, Ferrier-Pagès C, Reynaud S, Tambutté E, Zoccola D, Allemand D (2011) Coral biomineralization: From the gene to the environment. J Exp Mar Bio Ecol 408:58–78

Tambutté S, Tambutté E, Zoccola D, Caminiti N, Lotto S, Moya A, Allemand D, Adkins J (2007) Characterization and role of carbonic anhydrase in the calcification process of the azooxanthellate coral Tubastrea aurea. Mar Biol 151:71–83

Tanzil JTI, Brown BE, Dunne RP, Lee JN, Kaandorp JA, Todd PA (2013) Regional decline in growth rates of massive Porites corals in Southeast Asia. Glob Chang Biol 19:3011–3023

Tanzil JTI, Brown BE, Tudhope AW, Dunne RP (2009) Decline in skeletal growth of the coral Porites lutea from the Andaman Sea, South Thailand between 1984 and 2005. Coral Reefs 28:519–528

Taylor RB, Barnes DJ, Lough JM (1993) Simple-Models of Density Band Formation in Massive Corals. J Exp Mar Bio Ecol 167:109–125

Tomascik T, Sander F (1985) Effects of eutrophication on reef-building corals. Mar Biol 87:143–155

Trotter J, Montagna P, McCulloch M, Silenzi S, Reynaud S, Mortimer G, Martin S, Ferrier-Pagès C, Gattuso J-P, Rodolfo-Metalpa R (2011) Quantifying the pH "vital effect" in the temperate zooxanthellate coral Cladocora caespitosa: Validation of the boron seawater pH proxy. Earth Planet Sci Lett 303:163–173

Venn A, Tambutté E, Holcomb M, Allemand D, Tambutté S (2011) Live tissue imaging shows reef corals elevate pH under their calcifying tissue relative to seawater. PLoS One 6:

Warner ME, Fitt WK, Schmidt GW (1996) The effects of elevated temperature on the photosynthetic efficiency of zooxanthellae in hospite from four different species of reef coral: a novel approach. Plant Cell Environ 19:291–299

Watanabe T, Fukuda I, Katsunori C, Yeisin I (2003) Molecular analyses of protein components of the organic matrix in the exoskeleton of two scleractinian coral species. Comp Biochem Physiol Part B Biochem Mol Biol 136:767–774

Wells JW (1956) Scleractinia. Treatise on invertebrate paleontology F. Coelenterata. Geological Society of America & University of Kansas Press, pp 328–440

Woesik R Van, Woesik K Van, Woesik L Van (2013) Effects of ocean acidification on the dissolution rates of reef-coral skeletons. PeerJ 1–15

Chapter 3 – Skeletal records of bleaching reveal different thermal thresholds of Pacific coral reef assemblages

Nathaniel R. Mollica, Anne L. Cohen, Alice Alpert, Hannah C. Barkley, Russell E. Brainard, Jessica Carilli, Thomas M. DeCarlo, Elizabeth Drenkard, George Lohmann, Sangeeta Mangubhai, Kathryn Pietro, Hanny E. Rivera, Randi D. Rotjan, Celina Scott-Beuchler, Andrew Solow, and Charles Young

Published in Coral Reefs, May 2nd, 2019

3.1 Introduction

Reef-building corals exist in an obligate symbiosis with single celled dinoflagellates called zooxanthellae, which provide a significant component of the host energetic needs. When sea surface temperatures (SSTs) exceed a physiological threshold, the relationship between corals and zooxanthellae breaks down, the symbionts are expelled, and the coral loses pigmentation in a process called "bleaching" (e.g. Coles and Jokiel 1977). Prolonged or severe bleaching can lead to coral starvation and, eventually, death. Coral bleaching was first reported in 1963 (Donner et al. 2017), and regional-scale or mass bleaching of coral communities and reefs was first reported during the 1982/3 super El Niño (Hoegh-Guldberg and Smith 1989). As the oceans continued to warm over the subsequent three decades, episodes of mass bleaching increased in frequency and extent, and now occur with each El strong Niño (Hughes et al. 2018). By 2008, bleaching had caused irretrievable loss of an estimated 19% of reef area worldwide (Wilkinson 2008), and losses following the recent 2015-2016 El Niño are expected to exceed this estimate. As global temperatures rise, by a projected 1 to 2.5 °C over this century, (IPCC AR5 2014) there is mounting concern that coral communities will soon experience bleaching at a frequency from which they cannot recover.

Significant effort is currently invested in identifying coral reef ecosystems or communities that might survive ocean warming (Pratchett et al. 2008; Frieler et al. 2012; van Hooidonk et al. 2016; Beyer et al. 2018). These efforts are limited in large part, however, by two unknowns. First,

the spatial resolution of general circulation models (GCMs) is too coarse to resolve reef-scale hydrodynamics, meaning projections of future open ocean conditions may not apply to many shallow water reef systems. Statistical and dynamical downscaling of GCM output is one approach taken to specifically addressing this issue (Donner 2009; Frieler et al. 2012; van Hooidonk et al. 2016). Second, the thermal thresholds for bleaching of different reef systems are not well characterized. Currently, a single bleaching threshold based on 1°C warmer than the maximum monthly mean (MMM) SST is used to predict whether, and with what severity, bleaching will occur during heatwaves and in model projections of future global change scenarios (Heron et al. 2015). However, thermal thresholds differ amongst species (e.g. Coles and Jokiel 1977), amongst coral communities within and between reefs (e.g., Fisk and Done 1985; Rowan et al. 1997; Van Woesik et al. 2011) and examples exist of thermal thesholds changing over time (Maynard et al. 2008). While a few studies have incorporated inter-reef differences in thermal tolerance (van Hooidonk and Huber 2009; Donner 2011) and the potential for coral acclimatization (e.g. Logan et al. 2014) into projections of coral reef futures, these have been limited in assigning site-specific thermal thresholds by the paucity of observational bleaching records (van Hooidonk and Huber 2009).

This study addresses the second issue, i.e. the lack of constraint on coral thermal thresholds. Bleaching histories for reef locations around the globe have been compiled (e.g. Donner et al. 2017; Hughes et al. 2018), but all are limited by the paucity of observational data, especially but not limited to, remote reef locations. Here, we make a start at filling spatial and temporal gaps in bleaching records using signatures of bleaching archived in the skeletons of massive long-lived corals that survived, and recorded, multiple bleaching events extending back in time (Fig. 3.1). Skeletal "stress bands" have been linked, qualitatively, with anomalously high summertime SSTs and coral bleaching (Smithers and Woodroffe 2001; Hendy et al. 2003; Cantin et al. 2010; Carilli et al. 2010, 2012; Cantin and Lough 2014; Mallela et al. 2015). Recently, Barkley and Cohen (2016) and Barkley et al., (2018) demonstrated a statistically significant relationship between the prevalence of stress bands in massive *Porites spp.* corals and the severity of observed bleaching in the coral community on multiple reefs within the Palau archipelago, and on Howland and Jarvis Islands in the CEP. These observations support the utility of skeletal stress bands as proxies for historical bleaching severity in the absence of observational data.

In this study, we first build on the original calibration of bleaching incidence within a coral community (hereafter 'observed bleaching incidence') against the prevalence of stress bands in massive coral skeletons (hereafter 'stress band prevalence') (Barkley et al. 2018) by including new data from the Pacific and the Caribbean (Fig. 3.2). The new calibration includes 11 reef systems, multiple massive coral genera and represents multiple coral community compositions. Second, we apply the calibration to stress band records constructed from 8 central Pacific reef systems, spanning the time period 1982-2015. Third, we refine the NOAA thermal stress index (Degree Heating Weeks, DHW) calculation to enable estimates of thermal stress in the CEP, where SST variability on inter-annual timescales is dominant. We use a percentile-based method, independent of seasonality, to calculate the DHWs and cumulative thermal stress (Total Hotspot) for each heatwave at each site over the corresponding time period 1982-2015. We then compare the severity of the bleaching response to the level of thermal stress imposed on each reef during each event and construct reef-specific thermal sensitivity curves and a thermal tolerance index ($b_{½}$) for each reef system. Finally, we assess the thermal tolerance indices against multiple physiological and climatological factors to evaluate the potential mechanisms underpinning the different thermal tolerances exhibited by different reefs.

3.2 Materials and Methods

3.2.1 Collection of coral cores and identification of stress bands

247 skeletal cores were collected and analyzed from colonies of three massive coral genera (*Porites spp.*, *Orbicella spp.* and *Siderastrea siderea*) on eleven coral reefs in the Pacific Ocean and Caribbean. A subset of data from each core, specifically those years for which observational bleaching data exist, was used in the calibration. These cores are listed in Table A3.2. 122 *Porites* cores were then used to construct thermal histories for the eight Pacific reefs back to 1982, and generate the thermal sensitivity curves. These cores are listed in Table A3.3.

All cores were collected and analyzed using the same methods. Only live colonies were cored, establishing the top age, vertically i.e., parallel to the upward growth axis, and using either a pneumatic drill fitted with 3-cm diameter diamond tip coring bit or an hydraulic drill fitted with an 8-cm diameter bit. Core holes were sealed with a cement cap and underwater epoxy, secured flush with the colony surface to facilitate overgrowth of tissue and wound closure (e.g. Matson 2011), a 6 to 36-month process depending on the rate of coral growth and diameter of core. All

cores were first air dried in the field, then oven dried at 60 °C, and CT scanned intact, together with density standards, on the Siemens Volume Zoom Helical Computerized Tomography (CT) Scanner at Woods Hole Oceanographic Institution or the Siemens Biograph mCT scanner at the Biomedical Research Imaging Center (BRIC) at the University of North Carolina (protocol as per Barkley et al. 2015; DeCarlo et al. 2015).

Stress bands and annual growth bands were identified in the CT scan images of each core and quantified using the automated code coralCT for MATLAB which traces the density of individual corallites within the 3 dimensional core (DeCarlo and Cohen 2016). Revisions to version 1.1 of coralCT, which was designed primarily for *Porites spp.*, were made to accommodate the skeletal architecture of the Atlantic corals which have more prominent thecal walls than *Porites*. Specifically, a linear quadratic estimation algorithm (i.e. Kalman Filtering) improved polyp tracing along the core axis. The code was also revised to enable automated identification of stress bands (Barkley et al. 2018). Specifically, the density time-series for all corallites in the core (see DeCarlo et al. 2015, Data Repository Figure DR2) were averaged to create an "ensemble" mean density time series for all traceable corallites. The averaged density profile time-series was then detrended to account for shifts in mean density that may occur over time. Regions where skeletal density exceeded 2 standard deviations above the whole-core mean, a threshold chosen to account for the range in natural seasonal and inter-annual density variability, were identified as stress bands (Fig. 3.1C). To exclude fine-scale density anomalies such as worm borings, stress bands were defined as having a minimum width of 1 mm. Each CT scan was visually inspected to validate the presence and location of stress bands identified by the automated program.

The age model for each core was developed using annual growth bands also identified in the CT images. In corals with clear annual banding, the age model was constructed by counting the bands from the top of the core. Where banding was unclear or ambiguous, the band-based age model was validated using dissepiments. Specifically, the distance between successive monthly dissepiments was quantified from photographs taken under a dissecting microscope (Fig. A3.2). The estimate of annual extension derived from dissepiments was used to confirm the estimate derived from annual bands, following DeCarlo and Cohen (2017) (i.e. 12.4 dissepiments per year).

The thickness of the tissue in each core used in the bleaching history reconstruction was measured as an index of biomass or energetic reserve. The vertical distance between the top of the

core and the topmost dissepiment upon which the base of the tissue rests (e.g. Barnes and Lough 1992) was measured on a cut slab using a Nikon SMZ1500 stereomicroscope and SPOT imaging software (e.g. Barkley et al. 2018).

3.2.2 Bleaching Survey Data

Published bleaching accounts were used to calibrate the proportion of skeletal stress bands per event identified in the suite of cores against the observed bleaching incidence (represented by the percent coral cover observed to be bleached) recorded during that event (Table A3.4). In all cases, with the exception of the Phoenix Islands surveys in 2015 (Kanton, Rawaki, Enderbury, Nikumaroro), bleaching was observed during or after the peak SST anomaly obtained during each event. In the Phoenix Islands, ecological surveys and skeletal cores were obtained two months prior to the peak SST anomaly, and it is likely that the full extent of bleaching in 2015-16 was not captured by those surveys. However, since coring and surveys were conducted simultaneously, we expect the stress bands to track the severity of bleaching at the time, and we used this information in the calibration.

On Dongsha Atoll and Jarvis Island, bleaching estimates were obtained from photographic surveys conducted in June 2015 (DeCarlo et al. 2017) and November 2015 (Barkley et al. 2018) respectively. On Jarvis and Howland Islands in 2010, bleaching severity was assessed from Rapid Ecological Assesments (REA) and towed-diver surveys (Vargas-Ángel et al. 2011). In the Phoenix Islands (Kanton, Rawaki, Enderbury, and Nikumaroro) in 2015, bleaching information was estimated from photographic surveys (Mangubhai et al. 2015; Table A3.4). In the Caribbean, coral bleaching observations on Martinique, Barbados and Curacao in 1998, 2005 and 2010 were used in the calibration (Wilkinson 2008; Eakin et al. 2010; Estep et al. 2017). Results were reported as percent coral cover bleached, (Jarvis, Howland, Dongsha, and the Caribbean sites), or percent colony bleached (Phoenix Islands). We standardized the data as follows:

$$Observed\ Bleaching\ Incidence\ (\%) = \frac{bleached\ coral\ (m^2)}{total\ coral\ (m^2)} \quad (3.1)$$

3.2.3 Sea surface temperature data and data products

We used daily satellite SSTs (November 1981 – December 2016) from the AVHRR Pathfinder Version 5.3, 4-km dataset (nighttime only) (Casey et al. 2010). For reefs from which

cores were collected across multiple cells, the grid cells were averaged. Average weekly SSTs were calculated and temporal gaps in the Pathfinder data filled with mean-adjusted values from the IGOSS OIv2 1° x 1° resolution dataset (Reynolds et al. 2002). *In situ* temperature loggers deployed at Jarvis by Barkley et al., (2018), as well as our loggers deployed at Kanton, Enderbury, Nikumaroro, and Rawaki from June 2012 to September 2015 were used to validate satellite-derived SSTs for these central Pacific sites (Fig. A3.3). Average *in situ* temperatures were within ±0.25°C of satellite SSTs, with two exceptions. First, on the west side of Jarvis Island, upwelling of the Pacific Equatorial Undercurrent (EUC) lowers local temperatures relative to the east side of the island and satellite-derived SSTs, which consistently capture east side SSTs (Alpert et al. 2016). However, during El Niño, weakening of the EUC occurs, upwelling is diminished or entirely absent, and temperatures are homogenous around the island. Thus, during bleaching events, temperatures on Jarvis' west side are consistent with satellite-derived SSTs (Barkley et al. 2018). Second, in Kanton Lagoon, loggers deployed during the 2015 El Niño revealed that daytime temperatures in the lagoon consistently exceeded both satellite-derived SSTs and logged outer reef SSTs by up to 1°C. Kanton lagoon cores were used in the calibration because bleaching severity in the lagoon was recorded in 2015 at the same time the cores were collected. However, we did not include lagoon cores in the down-core historical bleaching reconstruction to evaluate thermal sensitivity because we could not constrain historical lagoon SST back to 1982 from the satellite data.

3.2.4 Estimation of the error on the calibration of stress band proportion against observed bleaching

The presence of a stress band in a single core during a known thermal stress event indicates that bleaching occurred, and stress bands have been used as a binary indicator of historical bleaching (e.g. Smithers and Woodroffe 2001; Carilli et al. 2010). Here we use stress bands to determine when bleaching occurred and quantify its severity. However, significant uncertainty exists in estimating the proportion of *Porites spp.* stress bands in the population based on cores extracted from a relatively small fraction of the population. Further, because bleaching is variable even on small spatial scales within a reef, there are non-trivial uncertainties associated with both the stress band proportion and the observed bleaching incidence. To best account for these uncertainties in calibrating the proxy, we used the Mantel-Haenszel estimator of the common odds ratio, $\hat{\psi}$ (Mantel and Haenszel 1959) (see Appendix A3 for detailed methods). To use the odds

ratio to predict bleaching incidence, a functional estimate of bleaching incidence was constructed by inverting the odds ratio:

$$p_{bi} = \left(1 + \frac{1-p_{sb}}{\hat{\psi} p_{sb}}\right)^{-1} \quad (3.2)$$

Where p_{bi} is the proportion of reef community bleached and p_{sb} is the proportion of stress bands (*sb*) observed. From the variance in both p_{sb} and $\hat{\psi}$ The associated variance of the prediction was calculated as follows:

$$Var\ p_{bi} \cong \left(\frac{\partial p_{bi}}{\partial p_{sb}}\right)^2 Var\ p_{sb} + \left(\frac{\partial p_{bi}}{\partial \hat{\psi}}\right)^2 Var\ \hat{\psi} \quad (3.3)$$

We use the variance on the predicted bleaching incidence ($Var\ p_{bi}$) to define a 2σ confidence interval for reconstructed bleaching incidence levels. The width of this confidence interval depends therefore on three things: the number of cores collected, the prevalence of stress bands among those cores, and the effectiveness of the common odds ratio at explaining the calibration data (or the quality of the fit).

3.2.5 Development and application of a percentile-based estimate of thermal stress

The NOAA Coral Reef Watch Degree Heating Week (DHW) index uses the amplitude and duration of the SST anomaly to estimate levels of thermal stress experienced by corals (Gleeson and Strong 1995) and assumes that thermally stressful conditions occur when temperatures exceed 1°C above the maximum monthly mean SST (MMM) to which corals are normally exposed. However, in the CEP, the SST regime is dominated by inter-annual variability rather than regular seasonal cycles and consequently the maximum temperature to which corals are normally exposed does not occur during the same month every year. This means that the MMM does not effectively describe the 'upper end' of temperatures in the CEP or other regions where seasonal variability is not dominant. The traditional DHW metric therefore, consistently overestimates the level of thermal stress in such regions.

To address this issue, we developed a percentile-based bleaching threshold which is independent of the timescale of SST variability and can be applied in any oceanographic environment. First, we calculated gap-filled Pathfinder SSTs from 1982-2016 for each grid cell containing the reef locations represented in the global bleaching database of Donner et al., (2017).

To establish the maximum heat to which corals are exposed during "normal" or non-extreme years, SSTs during ENSO neutral years between 1982 and 2012 (i.e., 1985-6, 1990, 1993-6, 2001, 2003-6, 2012 based on years when -1.25 < Nino 3.4 < 1.25 (Trenberth 1997)) were extracted and the site-specific distribution of weekly SSTs evaluated. A threshold percentile (e.g., 94th, 95th, 96th) was chosen to represent the high end of SSTs typically experienced by each coral community, and the SST value corresponding to that percentile at that site was substituted for the MMM +1°C threshold. We used the new threshold to calculate DHWs at each site. We repeated the exercise with different percentiles and compared the resulting DHWs to the observed bleaching levels at each site during bleaching years (Donner et al. 2017). The quality of each set of predictions was evaluated using the Gilbert Skill Score (or Equitable Threat Score, ETS) which maximizes predictive power while accounting for the increase in type 2 errors associated with lower thresholds (Fig. A3.1). A percentile of 94.4th resulted in the maximum ETS (0.68 on a scale of 0 to 1, see Appendix A3). It is important to note that this method is calibrated to maximize the predictive power of the 4 DHW alert level, and other commonly used alert levels (e.g. alert level 2 (8 DHW), under which mortality is likely) have not been at this time estimated (Liu et al. 2006).

3.2.6 Total Hotspot as an index of Cumulative Thermal Stress

The DHW Index was developed as a 3-month running forecasting metric to predict where bleaching is likely to occur. In this study, we compare the level of thermal stress experienced by the reef during each event, with the resulting bleaching severity. Thus, rather than DHW, we use the Total Hotspot (TH), which is the total number of weeks during which the site-specific thermal threshold is exceeded (Gleeson and Strong 1995). TH is calculated using the percentile-based threshold of 94.4th instead of the traditional MMM +1 threshold as follows:

$$TH_e = \sum_{w=1}^{n} H_w \tag{3.4}$$

Where TH is the Total Hotspot, for event e from the first week (w = 1) to the last week (n) during which SST exceeded the bleaching threshold. We use the TH index below to assess the sensitivity of each coral community to thermal stress.

3.3 Results

3.3.1 Stress band – bleaching calibration

Stress bands were identified in the majority of cores (with the notable exception of Kingman Reef), and only occurred in years in which SSTs were anomalously warm and TH exceeded zero (Table A3.4, Table A3.5). No stress bands occurred in years during which thermal stress was zero. For sites and years in which observational bleaching data are available, we regressed the proportion of stress bands against the observed severity of coral bleaching incidence at the same site during the same year. (Fig. 3.3). Stress bands are highly correlated with bleaching severity (r^2 = 0.945, p = 3.67e-12), consistent with Barkley and Cohen (2016) for Palau, and Barkley et al., (2018). The common odds ratio regression, used to estimate the error on the relationship between bleaching severity and stress band proportions (Methods, Eq. 3.2), was ψ = 1.11 ± 0.10 (2σ), implying a near 1 to 1 relationship (Fig. 3.3). We use this regression to predict bleaching levels at sites and during times where no observations were made. The error on these predictions is calculated using Equation 3.3 (methods) using the variance in the common odds ratio (ψ), the number of cores sampled, and the fraction of cores that exhibit stress bands. For a sample size of 15 cores, the maximum uncertainty on the estimate of bleaching severity is 28.7% (2σ), which occurs at a stress band proportion of 48.3% (Fig. 3.3 shaded region).

3.3.2 Thermal Stress Indices

In Figure 3.4, DHW and TH calculated using the traditional threshold method (i.e. 1 °C above the MMM, A-I) are compared with DHW calculated using the 94.4th percentile-based (J-Q) threshold for our study sites. In addition, we provide DHW and TH estimates for the northern Great Barrier Reef (GBR; 10.8° S and 142.9° E) (I and R), to highlight both the different levels and histories of thermal stress experienced by reefs in the CEP versus reefs in regions dominated by seasonal SST variability, and the relative change in estimated severity when the percentile-based method is applied. DHW events coincide with El Niño years at all CEP sites and their magnitude linked to size and type of El Niño event i.e., central vs. eastern Pacific El Niño (Ashok et al. 2007). Eastern Pacific events are felt most strongly at Jarvis (~160º W), whereas central Pacific events are felt most strongly in the Phoenix Islands. Further west, Maiana Island, is unaffected by eastern Pacific events instead experiencing its major thermal stress events in weak El Niño years (e.g. 2004).

At all our study locations the percentile-based bleaching threshold was higher than the MMM+1, causing lower DHW and TH estimates for each event relative to the traditional calculation. At equatorial sites, average DHW and TH for most events were substantially different. For example, DHWs derived by the percentile method was lower by an average of 6.3°C wk and 5.8°C wk at Jarvis and Kanton respectively, versus 4.5°C wk and 2.3°C wk for Dongsha and the GBR. TH decreased by 10.01 and 4.1°C, versus 2.14 and 0.88°C at the same sites. These results indicate that the traditional MMM+1 method overestimates thermal stress on central Pacific coral reefs relative to other reefs (confirming the bias observed by others, e.g. Donner 2011; Lough et al. 2018), and that the percentile method provides a non-biased method for all sites.

3.3.3 Reconstructed bleaching histories

We applied the stress band prevalence – observed bleaching incidence calibration (Fig. 3.3) to reconstruct the history and severity of bleaching at our eight central Pacific reef sites since 1982 (Fig. 3.5, Table A3.6). The young end of the reconstruction on each reef is determined by the date the most recent cores were collected (for example 2010 on Kingman, 2016 on Jarvis, 2012 on Howland and Maiana, see Table A3.3). We do not attempt to reconstruct bleaching in the Phoenix Islands in 2015 because the cores were retrieved two months prior to the peak SST, and thus may not capture the full severity of the bleaching that occurred there in 2015. Stress band counts at Jarvis Island back to 1960 are published elsewhere (Barkley et al. 2018).

Bleaching has been directly observed in the Phoenix Islands only in 2015, on Howland Island only in 2010, and no bleaching observations have been made on Maiana or Kingman, meaning our reconstructions significantly extend the bleaching database for this region across space and back in time. For all reefs, excluding Kingman, our analysis reveals a history of bleaching events, each occurring in response to El Nino-induced thermal stress. Cores collected on Kingman Reef in 2010 and 2012 revealed no stress bands, consistent with the absence of appreciable thermal stress (DHW > 4) over this time period (Fig. A3.4), and implying that Kingman Reef has never experienced significant bleaching.

3.3.4 Assessment of the thermal sensitivity of coral communities

Using the reconstructed bleaching histories (Fig. 3.5, Table A3.6) and the calculated thermal stress experienced by each reef during each bleaching event, we characterized the sensitivity of the coral community response to thermal stress (Fig. 3.6). For each site, the

relationship between thermal stress and bleaching severity follows a predictable, non-linear pattern. Because the bleaching thresholds of individual coral colonies on each reef are assumed to be normally distributed, we used a cumulative density function (CDF) to fit the data. A minimum amount of thermal stress is required to induce bleaching, therefore we used a lognormal CDF for the regression:

$$BI_j = \frac{100}{\sigma\sqrt{2\pi}} \int_0^{TH_j} \frac{e^{-(\ln(t)-\mu_i)^2/(2\sigma_i^2)}}{t} dt$$

where BI_j is coral bleaching incidence at a given Total Hotspot TH_j and μ_i and σ_i are regression parameters corresponding to mean and standard deviation of the associated normal distribution for each reef *i*. Data from Kanton, Rawaki, and Enderbury were pooled as the relationship between BI and TH was not significantly different between these reefs. For the purpose of this analysis, we excluded reconstructed BI events with greater than 35% error.

A single parameter index of the mean thermal tolerance of corals at each reef was estimated by converting μ_i to the half-point of each regression (i.e. the TH at which 50% bleaching is predicted) as follows:

$$b_{½} = e^{\mu_i}$$

Using $b_{½}$ as an index of thermal tolerance implies that Jarvis Island coral communities have the highest thermal tolerance ($b_{½}$ = 29.71 ± 1.06 SE), followed by the northern Phoenix Islands (Kanton/Enderbury/Rawaki) and that tolerances decrease westward, with Maiana Island exhibiting the lowest thermal tolerance index ($b_{½}$ = 3.04 ± 1.36 SE) of the CEP reefs studied here. We also compare the bleaching sensitivity of these CEP reefs to the GBR using spatial (Hughes et al. 2017) and temporal (Donner et al. 2017) bleaching observations versus percentile based TH estimates. The GBR data help to put the thermal tolerances of the central Pacific reefs in perspective, exhibiting an even lower thermal tolerance index than Maiana ($b_{½}$ =1.03 ± 1.04 SE).

3.4 Discussion

The occurrence of mass coral reef bleaching events associated with ocean warming has motivated efforts to better predict coral reef futures (Pandolfi et al. 2011). While some efforts are based predominantly on GCM projections of temperature (Beyer et al. 2018), others are

incorporating variable and potentially shifting thermal thresholds, as observed in nature (Coles and Jokiel 1977; Fisk and Done 1985; Rowan et al. 1997; Maynard et al. 2008; Van Woesik et al. 2012; Hughes et al. 2017). Nevertheless, characterizing the thermal tolerances of different reef communities and evaluating change over time are difficult because they require direct, repeat observations of coral communities during periods of thermal stress. Here we used skeletal stress bands to fill gaps in observational bleaching data on eight central Pacific coral reef islands since 1982. Our study builds on pioneering work by Emiliani et al. (1978) who identified stress bands in a *Montastrea* coral (now *Orbicella*), and by Hudson et al. (1976) who attributed anomalously high density bands in the same species to environmental stress. Subsequent work by Cantin and Lough (2014) construct bleaching histories from the GBR, and Carilli et al., (2009) used stress bands to evaluate effects of local stressors on bleaching incidence in the Caribbean and subsequently Barkley and Cohen (2016) showed that the proportion of stress bands reflected the severity of bleaching in the coral reef community. These observations paved the way for the use of skeletal records to provide quantitative information about reef responses to thermal stress in the absence of direct observations (DeCarlo et al. 2017; Barkley et al. 2018).

3.4.1 The stress band-bleaching relationship and a conceptual model of the mechanism

We expanded the original calibration of Barkley and Cohen (2016) using new observational bleaching data and measurements of stress band prevalence in three massive coral genera in the Pacific and Caribbean These results show that the relationship applies beyond just Pacific reefs and Pacific *Porites* corals, and leads naturally to the question: why is the prevalence of stress bands in massive corals so well correlated with the incidence of bleaching across the community of mixed coral taxa? We propose that within each population of massive corals, a range of thermal thresholds exist (Fig. 3.6B). When thermal stress is low, only the most sensitive massive corals in the population bleach, and they archive the bleaching as stress bands in their skeletons. Only the more sensitive corals of other species on the same reef also bleach. As thermal stress increases, massive corals with higher and higher thermal thresholds succumb to bleaching, as do the rest of the species in the coral community (Fig. 3.6C). Under this model, long-lived massive corals represent the full range of bleaching thresholds within their communities of mixed species on the reef. The Caribbean corals included in the calibration (Fig. 3.3) behave as the Pacific *Porites spp.* do, implying that the long-lived massive coral genera play a similar role on Caribbean reefs. While we attempted to avoid colony size bias during field sampling, we recognize that

bleaching reconstructions based on stress band prevalence do have the potential to underestimate the severity of bleaching during events in which mortality in the massive corals was high. If a substantial portion of massive colonies died, and were not represented in the core samples, the relative proportion of colonies that have stress bands would be lower, and underestimate the severity of the event. We can assume such a bias is minimal during most bleaching events as *Porites* tends to have lower mortality rates than other corals and because our record is relatively short (33 years). However, in applying this calibration to longer records, the considering and accounting for the compounding of potential bias is necessary.

3.4.2 Generation of bleaching histories

Using the new calibration, we generated bleaching histories for eight central Pacific reefs back through 1982. With the exception of Kingman Reef, each island experienced multiple episodes of thermal stress sufficient to cause coral bleaching (DHW>4) over this time period and our historical bleaching reconstruction reveals that each of the coral communities responded in a manner consistent with the degree of thermal stress imposed. Critically, seven of the reefs have experienced multiple severe (>30% bleaching) episodes within the last 4 decades, most of which had not been observed. For example, Howland Island experienced four substantive bleaching episodes in just 20 years, between 1990 and 2010. The Phoenix Islands – Kanton, Enderbury, Rawaki and Nikumaroro – all experienced multiple episodes of bleaching prior to 2015, but 2002/2003 (which coincided with the central Pacific El Niño) appears to have been the most significant (the upper bound of uncertainty in the reconstructed bleaching levels reach 100%). While direct observations did not occur in 2002/2003, our results are consistent with those of ecosurveys conducted several years later that recorded mass mortality of corals across the region (Obura and Mangubhai 2011).

3.4.3 Characterization of thermal sensitivity

Seven of the Pacific reefs studied experienced multiple episodes of bleaching at different levels of severity, and we were therefore able to characterize the reef-specific relationship between thermal stress and bleaching response. In these cases, we use Total Hotspot (TH) as a measure of the cumulative thermal stress experienced by each coral community during each event. In the absence of quantitative stress band data, we used observational bleaching data to construct a comparable response curve for the northern GBR, which reveals exceptionally low thermal

thresholds of GBR coral communities relative to those in the central Pacific. This observation raises the question: what are the biological and environmental factors underlying the relative thermal tolerance of the central Pacific reef assemblages?

3.4.4 Mechanisms of increased thermal tolerance

We established a thermal tolerance index ($b_{½}$) and evaluated the relationship between $b_{½}$ and the reef thermal history, water column nutrient concentrations, energetic status of the corals, presence or absence of upwelling, and cloud cover-based differences in irradiance at each of our study cites. For thermal history, we calculated the variance, range, median, and mean SSTs, and the median and mean of the TH per event for each reef over the satellite period. The best correlation with $b_{½}$ was the mean TH (OLS, $p < 0.001$). Thermal tolerance was significantly higher on reefs experiencing the most severe thermal stress events on average i.e., highest mean TH (Jarvis, Kanton, Rawaki, Enderbury), suggesting that thermal thresholds are likely linked to the history of thermal stress exposure (Fig. 3.7A). While our data do not allow for a mechanistic understanding of this relationship, the link between thermal history and coral thermal tolerance has been observed previously (e.g. Safaie et al. 2018). Indeed, the thermal threshold value used in the DHW calculation is based on the assumption that corals living at higher temperatures also bleach at higher temperatures, an observation made in field and laboratory based studies (Coles and Jokiel 1977; Van Woesik et al. 2012; Fine et al. 2013). Further, evidence suggests that corals in more variable SST environments, whether diurnal or seasonal or inter-annual time scales, have higher bleaching thresholds than corals living in more thermally-homogenous environments (McClanahan et al. 2007; Oliver and Palumbi 2011; Carilli et al. 2012; Safaie et al. 2018).

Critically, our data imply thermal tolerance on a community-scale, based on the relationship between stress band proportion in massive colonies and community-level bleaching incidence, and it is important that the drivers of community-level thermal tolerance may be different from those underlying resistance of individual colonies. Indeed, communities may develop higher thermal thresholds over time as repeated bleaching events kill more sensitive individuals and species, or selecting thermally-tolerant larvae during recruitment, and shift community composition towards more thermally tolerant taxa (Coles and Brown 2003; Golbuu et al. 2007; Maynard et al. 2008; Van Woesik et al. 2011; Fine et al. 2013; Barkley et al. 2018).

We also examined the potential role of water column nutrients and host energetic status in promoting thermal tolerance. High nutrient concentrations are thought to lower the bleaching thresholds of corals (Wooldridge 2009; D'Angelo and Wiedenmann 2014) so we compared average dissolved inorganic nutrient (DIN) concentrations (NO_3 + NO_2) during ENSO neutral conditions (Table A3.7) with the derived thermal tolerance of each reef community. We found a significant positive correlation (OLS, $p < 0.001$) between nutrient levels and thermal tolerance, inconsistent with prior hypotheses and laboratory experiments (Fig. 3.7B). While this evidence may suggest a role of nutrient uptake or heterotrophy in thermal tolerance, it is yet unclear whether the relationship we observe is direct. TH, nutrient concentrations and tissue thickness all covary across these sites and more testing is required to deconvolve these different factors.

Evidence exists that heterotrophic feeding can alleviate bleaching-induced starvation by supplementing the coral's energy budget (Grottoli et al. 2006; Rodrigues and Grottoli 2006; Hoogenboom et al. 2012). We used tissue thickness as a proxy for biomass and energetic reserve (Carilli et al. 2012) and found that average tissue thickness of cores collected during non-stressful (i.e. ENSO neutral) conditions was correlated with $b_{1/2}$ but the correlation was less significant (OLS, $p = 0.083$) (Fig. 3.7C). This result suggests that energetic reserve may not be playing a role in establishing thermal tolerance, and that energetically replete corals still bleach. However, it is likely that energetic status plays an important role in the survival of corals through bleaching, and in the post-bleaching recovery.

We also investigated the potential for cloud cover to mitigate the impact of thermal stress on coral bleaching using outgoing longwave radiation (OLR) as a proxy (Fig. A3.4A) for cloud cover (Kessler and Kleeman 2000). To compare the relative amount of total cloud cover observed at each site with the total thermal stress, the standardized cloudiness was integrated over each thermal stress episode (TC) and regressed against TH (Fig. A3.4B). Our analysis reveals that total cloud cover at our study sites is indeed elevated during thermal stress episodes but that cloudiness per °C·Week (i.e. the slope of the TH – TC regression) is highest where thermal tolerances are lowest (e.g. Maiana, the GBR). This suggests that differences in cloud cover cannot explain the differences in thermal tolerance observed in this study.

We conclude that the relatively high thermal tolerances observed on Jarvis and the northern Phoenix Islands most likely have arisen from adaptation over centuries or millennia of exposure

to repeated episodes of thermal stress driven by El Niño. Nevertheless, while coral reefs in the CEP have elevated thermal thresholds for bleaching relative to other reefs, they also experienced significantly higher levels of thermal stress than other reefs, and our bleaching reconstructions indicate that CEP coral communities bleach predictably in response to thermal stress. For this reason, elevated thermal thresholds of CEP coral communities are likely only one, albeit important, component of the strategy for coral reef survival in the dynamic, oft-times hostile environment of the CEP. New studies will shed light on questions about how the CEP coral communities survive the repetitive bleaching events they endure. This study shows that thermal tolerances of coral communities can be constrained using proxy data accrued across space and through time, in the absence of direct observations. Expansion of this approach to regions outside of the CEP are needed to evaluate potential limitations of the proxy as identified here, and to devise approaches for evaluating shifting thermal thresholds of coral reef communities using stress band data.

3.5 Figures

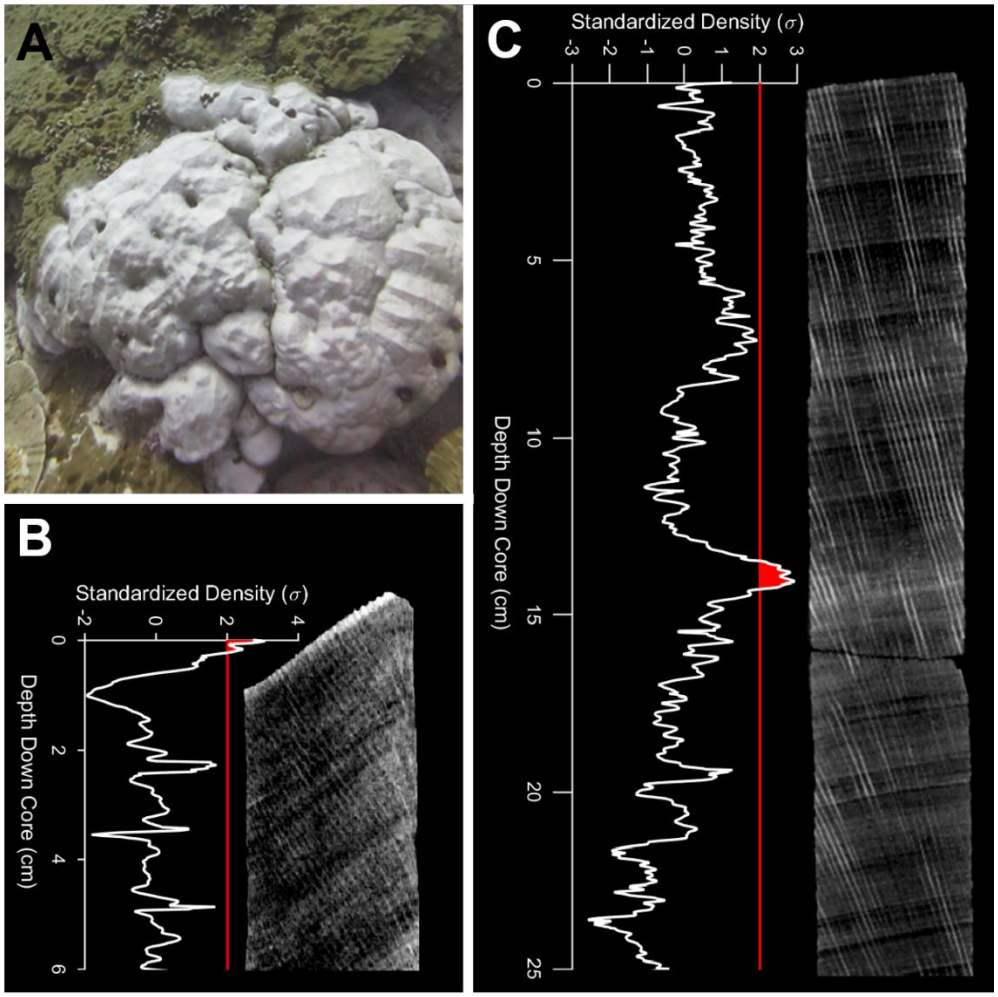

Figure 3.1: Incorporation of signatures of bleaching into a coral skeleton. **A:** *Porites lobata* colony #1032 (Phoenix Islands) bleached in 2015. B: The CT image of a core removed from the bleached colony revealed a high-density stress band at the top of the core. The density anomaly associated with the stress band is quantified using an automated image analysis routine written in Matlab (CoralCT, DeCarlo and Cohen 2016). Here, the stress band is identified as a 2σ excursion above the mean skeletal density (red shading). C: If the coral recovers and continues to grow, the stress band is incorporated into the skeleton and serves as a record of the bleaching event.

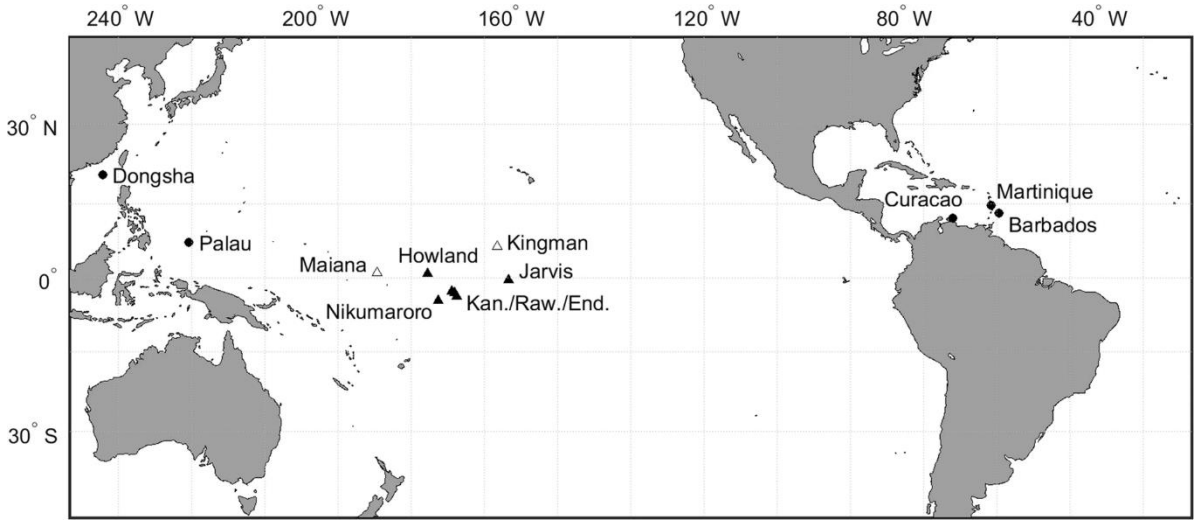

Figure 3.2: Map of reefs from which coral cores were collected and analyzed in this study. Black diamonds represent reef sites included in the calibration and for which thermal tolerance curves were constructed. Black circles are reefs included in the calibration but for which thermal tolerance curves were not constructed because they experienced fewer than three bleaching events over the study period (1982-2015). White diamonds are reefs for which thermal histories were reconstructed but were not included in the calibration due to a lack of observational bleaching data. Kingman Reef is shown by a white circle. No DHWs>4 exist at this site, no bleaching observations have been made, andno stress bands were evident in the cores.

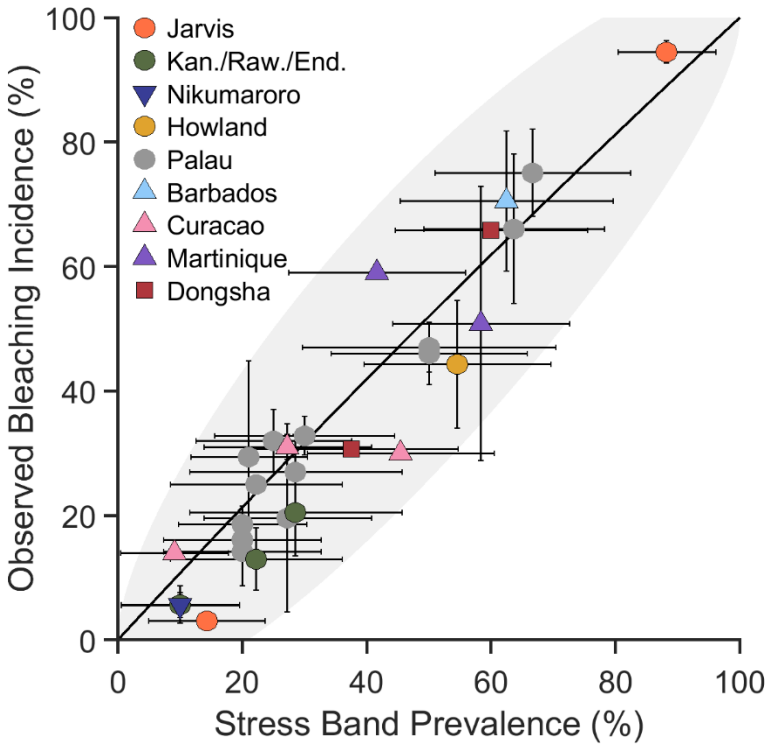

Figure 3.3: Stress band prevalence in three massive Pacific and Caribbean coral genera versus observed bleaching incidence at each site for the matching time periods. Vertical error bars show ±1 standard deviation on the observational bleaching data and horizontal error bars represent the standard error of a proportion of stress bands in the population of massive corals. The magnitude of the error is a function of the sample size (n = 10 to n = 38). The regression was computed using the Mantel-Haenszel common odds ratio. Shaded region shows 95% prediction interval in predicting bleaching incidence from a sample of n = 15 cores.

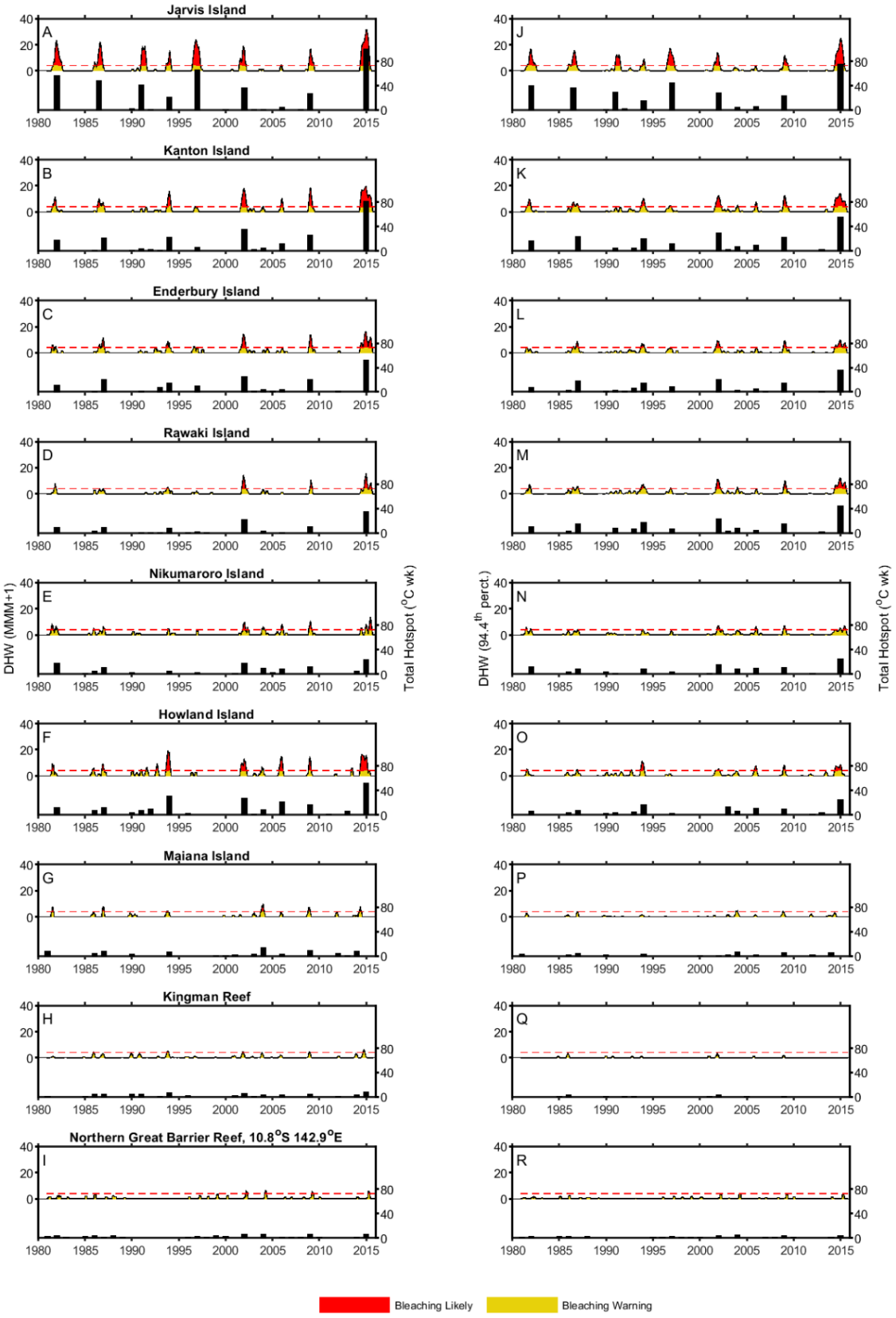
Jarvis Island
Kanton Island
Enderbury Island
Rawaki Island
Nikumaroro Island
Howland Island
Maiana Island
Kingman Reef
Northern Great Barrier Reef, 10.8°S 142.9°E
A
B
C
D
E
F
G
H
I
J
K
L
M
N
O
P
Q
R
DHW (MMM+1)
DHW (94.4th perct.)
Total Hotspot (°C wk)
Bleaching Likely
Bleaching Warning

Figure 3.4: Degree Heating Weeks (line curves) and Total Hotspot (bars) 1982-2015 calculated using the traditional bleaching threshold (NOAA Coral Reef Watch, MMM+1) (left panel) and the 94.4th percentile method (right panel). DHW events at locations with strong seasonal temperature cycles (e.g. GBR) are of similar magnitude by both methods, but are less severe at equatorial locations when calculated using the 94.4th percentile method. Pathfinder v5.3 4-km daily resolution dataset (nighttime only) was supplemented with the mean-adjusted IGOSSv2 weekly 1° x 1° gridded data product.

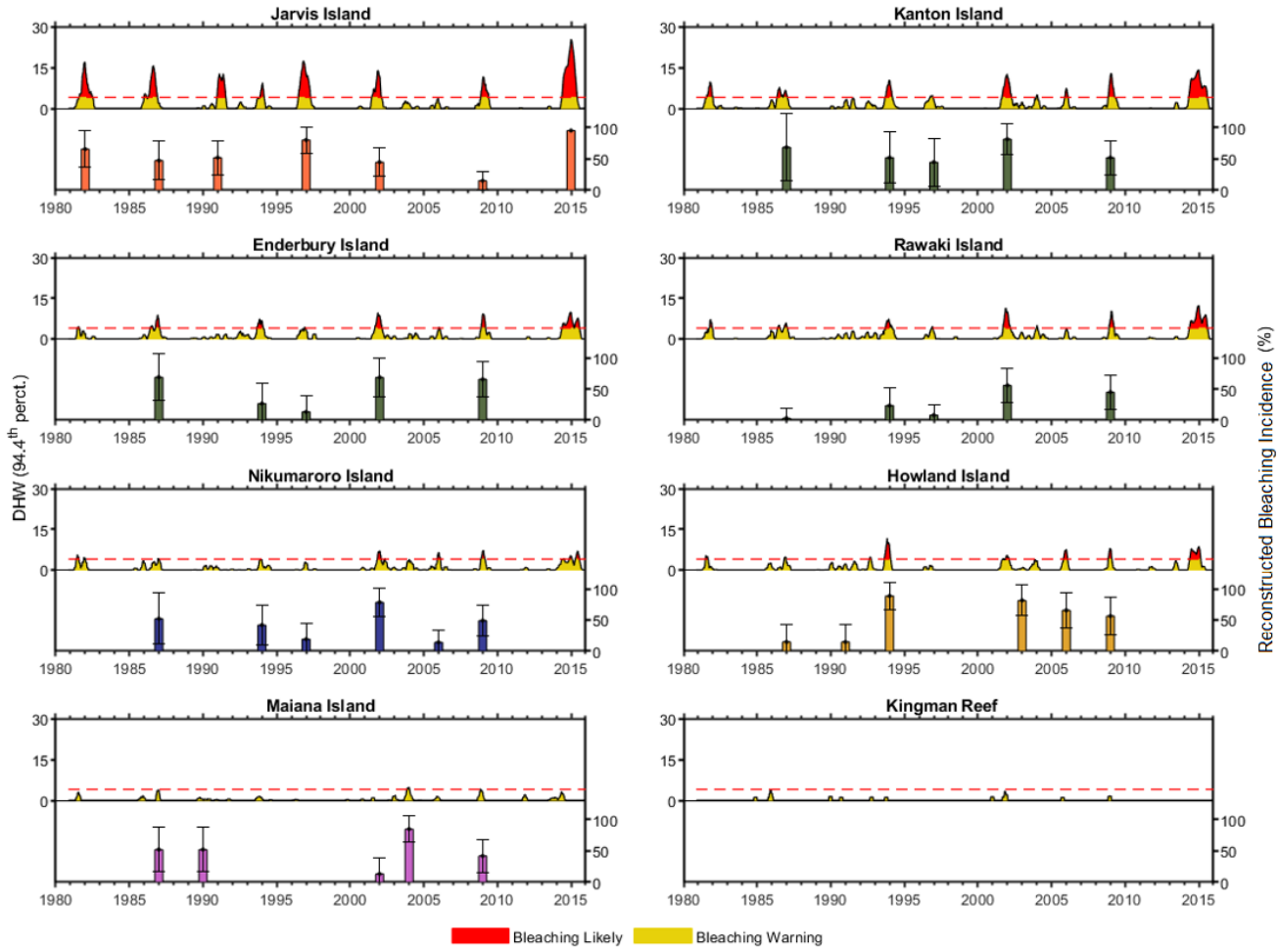

Figure 3.5: A history of bleaching events and their severity reconstructed from stress band records in populations of massive corals on each reef, shown with the reef-specific history of thermal stress represented by Degree heating Weeks calculated using the percentile method. Broken red line indicates 4 °C-weeks when bleaching is likely to occur. Error bars denote 2σ based on the variance of the bleaching reconstructions (Eq. 3.3).

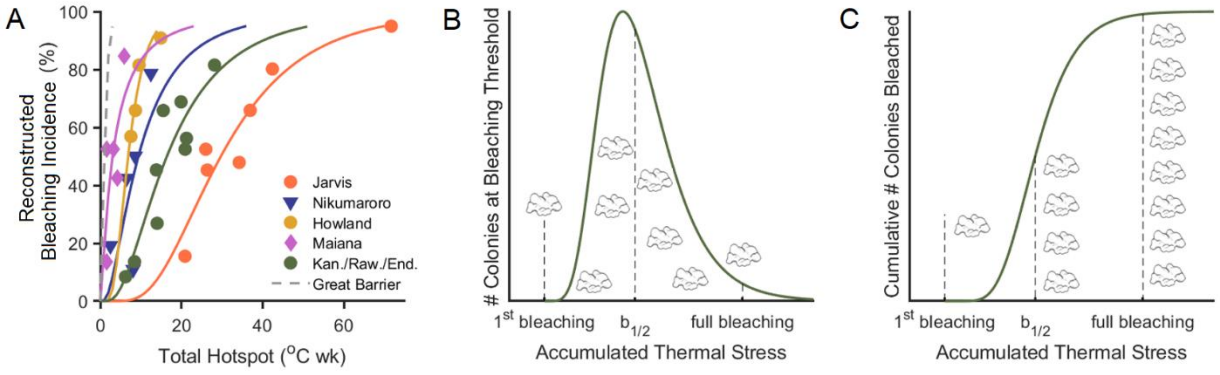

Figure 3.6A: The site-specific relationship between thermal stress (Total Hotspot) and percent bleaching incidence generated from bleaching reconstructions and DHW calculations in Fig. 3.5. Great Barrier Reef data (grey) are observed bleaching severity recorded during the 2002/2003 and 2015/2016 bleaching events (Donner et al. 2017; Hughes et al. 2017). B and C present a conceptual model to explain the mechanism by which massive corals record community bleaching incidence. **B:** bleaching thresholds of massive colonies in a population follow a lognormal distribution. **C:** The cumulative number of massive colonies bleached, as a function of thermal stress then follow a lognormal cdf. We use $b_{½}$, or the accumulated thermal stress (TH) at which the regession line predicts 50% bleaching as an index of thermal tolerance of the reef community.

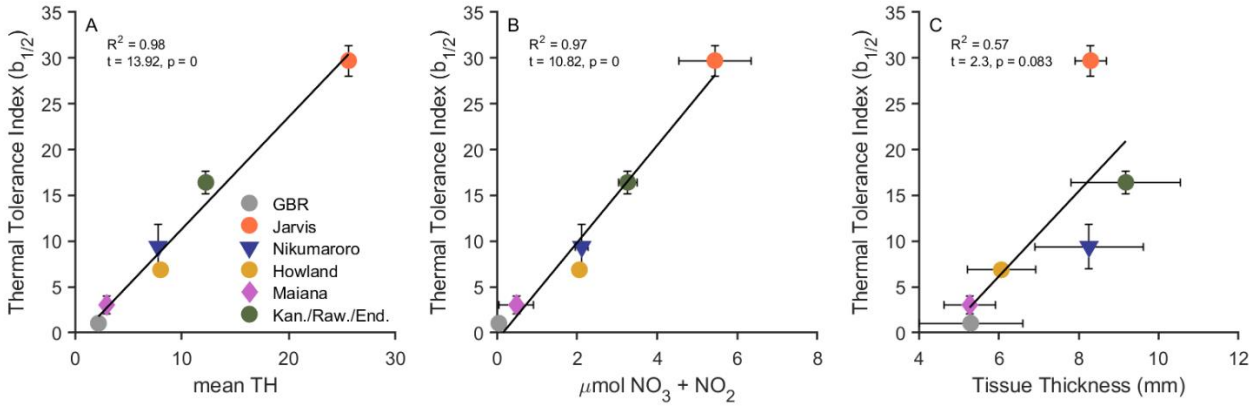

Figure 3.7: Thermal tolerance index ($b_{½}$) as a function of **A:** mean total hotspot over the instrumental period, **B:** nitrate + nitrite concentrations during non-stressful conditions (Table A3.7), and **C:** coral tissue thickness during non-stressful conditions (Table A3.8). Thermal tolerance is significantly related to thermal history (mean TH) (linear regression), consistent with evidence that corals experiencing regular, large thermal stress events are more resistant to stress than those experiencing relatively weaker events.

3.6 References

Alpert AE, Cohen AL, Oppo DW, Decarlo TM, Gove JM, Young CW (2016) Comparison of equatorial Pacific sea surface temperature variability and trends with Sr/Ca records from multiple corals. Paleoceanography 31:252–265

Ashok K, Behera SK, Rao SA, Weng H (2007) El Nino Modoki and its possible teleconnection. J Geophys Res 112:1–27

Barkley HC, Cohen AL (2016) Skeletal records of community-level bleaching in Porites corals from Palau. Coral Reefs 35:1407–1417

Barkley HC, Cohen AL, Brainard RE, Mollica NR, Rivera HE, Drenkard EJ, Young CW, Vargas-Ángel B, Lohmann GP, Decarlo TM, Alpert AE, Lino KC, Oliver TA, Pietro KR, Luu VH (2018) Repeat bleaching of a central Pacific coral reef over the past six decades (1960-2016). Nat Biol Commun

Barkley HC, Cohen AL, Golbuu Y, Starczak VR, Decarlo TM, Shamberger KEF (2015) Changes in coral reef communities across a natural gradient in seawater pH. Sci Adv 1–7

Barnes DJ, Lough JM (1992) Systematic variations in the depth of skeleton occupied by coral tissue in massive colonies of Porites from the Great Barrier Reef. J Exp Mar Bio Ecol 159:113–128

Beyer HL, Kennedy E V., Beger M, Chen CA, Cinner JE, Darling ES, Eakin CM, Gates RD, Heron SF, Knowlton N, Obura DO, Palumbi SR, Possingham HP, Puotinen M, Runting RK, Skirving WJ, Spalding M, Wilson KA, Wood S, Veron JE, Hoegh-Guldberg O (2018) Risk-sensitive planning for conserving coral reefs under rapid climate change. Conserv Lett e12587

Cantin NE, Cohen AL, Karnauskas KB, Tarrant AM, McCorkle DC (2010) Ocean Warming Slows Coral Growth in the Central Red Sea. 329:322–325

Cantin NE, Lough JM (2014) Surviving coral bleaching events: Porites growth anomalies on the great barrier reef. PLoS One 9:

Carilli J, Donner SD, Hartmann AC (2012) Historical temperature variability affects coral response to heat stress. PLoS One 7:1–9

Carilli JE, Norris RD, Black B, Walsh SM, Mcfield M (2010) Century-scale records of coral growth rates indicate that local stressors reduce coral thermal tolerance threshold. Glob Chang Biol 16:1247–1257

Carilli JE, Norris RD, Black BA, Walsh SM, McField M (2009) Local stressors reduce coral resilience to bleaching. PLoS One 4:1–5

Casey KS, Brandon TB, Cornillon P, Evans R (2010) The Past, Present, and Future of the AVHRR Pathfinder SST Program. Oceanogr from Sp Revisit 1–375

Coles SL, Brown BE (2003) Coral bleaching-capacity for acclimatization and adaptation. Adv Mar Biol 46:183–223

Coles SL, Jokiel PL (1977) Effects of temperature on photosynthesis and respiration in hermatypic

corals. Mar Biol 43:209–216

D'Angelo C, Wiedenmann J (2014) Impacts of nutrient enrichment on coral reefs: New perspectives and implications for coastal management and reef survival. Curr Opin Environ Sustain 7:82–93

DeCarlo TM, Cohen AL (2016) coralCT: software tool to analyze computerized tomography (CT) scans of coral skeletal cores for calcification and bioerosion rates.

DeCarlo TM, Cohen AL (2017) Dissepiments, density bands, and signatures of thermal stress in Porites skeletons. Coral Reefs 1–13

DeCarlo TM, Cohen AL, Barkley HC, Cobban Q, Young C, Shamberger KE, Brainard RE, Golbuu Y (2015) Coral macrobioerosion is accelerated by ocean acidification and nutrients. Geology 43:7–10

DeCarlo TM, Cohen AL, Wong GTF, Davis KA, Lohmann P, Soong K (2017) Mass coral mortality under local amplification of 2 °C ocean warming. Sci Rep 7:44586

Donner S (2011) An evaluation of the effect of recent temperature variability on\nthe prediction of coral. Ecol Appl 21:1718–1730

Donner SD (2009) Coping with commitment: Projected thermal stress on coral reefs under different future scenarios. PLoS One 4:

Donner SD, Rickbeil GJM, Heron SF (2017) A new, high-resolution global mass coral bleaching database. PLoS One 12:1–17

Eakin CM, Morgan JA, Heron SF, Smith TB, Liu G, Alvarez-Filip L, Baca B, Bartels E, Bastidas C, Bouchon C, Brandt M, Bruckner AW, Bunkley-Williams L, Cameron A, Causey BD, Chiappone M, Christensen TRL, Crabbe MJC, Day O, de la Guardia E, Díaz-Pulido G, DiResta D, Gil-Agudelo DL, Gilliam DS, Ginsburg RN, Gore S, Guzmán HM, Hendee JC, Hernández-Delgado EA, Husain E, Jeffrey CFG, Jones RJ, Jordán-Dahlgren E, Kaufman LS, Kline DI, Kramer PA, Lang JC, Lirman D, Mallela J, Manfrino C, Maréchal JP, Marks K, Mihaly J, Miller WJ, Mueller EM, Muller EM, Toro CAO, Oxenford HA, Ponce-Taylor D, Quinn N, Ritchie KB, Rodríguez S, Ramírez AR, Romano S, Samhouri JF, Sánchez JA, Schmahl GP, Shank B V., Skirving WJ, Steiner SCC, Villamizar E, Walsh SM, Walter C, Weil E, Williams EH, Roberson KW, Yusuf Y (2010) Caribbean corals in crisis: Record thermal stress, bleaching, and mortality in 2005. PLoS One 5:

Emiliani C, Hudson JH, Shinn EA, George RY (1978) Oxygen and Carbon Isotopic Growth Record in a Reef Coral from the Florida Keys and a Deep-Sea Coral from Blake Plateau. Science (80-) 627–628

Estep A, Sandin S, Vermeij M (2017) The State of Curaçao's Coral Reefs.

Fine M, Gildor H, Genin A (2013) A coral reef refuge in the Red Sea. Glob Chang Biol 19:3640–3647

Fisk DA, Done TJ (1985) Taxonomic and Bathymetric Patterns of Bleaching in Corals, Myrmidon Reef (Queensland). Proc Fifth Int Coral Reef Congr Tahiti 6:149–154

Frieler K, Meinshausen M, Golly A, Mengel M, Lebek K, Donner SD, Hoegh-Guldberg O (2012) Limiting global warming to 2 °C is unlikely to save most coral reefs. Nat Clim Chang 3:165–170

Gleeson MW, Strong AE (1995) Applying MCSST to coral reef bleaching. Adv Sp Res 16:151–154

Golbuu Y, Victor S, Penland L, Idip D, Emaurois C, Okaji K, Yukihira H, Iwase A, Van Woesik R (2007) Palau's coral reefs show differential habitat recovery following the 1998-bleaching event. Coral Reefs 26:319–332

Grottoli G, Rodrigues LJ, Palardy JE (2006) Heterotrophic plasticity and resilience in bleached corals. Nature 440:10–13

Hendy EJ, Lough JM, Gagan MK (2003) Historical mortality in massive Porites from the central Great Barrier Reef, Australia: Evidence for past environmental stress? Coral Reefs 22:207–215

Heron SF, Liu G, Eakin CM, Skirving WJ, Muller-Karger FE, Vera-Rodriguez M, de la Cour JL, Burgess TFR, Strong AE, Geiger EF, Guild LS, Lynds S (2015) NOAA Technical Report NESDIS 145 Climatology Development for NOAA Coral Reef Watch ' s 5-km Product Suite. 30

Hoegh-Guldberg O, Smith GJ (1989) The effect of sudden changes in temperature, light and salinity on the population density and export of zooxanthellae from the reef corals *Stylophora pistillata* Esper and *Seriatopora hystrix* Dana. J Exp Mar Bio Ecol 129:279–303

Hoogenboom MO, Campbell DA, Beraud E, DeZeeuw K, Ferrier-Pagès C (2012) Effects of light, food availability and temperature stress on the function of photosystem II and photosystem I of coral symbionts. PLoS One 7:

van Hooidonk R, Huber M (2009) Quantifying the quality of coral bleaching predictions. Coral Reefs 28:579–587

van Hooidonk R, Maynard J, Tamelander J, Gove J, Ahmadia G, Raymundo L, Williams G, Heron SF, Planes S (2016) Local-scale projections of coral reef futures and implications of the Paris Agreement. Sci Rep 6:39666

Hudson JH, Shinn EA, Halley RB, Lidz B (1976) Sclerochronology: A tool for interpreting past environments. Geology 4:361–364

Hughes TP, Anderson KD, Connolly SR, Heron SF, Kerry JT, Lough JM, Baird AH, Baum JK, Berumen ML, Bridge TC, Claar DC (2018) Spatial and temporal patterns of mass bleaching of corals in the Anthropocene. Science (80-) 359:80–83

Hughes TP, Kerry JT, Álvarez-Noriega M, Álvarez-Romero JG, Anderson KD, Baird AH, Babcock RC, Beger M, Bellwood DR, Berkelmans R, Bridge TC, Butler IR, Byrne M, Cantin NE, Comeau S, Connolly SR, Cumming GS, Dalton SJ, Diaz-Pulido G, Eakin CM, Figueira WF, Gilmour JP, Harrison HB, Heron SF, Hoey AS, Hobbs J-PA, Hoogenboom MO, Kennedy E V., Kuo C, Lough JM, Lowe RJ, Liu G, McCulloch MT, Malcolm HA, McWilliam MJ, Pandolfi JM, Pears RJ, Pratchett MS, Schoepf V, Simpson T, Skirving WJ, Sommer B, Torda G, Wachenfeld DR, Willis BL, Wilson SK (2017) Global warming and

recurrent mass bleaching of corals. Nature 543:373–377

IPCC AR5 (2014) Climate Change 2014: Synthesis Report.

Kessler WS, Kleeman R (2000) Rectification of the Madden-Julian Oscillation into the ENSO cycle. J Clim 13:3560–3575

Liu G, Strong AE, Skirving WJ, Arzayus F (2006) Overview of NOAA Coral Reef Watch Program's Near-Real- Time Satellite Global Coral Bleaching Monitoring Activities. Proc 10th Int Coral Reef Symp 1783–1793

Logan CA, Dunne JP, Eakin CM, Donner SD (2014) Incorporating adaptive responses into future projections of coral bleaching. Glob Chang Biol 20:125–139

Lough JM, Anderson KD, Hughes TP (2018) Increasing thermal stress for tropical coral reefs : 1871 – 2017. Sci Rep 1–8

Mallela J, Hetzinger S, Halfar J (2015) Thermal stress markers in Colpophyllia natans provide an archive of site-specific bleaching events. Coral Reefs 35:181–186

Mangubhai S, Rotjan R, de Villiers S, Braun C, Carilli J, Cavin J, Cohen A, Coker D, Cook C, Drenkard L, Gawne P, Harper S, Koethen J, Lasley R, Nand Y, Payet S, Rivera H, Sandin S, Kiareti A, Thorrold S, Young CC, Zgliczynski B (2015) Phoenix Islands Protected Area 2015 Expedition Report.

Mantel N, Haenszel W (1959) Issue Cover Volume 22 Issue 4 April 1959 < Previous Next > Statistical Aspects of the Analysis of Data From Retrospective Studies of Disease. J Natl Cancer Inst 22:719–748

Matson EG (2011) Core Plugs. Encycl Mod Coral Reefs 294–296

Maynard JA, Anthony KRN, Marshall PA, Masiri I (2008) Major bleaching events can lead to increased thermal tolerance in corals. Mar Biol 155:173–182

McClanahan TR, Ateweberhan M, Muhando C, Maina J, Mohammed SM (2007) Climate change and spatio-temporal variation in seawater temperature effects on coral bleaching and mortality in East Africa. Ecol Monogr 77:503–525

Obura D, Mangubhai S (2011) Coral mortality associated with thermal fluctuations in the Phoenix Islands, 2002-2005. Coral Reefs 30:607–619

Oliver TA, Palumbi SR (2011) Do fluctuating temperature environments elevate coral thermal tolerance? Coral Reefs 30:429–440

Pandolfi JM, Connolly SR, Marshall DJ, Cohen AL (2011) Projecting Coral Reef Futures Under Global Warming and Ocean Acidification. Science (80-) 333:418–422

Pratchett M, Munday P, Wilson S, Graham N, Cinner J, Bellwood D, Jones G, Polunin N, Mcclanahan T (2008) Effects Of Climate-Induced Coral Bleaching On Coral-Reef Fishes - Ecological And Economic Consequences.

Reynolds RW, Rayner NA, Smith TM, Stokes DC, Wang W (2002) An Improved In Situ and Satellite SST Analysis for Climate. 15:1609–1625

Rodrigues LJ, Grottoli AG (2006) Calcification rate and the stable carbon, oxygen, and nitrogen isotopes in the skeleton, host tissue, and zooxanthellae of bleached and recovering Hawaiian corals. Geochim Cosmochim Acta 70:2781–2789

Rowan R, Knowlton N, Baker A, Jara J (1997) Landscape ecology of algal symbionts creates variation in episodes of coral bleaching. Nature 388:265–9

Safaie A, Silbiger NJ, McClanahan TR, Pawlak G, Barshis DJ, Hench JL, Rogers JS, Williams GJ, Davis KA (2018) High frequency temperature variability reduces the risk of coral bleaching. Nat Commun 9:1–12

Smithers SG, Woodroffe CD (2001) Coral microatolls and 20th century sea level in the eastern Indian Ocean. Earth Planet Sci Lett 191:173–184

Trenberth KE (1997) The Definition of El Nino. Am Meteorol Soc

Vargas-Ángel B, Looney EE, Vetter OJ, Coccagna EF (2011) Severe, widespread El Niño-associated coral bleaching in the US Phoenix Islands. Bull Mar Sci 87:623–638

Wilkinson C (2008) Status of Coral Reefs of the World: Executive Summary. Glob Coral Reef Monit Netw 5–28

Van Woesik R, Houk P, Isechal AL, Idechong JW, Victor S, Golbuu Y (2012) Climate-change refugia in the sheltered bays of Palau: Analogs of future reefs. Ecol Evol 2:2474–2484

Van Woesik R, Sakai K, Ganase A, Loya Y (2011) Revisiting the winners and the losers a decade after coral bleaching. Mar Ecol Prog Ser 434:67–76

Wooldridge SA (2009) Water quality and coral bleaching thresholds: Formalising the linkage for the inshore reefs of the Great Barrier Reef, Australia. Mar Pollut Bull 58:745–751

Chapter 4 – Reconstructing Monthly SST Using LA-ICPMS on *Porites* Corals

Nathaniel R. Mollica, Anne L. Cohen, Forrest Horton

4.1. Introduction

Seasonal oscillations are the primary mode of climate variability in the Earth's oceans. Sub-annual changes in sea surface temperature (SST) drive marine species migrations, supply nutrients to the mixed layer, and constrain the habitat distributions of sessile marine organisms. Furthermore, observations (Schubert et al. 2004; Kosaka and Xie 2013) and coupled general circulation models (GCMs) (Seager and Vecchi 2010) indicate that seasonal temperatures in key ocean regions drive global variability in air temperature, ocean temperature, wind velocity, and precipitation. One key region is the central equatorial Pacific (CEP) – home to perhaps the most important climate phenomenon in the world oceans, the El Nino Southern Oscillation (ENSO). These coupled oscillations of SST and air pressure from east to west across the equatorial Pacific have global impacts on climate, including droughts, monsoons, and tropical cyclones. Climate scientists have long indexed ENSO by variations in SST in a region of the CEP known as the Nino 3.4 (5°N–5°S, 120°W–170°W). Problematically, however, SST observations are spatially inconsistent prior to the satellite era and increasingly sparse back through time. A more complete record of SST in the CEP and elsewhere is critical for understanding historical climate dynamics and predicting future changes to the global climate system. In this paper, we use data obtained from CEP corals to demonstrate that monthly SST reconstructions can be recovered using the Sr-U paleo proxy.

4.1.1 Inconsistencies among model and observational data products in the CEP

Data coverage in the Niño 3.4 prior to the satellite era is notoriously sparse (Fig. 4.1B–D). For example, almost no measurements were made in December 1890 (Fig. 4.1B) and large regions

remained unsampled into December 1970 (Fig. 4.1C). Consequently, the average error on uninterpolated SST estimates in the Niño 3.4 prior to 1982 is ± 2 °C (Fig. 4.1E). This is well within the magnitude of the expected SST warming response to anthropogenic forcing and all but the strongest ENSO events of the last century. Changes in observational techniques such as bucket versus engine intake temperatures and differences in the statistical methodologies used to interpolate the SST field from sparse inputs (Kaplan et al. 1998; Deser et al. 2010) exacerbate uncertainties in 20th century SST records in this critical region. Such data products that augment and interpolate these sparse measurements via statistical methods have made significant progress towards mitigating both measurement error and spatial gaps, but are ultimately limited by data quality and spatial resolution.

Existing SST records are insufficient for validating climate model simulations of 20th century Pacific SST. For example, in a recent analysis of 41 CMIP5 climate models (83 simulations), SST across the central-eastern equatorial Pacific increased over the 20th century (1900–2013 AD) in response to anthropogenic forcing. In 63% of the simulations, the east-west SST gradient weakened over this time period due to a weakening Walker circulation. However, these results are contrary to the mean trends in 5 observational datasets, which suggests the central and eastern Pacific cooled over this time period, while the western Pacific warmed, strengthening the east-west SST gradient (Coats and Karnauskas 2017; Seager et al. 2019). Such discrepancies between models and observational data either suggest that (a) current climate models are not capturing the response of the tropical Pacific to anthropogenic forcing or (b) that the observational record in the early 20th century is too sparse to accurately capture SST on the relevant spatial and temporal scales. Our inability to distinguish between these two scenarios has serious implications for our ability to accurately project future climate. Massive corals growing on coral reefs scattered across the equatorial Pacific have the potential to fill gaps in the observational record and thereby shed light on this conundrum with continuous, monthly-resolved records of proxy SST spanning the anthropogenic era.

4.1.2 Coral proxy records

Corals embed information about their oceanic environment in their skeletons as they grow, and their annual density bands and lunar dissepiments provide internal chronometers that enable

reconstructions with monthly resolution. Despite the availability of coral material within the Niño 3.4 region, however, few coral-based proxy records exist and just four extend further back in time than the mid-1900's (Fig. 4.2A). Two of these longer records are based on coral $\delta^{18}O$ ratios (Fig. 4.2A, B purple squares) (Evans et al. 1999; Cobb et al. 2003), which reflect a combination of seawater temperature and seawater $\delta^{18}O$ and thus have not been interpreted solely in terms of SST.

Two of the records are based on skeletal Sr/Ca ratios (Fig. 4.2A,B, green circles) (Nurhati et al. 2009, 2011; Thompson et al. 2015), which can be influenced by vital effects associated with the coral biomineralization process (de Villiers et al. 1994; Allison et al. 2001; Cohen et al. 2002; Gaetani and Cohen 2006). Although coral Sr/Ca often varies seasonally with SST and some Sr/Ca records capture SST variability and trends, results from this proxy have been inconsistent, lowering confidence in the interpretation of Sr/Ca-based SST records during the pre-satellite era.

Challenges associated with interpreting coral Sr/Ca records from the Niño 3.4 region are highlighted in Figures 4.3 and 4.4. In Figure 4.3, two long Sr/Ca records are compared with each other and with observational SSTs over the corresponding time period. One Sr/Ca record originates from Jarvis Island located in the bullseye of El Niño's impact on SST (0.37°S, 160.00°W) (Fig. 4.3B, blue) (Thompson et al. 2015). The other Sr/Ca record is from Palmyra Atoll (5.87°N, 162.08°W) (Fig. 4.3B, red) (Nurhati et al. 2011). Both Sr/Ca and SST records are detrended and presented as anomalies relative to the climatological mean.

Although confidence in the observational data from this region prior to 1982 is low (Fig. 4.1), co-variability of Jarvis and Palmyra SSTs is expected based on their respective locations and is observed throughout the satellite era when confidence in the SST estimates is high (Fig. 4.3A, solid lines). The Sr/Ca records, however, exhibit little co-variation (Fig. 4.3B) and are inconsistent with each other and with the satellite SSTs. This lack of coherence indicates that factors other than SST influence coral Sr/Ca variability.

Coral Sr/Ca records have also been used to evaluate whether eastern equatorial Pacific (EEP) SSTs are increasing (as GCM's and NOAA ERSST data products imply) or decreasing (as the HADISST data product implies) in response to anthropogenic forcing (Fig. 4.4). Interpreting Sr/Ca data generated from corals sampled at Wolf Island, Galapagos, Jimenez et al. (2018) suggest that EEP SSTs have increased since the start of their record in 1940, implying a warming trend

consistent with GCM simulations over the corresponding time period. Inconsistencies among coral Sr/Ca and between coral and satellite-based SST measurements cast doubt on this conclusion. In Figure 4.4, Sr/Ca data from the two Wolf Island corals (blue, red lines) are shown with satellite-era observational SSTs (black line) (1982–2010). Two results are notable. First, there is no long-term trend in the observational data since 1982 (black dashed line) and one of Sr/Ca records (red line), whereas the other Sr/Ca record indicates a statistically significant warming trend (blue line). Second, the two corals have Sr/Ca means that differ by ~0.07 mmol/mol, the equivalent of 1.1 °C. Together, these inconsistencies suggest that factors other than SST influence coral Sr/Ca ratios and that Sr/Ca proxy records are unreliable indicators of absolute temperature. Until these inconsistencies among and between the observational and coral SST datasets are reconciled, questions regarding the impact of anthropogenic forcing on CEP SST variability and trends will remain unresolved.

Previous work has shown that these inconsistencies can be resolved by incorporating additional geochemical information (i.e., the skeletal U/Ca ratio) in an improvement to the Sr/Ca proxy called Sr-U (Decarlo et al. 2016; Alpert et al. 2017; Rodriguez et al. 2019). Here, we demonstrate that Sr-U can be used to reconstruct monthly SSTs when paired with laser ablation inductively coupled plasma mass spectrometry (LA-ICPMS). We present two monthly resolved Sr-U records from the CEP that (1) capture the magnitude and phase of variability at their respective sites through two El Niño events and (2) provide a pan-*Porites* and possibly pan-species SST calibration for Sr-U. We also asses the methods capabilities in generating accurate temperatures from old and/or subfossil skeleton that may contain diagenetic material by selectively targeting pristine skeletal elements.

4.2 Methods

4.2.1 Coral Sr-U thermometry

Abiogenic aragonite precipitation experiments and the analysis of corals grown in culture under controlled temperature conditions showed that coral Sr/Ca ratios are influenced by both the mass fraction of aragonite precipitated in the calcifying fluid during biomineralization (Rayleigh

fractionation) and the temperature of the seawater in which skeletal growth occurs (Cohen et al. 2006, 2009; Gaetani and Cohen 2006; Gagnon et al. 2007). Based on this knowledge, and emerging observations of systematic covariation amongst trace element ratios in coral skeletons (e.g. Sinclair and Risk 2006) we previously developed a new coral-based paleo-thermometer, Sr-U, that uses U/Ca to deconvolve the influence of Rayleigh fractionation from that of seawater temperature on coral Sr/Ca (Decarlo et al. 2016; Alpert et al. 2017). U/Ca is used because it covaries with the carbonate ion concentration of the calcifying fluid (DeCarlo et al. 2015) and is thus a proxy for the mass fraction of aragonite precipitated by the coral.

Previous Sr-U studies (Alpert et al. 2017; Rodriguez et al. 2019) utilize multiple paired Sr/Ca and U/Ca values generated over two to three years of coral growth to calculate a single Sr-U value. By overlapping consecutive years, Sr-U values were generated at nominally annual resolution. These studies found that Sr-U values generated from multiple coral species in the Pacific and Atlantic oceans are strongly inversely correlated with observational SST over the temperature range 22 °C to 32 °C. Reconstructions from these studies showed that Sr-U accurately captures mean SSTs, multi-year variability, and century-long trends in the western tropical Atlantic. Conversely, records based on Sr/Ca alone did not capture mean SSTs and implied a cooling trend in the over the 20^{th} century (Alpert et al. 2017).

Bulk sampling of coral skeletons for Sr-U thermometry, as well as Sr/Ca and $\delta^{18}O$ analyses, utilizes a hand-held or automated micro-drill to remove coral powder along a continuous track parallel to the axis of maximum coral growth, attaining roughly monthly sampling resolution in *Porites* corals (Fig. 4.6A,B). Sr-U thermometry uses multiple paired Sr/Ca and U/Ca ratios to establish a Sr/Ca U/Ca regression, from which a single Sr-U value is calculated (Fig. 4.5G). Because this regression requires tens of individual measurements, data collected over multiple annual cycles must be used when bulk sampling thus limiting the Sr-U thermometer to approximately one-year resolution. Building on earlier work (Fallon et al. 1999; Hathorne et al. 2011; Serrato Marks et al. 2017; Vielzeuf et al. 2018 and others), we developed a laser ablation ICPMS technique to measure multiple Sr/Ca and U/Ca pairs *within* a single month of skeletal growth and, thus, calculate monthly Sr-U values. Our method is illustrated in Figure 4.5 (D-G) and described as follows.

4.2.2 Sample preparation.

Coral skeletal cores 3.5 cm-diameter (Fig. 4.6A) are slabbed along the axis of maximum growth, scored, and broken (to avoid losing material) into 7-cm long slices, embedded in epoxy and polished (Fig. 4.5C, D). We use a Zeiss Axioscope MosaiX microscope to image the sections at 10 X magnification and construct a monthly chronology based on successive dissepiments (Fig. 4.5E) (DeCarlo and Cohen 2017). Microscope visualization of the section also enables us to identify and avoid areas of skeleton that are diagenetically altered by dissolution or secondary aragonite infilling (e.g. Cohen and Hart 2004).

4.2.3 Pressed powder standards

Our primary coral standard is a packed powder of JCP-1 (AIST Japan, and our internal secondary coral standard is packed powder generated by subjecting a large (~500 g) piece of a modern coral (Jardin A, *Siderastrea siderea*, collected in Puerto Morelos, Mexico, abbreviated here as JAR) to a shatterbox, are analyzed between every 10 unknowns and NIST glass is analyzed at the beginning and end of each 5-hour analytical session to ensure long-term consistency.

4.2.4 Laser ablation ICPMS

We mount the coral thick sections and our standards into a S155 vacuum chamber attached to an ASI RESOlution-SE 193 nm ArF excimer laser ablation system. During ablation, the primary carrier gas consists of ~1000 mL/min of argon from the mass spectrometer. We supplement this with 500 mL/min of high purity helium and ~5 mL/min high purity dinitrogen to improve signal strength and stability. Approximately 25 circular, 50 μm-diameter ablation spots are selected between consecutive dissepiments, following three adjacent thecal walls in growth direction (Fig. 4.6F). This spot size is small enough to avoid centers of calcification, skeletal pores and diagenetic areas, while providing adequate material for precise analyses (Fig. A4.1). We utilize a notably low laser fluence (1.1 mJ/cm^2, which is monitored and maintained constant in the ASI RESOlution-SE) that produces consistent ablation and prevents rapid incision, which exacerbates down-hole fractionation and increases the risk of drilling through the sample into epoxy. We employed a single 64μm-diameter cleaning shot followed by a settling time of 20 s and a 50 s ablation interval with the laser pulse rate set to 10 Hz. The homogeneity of element ratios during coral ablation

suggest that these settings are sufficient in mitigating any potential down-hole fractionation effects (Fig. A4.1).

We transfer the sample gas through a signal smoothing squid on its way to an iCap Qc mass spectrometer, on which we sequentially measure ^{238}U, ^{88}Sr, and ^{48}Ca, with dwell times on each mass of 0.5, 0.01, and 0.001 milliseconds, respectively. To determine raw elemental ratios, we correct the counts per second measured at each mass based on the assumed normal abundances of these isotopes in nature. We developed a laser data reduction routine, described in Appendix A. This platform will enable users to import and process any raw data time series generated via LA-ICPMS. The routine also includes the capability to (a) align laser spot locations with coral thin section maps, (b) bin data into user defined intervals, (c) perform outlier analyses and screen laser data quality, (d) conduct Sr-U regressions. It is designed to be used for a wide range of laser setups, sampling resolutions, and compatible with multiple proxy calibrations.

In addition to the ^{238}U, ^{88}Sr, and ^{48}Ca data utilized in this chapter and chapter 5 of this thesis, we also collected ^{11}B, ^{25}Mg, and ^{138}Ba measurements during each spot. While these elements are neither examined in this chapter nor in chapter 5, each represents a valuable paleo archive, and will be the subject of future work. It should be noted that the data reduction routine described in Appendix A4 was constructed to process these elements as well, along with any other future analytes with minimal modification.

4.2.5 Calculating Sr-U

We bin ~25 Sr/Ca and U/Ca pairs every 2 mm down core, with a 1 mm overlap, consistent on average with monthly dissepiment spacings (Fig. 4.5G). We also calculate the average monthly Sr/Ca ratio from these data (See Appendix 4A). Over both cores analyzed, 86% of monthly Sr/Ca-U/Ca regressions were significant at the $p<0.05$ level (t-stat, OLS). We also tested bimonthly binning with a 1-month overlap. This increased the number of significant regressions to 97%, and significantly dampened variability that we attribute to outlying ablation points. This approach yielded an average relative uncertainty for Sr-U of 0.85%.

4.3 Results

Using the above method, we analyzed the top ~16 cm (representing the last 10 years of growth) from two coral cores from the CEP. Core J1222 was collected from a live coral on Jarvis Island (0.37°S, −159.98°W) in 2017 and core N1344 was collected from a live coral on Nikumaroro Island (4.68°S, 174.52°W) in 2018 (see locations in Figs. 4.2A and 4.11). Both corals survived the most recent El Niño in 2015–16.

We observed a large range in both Sr/Ca and U/Ca ratios within skeleton accreted over the course of a single month in both corals. Such fine-scale heterogeneity has been reported previously (Allison et al. 2001; Meibom et al. 2006; Allison and Finch 2009). In our data, we find a consistently strong, positive correlation (average r^2 = 0.82) between each of the ~25 Sr/Ca and U/Ca ratios collected between successive dissepiments (i.e., within a single month of growth). The wide range in Sr/Ca and U/Ca ratios over small length scales and their strong covariation indicates that coral Sr/Ca is strongly influenced by the mass fraction of aragonite (indicated by U/Ca) precipitated by the coral from each batch of calcifying fluid (Gaetani et al. 2011; DeCarlo et al. 2015).

4.3.1 Regression of laser Sr-U and Sr/Ca on SST

In Figure 4.6A, the Sr-U SST relationships for J1222 (blue) and N1344 (red) are plotted together. Monthly resolved Sr-U values from both corals show a strong, inverse correlation with monthly resolved SST over the temperature range 24–30.5 °C, as predicted by Sr-U theory (DeCarlo et al., 2016). Further, the Sr-U SST relationships in the two corals are indistinguishable from each other (Fig. 4.10C). This result indicates the potential for a universal Sr-U SST calibration for *Porites* similar to that observed in bulk analyses of Atlantic coral species (Rodriguez et al., 2019). The calibration we derive from these results is as follows:

$$\boldsymbol{SST}\ (^{\circ}\boldsymbol{C}) = -13.244 \pm 0.594\ \times\ \boldsymbol{SrU}\ +\ 146.88 \pm 5.33$$

Figure 4.6B shows the corresponding monthly Sr/Ca SST relationships. Sr/Ca from both corals also show an inverse correlation with SST, but the residuals from the two corals form two distinct populations (Fig. 4.6D), indicating that the Sr/Ca SST relationship differs between the two

corals, as has been shown for analogous bulk measurements. These coral-specific relationships confirm that factors other than temperature influence coral Sr/Ca, even at this sampling scale.

4.3.2 Jarvis Island record

In Figure 4.7, we present a continuous, 10-year, monthly-resolved Sr-U time-series generated from J1222 and N1344 using laser ablation, as well as the monthly Sr/Ca record generated by averaging all Sr/Ca values in each bin. The proxy datasets are plotted against satellite (OISST) data (black lines). Both Sr-U and Sr/Ca time-series are scaled to the SST data by calibrating the first two years of each time-series against SST and applying the calibration to the reminder of each record. It is notable that both Sr-U and Sr/Ca produce variability with consistent phase as the El Niño SST anomalies in 2010 and 2015. However, the relationship between Sr-U and SST remains consistent through the record, whereas the Sr/Ca SST relationship does not. The Sr/Ca record implies a significantly cooler 2010 ST anomaly than indicated by the instrumental dataset, as well as a warming trend over this period that is not apparent in the satellite record.

4.3.2 Nikumaroro Island record

We constructed a second, continuous 10-year, monthly-resolved Sr-U time-series from coral N1344, a *Porites* coral cored on Nikumaroro Island (4.68°S, 174.52°W) in 2018 (Fig. 4.9 B). Nikumaroro is located outside the Niño 3.4 and further into the Niño 4.0 region, south of the equator. We applied the same Sr-U SST calibration as above (i.e., based on the top 2 years of the Jarvis coral) to the Sr-U data generated from the Nikumaroro coral. We find that Sr-U captures the mean SST at Nikumaroro, as well as the timing and amplitude of SST variability in the observational record, including the existence and relative amplitudes of the 2009–10 and 2015–16 El Niños. Conversely, the Sr/Ca-only record derived from the same data returns SSTs that are too warm (Fig. 4.7D).

4.4 Discussion

As in calibrations derived from bulk sampling (Decarlo et al. 2016; Alpert et al. 2017; Rodriguez et al. 2019), LA-ICPMS Sr-U shows promise in mitigating vital effects that produce

decoupling and coral to coral offsets common in Sr/Ca records. Both Sr-U records correlate with SST on both a seasonal (i.e. 3 month moving average, $r = 0.79$, $p < 1e\text{-}33$ for J1222; $r = 0.42$, $p < 1e\text{-}5$ for N1344; $r = 0.84$, $p < 1e\text{-}72$ combined) and ENSO (i.e. 1-year moving average, $r = 0.83$, $p < 1e\text{-}40$ for J1222; $r = 0.33$, $p < 1e\text{-}3$ for N1344; $r = 0.80$, $p < 1e\text{-}62$ combined) time scale, although N1344 has a lower Pearson coefficient which is likely due to the smaller amplitude of SST variability resulting in a lower signal to noise ratio. Additionally, there remain slight discrepancies between Sr-U and instrumental SST (Fig. 4.7A,C). Notably these decouplings tend to occur during warm periods (e.g. J1222 Sr-U does not reach the peak SST recorded by satellite during the 2010 El Niño). Several factors may have resulted in these discrepancies, namely a deviation of local SST from regional SST, fluctuations in coral growth rate not reflected in sampling, or some component of coral vital effects not accounted for by the Sr-U proxy. While a definitive cause cannot be identified, here we provide a discussion of the likelihood and implications of each possibility.

An ever-present concern when generating proxy records from coral archives is the heterogeneity of the reef environment. Due to the complex bathymetry and resultant hydrodynamics of coral reefs, these environments are subject to systematic temperature variability on kilometer to meter scales (e.g. Venegas et al. 2019). Such spatial variability has been studied on Jarvis island (Barkley et al. 2018; Venegas et al. 2019), and found to vary by up to 0.5°C degrees around the east side of the island, and up to 2°C between the east and the west (where upwelling from the EUC occurs). The cores used in this analysis were selected opportunistically, and although in situ logger data has been collected at several locations on Jarvis island, the closest logger to colony J1222 was ~700 m away. At Nikumaroro island, loggers were deployed closer to the colony (~50 m), but for only part of the duration of the record (2012-2015) (Mollica et al. 2019). Despite these uncertainties, high resolution satellite SST (Pathfinder v5.3) is consistent with loggers deployed nearest to the sampled colonies both on Jarvis and Nikumaroro. Furthermore, the relationship between Sr-U and satellite SST is consistent between both colonies (Fig. 4.6), a result expected given the premise of the Sr-U thermometer (Decarlo et al. 2016) and the results of bulk analyses (Alpert et al. 2017; Rodriguez et al. 2019). However, the observed deviations in the Sr-U record may be a result of this imperfect control on measured SST.

Minor discrepancies in the agreement between the Sr-U and satellite SST may also be a result of variability in the coral growth rate. Where possible, monthly age models were verified by dissepiment, however during periods of the record where dissepiment preservation was poor a homogenous (i.e. 2mm bin with 1mm overlap sampling rate). If seasonal growth rates vary substantially during these periods, as has been seen in some higher latitude corals (DeCarlo and Cohen 2017), a bias towards faster growing time periods may occur. Additionally, the species of the two records, *Porites*, is known to not only calcify skeleton at the exterior surface of the colony, but also to thicken existing skeletal elements throughout the tissue layer (in these cores ~7mm) in a process called bio-smoothing (Barnes and Lough 1993; Gagan et al. 2012). However, these effects have been found to be limited to the top ~10% of the tissue layer in *Porites* corals (Mollica et al. 2018) and is lessened for faster growing colonies (Gagan et al. 2012). Given the growth rate of our corals (J1222 = 1.79 cm yr^{-1}, N1344 = 2.03 cm yr^{-1}), it is unlikely that the bio-smoothing process has had substantial impact on the overall record (especially when binned to 1mm resolution) but may account for short discrepancies during periods of low growth rate.

It should be noted however bio-smoothing prohibits our current sampling method (i.e. 50 µm spot size, which accounts for most of an individual skeletal element) from examining SST fluctuations at higher temporal resolution. Efforts in examining diurnal variability in element ratios are better suited to techniques capable of higher spatial resolution, e.g. Secondary Ion Mass Spectrometry (SIMS). While several studies have examined coral skeletal element ratios at this scale (e.g. Hart and Cohen 1996; Allison and Finch 2007), the current method of Sr-U calculation makes its use prohibitive at the needed resolution.

Discrepancies between ocean temperature around a colony and the Sr-U recorded in the coral skeleton could of course also be a result of the Sr-U proxy failing to record the correct SST. This could arise from erroneous measurements of either the Sr/Ca or U/Ca ratio of the coral skeleton, or a failure of the method to fully counteract vital effects in coral calcification at the monthly scale. While the precision of our consistency standard across all runs (see Appendix A) makes significant analytical error an unlikely factor, this analysis represents the first test of the Sr-U proxy at high resolution. When sampling 50 µm spots over a variety of skeletal elements in multiple corallites, heterogeneity between types of skeletal element (e.g. endothecal vs. exothecal)

and skeletal features (i.e. centers of calcification) become important (Allison 1996; Cohen et al. 2001; Meibom et al. 2004). We chose as large a spot size as possible to average out intra-element differences while still avoiding problematic sampling areas, and we detected no systematic patterns laterally across sampling tracks. That being said, the interior of *Porites* calyxes have complex 3-D architecture, and systematic differences in element ratios may not be apparent in a 2-D cross section.

Future investigation of the full spatial variability in element ratios across multiple concomitant calyxes at the micron scale would be required to definitively rule this out. Experimental work with tighter temperature control would also be required to robustly assess the efficacy of the Sr-U proxy in resolving consistent SST across different skeletal elements. We do not present such an analysis here and acknowledge that these concerns may be the cause of the discrepancies between the Sr-U and SST records. That being said, the efficacy of the proxy in its current state is encouraging as an enhancement to current high-resolution proxy methods, and demonstrably viable in its application to a variety of research questions.

Future work towards verifying and applying the proxy should include an expansion and formalization of an Sr-U – SST calibration for LA-ICPMS data. Ideally this would consist of two to three additional *Porites* corals spanning a wider range of SST with overlap of the two presented here. Such a dataset would confirm the applicability of Sr-U universally across at least the *Porites* genera, and add confidence to its applicability to fossil samples. Additional calibration data may also yield a more robust relationship and expand the calibration's utility to higher latitude reefs that experience a wider range of SST.

4.5 Conclusions

Quantifying the anthropogenic influence on 20th century temperature requires accurate temperature estimates that augment the spatially and temporally sparse instrumental record. Proxy records of past temperature change are also critical for evaluating the efficacy of model projections of future climate change. In some key regions such as the equatorial Pacific, SSTs strongly influence global climate patterns, yet remain poorly constrained over much of the last century.

This paucity of observational data has limited our ability to resolve conflicts between GCM projections and observational datasets. Furthermore, existing proxy reconstructions are neither consistent, nor coherent with observational data over this time period.

The new coral thermometer Sr-U shows great potential in resolving this conundrum by accurately resolving not only long-term mean SST and SST trends, but also the magnitude of interannual variability. Annual Sr-U has been shown to capture long term trends and decadal variability in the western tropical Atlantic (Alpert et al. 2017) and has been applied to generate SST records from fossil corals during key periods in Earth's climate history (Alpert et al. 2017; Rodriguez et al. 2019). In this paper we show the Sr-U proxy's ability to capture seasonal variations in SST when sampled monthly via LA-ICPMS.

Our primary goal in developing this method is to enable the generation of long, continuous records of SST with sufficiently high temporal resolution to resolve seasonal and ENSO variability. The Sr-U calibration presented here will be augmented with more records and evaluated across different species with the goal of applicability throughout long coral records and even in fossil material. The precision of sampling capable via LA-ICPMS complements this use, as targets can easily avoid diagenetically-altered material. This versatility allows for wide spread applications of this proxy across past and present tropical climate. It is our hope that this method enables the community to access and resolve these previously inaccessible questions.

4.6 Figures

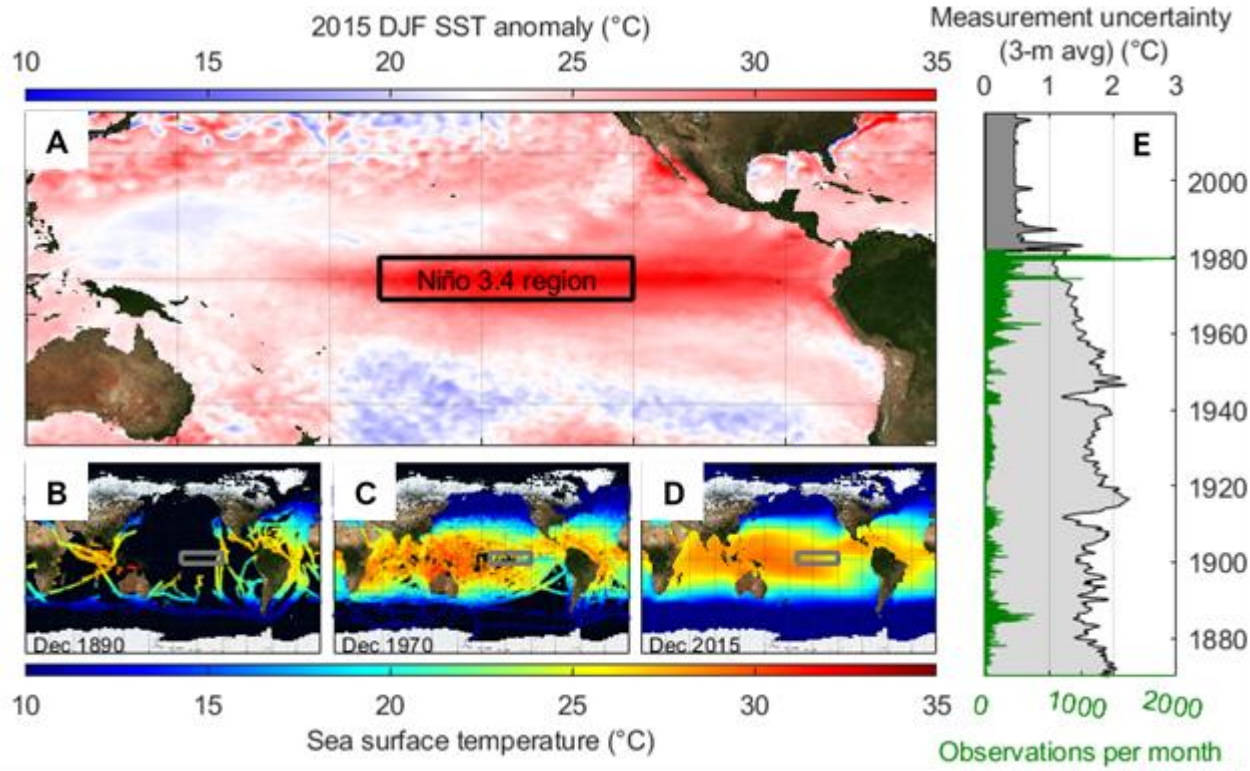

Figure 4.1: Pacific SST anomaly during the peak of the 2015–2016 El Niño heatwave (OISST v2, ¼° daily anomaly). The black rectangle outlines the Niño 3.4 region most commonly used to define ENSO. (**B-D)** SST measurements across the Pacific basin in December 1890 **(B**), December 1970 **(C),** and December 2015 **(D)** reveal the paucity of data in the 3.4 region (rectangle) prior to the satellite era. **(E)** The number of observations in the Nino 3.4 over the course of the instrumental record (dark green line). Data paucity prior to the satellite era leads to large uncertainties on the uninterpolated SSTs (light grey shading represents HADSST); dark grey shading is the 2σ uncertainty post-1982 (i.e., satellite) era.

.

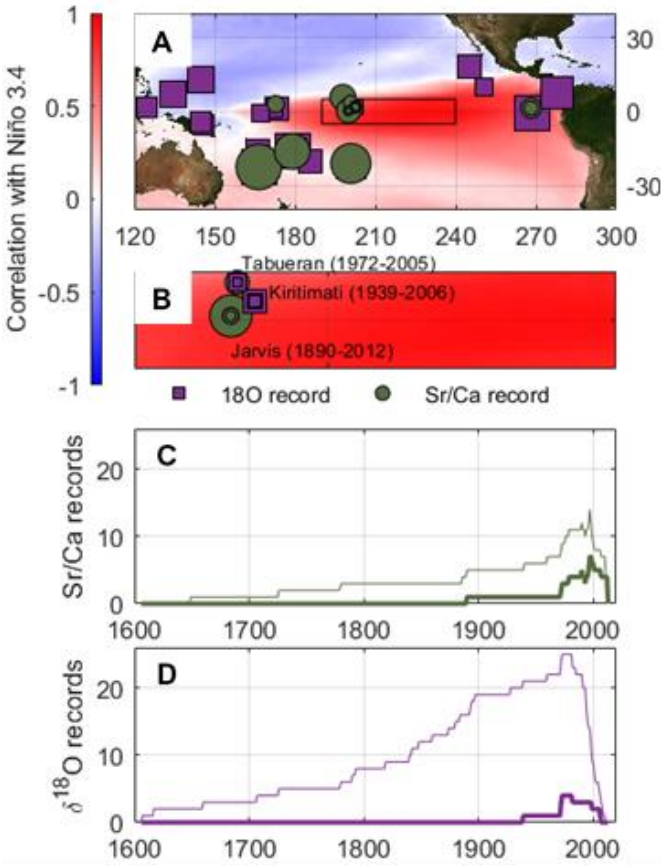

Figure 4.2: **(A)** Spatial correlation of Pacific basin SST (OISST v2, ¼° daily SST) with the Niño 3.4 SST (black box). Existing coral proxy SST records are shown. Sr/Ca records are tan circles; $\delta^{18}O$ records are purple squares. **(B)** shows existing coral proxy records in the Niño 3.4 region. Symbol size represents the relative length of each record. (**C)** and **(D**) show numbers and lengths of existing Sr/Ca **(C)** and $\delta^{18}O$ **(D)** coral proxy records across the Pacific (light lines) and Niño 3.4 (bold lines).

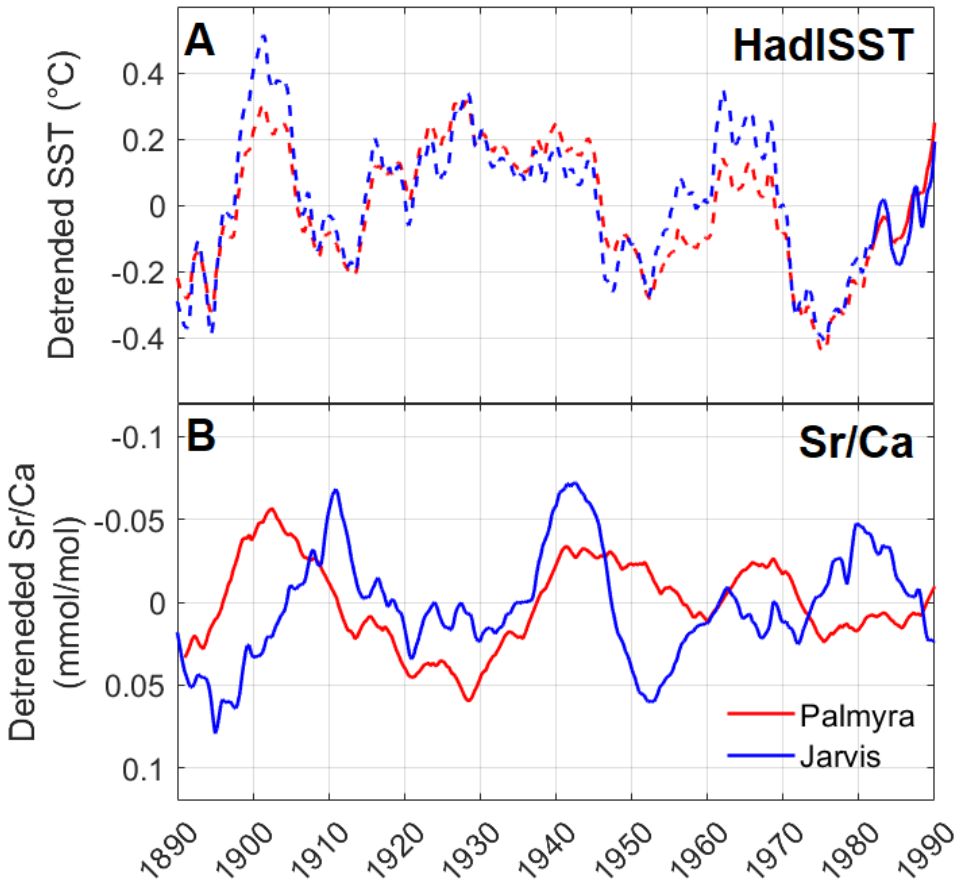

Figure 4.3: **(A)** Ten-year smoothed, detrended record of observational SST **(**HADISST) at Palmyra, 5.87°N, 162.08°W (red) (Nurhati et al. 2011) and Jarvis, 0.37°S, 160.00°W (blue) (Thompson et al. 2015) from 1890–1990 AD. Solid segments (1980–1990) represent satellite-era SST records that show strong co-variability between localities. (**B)** Ten-year smoothed detrended coral Sr/Ca records from each island from 1890–1990 AD exhibit little coherence with each other or with observational SSTs, even during the satellite era for which accurate SST records exist.

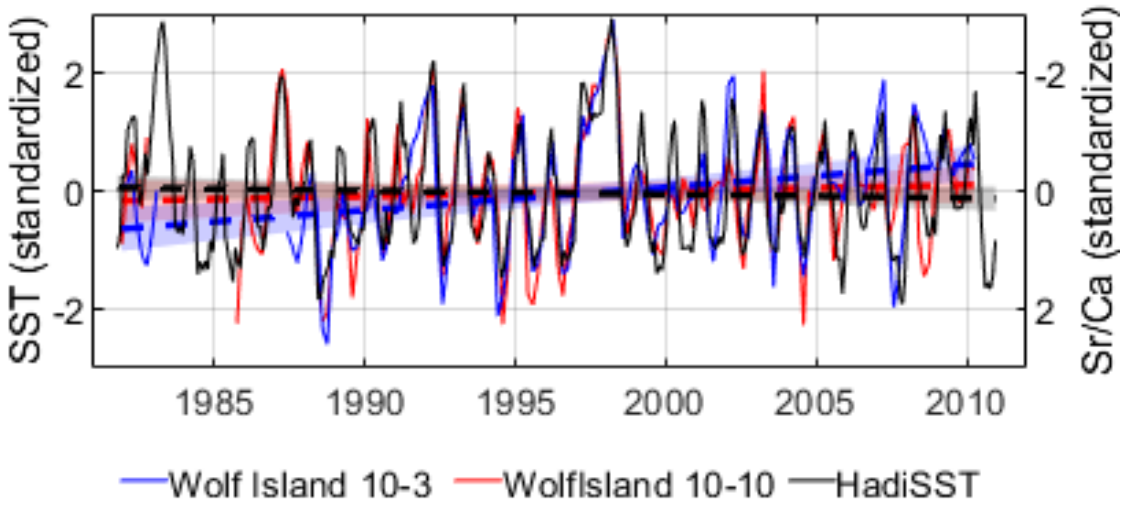

Figure 4.4: Satellite SST anomaly time-series from 1982–2010 at Wolf Island, Galapagos (black line), shown against coral-based Sr/Ca anomaly time series from two Wolf Island corals (red and blue lines) (Jimenez et al. 2018). The Sr/Ca datasets are offset from each other by 0.07 mmol/mol (~1.1 °C), but are standardized here to enable comparison with the satellite SST record. Linear trends in all datasets (dashed lines) are fit with a robust fitting algorithm that accounts for edge effects. Shaded areas represent error on linear trends. Throughout the record, seasonally-resolved Sr/Ca ratios oscillate with seasonal SSTs. One Sr/Ca record (blue) suggests a statistically significant warming trend of 0.39 °C per decade, whereas the observational record indicates no statistically significant trend.

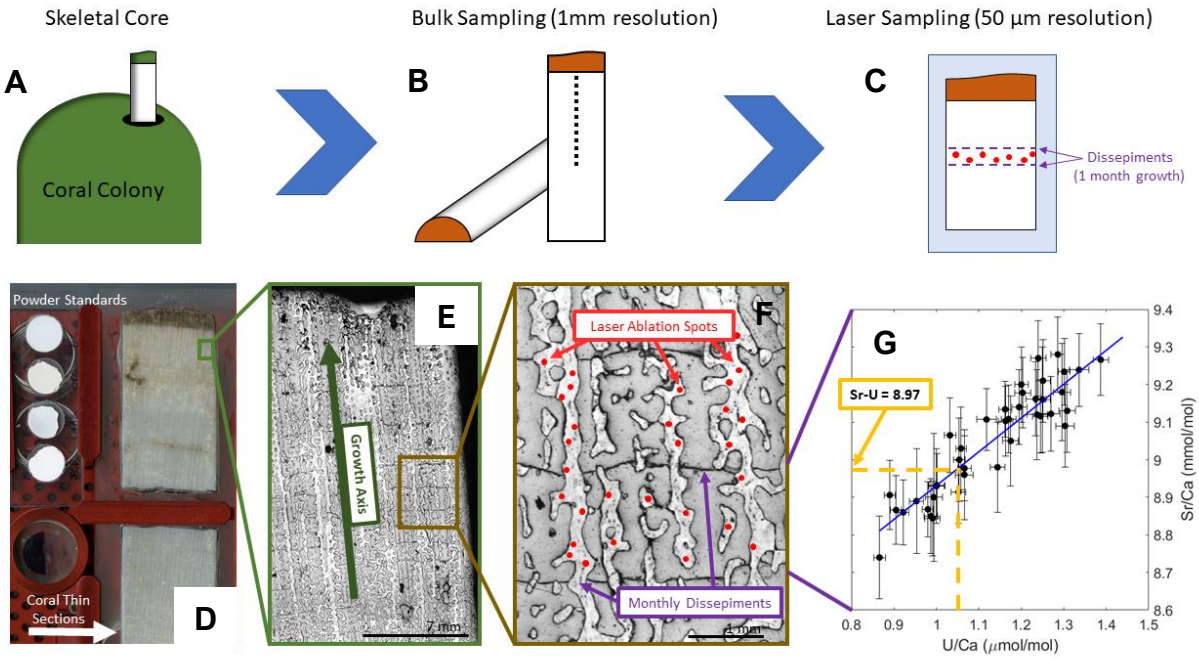

Figure 4.5: **(A)** Collection and **(B)** sampling of a coral core for bulk and **(C)** laser Sr-U measurements. Bulk sampling typically follows a track down the coral core, at a resolution of ~0.5–1 mm, encompassing multiple skeletal structures. For laser sampling, polished sections reveal monthly dissepimental sheets to guide monthly sampling. Other structure such as centers of calcification and secondary aragonite infilling can be identified and avoided with laser sampling. Our method generates 25 laser spots between each dissepiment pair, or approximated by average dissepimental spacing. (**D)** Coral sections are loaded into a laser chamber with packed powder carbonate standards representing a range of known Sr/Ca and U/Ca values. (**E** and **F**) laser spots are set along visible coral skeletal elements parallel to growth axis. (**G)** ~25 paired Sr/Ca and U/Ca measurements generated within the approximate dissepiment spacing (here ~1mm) are used to calculate a single, monthly Sr-U value.

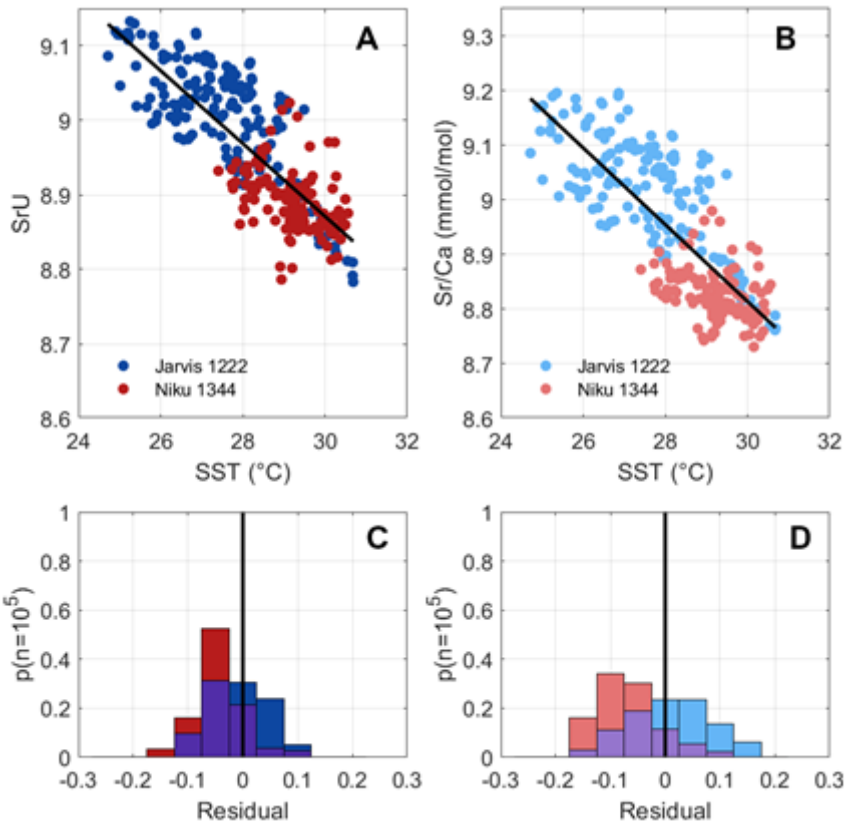

Figure 4.6: Monthly Sr-U **(A)** and Sr/Ca **(B)** from J1222 (blue) and N1344 (red) plotted versus monthly satellite SST (OISST v2, ¼°) verified with *in situ* logger data from each site. Sr-U correlates with SST, and corals fall along the same regression line whereas Sr/Ca-SSTs for the two corals are offset. A bootstrap resampling of the datasets (**C** and **D**), show the Sr-U residuals were fully overlapping whereas the Sr/Ca residuals were significantly different for each core.

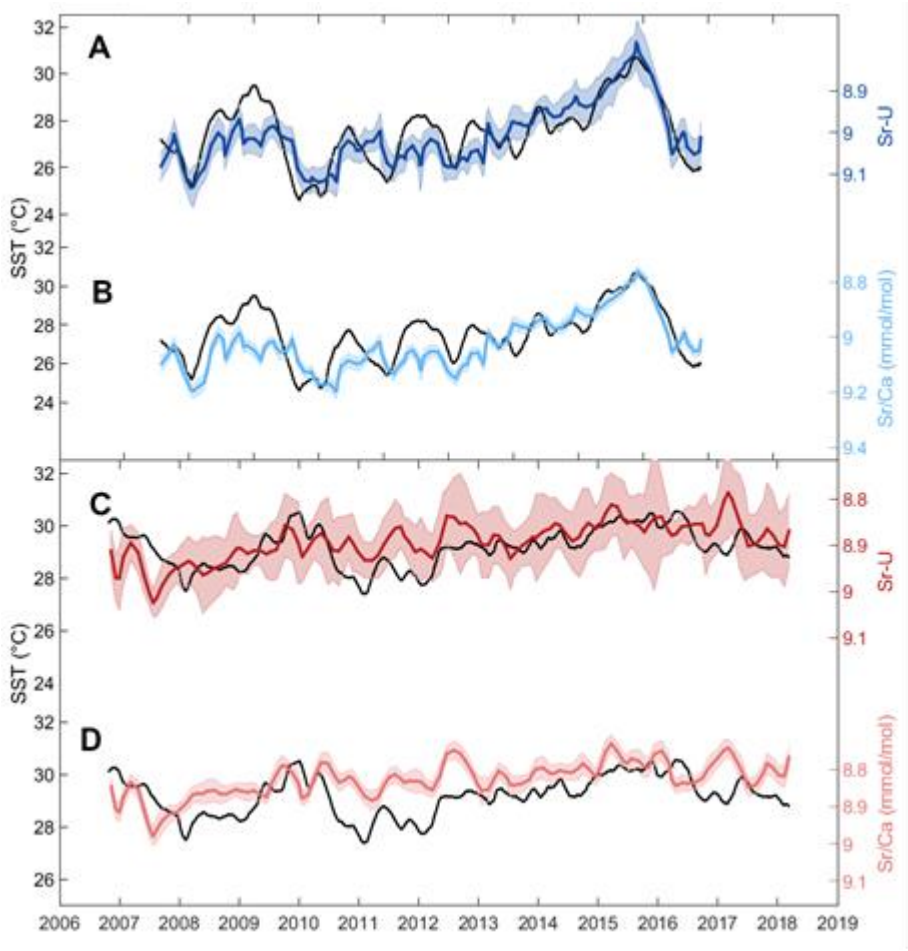

Figure 4.7: Monthly resolved Sr-U (**A**) and Sr/Ca (**B**) coral J1222 (Jarvis Island) shown versus satellite SSTs verified against in situ logger data. Corresponding plots for N1344 are shown in (**C**) and (**D**). Both the Sr-U and the Sr/Ca capture the general shape and variability in the SST record, and record two ENSO events (2010 and 2015), but the Sr-U record accurately tracks the SST trend whereas the Sr/Ca does not.

4.7 References

Allison N (1996) Geochemical anomalies in coral skeletons and their possible implications for paleoenvironmental analyses. Mar Chem

Allison N, Finch AA (2007) High temporal resolution Mg/Ca and Ba/Ca records in modern Porites lobata corals. Geochemistry, Geophys Geosystems 8:

Allison N, Finch AA (2009) Reproducibility of minor and trace element determinations in Porites coral skeletons by secondary ion mass spectrometry. Geochemistry, Geophys Geosystems 10:

Allison N, Finch AA, Sutton SR, Newville M (2001) Strontium heterogeneity and speciation in coral aragonite: Implications for the strontium paleothermometer. Geochim Cosmochim Acta 65:2669–2676

Alpert AE, Cohen AL, Oppo DW, DeCarlo TM, Gaetani GA, Hernandez-Delgado EA, Winter A, Gonneea ME (2017) Twentieth century warming of the tropical Atlantic captured by Sr-U paleothermometry. Paleoceanography 32:146–160

Barkley HC, Cohen AL, Brainard RE, Mollica NR, Rivera HE, Drenkard EJ, Young CW, Vargas-Ángel B, Lohmann GP, Decarlo TM, Alpert AE, Lino KC, Oliver TA, Pietro KR, Luu VH (2018) Repeat bleaching of a central Pacific coral reef over the past six decades (1960-2016). Nat Biol Commun

Barnes DJ, Lough JM (1993) On the nature and causes of density banding in massive coral skeletons. J Exp Mar Bio Ecol 167:91–108

Coats S, Karnauskas KB (2017) Are Simulated and Observed Twentieth Century Tropical Pacific Sea Surface Temperature Trends Significant Relative to Internal Variability? Geophys Res Lett 44:

Cobb KM, Charles CD, Cheng H, Edwards RL (2003) El Niño/Southern Oscillation and tropical Pacific climate during the last millennium. Nature 424:271–276

Cohen AL, Gaetani GA, Lundälv T, Corliss BH, George RY (2006) Compositional variability in a cold-water scleractinian, Lophelia pertusa: New insights into “vital effects.” Geochemistry,

Geophys Geosystems 7:

Cohen AL, Hart SR (2004) Deglacial sea surface temperatures of the western tropical Pacific: A new look at old coral. Paleoceanography 19:1–6

Cohen AL, Layne GD, Hart SR, Lobel PS (2001) Kinetic control of skeletal Sr/Ca in a symbiotic coral: Implications for the paleotemperature proxy. Paleoceanography 16:20–26

Cohen AL, McCorkle DC, De Putron S, Gaetani GA, Rose KA (2009) Morphological and compositional changes in the skeletons of new coral recruits reared in acidified seawater: Insights into the biomineralization response to ocean acidification. Geochemistry, Geophys Geosystems 10:

Cohen AL, Owens KE, Layne GD, Shimizu N (2002) The effect of algal symbionts on the accuracy of Sr/Ca paleotemperatures from coral. Science (80-) 296:331–333

DeCarlo TM, Cohen AL (2017) Dissepiments, density bands, and signatures of thermal stress in Porites skeletons. Coral Reefs 1–13

Decarlo TM, Gaetani GA, Cohen AL, Foster GL, Alpert AE, Stewart JA (2016) Coral Sr-U thermometry. Paleoceanography 626–638

DeCarlo TM, Gaetani GA, Holcomb M, Cohen AL (2015) Experimental determination of factors controlling U/Ca of aragonite precipitated from seawater: Implications for interpreting coral skeleton. Geochim Cosmochim Acta 162:151–165

Deser C, Phillips AS, Alexander MA (2010) Twentieth century tropical sea surface temperature trends revisited. Geophys Res Lett 37:1–6

Evans MN, Fairbanks RG, Rubenstone JL (1999) The thermal oceanographic signal of El Niño reconstructed from a Kiritimati Island coral. J Geophys Res Ocean 104:13409–13421

Fallon SJ, McCulloch MT, Van Woesik R, Sinclair DJ (1999) Corals at their latitudinal limits: Laser ablation trace element systematics in Porites from Shirigai Bay, Japan. Earth Planet Sci Lett 172:221–238

Gaetani GA, Cohen AL (2006) Element partitioning during precipitation of aragonite from seawater: A framework for understanding paleoproxies. Geochim Cosmochim Acta 70:4617–

4634

Gaetani GA, Cohen AL, Wang Z, Crusius J (2011) Rayleigh-based, multi-element coral thermometry: A biomineralization approach to developing climate proxies. Geochim Cosmochim Acta 75:1920–1932

Gagan MK, Dunbar GB, Suzuki A (2012) The effect of skeletal mass accumulation in Porites on coral Sr/Ca and ??^{18}O paleothermometry. Paleoceanography 27:1–16

Gagnon AC, Adkins JF, Fernandez DP, Robinson LF (2007) Sr/Ca and Mg/Ca vital effects correlated with skeletal architecture in a scleractinian deep-sea coral and the role of Rayleigh fractionation. Earth Planet Sci Lett 261:280–295

Hart SR, Cohen AL (1996) An ion probe study of annual cycles of Sr / Ca and other trace elements in corals. Geochim Cosmochim Acta 60:3075–3084

Hathorne EC, Felis T, James RH, Thomas A (2011) Laser ablation ICP-MS screening of corals for diagenetically affected areas applied to Tahiti corals from the last deglaciation. Geochim Cosmochim Acta 75:1490–1506

Jimenez G, Cole JE, Thompson DM, Tudhope AW (2018) Northern Galápagos Corals Reveal Twentieth Century Warming in the Eastern Tropical Pacific. Geophys Res Lett 45:1981–1988

Kaplan A, Cane MA, Clement AC, Blumenthal MB, Rajagopalan B (1998) Analyses of global sea surface temperature 1856-1991. J Geophys Res 103:

Kosaka Y, Xie S (2013) Recent global-warming hiatus tied to equatorial Pacific surface cooling. Nature 501:403–407

Meibom A, Cuif JP, Hillion F, Constantz BR, Juillet-Leclerc A, Dauphin Y, Watanabe T, Dunbar RB (2004) Distribution of magnesium in coral skeleton. Geophys Res Lett 31:1–4

Meibom A, Yurimoto H, Cuif JP, Domart-Coulon I, Houlbreque F, Constantz B, Dauphin Y, Tambutté E, Tambutté S, Allemand D, Wooden J, Dunbar R (2006) Vital effects in coral skeletal composition display strict three-dimensional control. Geophys Res Lett 33:2–5

Mollica NR, Cohen AL, Alpert AE, Barkley HC, Brainard RE, Carilli JE, Decarlo TM, Drenkard EJ, Lohmann P, Mangubhai S (2019) Skeletal records of bleaching reveal different thermal

thresholds of Pacific coral reef assemblages. Coral Reefs

Mollica NR, Guo W, Cohen AL, Huang K-F, Foster GL, Donald HK, Solow AR (2018) Ocean Acidification Affects Coral Growth by Reducing Skeletal Density. Proc Natl Acad Sci

Nurhati IS, Cobb KM, Charles CD, Dunbar RB (2009) Late 20th century warming and freshening in the central tropical Pacific. Geophys Res Lett 36:2–5

Nurhati IS, Cobb KM, Di Lorenzo E (2011) Decadal-scale SST and salinity variations in the central tropical pacific: Signatures of natural and anthropogenic climate change. J Clim 24:3294–3308

Rodriguez LG, Cohen AL, Ramirez W, Oppo DW, Pourmand A, Edwards RL, Alpert AE, Mollica N (2019) Mid-Holocene, Coral-Based Sea Surface Temperatures in the Western Tropical Atlantic. Paleoceanogr Paleoclimatology 34:1234–1245

Schubert SD, Suarez MJ, Pegion PJ, Koster RD, Bacmeister JT (2004) Causes of Long-Term Drought in the U . S . Great Plains. Am Meteorol Soc 485–503

Seager R, Cane M, Henderson N, Lee D, Abernathey R (2019) Strengthening tropical Pacific zonal sea surface temperature gradient consistent with rising greenhouse gases. Nat Clim Chang 9:

Seager R, Vecchi GA (2010) Greenhouse warming and the 21st century hydroclimate of southwestern North America. Proc Natl Acad Sci

Serrato Marks G, LaVigne M, Hill TM, Sauthoff W, Guilderson TP, Roark EB, Dunbar RB, Horner TJ (2017) Reproducibility of Ba/Ca variations recorded by northeast Pacific bamboo corals. Paleoceanography 32:966–979

Sinclair DJ, Risk MJ (2006) A numerical model of trace-element coprecipitation in a physicochemical calcification system: Application to coral biomineralization and trace-element “vital effects.” Geochim Cosmochim Acta 70:3855–3868

Thompson DM, Cole JE, Shen GT, Tudhope AW, Meehl GA (2015) Early twentieth-century warming linked to tropical Pacific wind strength. Nat Geosci 8:117–121

Venegas RM, Oliver T, Liu G, Heron SF, Clark SJ, Pomeroy N, Young C, Eakin CM, Brainard RE (2019) The Rarity of Depth Refugia from Coral Bleaching Heat Stress in the Western and

Central Pacific Islands. Sci Rep 9:1–12

Vielzeuf D, Gagnon AC, Ricolleau A, Devidal JL, Balme-Heuze C, Yahiaoui N, Fonquernie C, Perrin J, Garrabou J, Montel JM, Floquet N (2018) Growth kinetics and distribution of trace elements in precious corals. Front Earth Sci 6:1–18

de Villiers S, Shen GT, Nelson BK (1994) The Sr/Ca-temperature relationship in coralline aragonite: Influence of variability in (Sr/Ca)Seawater and skeletal growth parameters. Geochim Cosmochim Acta 58:197–208

Chapter 5 – One Hundred Years of Heat Stress and Coral Bleaching in the Central Equatorial Pacific

Nathaniel R. Mollica, Anne L. Cohen, Andrew R. Solow

5.1 Introduction

Tropical coral reef ecosystems provide the physical, biological, cultural and economic backbone of an estimated 500 million people worldwide (Wilkinson 2004). Barrier and fringing reefs protect over 150,000 km of tropical coastline from waves, storms and tsunamis, (Ferrario et al. 2014), an ecosystem service valued at ~4 billion USD a year (Beck et al. 2018). Tropical reefs are inhabited by approximately 830,000 species globally (Fisher et al. 2014) including ¼ of all fish species making them among the most biodiverse ecosystems on earth. Yet coral reefs are in rapid decline. Unsustainable fishing practices, nutrient and sediment pollution, diseases and invasive species, and coral bleaching events have had catastrophic effects on many of the world's coral reefs, resulting in a loss of 50-75% of global coral cover to date (Bruno et al. 2019). Many coral reef countries are taking unprecedented measures to manage local stressors and to invest in coral reef protections, in a massive effort to sustain their livelihoods (Selig and Bruno 2010). But anthropogenic ocean warming is a global threat to which even the best managed and protected coral reefs in the world are susceptible.

Global climate models project a sharp increase in rates of ocean warming through this century. However, most alarming for coral reef ecosystems are projected increases in the magnitude, frequency, and duration of marine heat waves (MHWs) (Frölicher et al. 2018). These heat waves, predominantly driven by the El Niño Southern Oscillation (ENSO), were first associated with global scale coral bleaching in 1982-1983. Subsequent global bleaching events associated with the 1987-1988, 1997-1998, 2009-2010, and 2015-2016 El Niño MHWs have resulted in seemingly irreversible declines in global coral cover (Wilkinson 2004; Hughes et al.

2018). In 2015-2016, an MHW associated with a so-called Super El Nino killed ~25% of corals across the global tropics.

Projections of coral reef futures under 21st century climate change indicate moderate declines in the most optimistic cases (Logan et al. 2014) with most predicting complete devastation resulting from annual severe bleaching (Hoegh-Guldberg 1999), projected to occur on most reefs by 2043 (van Hooidonk et al. 2016). The major unknown in each of these projections is whether corals can adapt or acclimate to anthropogenic warming at the rapid pace at which climate change is occurring. Some studies suggest most corals are incapable of adaptation on the timescale required (Hoegh-Guldberg 1999), yet emerging evidence suggests that adaptation or acclimation potential exists. Some corals exposed to large diel temperature variability (Palumbi et al. 2014; Safaie et al. 2018) or chronic high temperatures (Van Woesik et al. 2012; Mollica et al. 2019) appear genetically primed or adapted to high levels of heat stress. For example, several studies show branching *Acropora sp.* collected from high variability environments on Ofu island (American Samoa) have higher thermal tolerances (Oliver and Palumbi 2011; Palumbi et al. 2014), although this is not the case for massive species (Klepac and Barshis 2020). Another recent study indicates that directional selection, a process by which extreme heat events weed out thermally sensitive individuals within a coral community resulting in elevated baseline thermal thresholds of the recovered populations, may be occurring in reefs in the Phoenix Islands Protected Area (PIPA) (Fox et al., *Science, in review*). Given the projections of more frequent and severe MHWs, a robust scientific understanding of the mechanisms of resilience and the circumstances that enhance both resilience and recovery are therefore key components of the global strategy to ensure coral reef futures under global climate change.

To uncover how these mechanisms have and are acting on reefs today, we must study reefs that have survived multiple MHWs. Few reefs have experienced a long history of thermal stress capable of producing bleaching, however one such region is the Central Equatorial Pacific (CEP). Reefs here have been subject to heat waves from El Niño for hundreds if not thousands of years. These reefs therefore could provide key insights into 1) whether adaptation can occur at a pace fast enough to keep up with global warming resilience; 2) the mechanisms underpinning resilience and recovery and 3) the environmental and ecological circumstances that optimize resilience and recovery. However, efforts to make these insights in the CEP and other regions have been limited

by three main factors. First, ecological surveys conducted during bleaching events are usually limited to coral reefs that are accessible by boat or airplane, and even those that are monitored, include a very small fraction of total reef area that is accessible to divers. Second, the bleaching histories of coral reef ecosystems are not known. Few reports of bleaching were published prior to 1998, and subsequent events monitored in a few select locations, mostly opportunistically. Third, lack of accurate on-reef temperature measurements prior to the satellite era limit our knowledge of the history of thermal stress to which coral reef communities have been exposed, the amplitude and duration of stress events, and the secular warming trend. Shipboard and mooring temperature measurements are often insufficient to quantify MHW severity pre-1982 and aggregations of such measurements are often spatially and temporally sparse near coral reefs, especially Pacific reefs, prior to the 1970s (See Fig. 4.1) (Kennedy et al. 2011). Small changes in temperature and the duration of such temperature anomalies matter in a coral reefs' response to MHWs yet interpolated SST products may yield unreliable metrics of thermal stress. Together, these gaps in data limit our ability to accurately assess these questions about adaptation and reef resilience,

In this study we address these gaps in knowledge by 1) Constructing coral reef bleaching histories across space and through time using a novel coral skeletal bleaching proxy and 2) developing and applying a new tool with which to reconstruct accurate, monthly resolved on-reef temperature histories. By comparing the history of bleaching with the history of thermal stress events we have been able to evaluate changes in the sensitivity of corals to increasing levels of thermal stress over time.

The study focuses on corals collected on seven islands in the Niño 4 region of the CEP (Fig. 5.1). First, we use a logistic model to pool stress band records of coral cores collected from the dominant reef building *Porites sp.* on each reef into a regional-scale history of coral reef bleaching and assess the severity of the 2015-2016 bleaching event in the context of the last century. Second, we generate a history of monthly-resolved on-reef SSTs using the new laser Sr-U method, focusing on Jarvis Island. Using both the bleaching and SST records, we then evaluate temporal patterns and potential shifts in thermal sensitivity of *Porites*, and discuss the implications for the broader coral reef community.

5.2 Methods

5.2.1 Coral stress bands as a proxy for bleaching

174 *Porites* coral cores from 7 islands in the CEP (Fig. 5.1) were analyzed for skeletal stress bands following the method described in chapter 2. Briefly, the cores were CT scanned and the resulting 3D images were used to compute skeletal density along the coral growth axis. Abrupt anomalously high-density bands (stress bands) were identified and aged using annual banding patterns. Stress bands serve as indicators of times in a coral's life during which it bleached. In chapter 3 the proportion of stress banding in a collection of coral cores during a given bleaching event is then used to estimate prevalence of bleaching within a reef community. Recent evidence shows that while community bleaching and *Porites* stress banding may correlate, the mechanisms by which *Porites* and other members of the community adapt or acclimatize to thermal stress is fundamentally different on CEP reefs. Due to the length of the bleaching record generated here, there is potential for significant shifts in thermal tolerance between species. We therefore limit the interpretation of this record to the *Porites* community on each reef.

5.2.2 Pooling reef sites to assess bleaching on a regional scale using a logistic model

Although the total number of corals sampled across the region was large (n = 174), colony size and distribution constrained sampling such that few records extend into the early 20th century with some islands having longer records than others (Fig. A5.1). Because of the comparative paucity of cores covering the early part of the record, we use a logistic model to enhance our reconstruction of bleaching.

The severity of a bleaching event at each island was estimated using two regression parameters – the 'regional severity' of the event, γ, and the relative tolerance of the coral community at that island β. A unique γ was estimated for each event during which at least one stress band was identified at one island. Thus, for each island j and event k, stress band prevalence was estimated as:

$$p_{jk} = \frac{\exp(\beta_j + \gamma_k)}{1+\exp(\beta_j + \gamma_k)} \tag{5.1}$$

Estimates were then averaged across all the studied islands to produce a region-scale stress band prevalence. We validated the estimated stress band prevalences against bias-adjusted regional averages of the observed stress band counts (Fig 5.6). Uncertainty in the estimates of regional scale bleaching are derived via the delta method using the covariance matrix of fitted gamma and beta parameters. The RMSE of the estimates was 8.6%, with $r^2 = 8.32, p < 0.001$. Based on the consistency with observations from both high-n and low-n events, we confidently use these estimates to reconstruct regional community bleaching over the full record, spanning the last century. Stress band prevalence for each event was then converted to an estimate of reef community bleaching using the established relationship for massive *Porites* in the CEP (Fig 5.2b) (Mollica et al. 2019).

5.2.3 A centennial scale proxy SST record from Jarvis island

A 196 cm long *Porites* skeletal core (J018) collected from a living colony at Jarvis island was used to reconstruct a monthly resolved Sr-U proxy record of SST on the reef. The core was prepared and sampled following the methodology used in chapter 4 of this thesis. Briefly, the core was slabbed along the axis of maximum growth, scored, and made into 7 cm thick sections. Laser spots were targeted along the growth axis of each section at a frequency of roughly 12 spots per mm^2 distributed randomly within a track spanning 2 mm laterally, or 24 spots per mm down core. A coarse (annual) age model was made for the core using CT images, and a sample near the base of the core was dated by U-Th to be 1931±1 (following the methods of Burns et al. (2016), see table A5.2), which is consistent with banding estimates of growth rate (2.4 cm per year), although slightly younger than the corresponding band age at that point (1927). This may be a result of bias from secondary crystal growth (minor amounts of which were found in the corresponding thick section, and avoided during laser sampling) or inaccuracies in the band-based age model. Sr-U was calculated from binned Sr/Ca and U/Ca element ratios collected at each laser spot using a bin size of 4 mm with a boxcar overlap of 2 mm. This produced roughly 12 Sr-U values per year, varying with local growth rate of the coral.

Based on analyses presented in chapter 4 we do not expect data products synthesizing instrumental SST measurements to precisely capture the temperature at Jarvis island, especially prior to the satellite era. However, we can with reasonable certainty expect the timing and phase of interannual (i.e. ENSO cycle) variability to be consistent between interpolated instrumental

SSTs and our proxy record. In the absence of a sub-annual age model for J018 we therefore tune the age model of the proxy record to reflect this coarse variability as follows. The record was mapped with homogenous spacing from May 2012 (time of collection) to January 1925 (start of the record based on annual banding). The signal was then standardized and smoothed to a 6-point running average, and aligned with a similarly standardized and smoothed HadISST record from the 1 by 1-degree cell that encloses Jarvis island. The MATLAB dynamic time warping (DTW) function was then used to align the two signals. The warping path was restricted to 6 samples (~half a year) strait-line fit between the two series to prevent overfitting. The resulting age model was then applied to the unsmoothed data.

The monthly-aged Sr-U record generated J018 was then converted to SST using the calibration presented in Chapter 4. Because of the limited number of corals included in the calibration so far, we compared the chapter 4 calibration (Fig. 5.5, grey shaded region) to a calibration consisting of N1344, J1222, and the top 10 years of J018. There is no significant difference between the two relationships, lending further credence to the assumption of a universal Sr-U calibration (at least for *Porites* corals). The resulting Sr-U SST record is presented in figure 5.3. While the calibration data for each of the three corals (when considered individually over their respective calibration periods) have slightly different relationships with SST (Fig. A5.3), the prediction envelops ($p < 0.05$) of each individual regression overlap near completely, suggesting no significant difference in the reconstructed SST. Of note is the difference in slope between the three relationships; in particular, J018 is significantly steeper than N1344. This may be evidence of a slightly nonlinear relationship with SST, however given that the two datasets only barely overlap and are more restricted in the Sr-U domain than the J1222 data (which shows no evidence of nonlinearity), we attribute these differences in slope to the limited SST range exhibited by each coral. In addition, the steeper J018 data may be a result of the underrepresentation of the 2010 MHW (see section 5.3.3).

5.2.4 Calculating Thermal stress as Degree Heating Months (DHM)

Degree Heating Weeks (DHW) are the gold standard of quantifying thermal stress for coral reefs during MHWs (Gleeson and Strong 1995). However, they were developed for satellite SST measurements made at high temporal and spatial resolution, largely as a forecasting metric (e.g. van Hooidonk and Huber 2009). In an effort to quantify the impacts of marine heatwaves prior to

the satellite era on coral reefs, a lower resolution Degree Heating Month (DHM) has been calculated from the coarser SST products made from temperature measurements pre-satellite (HadISST, ERSST, Kaplan Extended SST, etc.) and GCM output (Donner 2005; Donner et al., 2007; Lough et al., 2018; etc.). Calculating DHMs has not been standardized across studies using the metric, but does rely on the same threshold for accrual of thermal stress (the maximum monthly mean). Here we calculate DHM for two instrumental data products (HadISST v.1.1 and ERSSTv5) as well as the J018 Sr-U proxy record via the percentile-based threshold established for Jarvis island in Chapter 3 (Mollica et al., 2019). For comparison with the region wide estimates of bleaching, we calculate DHM using the average SST in the Niño 4 region and the average threshold of the 7 islands. It should be acknowledged that DHM over the whole of the Niño 4 region does not reflect the thermal stress experienced at any one reef, as thermal stress varies significantly within the region, most prominently with longitude (e.g. Fig. 5.1). A more accurate approach would utilize a weighted average of SST from each reef, however the paucity of the instrumental record precludes this type of analysis for much of the record (three of the reefs included in the regional bleaching estimate fall in the same cell of the HadISST). In the future, proxy records may shed light on the variations in thermal stress among these islands, but at this time we are limited to a regional estimate of SST and thermal stress.

5.2.5 Analytical and empirical conversion of Jarvis thermal tolerance curve

Because TH used in constructing the thermal tolerance curve for Jarvis island in chapter 2 are calculated using DHW, and the TH used here are calculated using DHM, the relationship must be converted. However, due to the properties of the lognormal CDF function (i.e. it truncates at 0) the conversion is not straightforward. DHM, by the nature of their calculation, truncate small DHW events, and thus an event with positive DHW may have zero DHM and a zero Total Hotspot when calculated from monthly resolution SST. We use an empirical linear relationship between DHW and DHM calculated using the chapter 2 dataset to convert the thermal tolerance curve to monthly Total Hotspot (Fig. 5.4f, solid orange line). However, because this curve truncates at zero TH, it no longer has the functional form of the lognormal CDF. We therefore also evaluate an analytical conversion using DHM calculated form the chapter 2 dataset. We find that the data presented here are more closely in line with the empirical conversion.

5.3 Results

5.3.1 CEP reefs bleach in response to El Niño events

Stress bands corresponding to colony bleaching were identified in coral cores collected at all sites, concurrent with historical El Niños (as described by SOI, MEI, etc). Our earliest identified stress band was deposited in 1897, six years above the base of the oldest core. Regional pooling via logistic regression (Methods 5.2.2) was conducted for all detected bleaching events post 1930, at which time records at 3 islands were extant. Bleaching events were generally coincident with SST anomalies in the Niño 4 region (Fig. 5.2a,b). Several bleaching events early in the record (e.g. 1945, 1953) occur during less prominent peaks in the Niño 4 index, possibly a result of underestimated temperatures due to a paucity of observations in the region during the early part of the 20^{th} century.

5.3.2 Stationarity of the Centennial Bleaching Record

In our record, severe (greater than 30%) bleaching events have occurred regularly in the CEP since at least 1930, the earliest El Niño event in our record. Over this time period, there is no significant trend ($p = 0.926$) in the severity of bleaching response during stress events, suggesting that ocean warming had negligible effects on the impact of MHWs on coral communities in this region prior to 2015.

Despite the lack of trend in the magnitude of bleaching events, the frequency of bleaching events in our record increases during the last 30 years from 1.5 per decade to 2.67 per decade. While the increase in frequency in our record could also be explained by a sampling bias (i.e. more core records span recent years, making the detection of low-level bleaching events more likely during the last 30 years), an increase in the frequency of coral bleaching events has been observed in other regions and globally (Donner et al. 2017; Hughes et al. 2018), and has been shown to be a result of more frequent severe El Niño driven MHWs (Hughes et al. 2018).

In contrast to the past 100 years, the 2015/2016 MHW was significantly (95 percent prediction interval, $p < 0.001$) more devastating; bleaching exceeded all previous events in the record at every reef, and caused an average $95.2 \pm 2.2\%$ (2σ) bleaching across the region. It was unprecedented in terms of both regional peak temperature and anomaly duration (Fig. 5.2b), and globally produced the most widespread coral bleaching event in instrumental history (Hughes et al. 2018). This was heralded by a 2014 shift in from cool phase of the PDO that had lasted since

2008 into one of the most consistently warm PDO phases on record after the most recent warming hiatus.

5.3.3 Monthly Sr-U proxy records 20th century SST

The lack of trend in regional bleaching severity over the 20th century raises a significant question: have CEP reefs steadily increased their thermal tolerance as they adapt to increasingly severe MHWs, or has the severity of MHWs remained stationary prior to 2015, and little to no adaptation has occurred over the time period. Due to the paucity of the instrumental record (particularly in this area, see Chapter 4 Fig. 4.1b) prior to the satellite era, resolving this question with existing data products is unlikely. To investigate the capability of coral proxy records in resolving MHWs, we generated a monthly resolved Sr-U record from one coral collected at Jarvis island (J018, 1925-2012). SST was calculated using the calibration given in chapter 4 of this thesis, and validated using satellite SST measurements (Gap-filled Pathfinder v5.3 from 1982-2012) (Chapter 3; Mollica et al., 2019) and found to have an excellent correlation ($r^2 = 0.702$, $p < 0.001$). A monthly age model was generated from the core using a combination of annual bands, U-Th dating, and dynamic time warping of the smoothed Sr-U signal (Methods 5.2.3). We then applied this calibration down core to reconstruct historical SST at Jarvis (Fig. 5.3).

To compare instrumental and Sr-U temperature pre-satellite, we adjusted SST from the 1° x 1° grid cell of the HadISSTv1.1 gridded data product containing Jarvis island based on higher resolution (4 km Pathfinder v5.3) satellite SST from the site of collection (via linear regression). Over the satellite era, two notable divergences occur between the two records – 2010, during which Sr-U SST significantly underrepresents the peak of the El Niño, and 1983, during which the peak of the El Niño is exaggerated. Neither of these discrepancies can be readily attributed to analytical error, and in fact the 2010 El Niño is also underpredicted in the Jarvis 1222 calibration coral (Chapter 4 Fig. 4.7) making analytical error unlikely. It may be that during the 2010 marine heatwave, SST at the site of collection was mitigated by local factors (e.g. upwelling on a scale not captured by satellite or logger placement) that were unique to that event. The 1983 excursion may be a result of abnormalities in coral skeletal deposition during bleaching events that the Sr-U proxy is incapable of resolving (although this coral did not bleach for a prolonged enough period to deposit a stress band during 1987, similar abrupt spikes in the record appear in 1998 and 1941, two events when the coral did form a stress band). To mitigate the effect of such spikes in

calculating the severity of MHWs, we bootstrap resample the data assuming a normal error distribution (Methods 5.2.5).

HadISST and the Sr-U reconstructed SST show significantly less agreement pre-1982, highlighting the uncertainties and scarcity in early instrumental measurements in this area. Over the length of the record, the trend in Sr-U SST (0.35 ± 0.098, °C per century, linear robust regression) is warming significantly compared to the adjusted HadISST (-0.0921 ± 0.13 °C per century) which is within error or stationarity. Although a warming trend is also observed in the ERSSTv5 data product when adjusted similarly (1.34 ± 0.14 °C per century), the effect in our record is more muted, and in fact 20th century warming in the area has been shown to be driven by ENSO variability (Coats and Karnauskas 2017). It is therefore unlikely that the background SST trend has had appreciable effect on coral thermal tolerance at Jarvis relative to changes in MHW severity.

5.3.5 Sr-U versus Sr/Ca

Given the anomalies in the Sr-U SST record (e.g. the underrepresentation of 2010, the jagged portion of 1998, etc.) and the potential effect of stress band formation on the Sr-U proxy, it is worth assessing the quality of the Sr/Ca proxy during these time periods, and over the record as a whole. To do this, we constructed an internal calibration for both Sr/Ca and Sr-U over the top 10 years of the record, and compared 1) the quality of each calibration, 2) the ability of each proxy to capture the mean, variance, and extreme event magnitude over the satellite era. The results are summarized in table 5.1. Overall, the Sr-U proxy does significantly better in terms of error in predicted SST, calibration variance explained, as well as capturing the mean and variance over the satellite period. We attribute the deviations during extreme events to be a product of significant alteration of the calcification process during bleaching (perhaps due to significant changes in the residence time of fluid in the calcifying space). While the Sr-U proxy does not fully correct for these changes, it does improve the capture of extreme SSTs over Sr/Ca alone. Further development of the proxy to account for these deviations may include the use of an additional geochemical signal or structural marker that is able to indicate periods of coral bleaching or decoupling if the Sr-U proxy, or refinement of the sampling method during times of bleaching or slow growth.

5.3.4 Assessing changes in thermal tolerance of CEP corals

Corals at Jarvis island have been shown to exhibit a predictable response to thermal stress when quantified as Total Hotspot (TH), or the sum of weekly temperatures above an established bleaching threshold (See Chapter 2). Here we quantify MHW severity in a similar manner but at a monthly scale (the resolution of our Sr-U record) using degree heating months (DHMs, Methods 5.2.5). A bootstrap resampling of the Sr-U SST was used to calculate TH for each MHW and compared to the regional bleaching estimates (Fig. 5.4c) and the reconstructed bleaching at Jarvis Island (Fig. 5.4f). We calculated TH for each event using both the HadISST and ERSST for the Niño 4 region (Fig. 5.4a,b) and the adjusted HadISST and ERSST at Jarvis island (Fig. 5.4d,e). Given that the severity of 2015, even in terms of both thermal stress and response, is a clear departure from the pattern of previous events it was excluded from all subsequent analyses.

Based on the island-specific relationships between TH and reconstructed community bleaching observed during the satellite era (Chapter 3 Fig. 3.6), bleaching events recorded at a reef (or collection of reefs) with a static thermal tolerance are expected to fall along a predictable relationship with a functional form of a lognormal cumulative distribution function (CDF). If thermal tolerance of the same community was instead increasing, bleaching events would follow a series of lognormal CDFs translating to higher and higher TH values for the same level of bleaching. The regional bleaching estimates do not follow this functional form when compared to the HadISST and ERSST for the Niño 4 region when considered as a whole, however there are significant relationships characteristic of thermal tolerance curves when considering only the satellite era (Fig. 5.4a,b red curve) in both the ERSST and HadISST ($p<0.01$ in both cases). For both products, TH prior to the satellite era fall to the left (less tolerant side) of the curve, which could imply two things: first, thermal tolerance has increased in the region over the time period, or second, instrumental SST pre-satellite did not capture peak thermal stress during MHWs, leading to underestimates of TH. While a robust differentiation between these two causes cannot be made at a regional scale with the current data, we consider it likely that the second factor plays a large roll in the observed pattern given the numerous events for which bleaching was observed but TH from either or both the ERSST and HADISST was zero.

To use proxy SST to resolve this issue in assessing the regional thermal tolerance, a record from each reef would be required and is beyond the scope of this thesis. The J018 Sr-U record

cannot be extrapolated to the region as a whole as TH from the Jarvis island record do not correlate with regional bleaching (Fig. 5.4c), suggesting Jarvis SST does not accurately capture the impact of MHW on the entire Niño 4 region. However, the J018 Sr-U record does allow for the assessment of thermal tolerance at Jarvis island. When examining the bleaching record at Jarvis alone, the thermal tolerance tendencies observed in the regional data (Fig. 5.4a,b) are not observed; in fact, bleaching levels show no apparent pattern when compared to TH calculated using either the adjusted HadISST and ERSST at Jarvis (Fig. 5.4d,e). However, the Sr-U based TH is consistent with a single lognormal CDF over the entire record – strong evidence that Jarvis has held a static thermal threshold over the 20th century.

We compared both an analytical and empirical conversion of the thermal tolerance curve fit to satellite based TH in Chapter 3 (Fig. 3.6a) to the extended bleaching dataset and found that both forms are roughly consistent (Methods 5.2.6). The empirical form is more closely correlated with the observations (r^2 = 0.45), and there is no systematic difference between residuals from events early in the record (cool colors) and those later in the record (warm colors) (Fig. 5.4f). It also overlaps the error envelope of thermal tolerance curve fit using the 20th century data for all but the lowest TH values, where the deviations discussed in 5.2.5 likely impact its applicability. There is one predominant outlier from this relationship, 1966, in which bleaching was significantly higher than expected for the associated TH. The Sr-U SST record during this event is over 1 °C less than either the adjusted HadISST and the ERSST, which may suggest the proxy underestimated SST during this event similar to the 2010 event during the satellite record. It is possible but unlikely that this point is evidence of a lower thermal tolerance earlier in the record, as the 1943 event is consistent with the static thermal threshold curve (although there are only 3 cores at Jarvis that extend back to this event giving any estimate of bleaching severity a high uncertainty). We therefore neglect this outlier, and conclude that no significant shift in thermal tolerance at Jarvis island has occurred over the 20th century.

5.4 Discussion

For at least the last 10,000 years, the CEP has experienced more regular, severe heat waves (produced by ENSO) than any other ocean region, making it ground zero for coral thermal stress

(Carré et al. 2014). Because our record shows severe bleaching events have occurred in the CEP for over a hundred years (as far back as our record extends) coincident with strong El Niño events, and ENSO amplitude is estimated to have remained roughly constant over the last 4,000 years, (Carré et al. 2014) it is conceivable that mass coral bleaching in the CEP has been occurring for millennia. Repetitive bleaching may therefore have been commonplace for these reefs long before it became a global phenomenon, in contrast to long term records of coral bleaching from other regions (Hughes et al. 2018; DeCarlo et al. 2019).

Despite this regular severe heat stress, and a correspondingly severe bleaching response, coral reefs in the CEP have not only survived but thrived; prior to the 2015-2016 super El Niño these reefs boasted relatively high coral cover among reefs globally (e.g. Obura and Mangubhai 2011; Barkley et al. 2018) which they have maintained through or recovered after MHWs, in contrast to other regions (e.g. Caribbean, or the Great Barrier Reef) (Hughes et al. 2017; Oliver et al. 2018). Several mechanisms for this resilience have been suggested, including a balance between major selective pressure from repeated severe bleaching and multi-year recovery periods (Fox et al., *Science, in Review*), coral acclimatization through development of a thicker tissue layer (Mollica et al. 2019), and a more resistant host-symbiont relationship developed under large-magnitude high-frequency variability (Safaie et al. 2018). However, the effectiveness of these mechanisms has not been evaluated in the context of centennial scale warming and interannual variability such as ENSO or PDO.

The coupled bleaching and Sr-U derived SST records presented in this chapter indicate that *Porites* corals at Jarvis have maintained a constant thermal tolerance over the 20th century. Furthermore, no significant difference in thermal tolerance was observed in the young *Porites* colonies relative to the older colonies sampled. We therefore conclude that *Porites* colonies on Jarvis, at least those that have survived multiple heatwaves, have neither increased their individual thermal tolerance through methods of adaptation or acclimatization, nor have they experienced significant selective pressure in their new recruits. These characteristics were also observed in the *Porites* of the Great Barrier Reef (GBR) and nearby Coral Sea by DeCarlo et al., (2019) with the exception of the anomalous 2016 event. These observations raise important questions:

First, why is there no increase in the thermal tolerance of *Porites* populations following MHWs severe enough to produce selective pressure in other species? It is evident purely by the

age of some of the colonies sampled in this study that many *Porites* in the CEP have bleached during, yet survived, a long history of severe MHWs. The differences in the degree of stress required for a *Porites* colony to bleach, form a stress band, and die from catabolysis can be substantial (DeCarlo et al. 2019; Mollica et al. 2019). One hypothesis as to their survival mechanism involves the unusually thick tissue layer characteristic of CEP *Porites*. Perhaps these nutrient reserves support colonies through lengthy bleaching, and under extreme conditions allow polyps to retreat and survive deep inside the skeleton (Ellen Park, SSF thesis, WHOI 2019). DeCarlo et al., (2019) found that *Porites* in both the GBR and Coral Sea, after decades of maintaining a consistent thermal tolerance, produced significantly fewer stress bands during the 2016-2017 MHW despite having been observed to bleach. They hypothesize that this abrupt shift in thermal tolerance is a result of acclimation following the 2015-2016 MHW, just one year prior (this pairing of two severe MHWs only one year apart does not occur earlier in their record, nor does it occur in our SST reconstruction from Jarvis). They suggest that this increase in tolerance is a result of stress priming, which, although due to the time between events is unlikely to be a result of temporary upregulations in heat shock proteins as observed in Mcclanahan et al. (2019) could be the result of an increase in tissue biomass in response to the first event.

Second, given these coping mechanisms for extreme stress, why then do *Porites* on different CEP reefs (Mollica et al. 2019) and elsewhere (DeCarlo et al. 2019) exhibit different thermal tolerances? If chronic differences in tissue thickness drives the difference in tolerance between these reefs, then these differences must have arisen from selective pressure. However, if this is the case, the lack of adaptation over the bleaching history reconstructed in this study suggests that such pressure is acting on a much longer timescale than in other species. This is consistent with the longevity of *Porites* in the CEP.

Third, what then is the capacity of these reefs in the CEP to adapt to 21st century climate change? It is possible, given the projected increases in El Niño frequency (Cai et al. 2014), that the acclimation observed by DeCarlo et al. (2019) may also occur in the CEP, although whether this priming has lasting effects remains to be seen. An increase in the frequency of the PDO (Xu and Hu 2018) may also produce more frequent intense MHWs in the region, as ENSO heatwave are amplified by positive PDO phases. This effect may be dampened, however, by predictions of simultaneous dampening of PDO spatial SST anomalies. While the uncertainties in interpolated

SST products preclude a robust analysis, there is evidence that unlike Jarvis, some of the other reefs in the CEP may have experienced adaptation over the last 100 years. When compared to estimates of thermal stress in the Niño 4 index, our regional bleaching estimates suggest that the region as a whole has become more thermally tolerant (Fig. 5.4a,b). To definitively evaluate this possibility, accurate SST must be obtained for each of these reefs. To this end, the Sr-U proxy shows definitive promise in reconstructing seasonal and interannual variability in ocean temperature, and in capturing the magnitude of historical MHWs.

Given the disparity between the adaptive mechanisms of *Porites* and other species, it is unlikely that long term conclusions regarding thermal tolerance can be extrapolated from these massive colonies to other members of the community (as was done in recent decades in Chapter 3). While these centenarian corals have lived through and recorded their response to numerous bleaching events, shorter lived coral species (e.g. *Acropora*, *Pocillopora*) may have turned over their population as many as 10 times during the 20th century. The Jarvis Sr-U record suggests multiple MHWs capable of exerting significant selective pressure on these species have occurred over the last 100 years, which could have substantially increased their tolerance as observed in Fox et al. (*Science, in Review*). In light of this potential decoupling between the *Porites* and less tolerant reef species stress we do not generalize the static thermal threshold of the Jarvis *Porites* to the broader community.

Finally, the impacts of the unprecedented 2015-2016 super El Niño must be taken into account when considering the future of these reefs. Despite a long history of surviving prolonged elevated temperatures, if 2015-2016 heralds a new regime of MHWs, these reefs may lack the capacity to survive new levels thermal stress. Although the increasing frequency of heatwaves expected in the region (Hooidonk et al. 2016; Hughes et al. 2018) may provide opportunities for acclimation to persist between events, the recovery time that these reefs have been allowed to see (~5-10 years) may decrease to the point at which the reefs cannot recover quickly enough before the next event. The future of these reef systems, along with others around the globe are therefore ultimately dependent on our ability to reduce emissions and curb the trajectory of warming.

5.5 Figures

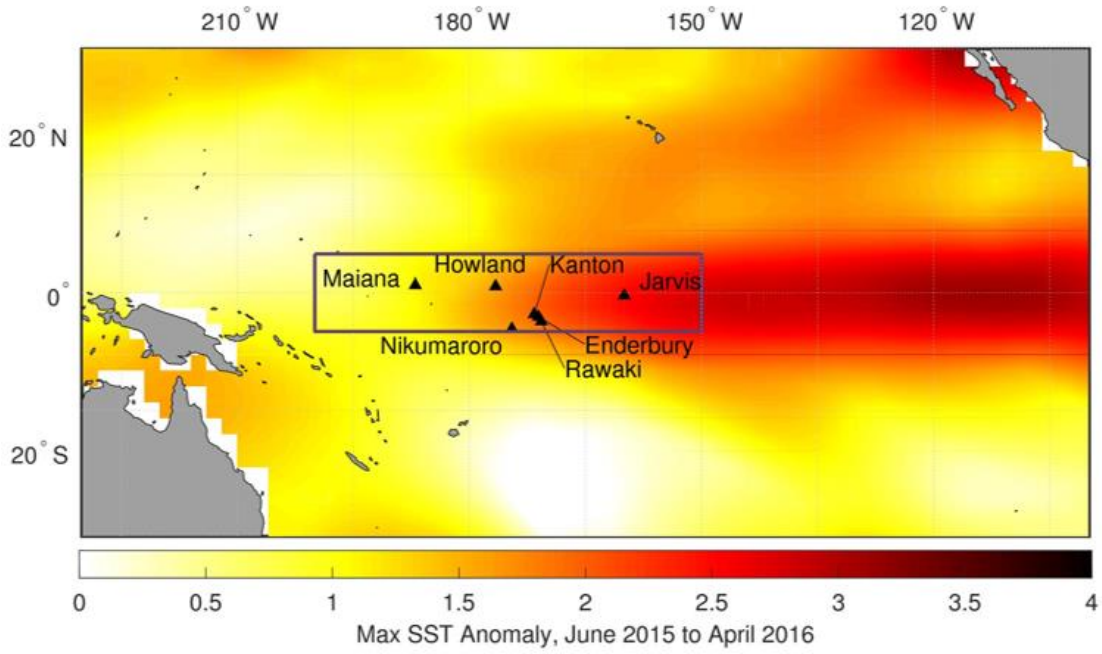

Fig. 5.1. The seven reef sites (black triangles) used in our record, overlain on the max SST anomaly (ERSSTv5) during the 2015-2016 MHW. The box outlines the Niño 4 region. In this study we use the seven reefs shown to compute a regional coral bleaching estimate for MHWs in the Niño 4 region, and use the average SST within the region to index the associated thermal stress.

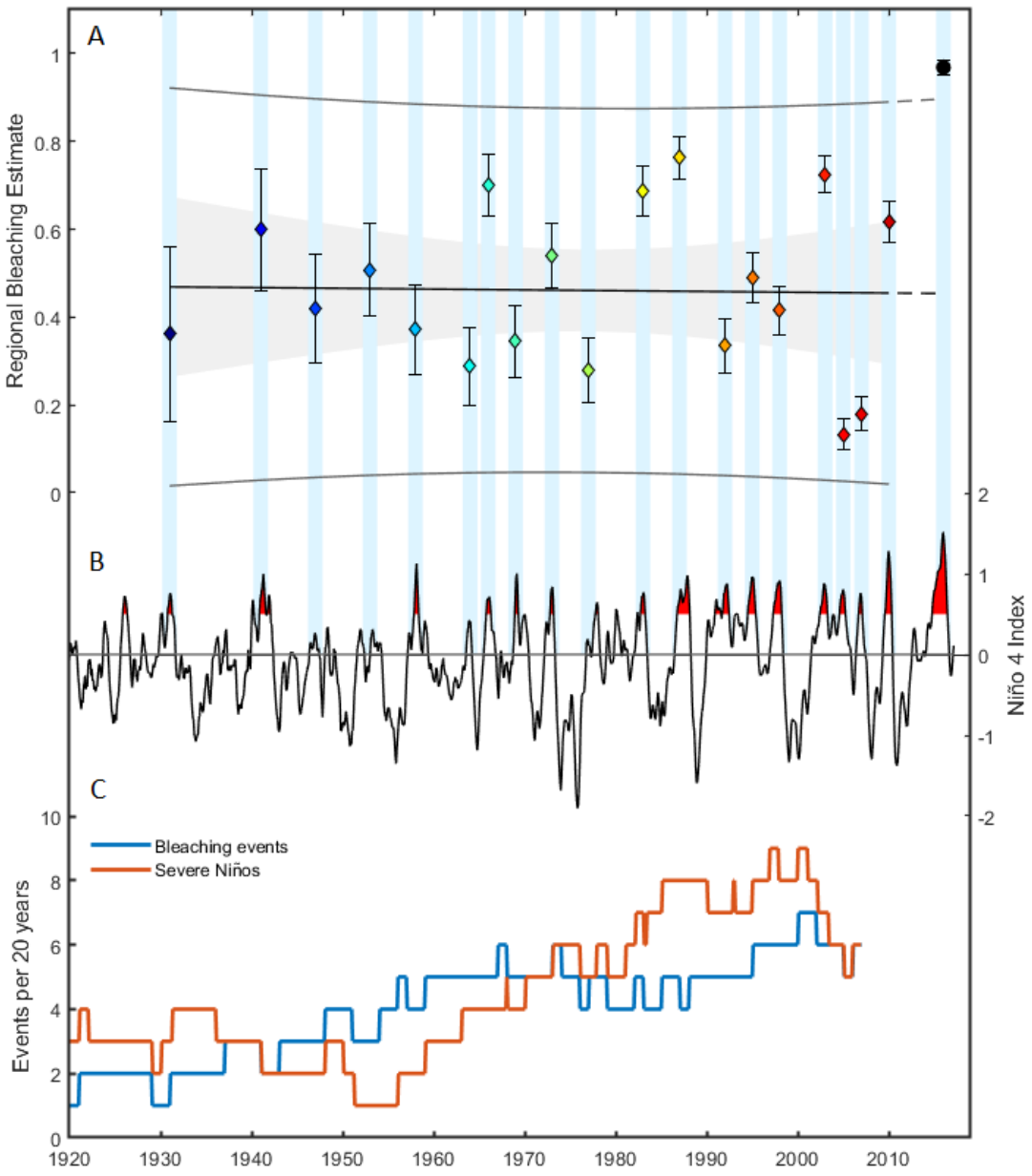

Fig. 5.2. A: Reconstructed estimates of coral bleaching using the logistic model over the last 100 years. There is no significant trend (p = 0.659) prior to the 2015-2016 MHW, the severity of which exceeded 95% prediction bounds on the prior trend, demonstrating the unprecedented nature of the event. B: Niño 4 index, with temperature anomalies above 0.5 degrees C highlighted in red. El Niño events corresponding to reconstructed bleaching events are highlighted in blue. C: Frequency of bleaching events in 20-year windows compared to strong El Niños. Logistic regression was used to augment time periods of low core counts by estimating island and event characteristics using the entire record (see supplementary material).

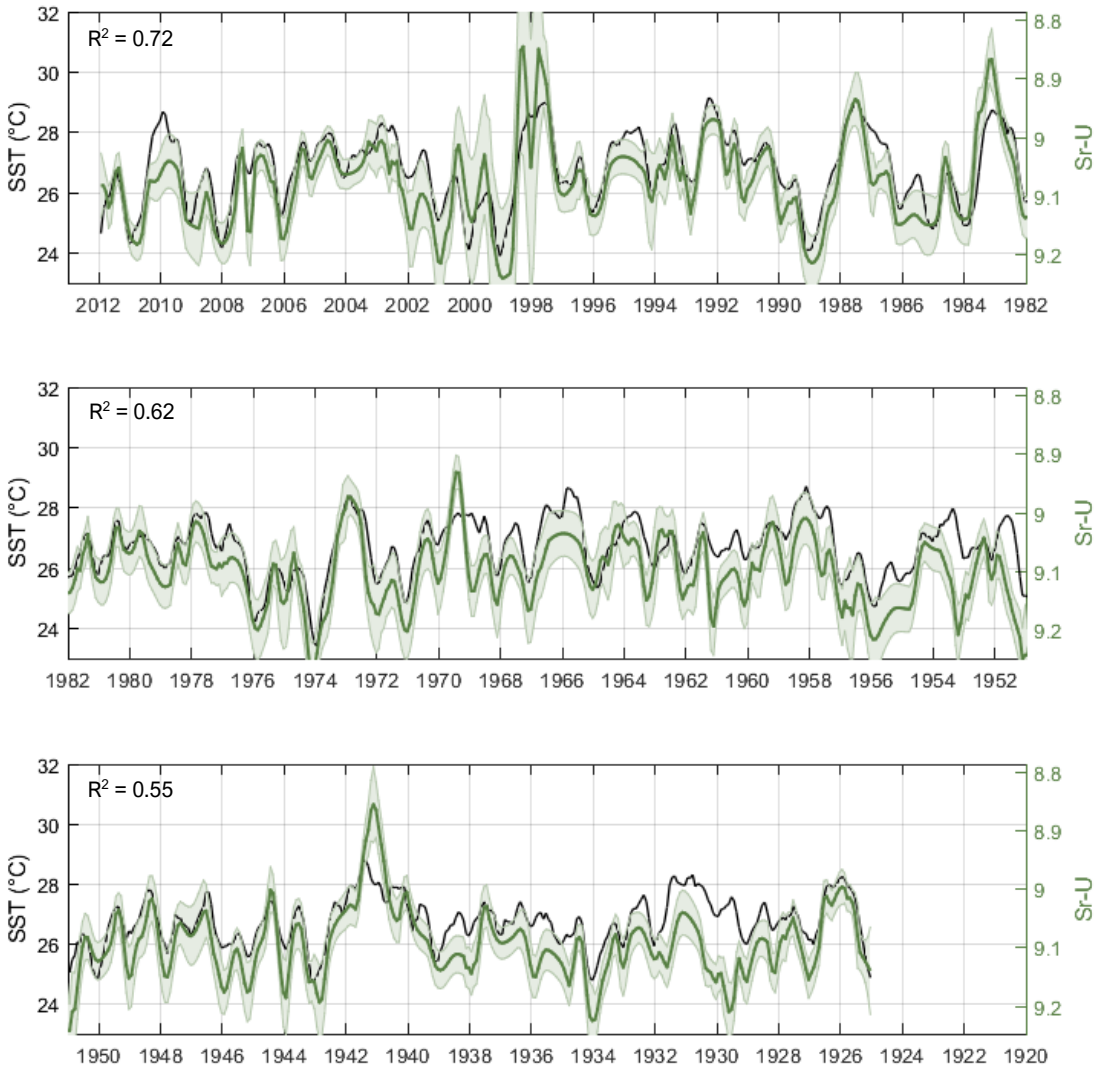

Fig. 5.3. Monthly Sr-U reconstruction of SST at Jarvis island (from core J018). The Sr-U (green) has been aligned with the SST axis using the calibration presented in chapter 4. The adjusted HadISST (black) has been binned in the same manner as the Sr-U. Agreement between the two records is high during the satellite era (top panel), however discrepancies are increasingly observed moving back in the record, highlighting the uncertainties in the instrumental record pre-satellite.

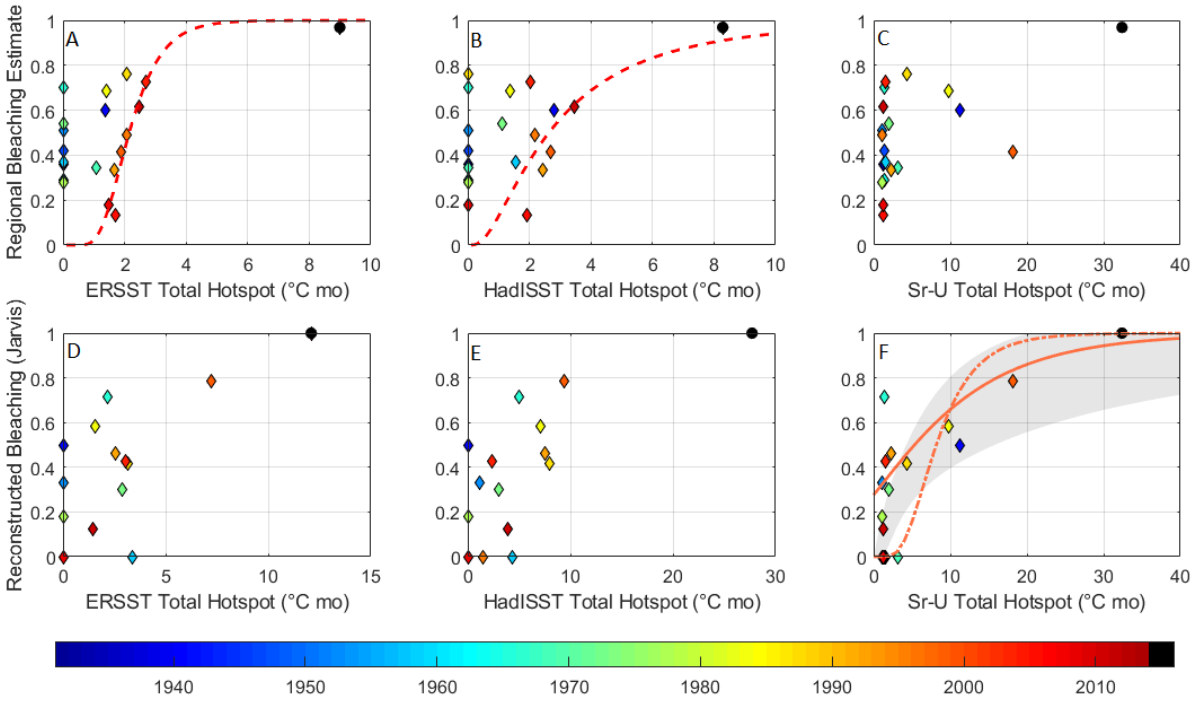

Fig. 5.4. a-c: Comparison of regional bleaching estimates and associated thermal stress (as measured by TH) when calculated using the ERSST in the Nino 4 region, HADISST in the Nino 4 region, and the J018 Sr-U proxy record. No significant relationship is observed in the regional bleaching estimates when considered as a whole. However, when considering only the satellite era, significant ($p<0.01$) thermal tolerance curves (calculated following Chapter 3) are found using the ERSST and HadISST (red dashed lines). The earlier points in the record (pre-1981; cool colors) all fall to the left of the red lines, implying one of two things: 1) coral thermal tolerance in the region has increased, or 2) heat wave SSTs pre-satellite fail to capture the magnitude of thermal stress during heatwaves (see discussion). No relationship exists in either the early or late part of the record when comparing regional bleaching to the Jarvis Sr-U. **d-f:** Comparison of reconstructed bleaching at Jarvis with TH calculated using ERSSTv5 and HadISSTv1.1 grid cells enclosing Jarvis (both of which were adjusted using high resolution satellite SST, see methods 5.3.3), and the J018 Sr-U proxy record. Bleaching at Jarvis island is not significantly related to either TH when using the Jarvis-adjusted ERSST or the HadISST, but is significantly related to TH calculated from the Sr-U proxy record (prediction envelope shown in grey). The relationship is broadly consistent with both the empirical (solid orange line) and analytical (dot-dashed orange

line) conversions of the thermal tolerance curve observed during the satellite era (chapter 3), and closest to the empirical.

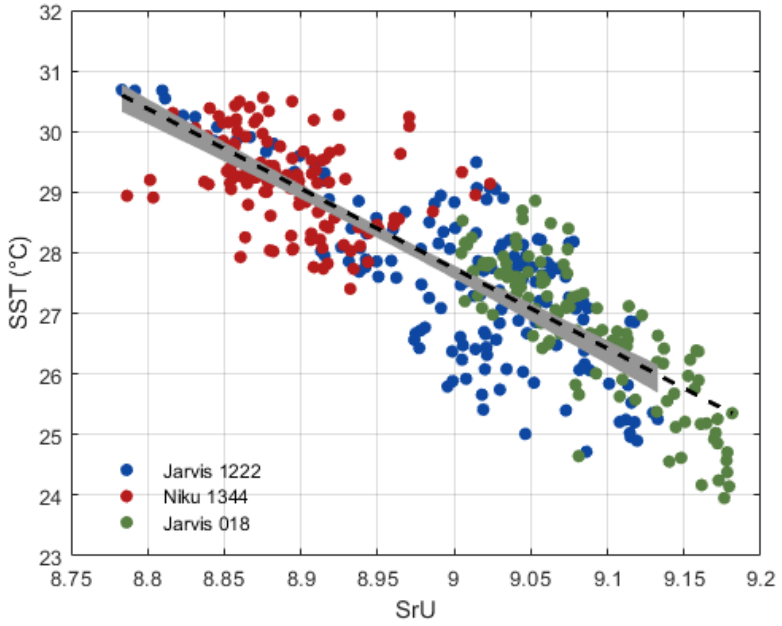

Fig. 5.5 Calibration of Sr-U to SST reproduced form chapter 4. The top 10 years of J018 have been added to the plot (green points). When considered as a 3-coral calibration, the regression (dashed black line) is within error of the 2-coral calibration (grey shaded region), lending credence to the universal Sr-U calibration hypothesis, at least in *Porites*. While J018 alone is slightly steeper than the 3-coral calibration, validation of J018 record over the entire satellite era when the 2-coral calibration is applied yields better results, suggesting this effect may be flattened over a larger range in SST.

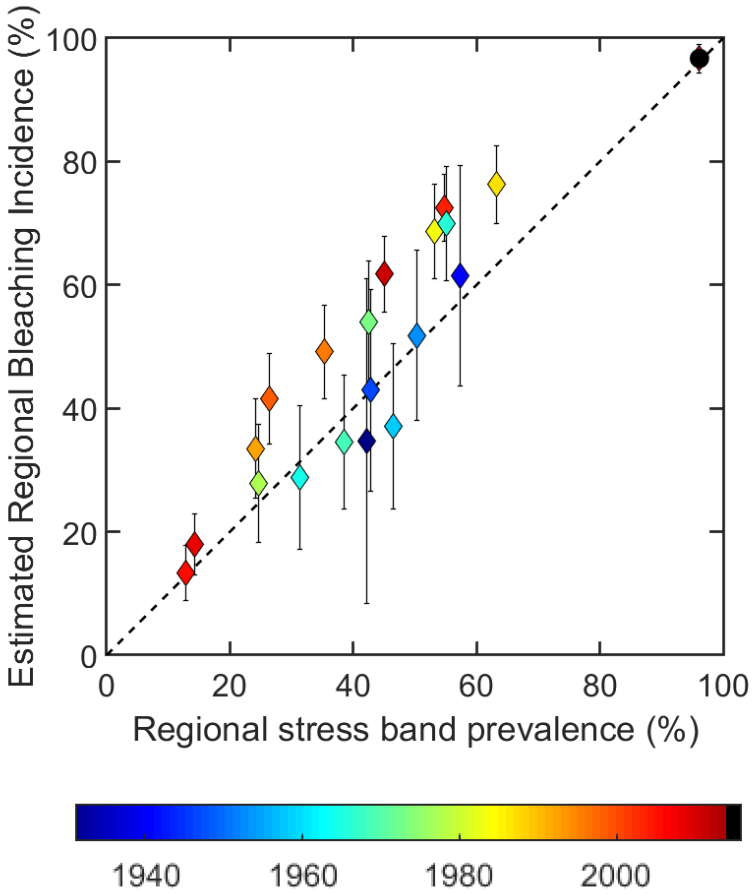

Fig. 5.6. Comparison of model estimations of bleaching incidence against bias corrected observations. The RMSE of the model is 8.6%, and is significant about the 1 to 1 line (dashed) ($r^2 = 8.32, p < 0.001$). Events are color coded by year, with the unprecedented 2015 event designated as a black circle.

Table 5.1. Comparison of Sr/Ca and Sr-U internal calibrations for J018

	Sr/Ca	*Sr-U*
Calibration equation	$SST\ (°C) = -11.70\ Sr/Ca\ +\ 133.1$	$SST\ (°C) = -17.59\ SrU\ +\ 186.6$
R^2	0.58	**0.72**
p	>0.01	>0.01
RMSE[1]	0.63	**0.53**
Satellite era		
$\mu_{inst} - \mu_{proxy}\ (^oC)$	-0.14	**-0.07**
$\sigma^2_{inst} - \sigma^2_{proxy}\ (^oC)$	-0.29	**-0.14**
2010 Peak SST difference	-1.52	**-1.01**
1998 Peak SST difference	-4.47	**1.06**
1983 Peak SST difference	**-1.28**	-2.4

[1]RMSE is robust estimate of sigma based on MATLAB robustfit algorithm.

5.6 References

Barkley HC, Cohen AL, Brainard RE, Mollica NR, Rivera HE, Drenkard EJ, Young CW, Vargas-Ángel B, Lohmann GP, Decarlo TM, Alpert AE, Lino KC, Oliver TA, Pietro KR, Luu VH (2018) Repeat bleaching of a central Pacific coral reef over the past six decades (1960-2016). Nat Biol Commun

Beck MW, Losada IJ, Menéndez P, Reguero BG, Díaz-Simal P, Fernández F (2018) The global flood protection savings provided by coral reefs. Nat Commun 9:

Bruno JF, Côté IM, Toth LT (2019) Climate Change, Coral Loss, and the Curious Case of the Parrotfish Paradigm: Why Don't Marine Protected Areas Improve Reef Resilience? Ann Rev Mar Sci 11:

Burns SJ, Godfrey LR, Faina P, McGee D, Hardt B, Ranivoharimanana L, Randrianasy J (2016) Rapid human-induced landscape transformation in Madagascar at the end of the first millennium of the Common Era. Quat Sci Rev 134:92–99

Cai W, Borlace S, Lengaigne M, van Rensch P, Collins M, Vecchi G, Timmermann A, Santoso A, McPhaden MJ, Wu L, England MH, Wang G, Guilyardi E, Jin F-F (2014) Increasing frequency of extreme El Niño events due to greenhouse warming. Nat Clim Chang 5:1–6

Carré M, Sachs JP, Purca S, Schauer AJ, Braconnot P, Falcón RA, Julien M, Lavallée D (2014) Holocene history of ENSO variance and asymmetry in the eastern tropical Pacific. Science (80-) 345:

Coats S, Karnauskas KB (2017) Are Simulated and Observed Twentieth Century Tropical Pacific Sea Surface Temperature Trends Significant Relative to Internal Variability? Geophys Res Lett 44:

DeCarlo TM, Harrison HB, Gajdzik L, Alaguarda D, Rodolfo-metalpa R, Olivo JD, Liu G, Patalwala D, Mcculloch MT (2019) Acclimatization of massive reef-building corals to consecutive heatwaves. Proc R Soc B 286:

Donner SD, Rickbeil GJM, Heron SF (2017) A new, high-resolution global mass coral bleaching database. PLoS One 12:1–17

Ferrario F, Beck MW, Storlazzi CD, Micheli F, Shepard CC, Airoldi L (2014) The effectiveness of coral reefs for coastal hazard risk reduction and adaptation. Nat Commun 5:3794

Fisher R, O'Leary RA, Low-Choy S, Mengersen K, Knowlton N, Brainard RE, Caley MJ (2014) Species Richness on Coral Reefs and the Pursuit of Convergent Global Estimates. Curr Biol 25:500–505

Frölicher TL, Fischer EM, Gruber N (2018) Marine heatwaves under global warming. Nature 560:360–364

Gleeson MW, Strong AE (1995) Applying MCSST to coral reef bleaching. Adv Sp Res 16:151–154

Hoegh-Guldberg O (1999) Climate Change, coral bleaching and the future of the world' s coral reefs. Ove Hoegh-Guldberg. Mar Freshw Res 50:839–866

van Hooidonk R, Huber M (2009) Quantifying the quality of coral bleaching predictions. Coral Reefs 28:579–587

Hooidonk R Van, Maynard J, Tamelander J, Gove J (2016) Local-scale projections of coral reef futures and implications of the Paris Agreement. Nat Publ Gr 1–8

van Hooidonk R, Maynard J, Tamelander J, Gove J, Ahmadia G, Raymundo L, Williams G, Heron SF, Planes S, Hooidonk R Van, Maynard J, Tamelander J, Gove J (2016) Local-scale projections of coral reef futures and implications of the Paris Agreement. Sci Rep 6:39666

Hughes TP, Anderson KD, Connolly SR, Heron SF, Kerry JT, Lough JM, Baird AH, Baum JK, Berumen ML, Bridge TC, Claar DC (2018) Spatial and temporal patterns of mass bleaching of corals in the Anthropocene. Science (80-) 359:80–83

Hughes TP, Kerry JT, Álvarez-Noriega M, Álvarez-Romero JG, Anderson KD, Baird AH, Babcock RC, Beger M, Bellwood DR, Berkelmans R, Bridge TC, Butler IR, Byrne M, Cantin NE, Comeau S, Connolly SR, Cumming GS, Dalton SJ, Diaz-Pulido G, Eakin CM, Figueira WF, Gilmour JP, Harrison HB, Heron SF, Hoey AS, Hobbs J-PA, Hoogenboom MO, Kennedy E V., Kuo C, Lough JM, Lowe RJ, Liu G, McCulloch MT, Malcolm HA, McWilliam MJ, Pandolfi JM, Pears RJ, Pratchett MS, Schoepf V, Simpson T, Skirving WJ, Sommer B, Torda G, Wachenfeld DR, Willis BL, Wilson SK (2017) Global warming and

recurrent mass bleaching of corals. Nature 543:373–377

Kennedy JJ, Rayner NA, Smith RO, Parker DE, Saunby M (2011) Reassessing biases and other uncertainties in sea-surface temperature observations measured in situ since 1850 , part 1 : measurement and sampling uncertainties. J Geophys Res 116:

Klepac CN, Barshis DJ (2020) Reduced thermal tolerance of massive coral species in a highly variable environment: Reduced heat tolerance of massive corals. Proc R Soc B Biol Sci 287:19–21

Logan CA, Dunne JP, Eakin CM, Donner SD (2014) Incorporating adaptive responses into future projections of coral bleaching. Glob Chang Biol 20:125–139

Mcclanahan TR, Darling ES, Maina JM, Muthiga NA, Stéphanie D, Jupiter SD, Arthur R, Wilson SK, Mangubhai S, Nand Y, Ussi AM, Humphries AT, Patankar VJ, Guillaume MMM, Keith SA, Shedrawi G, Julius P, Grimsditch G, Ndagala J, Leblond J (2019) Temperature patterns and mechanisms influencing coral bleaching during the 2016 El Niño. Nat Clim Chang 9:

Mollica NR, Cohen AL, Alpert AE, Barkley HC, Brainard RE, Carilli JE, Decarlo TM, Drenkard EJ, Lohmann P, Mangubhai S (2019) Skeletal records of bleaching reveal different thermal thresholds of Pacific coral reef assemblages. Coral Reefs

Obura D, Mangubhai S (2011) Coral mortality associated with thermal fluctuations in the Phoenix Islands, 2002-2005. Coral Reefs 30:607–619

Oliver JK, Berkelmans R, Eakin CM (2018) Coral Bleaching in Space and Time. In: van Oppen M.J.H., Lough J.M. (eds) Coral Bleaching. Springer, Cham,

Oliver TA, Palumbi SR (2011) Do fluctuating temperature environments elevate coral thermal tolerance? Coral Reefs 30:429–440

Palumbi SR, Barshis DJ, Bay R a (2014) Mechanisms of reef coral resistance to future climate change. Science (80-) 344:895–898

Safaie A, Silbiger NJ, McClanahan TR, Pawlak G, Barshis DJ, Hench JL, Rogers JS, Williams GJ, Davis KA (2018) High frequency temperature variability reduces the risk of coral bleaching. Nat Commun 9:1–12

Selig ER, Bruno JF (2010) A Global Analysis of the Effectiveness of Marine Protected Areas in Preventing Coral Loss. PLoS One 5:

Wilkinson C (2004) Status of Coral Reefs of the World. Australian Institute of Marine Science, Townsville, MC

Van Woesik R, Houk P, Isechal AL, Idechong JW, Victor S, Golbuu Y (2012) Climate-change refugia in the sheltered bays of Palau: Analogs of future reefs. Ecol Evol 2:2474–2484

Xu Y, Hu A (2018) How would the Twenty-First-Century warming influence pacific decadal variability and its connection to North American Rainfall: Assessment based on a revised procedure for the IPO/PDO. J Clim 31:1547–1563

Chapter 6 – Future Directions

6.1 Introduction

The harsh reality of modern coral reefs is that, like so many of nature's wonderful ecosystems, they are under direct and imminent threat from anthropogenic climate change. In the face of this reality, fatalism and tragic drama have become wide spread among the coral reef research community, coloring many recent publications with the gloomy air of documenting the extinction and disappearance of coral reefs as we know them today. While some researchers may be playing up this gloom and doom sentiment to garner a larger spotlight on the threats (and thereby generate interest in saving coral reefs), I feel that this is a counterproductive and possibly dangerous practice for two reasons. First, it obfuscates the truth evident in many recent studies, including this thesis, that suggest some reefs may have the capacity to survive and even thrive in a warming world through local environmental mitigations (Wall et al. 2014; DeCarlo et al. 2017) or adaptive capabilities (Rivera *PhD Thesis*, 2019; Fox et al., *In Review*; Oliver and Palumbi 2011; Mollica et al. 2019). These success stories must be highlighted and pursued such that identification and protection of climate resilient reefs occurs as soon as possible, as they will provide a bastion to coral and reef species should the worst projections of warming be realized. Second, coral reef fatalism often dismisses restoration efforts as inconsequential in the scope of global reef futures in GCM projections. This has led to a breakdown in communication between coral reef managers and scientists, which in turn has resulted in a significant proportion of coral restoration work being undertaken with little or no scientific input or detailed monitoring (Bostrom Einarsson et al., 2020).

If we are to make any effort at saving coral reefs and the species therein, there are several truths that must be acknowledged. Most important of these is that tropical reefs have already lost over 50-75% of coral cover to bleaching, increased disease outbreaks, sedimentation and nutrient pollution, and other anthropogenic stressors in only the last 40 years (Bruno et al. 2019). In even the most optimistic IPCC projections, warming will continue for at least another 20 years, which means that conditions will worsen. The next truth is that coral reefs have never in their 500-million-year history been exposed to warming at the rate it is occurring today. Acclimatization and adaptation strategies that these species may have relied upon in their genetic history may not be

capable of handling the steep warming curve and pronounced heat wave events of the 21st century. So, what does this mean for coral reef conservation? It is likely too late for even dramatic reductions in global scale carbon output to save the majority of coral reefs. To be effective, conservation efforts must therefore have two focuses:

1) To identify and protect those reef communities that have the best chance of surviving 21st century warming through demonstrated higher thermal tolerance, local environmental processes that mitigate heat stress, or historically proven adaptive capability.
2) To bridge the decades of inescapable warming in the near future by protecting coral biodiversity through active restoration efforts aimed at preserving endangered coral species, actively propagating thermally tolerant individuals, and fostering local community interest and involvement in mutually beneficial reef preservation

These efforts will only be effective in so far as anthropogenic warming is curbed substantially in the next century, however coral reef optimists have already identified these focuses and efforts are being made in both directions.

6.2 Identifying and protecting tolerant reefs

At this point, there exists no single definitive test for identifying thermally tolerant or resilient corals prior to their exposure to extreme heat. The gold standard for such a test would be 1) minimally destructive, 2) easily administered with minimal training, and 3) economically feasible. The obvious route would be the detection of a genetic marker related to thermal tolerance, as most genetic tests meet all three criteria. However, the genomic understanding of coral thermal tolerance is still in its infancy. Studies have shown heat stressed corals change expression of hundreds of genes (Meyer et al. 2011; Barshis et al. 2013), and while only a fraction of these are likely to correspond to thermal defense mechanisms, the difference in response of proven thermally tolerant individuals suggests there is no single 'thermal tolerance gene,' but rather tens of genes working in concert for any hypothesized tolerance strategy (i.e. production of heat shock proteins, elimination of radicals). Population genetics has recently yielded exciting results in identifying thermally tolerant corals within the Palauan reef system (Rivera 2019) and across a latitudinal gradient in the Great Barrier Reef (Dixon et al. 2015) although these approaches are not

yet independent of some stress test validation. The use of CRISPR mutagenesis has also shown recent promise as a tool to evaluate the importance of gene function in coral thermal tolerance, but has not yet been put to expansive use (Cleves et al. 2020). While a coral genomics tool for identifying tolerant corals may become viable in the future, current efforts focus on identifying tolerant corals post stress, either via direct stress testing or after natural marine heatwaves.

In the absence of a genetic assay for thermal tolerance, heat stress experiments are a more empirical option and have been employed extensively in recent years. One of the more significant developments towards experimental stress testing is the CBASS (a portable hot box) which can be used in the field to conduct short-term (i.e. 18 hour to 3 day) bleaching experiments on collected fragments of coral (Palumbi et al. 2014). This technique offers advantages over more traditional heat stress experiments in its portability, ease of use, and cost efficiency. CBASS stress testing has also recently been shown to identify thermally tolerant corals with the same level of accuracy as long term (i.e. 21 day) experiments (Voolstra et al. 2020). While these results are promising, in isolating coral test subjects from their natural environment these experiments may omit environmental factors that influence bleaching susceptibility (i.e. flow regime, light exposure, nutrient availability). While an in situ experimental setup is not currently feasible, a more accurate reconstruction of the coral's natural environment may improve the applicability of this technique.

We can also make use of natural bleaching events to identify thermally tolerant corals. In this thesis, I identify thermally tolerant coral populations after they have been subjected to repeat stress using skeletal records of bleaching, i.e. stress bands. By making use of natural marine heatwaves, skeletal stress bands can be used to recover thermal tolerance information about both massive corals and the communities around them years to decades after bleaching events. However, this technique is not without issue – namely it requires both a prolonged history of thermal stress events to gauge the tolerance of the sampled population, and a significant number of large *Porites* (or potentially other massive species) colonies that can be sampled within the testing area. While data suggest that these massive colonies are representative of the broader community in the reefs in this study (Fig. 2.2), this may not be the case everywhere. In terms of meeting the criteria for this 'gold standard' test, current detection methods for stress bands are costly (requiring CT scanning) and more destructive than tissue biopsy. Future development of the

proxy should look towards an in-situ method of stress band detection, perhaps through the use of acoustic or nuclear instruments common in borehole logging.

Improvements to each of these techniques could lead to one or more becoming the gold standard of detecting coral thermal tolerance, however all require sampling on a colony scale making the logistics of their application across the hundreds of thousands of km^2 that comprise the world's reefs infeasible. Therefore, any in situ assay must be paired with the capability of remotely identifying likely candidates for thermal tolerance. In order to identify potential climate tolerant reef communities from afar, our best resort is high resolution hydrodynamic modelling (e.g. Regional Ocean Modeling System, ROMS). Localized reef environments capable of promoting thermal tolerance (e.g. long residence times leading to chronically high water temperatures or shallow reef substrate subject to high temperature variability) are a result of complex geomorphology on scales difficult to resolve with even high-resolution (4km) satellite SST. Given accurate bathymetry, ROMS nested in coarser regional datasets have been shown to provide accurate temperatures across even complex reef environments on the scale of meters (REFS). The use of ROMS in identifying possible thermally tolerant communities is also in its infancy, however its potential to inform the selection of field sites for tolerance assay is significant. Pairing these two methods will allow us to quickly and efficiently identify reef communities that have the best chance of surviving 21st century warming.

6.3 Active restoration efforts

If these efforts are successful, it is critical that scientific involvement in the conservation process not stop at this point and simply turn over the responsibility to local governments and stakeholders. Over the last few decades, coral restoration has begun to gain both publicity and support, however efforts have suffered from two key issues: 1) poor design of many projects due to insufficient scientific foundation (e.g. lack of experimental control, poorly chosen reference systems), and 2) lack of consistent monitoring of existing projects, with little to no reporting on the long-term success or failure (Bostrom-Einarsson et al. 2020). These challenges have led resource managers to be reluctant in undertaking large and long-term restoration projects, and have prevented the development of scalable restoration efforts. Greater scientific involvement in restoration efforts will serve to close this gap by developing more efficient and longer lasting

restoration methods. Several such techniques have already been developed, but scalability remains the biggest scientific impediment to coral reef restoration.

Coral gardening was among the first developments in reef restoration, adding a nursery phase to transplant efforts. This process aims at increasing transplant success by allowing outplants to grow to an optimal size threshold, and also allows nurseries to maintain a standing stock of coral from which outplants can be made. However, while some studies report high rates of survival (Putchim et al. 2008), a recent review of transplant studies concluded that on average gardened corals had only a 2% higher survival rate than direct transplants (Bostrom-Einarsson et al. 2020). This disparity between anticipated result and observed outcome highlights a lack of robust experimental validation. Future efforts in coral gardening could be improved by optimizing survivability in several ways. Targeting thermally tolerant coral individuals for replication increases the likelihood of restoration efforts lasting through future bleaching events. Also, pairing outplanting with substrate stabilization techniques has been shown to enhance coral recruitment significantly (Lindahl 2003).

Gardening has also been primarily limited to fast growing branching coral genera, and while propagation of these genera is easier as they are more amenable to fragmentation, these same genera are among the least thermally tolerant (Loya et al. 2001). To both maintain biodiversity and stability of reef systems through anthropogenic warming, the massive slow growing species (e.g. *Porites, Montastrea*) that form the backbone of reef construction must be preserved. Micro-fragmentation, a recent technique developed to accelerate the propagation of polyps in massive corals, has shown incredible promise in both the growth and survival of gardened outplants (Forsman et al. 2015). Using this method, new coral can be 're-skinned' over dead colonies, not only restoring live coral cover to a reef but substantially reducing deterioration of substrate. However, while promising, this technique also suffers from a lack of scalability. To be attractive to coral reef managers, local scale efforts in outplanting should focus on 1) identifying and propagating thermally tolerant corals to maximize survivability, and 2) focus on reef areas less susceptible to local stressors (i.e. pristine or protected areas) and global stressors (i.e. heat mitigating hydrodynamics, low rates of warming).

One restoration technique that shows promise in terms of scalability is larval enhancement. This method seeks to increase rates of coral fertilization by collecting or rearing larvae and

distributing them onto the reef either directly or via settlement structures. Two methods have been utilized to date; one study harvested embryos reared in a coral nursery, and settled them onto concrete tetrapods which were then scattered onto the reef (Chamberland et al. 2017). The second study reared collected embryos in holding tanks on the reef, after which the larvae were released into enclosures over target substrate (Heyward et al. 2002). While both efforts were significantly faster than outplanting, they observed lower rates of success. Nevertheless, larval enhancement shows the most promise of current restorations in scaling to the thousands of square kilometers of reef area threatened by ocean warming. Further development of this technique in terms of both survivability of recruits and dispersal efficiency could potentially have massive results. If collected from a sufficiently genetically diverse population, recruits placed via larval enhancement will also be less sensitive to disease, a problem inherent in propagation-based techniques. And, like other methods of coral planting, larval enhancement would also benefit from identifying and replicating thermally tolerant individuals.

6.4 Conclusions

The most important steps scientific advancement can make toward helping coral reefs survive anthropogenic warming are not as passive observers, but as active defenders. Identifying, protecting, nurturing reef communities that are capable of surviving 21st century warming is central to this effort. Considerable scientific effort has been made in this direction, but improvements can still be made. In the face of the inescapable warming projected over the coming decades, active restoration efforts must be employed to maintain both the abundance and biodiversity of these tolerant reef systems. While restoration techniques are not yet viable on the scale necessary, recent advances in these techniques have improved their success rate and potential use over large spatial scales. However, even with a concerted effort to give these reefs the best chance possible in surviving warming, all corals have a limit to their thermal tolerance. Without the abatement of anthropogenic warming through the reduction of fossil fuel emissions, these efforts will be in vain.

6.5 References

Barshis DJ, Ladner JT, Oliver TA, Seneca FO, Traylor-Knowles N, Palumbi SR (2013) Genomic basis for coral resilience to climate change. Proc Natl Acad Sci 110:1387–1392

Bostrom-Einarsson L, Babcock RC, Baryaktarov E, Ceccarelli D, Cook N, Ferse S, Hancock B, Harrison P, Hein M, Shaver E, Smith A, Suggett D, Stewart-Sinclair P, Vardi T, McLeod I (2020) Coral restoration – A systematic review of current methods, successes, failures and future directions. PLoS One 13:1–24

Bruno JF, Côté IM, Toth LT (2019) Climate Change, Coral Loss, and the Curious Case of the Parrotfish Paradigm: Why Don't Marine Protected Areas Improve Reef Resilience? Ann Rev Mar Sci 11:

Chamberland VF, Petersen D, Guest JR, Petersen U, Brittsan M, Vermeij MJA (2017) New Seeding Approach Reduces Costs and Time to Outplant Sexually Propagated Corals for Reef Restoration. Sci Rep 7:1–12

Cleves P, Tinoco A, Bradford J, Perrin D, Bay L, Pringle J (2020) Reduced heat tolerance in a coral carrying CRISPR-induced mutations in the gene for a heat-shock transcription factor. Proc Natl Acad Sci USA 117:28899–28905

DeCarlo TM, Cohen AL, Wong GTF, Davis KA, Lohmann P, Soong K (2017) Mass coral mortality under local amplification of 2 °C ocean warming. Sci Rep 7:44586

Dixon G, Davies S, Aglyamova G, Meyer E, Bay L, Matz M (2015) Genomic Determinants of Coral Heat Tolerance Across Latitudes. Science (80-) 348:2014–2016

Forsman ZH, Page CA, Toonen RJ, Vaughan D (2015) Growing coral larger and faster: Micro-colony-fusion as a strategy for accelerating coral cover. PeerJ

Heyward AJ, Smith LD, Rees M, Field SN (2002) Enhancement of coral recruitment by in situ mass culture of coral larvae. Mar Ecol Prog Ser 230:113–118

Lindahl U (2003) Coral reef rehabilitation through transplantation of staghorn corals: Effects of artificial stabilization and mechanical damages. Coral Reefs 22:217–223

Loya Y, Sakai K, Yamazato K, Nakano Y, Sambali H, Van Woesik R (2001) Coral bleaching: The winners and the losers. Ecol Lett 4:122–131

Meyer E, Aglyamova G V., Matz M V. (2011) Profiling gene expression responses of coral larvae (Acropora millepora) to elevated temperature and settlement inducers using a novel RNA-Seq procedure. Mol Ecol 20:3599–3616

Mollica NR, Cohen AL, Alpert AE, Barkley HC, Brainard RE, Carilli JE, Decarlo TM, Drenkard EJ, Lohmann P, Mangubhai S (2019) Skeletal records of bleaching reveal different thermal thresholds of Pacific coral reef assemblages. Coral Reefs

Oliver TA, Palumbi SR (2011) Do fluctuating temperature environments elevate coral thermal tolerance? Coral Reefs 30:429–440

Palumbi SR, Barshis DJ, Bay R a (2014) Mechanisms of reef coral resistance to future climate change. Science (80-) 344:895–898

Putchim L, Thongtham N, Hewett A, Chansang H (2008) Survival and growth of Acropora spp. in mid-water nursery and after transplantation at Phi Phi Islands , Andaman Sea , Thailand. 11th Int Coral Reef Symp Ft Lauderdale, Florida 1258–1261

Rivera HE (2019) Genetic connectivity, adaptation, and phenotypic plasticity of corals and anemones under thermal stress. Dr Thesis

Voolstra CR, Buitrago-López C, Perna G, Cárdenas A, Hume BCC, Rädecker N, Barshis DJ (2020) Standardized short-term acute heat stress assays resolve historical differences in coral thermotolerance across microhabitat reef sites. Glob Chang Biol 26:4328–4343

Wall M, Wall M, Putchim L, Schmidt GM, Jantzen C, Khokiattiwong S (2014) Large-amplitude internal waves benefit corals during thermal stress Large-amplitude internal waves benefit corals during thermal stress. Proc R Soc B

Appendix A2 – Supplementary text, figures, and data for chapter 2

A2.1 Correlation between coral skeletal density and R_{ECM} on the seasonal scale

Coral skeletal density shows a significant correlation ($p < 0.05$) with R_{ECM} on the seasonal scale in 5 out of the 9 cores analyzed in this study, consistent with the control of the skeletal thickening rate on skeletal density (Fig. A2.3). Seasonal R_{ECM} was estimated following the same method as the annual R_{ECM} (Methods), except that seasonal seawater temperatures were estimated at the same resolution as the boron isotope measurements (e.g. 6-8 samples per year). The rate of skeletal extension was assumed constant throughout the year.

Note, the absence of such correlation in some cores can be due to improper alignment between the density profile and the sampling track for boron isotope measurements. Density determined by CT scanning represents average density across all continuous polyps in the core, while boron isotope sampling was conducted along a single polyp. This misalignment issue can be accounted for if certain amount of shift in the density profile is applied. For example, the correlation between the coral skeletal density and R_{ECM} in core Green Island 701 improves significantly (from $p=0.098$ to $p < 0.001$), if a 1mm shift is applied. For other cores, e.g. Saboga 192 and Airai 23, the skeletal density shows minimal annual cyclicity. Accordingly, there are poor correlation between the coral skeletal density and R_{ECM}.

A2.2. Elevation of DIC concentration in coral ECM

Several studies have attempted to quantify the DIC concentrations within the coral ECM with different geochemical methods. For example, Allison et al. estimated a factor of 1.4 times elevation of DIC concentrations in *Porites* coral ECM (Allison et al. 2014), by combining estimates of ECM pH from $\delta^{11}B$ and estimation of ECM CO_3^{2-} and HCO_3^- concentrations from B/Ca ratios. However, McCulloch et al. recently estimated a much higher elevation (i.e. a factor of 2.6) of DIC concentration in *Porites* coral ECM using a similar approach (Holcomb et al. 2016).

This difference results mainly from the different ways the two studies used to derive the boron partition coefficient between seawater and aragonite. McCulloch et al. also suggested the DIC elevations in coral ECM vary seasonally, with elevation factors fluctuating by 0.74 on average. However, the annual average DIC elevations estimated from their data are relatively constant, ranging by 0.20 between years. In a study using the same approach, Comeau et al. found DIC in the ECM to be elevated by a factor of 1.8 in *A. youngei*, and 1.7 in *P. damicornis* (Comeau et al. 2017). Elevation of DIC concentration in coral ECM was also suggested by Furla et al., who observed that *S. pistillata* corals growing in calcium and carbon labeled seawater show only about 20~25% of the C^{14}/Ca^{45} ratio of the surrounding seawater in their skeletons and thus estimated a DIC elevation factor of ~3 in the their ECM (Furla 2000). In contrast, Cai et al. reconstructed the full carbonate chemistry of the ECM in *O. faveolata, T. reniformis,* and *A. millepora* corals, based on in situ electrode measurements of ECM pH and CO_3^{2-} concentrations, and suggest DIC concentrations in their ECM can be similar to seawater (e.g. an elevation factor of 0.7 to 3.9). These variations in estimated DIC elevation factors could suggest differences in DIC elevation among different coral species and individuals.

In this study, we adopt a DIC elevation factor (i.e. α) of 2 and refine this estimation using a Bayesian statistical approach (See section A2.4). Consideration of seasonal variations in ECM DIC elevations similar to what suggested by McCulloch et al. does not affect our conclusions (Fig. A2.3).

A2.3. *Porites* skeletal growth model

We modeled skeletal growth of *Porites* corals as a two-step process: daily vertical extension (E), followed by thickening around the interior to the depth of the tissue layer (T_d). Coral poly is approximated as ring in our model. Each new skeletal element is prescribed a height equivalent to the daily extension (E) and an initial wall thickness of w_o. Skeletal thickening occurs throughout the tissue layer, and its rate is controlled by the aragonite precipitation rate in the ECM (R_{ECM}) and decreases with depth in the tissue layer:

$$R(z) = R_{ECM} \times e^{-\frac{\lambda \times z(t,E)}{T_d}} \quad [A2.1]$$

where z is the depth at which the skeletal element resides relative to top of the tissue layer and is a function of time (t) and extension rate (E), R(z) is the thickening rate at depth z, λ is the decay constant. The wall thickness of polyp ring increase as thickening of skeletal elements continues:

$$\frac{dw}{dt} = \frac{R(z)}{\rho_{arag}} = \frac{R_{ECM}}{\rho_{arag}} \times \ e^{-\frac{\lambda \times z(t,E)}{T_d}} \qquad [A2.2]$$

where $\frac{dw}{dt}$ is the change in wall thickness at a given depth z within the tissue layer due to thickening, and ρ_{arag} is the density of aragonite (i.e. 2.94 g cm^{-3})(5). The final wall thickness of the polyp (w_f) can then be calculated as:

$$w_f = w_o + \int_{t=0}^{t=t_f} \frac{R_{ECM}}{\rho_{arag}} \times \ e^{-\frac{\lambda \times z(t,E)}{T_d}} dt \qquad [A2.3]$$

where $\frac{dw}{dt}$ is integrated over the entire period for which each skeletal element remains in the tissue layer (t_f). The final density of the skeleton was then calculated based on the fraction of the ring filled with aragonite (Eq. 3 in the main text).

A2.4. Estimation of model parameters with a Bayesian inference method

There are limited experimental constraints on several parameters in our skeletal growth model, including the initial thickness of new skeletal framework (w_o), the decline of thickening rate with depth in the tissue (λ), and the DIC elevation within the ECM (α). We estimated these parameters with a Bayesian inference method. Bayesian inference begins with a prior distribution for the parameter (or parameters) of interest that reflects prior information. The prior distribution is then updated with new data via Bayes' Rule to form the posterior distribution of the parameter that reflects both prior information and the information contained in the data. A point estimate of the parameter is then given by its posterior mean and a measure of estimation precision is given by its posterior standard deviation.

A2.4.1 Constructing prior distributions for free parameters

$\boldsymbol{w_o}$**.** The new skeletal framework in our model is analogous to the early mineralization zones (EMZ) observed in *Porites* skeletons, which are thought to represent rapid initial growth at the apex of skeletal elements every 24 hours (Cuif and Dauphin 2005; Northdruft and Webb 2007; Shirai et al. 2012). Here we consider the EMZ to consist of the dark, organic rich, centers of calcification and the immediately associated fibers (Fig. A2.2). As w_o is a nonzero positive quantity, we adopt a log-normal distribution prior for w_o, with a mean and variance of the experimentally determined sizes of EMZ (i.e. 35.4 μm, 29.6 μm respectively).

$\boldsymbol{\lambda}$**.** The decrease of skeletal thickening rate within the tissue layer of *Porites* is a poorly understood process. Barnes and Lough first described this feature in *Porites* coral cores from the Great Barrier Reef, noting a high amount of skeletal thickening near the colony surface and then rapid decrease toward the base of the tissue layer (Barnes and Lough 1993). Similar trends have later also been observed in Indo-Pacific *Porites* (Gagan et al. 2012). Following previous modeling studies (Elman 1991; Taylor et al. 1993), we simulate this decrease as an exponential function with decay constant λ. However, to our knowledge there have been no quantitative estimates of λ. We therefore adopt a uniform prior distribution for λ greater than zero.

α. As discussed in section A2.2, existing estimates for the DIC elevation factor in the ECM (α) vary significantly among different species and methods. We chose to adopt a log-normal distribution prior for α with a mean 2.0. To reflect the large differences between studies, a distribution with standard deviation 2 times that of the log of observed experimental values in (Mcculloch et al. 2017) (i.e. 0.14) was used.

A2.4.2 Evaluating likelihood and posterior distributions of parameter estimates

A joint prior distribution was assembled to reflect the combined probability of all possible combinations of these three parameters. We then simulate the density of each core from this study using all possible combinations of parameters described by the joint prior based on our skeletal growth model. The likelihood of each combination of parameters was evaluated by comparing our measured densities with the associated model predictions assuming normally distributed sample error. This joint likelihood function was then used to update the prior via Bayes' theorem to form the posterior (Fig. A2.4a-c). A univariate distribution for each parameter was generated from the joint posterior by evaluating the maximum probability of the other two parameters for any given

value. For example, for each possible $\alpha = \alpha_i$, there exists a two-parameter posterior of dw_1 and λ. The maximum of this 2D distribution was taken to be the probability of α_i, $p(\alpha_i)$. This was then repeated for the other two parameters.

In the end, our Bayesian inference method yields the following estimates of each parameter: $w_o = 59\ ^{+23}_{-24}\ \mu m$, $\lambda = 12.8\ ^{+11.9}_{-6.2}$, and $\alpha = 2.05\ ^{+0.39}_{-0.38}$ (2 σ).

A2.4.3 Validating Bayesian estimated parameters using skeletal density profiles

We examined skeletal density profiles from within the tissue layer of 5 cores collected in this study (those that were not damaged at the top). A composite profile was then produced by normalizing the individual profiles to their respective tissue thicknesses (T_d) and fit with an exponential regression for which a 95% confidence interval was calculated (Fig. A2.4d). We then employ our *Porites* skeletal growth model to generate predictions of the density profile within the tissue layer, using the normalized T_d and average r_o, E, and R_{ECM} from the five cores. Because the model predicted curve falls within the 95% confidence interval of the exponential fit, and replicates the normalized density profile reasonably well, we accept these parameters as satisfactory for our predictions.

A2.5. Sensitivity of model predicted density to different model parameters

While R_{ECM} plays a significant role in skeletal density in our model, other measured model parameters (r_o, T_d, E) also exert significant controls, as do the estimated model parameters (w_o, λ, Fig. A2.5). In brief, predicted density is directly proportional to R_{ECM}, T_d, w_o, and λ (e.g. an increase in λ leads to a higher predicted density), while it is inversely proportional to r_o and E. We evaluate below the sensitivity of the model predicted density to each parameter, by individually varying each parameter by up to 50% while holding all the other parameters constant at the mean value observed in our cores.

R_{ECM}: As discussed in the main text, the model predicted density is sensitive to R_{ECM}, yielding a 0.54% change in density for every 1% change in R_{ECM}. R_{ECM} is most sensitive to temperature; in the context of 20th century climate change, we project a mean temperature rise of 2.5 degrees at reef locations (based on CESM-BGC output), which corresponds to an 83% increase

in R_{ECM}. In comparison, CESM-BGC projected change in seawater pH (i.e. -0.3 units) and in DIC (i.e. 120 µmol/kg) produces smaller changes in R_{ECM}, -32% and 11% respectively.

r_o: Among all the model parameters, r_o has the strongest effect on the model predicted density, producing a -1% change in density for every 1% change in r_o. r_o varies among different coral species, and is often used for identifying coral taxonomy (Veron and Stafford-Smith 2000). Little is known about how r_o changes with environmental factors. Tambutté et al. (Tambutté et al. 2015) observed that calyx radii of *S. pistillata* growing in low pH seawater (i.e pH = 7.2) increased by over 50% compared to those in normal seawater. Note, however, this increase was based on measurement of the interior radii of the calyx, and so is not directly comparable to r_o in our model. In the Andaman Sea, Tanzil et al. (Tanzil et al. 2009) found that the average cross section areas of *Porites* polyps varied significantly between reefs (with a standard deviation of ~10%), but there was no consistent trend through time.

E: The model predicted density is also sensitive to changes in *E,* producing -0.30% in density for every 1% change in E. Many environmental factors are thought to affect the rate of coral extension, particularly temperature and irradiance. Some studies suggest coral extension increases linearly with sea surface temperature (Nie et al. 1997; Lough and Barnes 2000), while others show sharp decreases in coral extension above a threshold temperature or after bleaching events (Cooper et al. 2008; De'ath et al. 2009; Cantin et al. 2010; Hetzinger et al. 2016). Coral extension has also been found to decrease with lower irradiance (Baker and Weber 1975; Huston 1985), but is relatively insensitive to ocean acidification (Fabricius et al. 2011; Barkley et al. 2015; Tambutté et al. 2015).

T_d: The model is least sensitive to changes in T_d, resulting in 0.28% change in density for every 1% change in T_d. Changes in T_d are generally thought to be related to nutrient concentrations in seawater, and are not affected by ocean acidification (Fabricius et al. 2011; Barkley et al. 2015).

w_o: The model is less sensitive to changes in w_o than R_{ECM}, resulting in 0.36% change in density for every 1% change in w_o. w_o is thought to be a phenotypic characteristic of Porites; no evidence has shown a change in EMZ size in response to external stimuli.

λ: The model is similarly sensitive to the estimated value of λ as it is to E, resulting in -0.31% change in density for every 1% change in λ. As stated above, the rate of decrease in skeletal

thickening within the tissue layer is a poorly understood process, and has also not been linked to any external stimuli.

A2.6. Comparison between model predicted density and measured density in the existing studies

To enable density predictions, our model requires several input parameters specific to each coral, including extension rate (E), polyp radius (r_o), and tissue thickness (T_d). In addition, seawater carbonate chemistry parameters are needed to estimate R_{ECM}. No studies examined in our model-data comparison reported all of these parameters. When not reported, the values of these parameters were either adopted from other studies reporting such parameters in the region (e.g. T_d and seawater chemistry) or assumed representative average values for each taxon (e.g. r_o). The performance of our model is directly related to the uncertainties associated with these measured or estimated parameters.

Great Barrier Reef: r_o was not reported for Great Barrier reef cores (Lough and Barnes 2000). But each core was identified at the species level (unlike the Andaman Sea cores). This allowed for a relatively precise estimation of r_o (Fig. A2.6b, (Veron and Stafford-Smith 2000)), which contributes to more satisfactory predictions generated at these locations. For some cores, there are insufficient in situ measurements about their seawater carbonate chemistry. In these cases, we used pH, T, S, and DIC output from the CESM-BGC historical run (1900-2005) to estimate the seawater conditions during time period when density was reported. This could introduce uncertainties in the estimated R_{ECM}, because the physicochemical conditions of the reef environments can be significantly different from the open ocean conditions (as estimated with output from the CESM-BGC historical run).

Galapagos: Neither r_o nor T_d were measured for Galapagos corals (28). Instead, we adopted the mean r_o values from our cores and the T_d (i.e. 6.5mm) estimated from nearby sites (Wellington et al. 1996; Linsley et al. 1999) in the model predictions. Despite these limitations, the model predicted density strongly correlates with measured density ($p=0.001$).

Andaman Sea: Data about the Andaman Sea corals were compiled from two studies (Tanzil et al. 2009, 2013). r_o and T_d were reported in (Tanzil et al. 2009) but not in (29). The mean

values of r_o and T_d reported in (15) were assumed to representative of corals reported in (Tanzil et al. 2013). Seawater carbonate chemistry parameters were estimated from the CESM-BGC historical run for this region. This, combined with the lack of r_o and T_d measurements at most sites, could explain the less satisfactory agreement between model predicted density and measured density (Fig A2.6d).

Arabian Gulf: r_o was not reported for Arabian Gulf cores (Poulsen et al. 2006). However, similar to Great Barrier Reef corals, each core was identified at the species level, which enables a relatively precise estimation of r_o. Seawater carbonate chemistry was also estimated from the CESM-BGC historical run for this region. However, these reefs are less sheltered from the open ocean compared to other reefs, e.g. the Andaman Sea reefs, and thus the estimates from the CESM-BGC historical run may be more representative.

Caribbean: r_o was not measured for Caribbean corals (Crook et al. 2013). All corals collected from the Caribbean were *Porites astreoides,* for which a wide range of calyx radii (i.e. 0.6 to 1.3 mm) have been reported (Szmant 1986; Veron and Stafford-Smith 2000). In the model simulation, we adopted the r_o values reported for nearby Caribbean sites (i.e. 1.3 mm). In addition, there are potential differences in both calcification mechanism and polyp structure between *P. astreoides* (the only Atlantic coral used in this study) and the coral species in our study that were used to estimate important model parameters (e.g. dw_1, λ, and α). All these could have contributed to the less satisfactory agreement between the model predicted density and measured density (Fig. A2.6f).

A2.7. Correlation between skeletal density and extension in some corals

Negative correlations between coral skeletal density and extension were observed for corals in both the Great Barrier reef (Lough and Barnes 2000) and in the Andaman Sea (Tanzil et al. 2013). Such correlations have been suggested as evidence for extension exerting a major control on skeletal density. For all the cores examined in our model-data comparison, such correlation is observed only in these two studies, yielding an apparent slope that is consistent with our model predicted sensitivity of density to extension (Fig. A2.7). Cores from all studies, except those from the Caribbean and Galapagos, fall near this correlation.

The skeletal extension in the corals examined in our model-data comparison vary significantly from 0.2 to 2.4, representing a -78 to +71% variation around the mean value. This is larger than variations in the estimated R_{ECM} for these coral, i.e. 0.15 to 0.48 g cm^{-2} yr^{-1}, or -54 to +58% variation around the mean value. This suggests that both extension and R_{ECM} control the variability of skeletal density in these corals.

A2.8. Projecting changes in *Porites* skeletal density over the 21st century

To evaluate the impact of 21st century climate change on *Porites* skeletal density, we force our skeletal growth model with sea surface T, DIC, and pH outputs from the Community Earth System Model Biogeochemical run (CESM-BGC) in the RCP 8.5 projection for the years 2006-2015 and 2090-2099. As stated in the main text, this CESM-BGC run predicts 0.25 to 0.35 units decrease in seawater pH, -50 to 250 µmol/kg change in DIC, and 1.7 to 3 ^{o}C increase in sea surface temperatures at global reefs by the end of the 21st century. We conducted model simulations to determine the effects of each individual seawater parameter on coral skeletal density change at reef locations by assuming all parameters (i.e. DIC, pH, or T) is fixed at beginning of century values except the one of interest (Figure A2.8a-f). All other model parameters (i.e. r_o, T_d, E, λ, w_o, and α) were also held constant in these simulations. . It should be noted that the error included in these estimates represents only uncertainty propagated from the estimated model parameters, and does not account for uncertainties in GCM output as only one CESM-BGC run has been conducted.

Effects of rising seawater temperature: Due to the coupled nature of the CESM-BGC run output variables (i.e. the simulated pH, DIC, and T are not independent of each other), the projected change in Ω_{SW} includes the effect of rising seawater temperature. Accordingly, our model projected changes in *Porites* skeletal density due to ocean acidification (Fig. 4 and Fig. A2.8h) alone automatically includes the effects of temperature on certain aspects of coral calcification process (e.g. on Ω_{SW}). Note, temperature also affects the reaction kinetics parameters of aragonite precipitation (i.e. k and n, Eq. 1) and will lead to higher aragonite precipitation rates and thus R_{ECM} at higher temperatures. If these later temperature effects were also included, our model would predict a global increase in *Porites* skeletal density by ~29 ± 3% on average (Fig. A2.8i), similar to predictions from other model studies that include such temperature effects (McNeil et al. 2004).

However, there are large uncertainties regarding how rising sea surface temperatures will affect coral calcification, particularly related to its effects on zooxanthelae photosynthesis and coral bleaching (Coles and Jokiel 1977; Warner et al. 1996; Hooidonk et al. 2016). We therefore, as stated in the main text, focus on evaluating the changes in *Porites* skeletal density derived solely from ocean acidification in our model projections and hold the kinetics parameters of aragonite precipitation constant as calculated at the beginning of century temperatures.

A2.9 Supplementary figures and tables

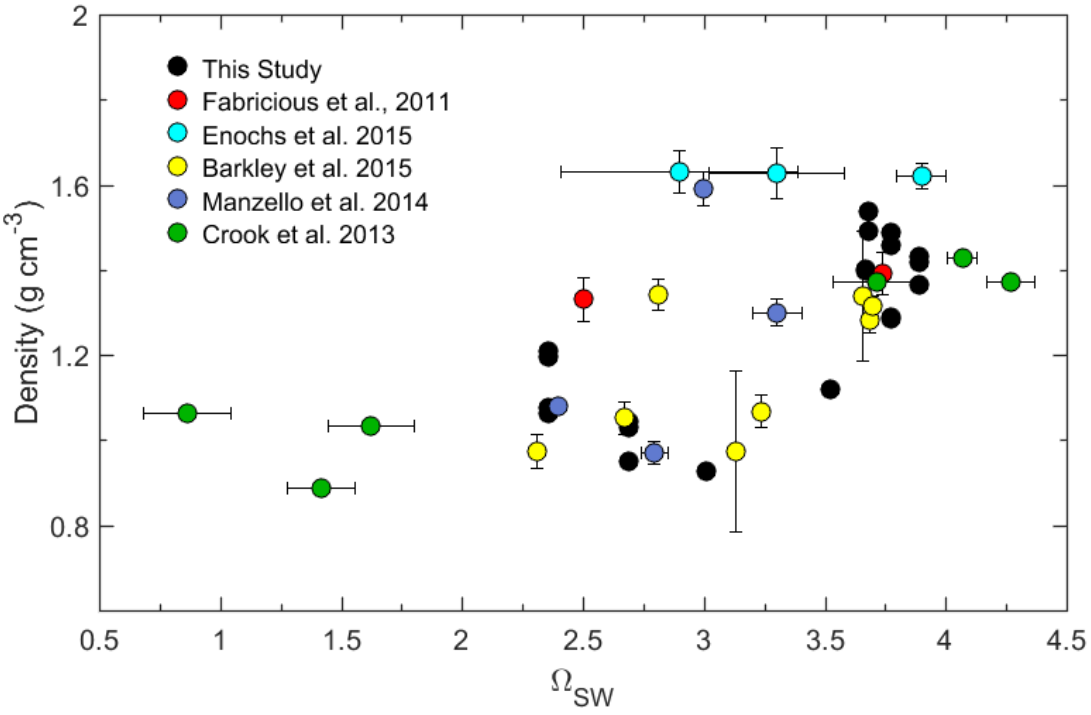

Figure A2.1. Variations of skeletal density with seawater aragonite saturation state in different reefs. Error bars indicate the standard deviation of reported density and Ω_{sw}.

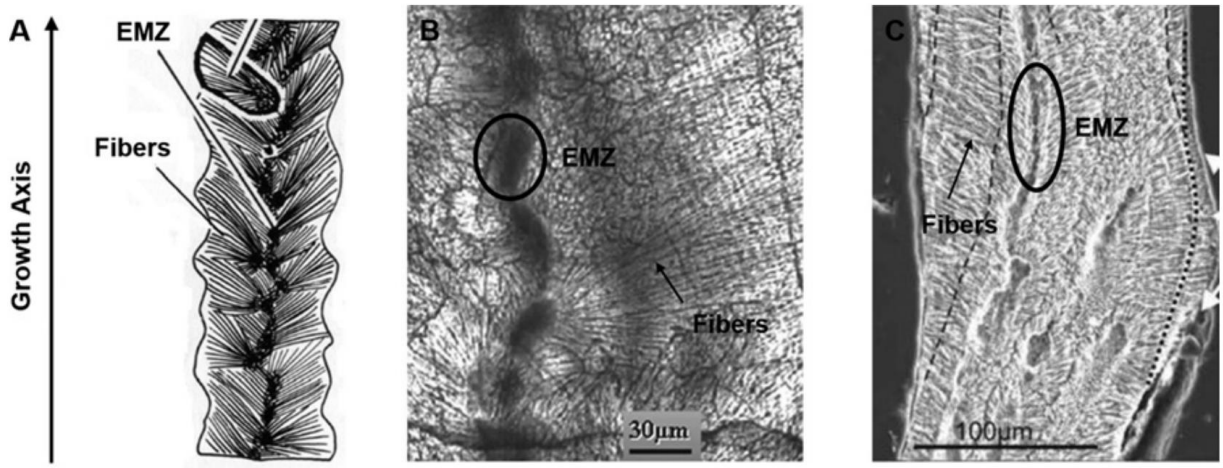

Figure A2.2: Microstructures of *Porites* coral skeleton examined at micron-length scale showing Early Mineralization Zone (EMZ) and thickening fiber bundles, as depicted: **A**) schematically (Wells 1956), **B**) a petrographic thin-section viewed under polarized light (Cohen and McConnaughey 2003), and **C**) a Scanning Electron Microscopy image of a polished etched section (Northdruft and Webb 2007). Each shows the continuous line of EMZs and growth of aragonite crystals perpendicular to the EMZs. These figures and images of coral skeleton show EMZ and immediately associated crystal fibers oriented parallel to the axis of upward growth, thus driving skeletal extension, whereas the mature bundles of elongate fibrous crystals serve to thicken the skeleton and relate directly to skeletal density. Strong biological control of EMZ accretion may explain our finding that skeletal extension is not sensitive to calcifying fluid pH or ocean acidification.

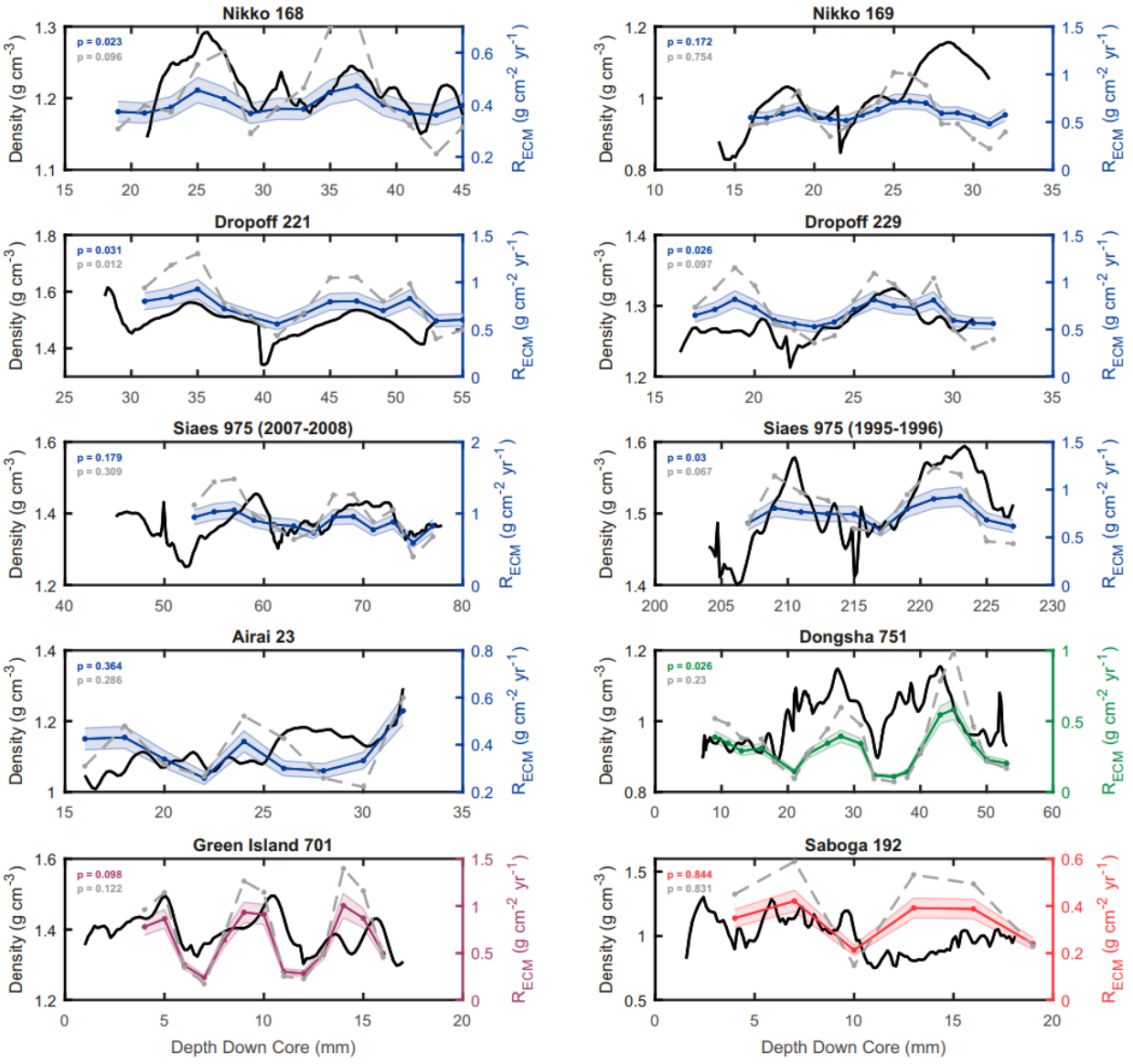

Figure A2.3. Correlation between coral skeletal density and R_{ECM} on seasonal scales for all cores analyzed in this study. As in the corresponding main text figures, a DIC elevation factor of 2 was used to compute R_{ECM}. Dashed grey line shows R_{ECM} estimates when seasonally varying α centered at 2 and an amplitude of 0.74 over which high DIC elevation coincides with summer temperatures, as was observed in (Mcculloch et al. 2017).

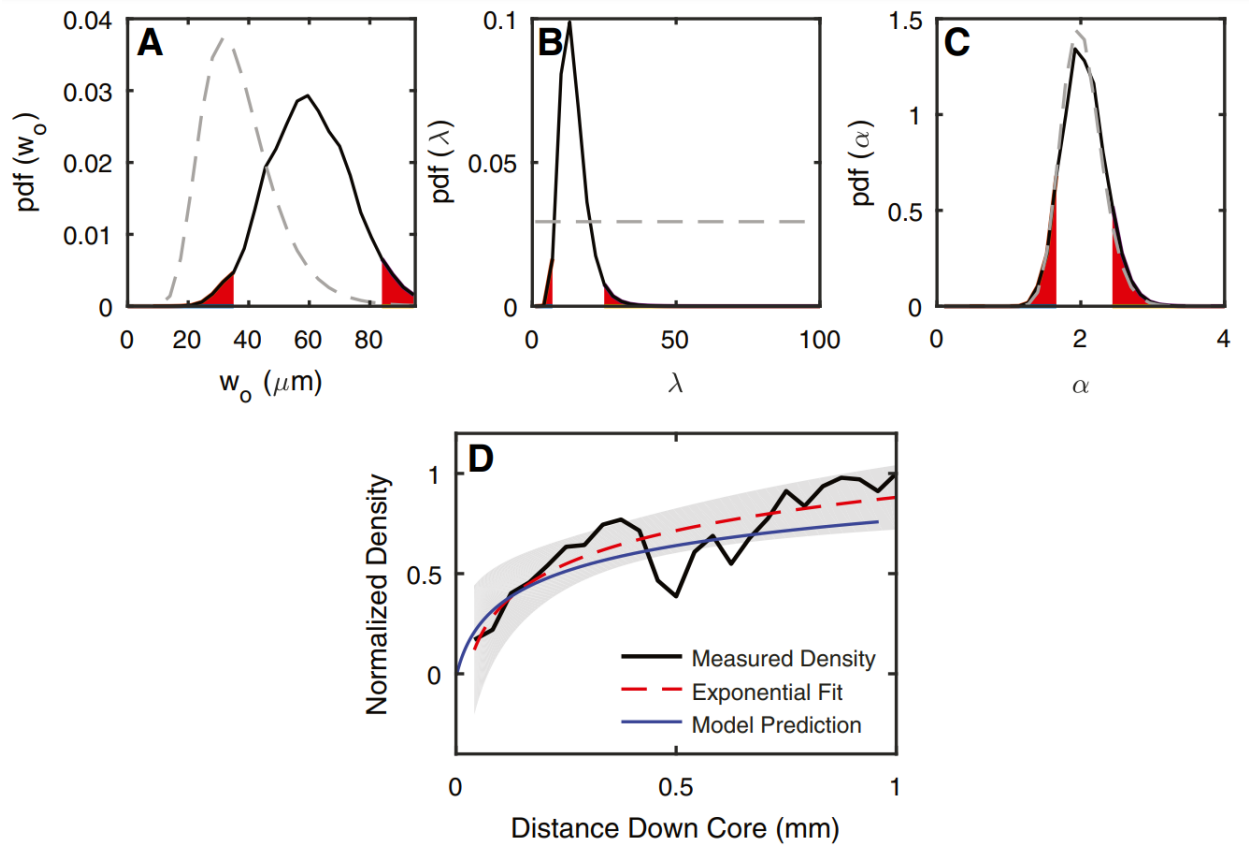

Figure A2.4. Estimation of model parameters based on the Bayesian inference method. (A–C) Probability density functions (pdfs) of prior (dashed lines) and univariate posterior (solid lines) for each parameter derived from the Bayesian method, with 95% confidence intervals shown in red. (D) Composite density profile (black line) with exponential fit (red line) and associated 95% confidence intervals (gray envelope). The blue line represents model prediction based on our estimated parameters, which falls within the confidence envelope.

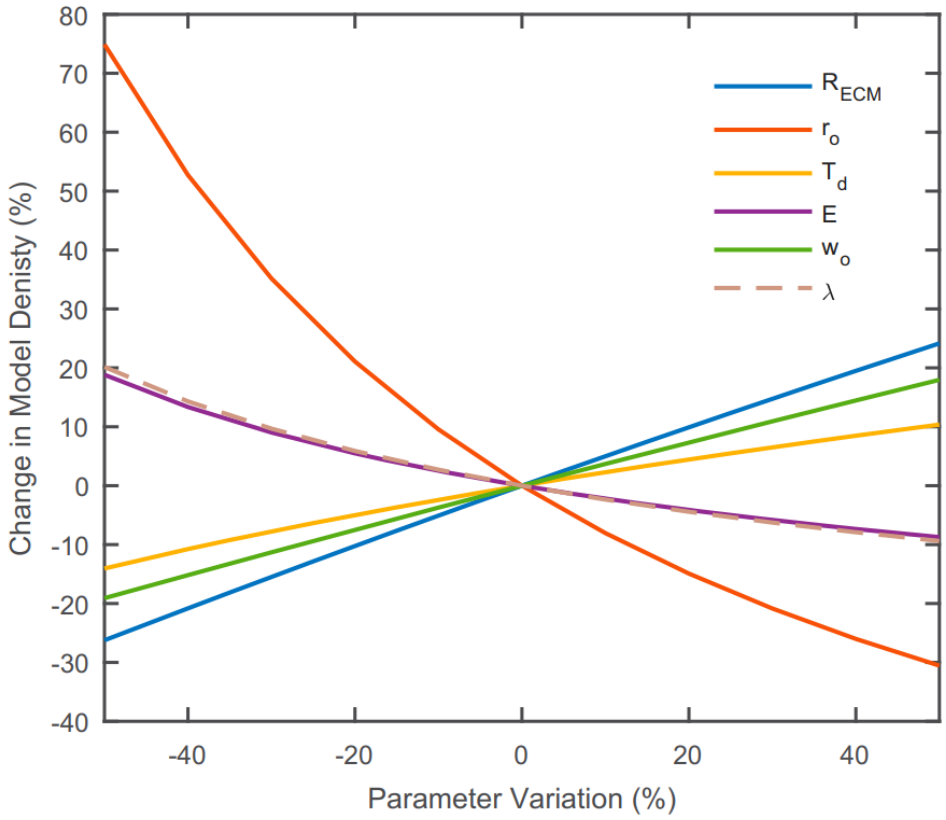

Figure A2.5. Sensitivity of model predicted density to key model parameters, R_{ECM}, $r_{o,}$, T_d, E, w_o, and λ. The reference point in these sensitivity evaluations were set to be the mean values of each parameter in our cores.

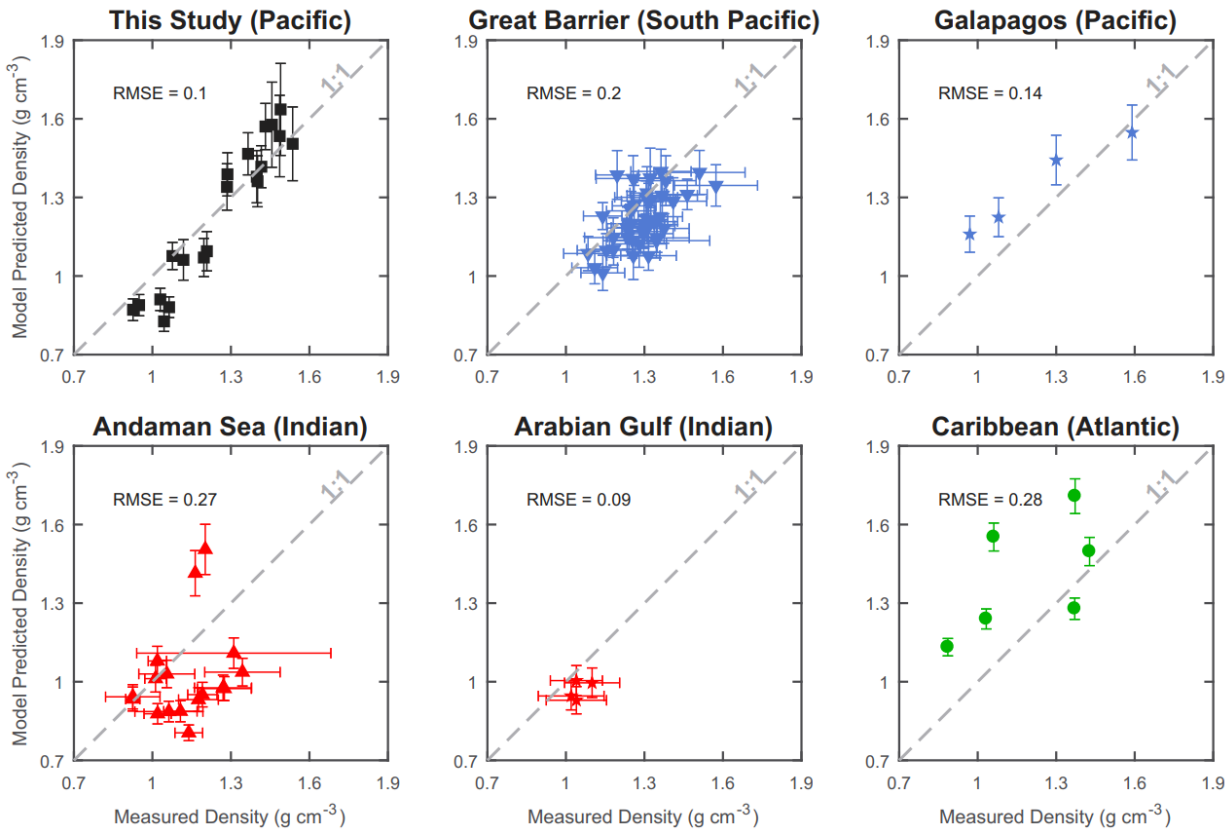

Figure A2.6. Comparisons between model predicted density and measured density for different reefs. Horizontal error bars denote 2σ uncertainties in site average densities. Vertical error bars represent uncertainties in model prediction, propagated from uncertainties in estimated parameters α, λ, and dw_1 as well as in situ measurements of seawater conditions (where available). Root-mean-square error (RMSE) relative to the 1:1 line is shown for each set of predictions

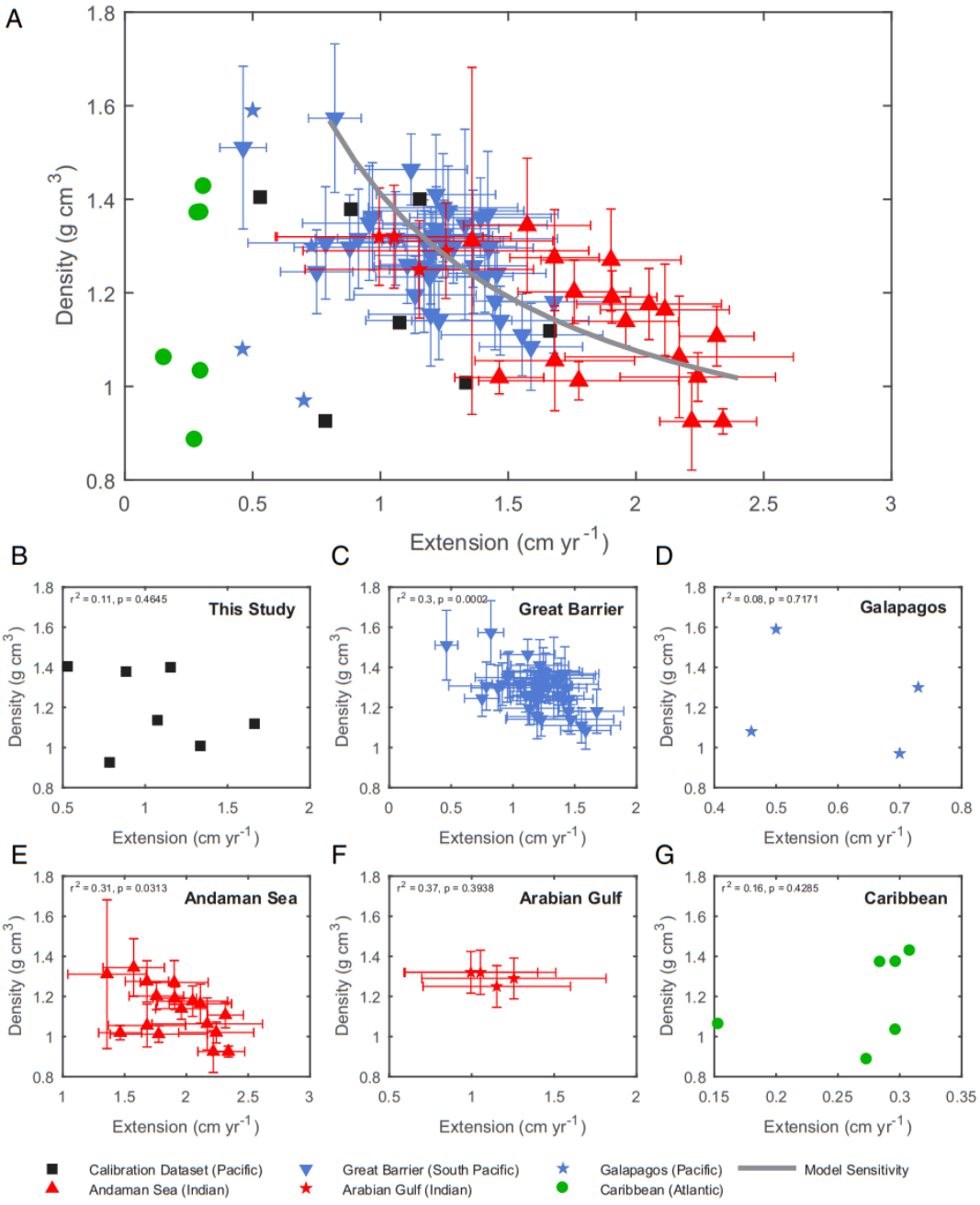

Figure A2.7. Variations of skeletal density and extension in different reefs. Points from the Galapagos, Great Barrier, and the Andaman Sea represent site average density and extension, for which error bars denote 2σ uncertainties. Shown in (b-g) are data from each reef/region. Only the cores from the Great Barrier Reef and the Andaman Sea show a significant correlation between skeletal density and extension when examined separately.

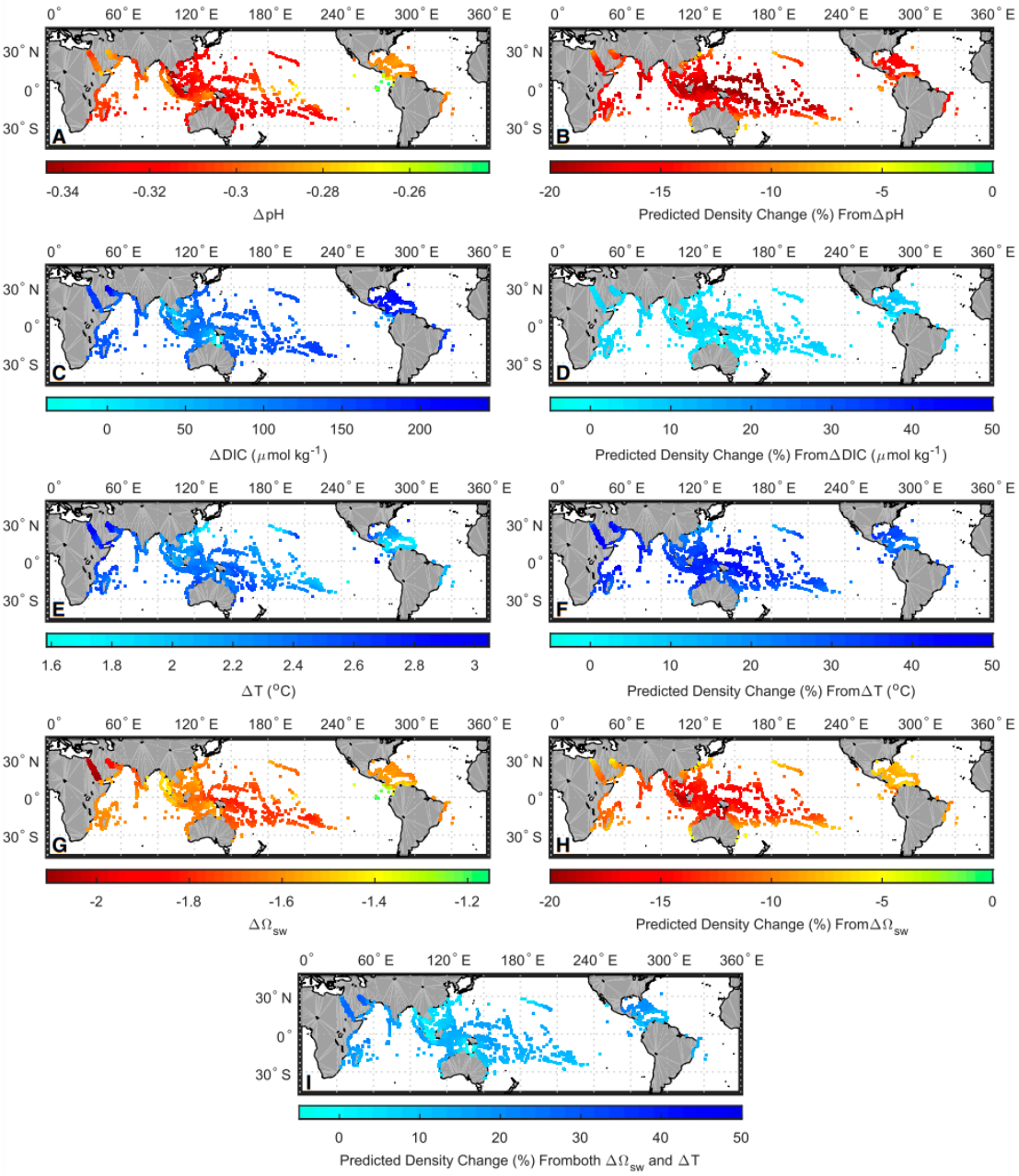

Figure A2.8. Projected change in seawater pH, DIC, T, and Ω_{sw} and the corresponding changes in *Porites* skeletal density over the 21st century. Changes in seawater physicochemical conditions were based on outputs from CESM-BGC RCP 8.5 run from the years 2006-2015 and 2090-2099. Skeletal extension, initial radius, and tissue thickness were held constant in our model simulations. The combined effect considering changes in all seawater parameters, including the effect of temperature on the kinetics of aragonite precipitation, is shown in subplot **I**.

Table A2.1 – Characterization of *Porites* core samples in this study, including seawater conditions, coral skeletal parameters, boron isotope compositions, and estimated pH and abiogenic aragonite precipitation rate in the coral calcifying medium.

Site	Core ID	Year	SST (°C)	S	pH	DIC (µmol kg^{-1})	Extension (cm yr^{-1}) E	Density (g cm^{3}) ρ	Calcification (g cm^{-2} yr^{-1})	Tissue thickness (cm) T_d	Polyp Radius (cm) r_o	$\delta^{11}B$ (‰)	pH_{ECM}	Rate (g cm^{-2} yr^{-1}) R_{ECM}
Nikko*	168	2009	30.26 ± 0.75	32.41 ± 0.63	7.84 ± 0.03	1785.7 ± 30.4	1.25	1.21	1.51	0.394	0.054	22.67 ± 0.21	8.36 ± 0.02	0.54 ± 0.09
		2008	30.26 ± 0.75	32.41 ± 0.63	7.84 ± 0.03	1785.7 ± 30.4	1.31	1.20	1.57	0.394	0.054	22.61 ± 0.25	8.36 ± 0.02	0.55 ± 0.09
Nikko*	169	2009	30.26 ± 0.69	32.41 ± 0.63	7.84 ± 0.03	1785.7 ± 30.4	0.99	1.06	1.06	0.463	0.078	22.27 ± 0.21	8.33 ± 0.02	0.51 ± 0.08
		2008	30.26 ± 0.69	32.41 ± 0.63	7.84 ± 0.03	1785.7 ± 30.4	0.74	1.08	0.79	0.463	0.078	22.61 ± 0.22	8.36 ± 0.02	0.55 ± 0.09
Dropoff*	221	2008	29.80 ± 0.43	33.69 ± 0.31	8.05 ± 0.02	1865.7 ± 29.6	1.03	1.49	1.53	0.333	0.042	23.73 ± 0.23	8.43 ± 0.02	0.74 ± 0.08
		2007	29.80 ± 0.43	33.69 ± 0.31	8.05 ± 0.02	1865.7 ± 29.6	0.97	1.46	1.42	0.333	0.042	23.77 ± 0.24	8.43 ± 0.02	0.74 ± 0.08
Dropoff*	229	2008	29.80 ± 0.44	33.69 ± 0.31	8.05 ± 0.02	1865.7 ± 29.6	0.85	1.29	1.09	0.451	0.061	23.30 ± 0.28	8.40 ± 0.02	0.66 ± 0.07
		2007	29.80 ± 0.44	33.69 ± 0.31	8.05 ± 0.02	1865.7 ± 29.6	0.68	1.29	0.88	0.451	0.070	23.58 ± 0.27	8.42 ± 0.02	0.71 ± 0.08
Siaes	975	2008	29.21 ± 0.50	33.98 ± 0.12	8.04 ± 0.01	1860.9 ± 25.7	1.23	1.40	1.72	0.543	0.057	24.20 ± 0.11	8.46 ± 0.01	0.36 ± 0.16
		2007	29.21 ± 0.50	33.98 ± 0.12	8.04 ± 0.01	1860.9 ± 25.7	1.08	1.40	1.51	0.543	0.056	23.72 ± 0.42	8.43 ± 0.02	0.33 ± 0.15
		1996	29.29 ± 0.65	33.98 ± 0.12	8.04 ± 0.01	1860.9 ± 25.7	1.14	1.49	1.70	0.543	0.041	23.14 ± 0.47	8.39 ± 0.03	0.35 ± 0.16
		1995	29.29 ± 0.65	33.98 ± 0.12	8.04 ± 0.01	1860.9 ± 25.7	1.34	1.54	2.06	0.543	0.043	23.67 ± 0.26	8.43 ± 0.02	0.54 ± 0.21
Airai	23	2009	29.63 ± 0.70	33.06 ± 0.62	8.03 ± 0.04	1805.6 ± 59.1	1.66	1.12	1.86	0.655	0.050	21.32 ± 0.85	8.27 ± 0.04	0.53 ± 0.21
Donghsa	751	2010	26.40 ± 2.33	33.54 ± 0.49	7.96 ± 0.07	1819.7 ± 45.5	1.25	1.03	1.29	0.857	0.075	23.78 ± 0.43	8.47 ± 0.07	0.51 ± 0.20
		2011	26.40 ± 2.33	33.54 ± 0.49	7.96 ± 0.07	1819.7 ± 45.5	1.51	1.04	1.58	0.857	0.074	23.46 ± 0.34	8.45 ± 0.06	0.23 ± 0.08
		2012	26.40 ± 2.33	33.54 ± 0.49	7.96 ± 0.07	1819.7 ± 45.5	1.24	0.95	1.18	0.857	0.077	23.65 ± 0.27	8.46 ± 0.06	0.35 ± 0.07
Green Is	701	2010	27.02 ± 1.88	33.50 ± 0.50	8.10 ± 0.01	1913.2 ± 27.7	0.54	1.37	0.74	0.602	0.077	24.74 ± 0.65	8.52 ± 0.06	0.72 ± 0.08
		2011	27.02 ± 1.88	33.50 ± 0.50	8.10 ± 0.01	1913.2 ± 27.7	0.60	1.42	0.85	0.602	0.073	24.58 ± 0.67	8.51 ± 0.06	0.65 ± 0.08
		2012	27.02 ± 1.88	33.50 ± 0.50	8.10 ± 0.01	1913.2 ± 27.7	0.45	1.43	0.64	0.602	0.078	24.48 ± 0.61	8.51 ± 0.06	0.57 ± 0.09
Saboga	192	2008	26.50 ± 1.02	30.90 ± 2.54	8.04 ± 0.02	1778.5 ± 44.5	0.78	0.93	0.73	0.701	0.073	22.11 ± 0.31	8.37 ± 0.05	0.65 ± 0.09
Average			28.47 ± 1.22	33.10 ± 0.62	7.98 ± 0.03	1838.83 ± 33.6	0.95	1.21	1.12	0.562	0.063	23.42 ± 0.35	8.43 ± 0.04	0.54 ± 0.11

For Palau cores, seawater salinity, pH, and DIC were averaged over discrete samples taken from the corresponding reef sites between 2011 and 2015. Seawater conditions for Donghsa atoll and Green island sites are based on measurements of seawater samples taken at the time of collection only. No in situ seawater measurements were made when Saboga 192 core was collected, therefore seawater conditions at this site were estimated from values reported in Manzello et al. (2008) for the same location.

* For these coral cores, boron isotope compositions were determined and reported by DeCarlo et al. (2016).

A2.10 References

Allison N, Cohen I, Finch AA, Erez J, Tudhope AW, Facility EIM (2014) Corals concentrate dissolved inorganic carbon to facilitate calcification. Nat Commun 5:5741

Baker PA, Weber JN (1975) Coral growth rate: Variation with depth. Phys Earth Planet Inter 10:135–139

Barkley HC, Cohen AL, Golbuu Y, Starczak VR, Decarlo TM, Shamberger KEF (2015) Changes in coral reef communities across a natural gradient in seawater pH. Sci Adv 1–7

Barnes DJ, Lough JM (1993) On the nature and causes of density banding in massive coral skeletons. J Exp Mar Bio Ecol 167:91–108

Cantin NE, Cohen AL, Karnauskas KB, Tarrant AM, McCorkle DC (2010) Ocean Warming Slows Coral Growth in the Central Red Sea. 329:322–325

Cohen AL, McConnaughey TA (2003) Geochemical Perspectives on Coral Mineralization. Rev Mineral Geochemistry 54:151–187

Coles SL, Jokiel PL (1977) Effects of temperature on photosynthesis and respiration in hermatypic corals. Mar Biol 43:209–216

Comeau S, Cornwall CE, McCulloch MT (2017) Decoupling between the response of coral calcifying fluid pH and calcification to ocean acidification. Sci Rep 7:7573

Cooper TF, De'ath G, Fabricius KE, Lough JM (2008) Declining coral calcification in massive Porites in two nearshore regions of the northern Great Barrier Reef. Glob Chang Biol 14:529–538

Crook ED, Cohen AL, Rebolledo-Vieyra M, Hernandez L, Paytan A (2013) Reduced calcification and lack of acclimatization by coral colonies growing in areas of persistent natural acidification. Proc Natl Acad Sci U S A 110:11044–9

Cuif JP, Dauphin Y (2005) The Environment Recording Unit in coral skeletons – a synthesis of structural and chemical evidences for a biochemically driven, stepping-growth process in bres. Biogeosciences 2:61–73

De'ath G, Lough JM, Fabricius KE (2009) Declining coral calcification on the Great Barrier Reef. Science (80-) 323:116–119

Elman JL (1991) On the inclusion of trace materials into massive coral skeletons. Mach Learn 7:195–225

Fabricius KE, Langdon C, Uthicke S, Humphrey C, Noonan S, De 'ath G, Okazaki R, Muehllehner N, Glas MS, Lough JM (2011) Losers and winners in coral reefs acclimatized to elevated carbon dioxide concentrations. Nat Clim Chang 1:165–169

Furla P (2000) Furla P , Galgani I , Durand I , Allemand D .. Sources and mechanisms of inorganic carbon transport for coral calcification and photosynthesis . J Exp. J Exp Biol 3445–3457

Gagan MK, Dunbar GB, Suzuki A (2012) The effect of skeletal mass accumulation in Porites on coral Sr/Ca and ??^{18}O paleothermometry. Paleoceanography 27:1–16

Hetzinger S, Pfeiff M, Dullo W, Zinke J (2016) A change in coral extension rates and stable isotopes after El Niño- induced coral bleaching and regional stress events. 1–10

Holcomb M, DeCarlo T, Gaetani G, McCulloch M (2016) Factors affecting B/Ca ratios on synthetic aragonite. 67–76

Hooidonk R Van, Maynard J, Tamelander J, Gove J (2016) Local-scale projections of coral reef futures and implications of the Paris Agreement. Nat Publ Gr 1–8

Hughes TP (1987) Skeletal density and growth form of corals. 35:259–266

Huston M (1985) Variation in coral growth rates with depth. Coral Reefs 4:19–25

Linsley BK, Messier RG, Dunbar RB (1999) Assessing between-colony oxygen isotope variability in the coral Porites iobata at Clipperton Atoll. Coral Reefs 18:13–27

Lough JM, Barnes DJ (2000) Environmental controls on growth of the massive coral Porites. J Exp Mar Bio Ecol 245:225–243

Manzello DP, Enochs IC, Bruckner A, Renaud PG, Kolodziej G, Budd DA, Carlton R, Glynn PW (2014) Galapagos coral reef persistence after ENSO warming across an acidification gradient.

Geophys Res Lett 41:9001–9008

Mcculloch MT, Olivo JPD, Falter J, Holcomb M, Trotter JA (2017) Coral calcification in a changing World and the interactive dynamics of pH and DIC upregulation. 1–8

McNeil BI, Matear RJ, Barnes DJ (2004) Coral reef calcification and climate change : The effect of ocean warming. 31:2–5

Nie B, Chen T, Zhu ML, Wang Y, Zhong J, Zhu Y (1997) Relationship between coral growth rate and sea surface temperature in the northern part of South China Sea during the past 100 a. Sci China Ser D Earth Sci 40:173–182

Northdruft LD, Webb GE (2007) Microstructure of common reef-building coral genera Acropora, Pocillopora, Goniastrea and Porites: constraints on spatial resolution in geochemical sampling. Facies - Carbonate Sedimentol Paleoecol 53:1–26

Poulsen A, Burns K, Lough J, Brinkman D, Delean S (2006) Trace analysis of hydrocarbons in coral cores from Saudi Arabia. Org Geochem 37:1913–1930

Shirai K, Sowa K, Watanabe T, Sano Y, Nakamura T, Clode P (2012) Visualization of sub-daily skeletal growth patterns in massive Porites corals grown in Sr-enriched seawater. J Struct Biol 180:47–56

Szmant AM (1986) Coral Reefs Reproductive ecology of Caribbean reef corals. 43–53

Tambutté E, Venn AA, Holcomb M, Segonds N, Techer N, Zoccola D, Allemand D, Tambutté S (2015) Morphological plasticity of the coral skeleton under CO2-driven seawater acidification. Nat Commun 6:7368

Tanzil JTI, Brown BE, Dunne RP, Lee JN, Kaandorp JA, Todd PA (2013) Regional decline in growth rates of massive Porites corals in Southeast Asia. Glob Chang Biol 19:3011–3023

Tanzil JTI, Brown BE, Tudhope AW, Dunne RP (2009) Decline in skeletal growth of the coral Porites lutea from the Andaman Sea, South Thailand between 1984 and 2005. Coral Reefs 28:519–528

Taylor RB, Barnes DJ, Lough JM (1993) Simple-Models of Density Band Formation in Massive

Corals. J Exp Mar Bio Ecol 167:109–125

Veron JE., Stafford-Smith M (2000) Corals of the world. Vol 1-3. Australian Institute of Marine Science, Townsville MC, Qld, Australia

Warner ME, Fitt WK, Schmidt GW (1996) The effects of elevated temperature on the photosynthetic efficiency of zooxanthellae in hospite from four different species of reef coral: a novel approach. Plant Cell Environ 19:291–299

Wellington GM, Dunbar RB, Merlen G (1996) Calibration of stable oxygen isotope signatures in Galpagos corals. Paleoceanography 11:467–480

Wells JW (1956) Scleractinia. Treatise on invertebrate paleontology F. Coelenterata. Geological Society of America & University of Kansas Press, pp 328–440

Appendix A3 – Supplementary text, figures, and data for chapter 3

A3.1 Formulation of the Mantel-Haenszel estimator

An odds ratio can be used to estimate the chance of an outcome occurring (in this case the formation of a stress band) relative to another, independently observed outcome (in this case coral bleaching). Here we use it to estimate a given coral community's propensity to form stress bands at different levels of bleaching, and to compare the prevalence of stress banding on different reefs. In this context, the common odds ratio can be expressed as:

$$\psi = \frac{p_{bi}/(1 - p_{bi})}{p_{sb}/(1 - p_{sb})}$$

Where p_{bi} is the probability of a coral bleaching at a given time, and p_{sb} the probability that a coral has a stress band associated with the same time. If sampled colonies are assumed to follow a binomial distribution in both the probability to bleach and to form a stress band formation, the Mantel-Haenszel estimator of the common odds ratio can be expressed as follows:

$$\hat{\psi} = \frac{\sum_{j=1}^{J} X_j(n_j - Y_j)/N_j}{\sum_{j=1}^{J} Y_j(m_j - X_j)/N_j}$$

Where X_j is the number out of m_j corals that produce stress bands, and Y_j is the number out of n_j corals that bleach for an event j. Because bleaching data is commonly reported in percent cover bleached, and not the number of colonies bleached, we estimated Y_j as the number of square meters bleached (Y_j^*) out of a total of n_j^* square meters. Substituting these values into the equation above, and treating each bleaching event on each reef as an individual event j, we estimated a common odds ratio of $\hat{\psi}$ = 1.11, which implies a near 1 to 1 association between the amount of stress bands observed in the coral colonies, and the amount of coral cover bleached. The variance in this relationship was estimated using Equation 2 in the main text, and converted to 2σ = 0.10,

implying a very consistent odds ratio between stress band prevalence and observed community bleaching among reefs, and between events at a single reef (where more than one were observed).

A3.2 Calibration of the percentile based bleaching threshold

We calibrated the ENSO-Neutral Percentile based model of thermal stress to select a percentile of the climatological SST that maximizes bleaching prediction. We compared bleaching predictions made using a range of threshold percentiles (84.0^{th} to 99.9^{th}) to the database of bleaching observations recently published by Donner et al., (2017). In this analysis, we considered each year at each site an individual event for a total of $n = 21{,}384$ predictions. In keeping with the traditional NOAA methodology, bleaching was predicted for an event if the DHW exceeded 4 °C·weeks during a given year at each site. The overall quality of prediction was assessed using the Gilbert or Equitable Threat Score (ETS) (Fig. A3.1):

$$ETS = \frac{S - S_r}{S + F_1 + F_2 - S_r}$$

Where S is total number of correct predictions (i.e. bleaching occurred and was predicted or did not occur and was not predicted) and F_1 and F_2 are type 1 and type 2 errors. S_r are successes that can be attributed to random chance, and are defined as:

$$S_r = (S + F_1)(S + F_2)/n$$

Possible ETS range from -⅓ to 1, with 1 indicating perfect predictive power. Using this metric, the maximum predictive power of the percentile-based model was found to be at a threshold percentile of 94.4. We then compared the calibrated ENSO-Neutral Percentile based model to the traditional MMM model to evaluate the quality of our predictions versus those made using the established method. When comparing the predictive power of two models using scarce data, such as bleaching observations, it is critical to assess both type I (false positive) and type II (false negative) errors as well as the accuracy of predictions as a whole. While some amount of type I errors is expected (bleaching may likely have occurred but not been documented), an abundance of type II errors suggests the number of correct predictions a model makes may be a result of over-

prediction. As can be seen in Table A3.1, the ENSO-Neutral percentile based DHW have a higher ETS, and more often correctly predict the bleaching state.

While the ideal validation for this new model would be to compare predictive power in the Central Pacific relative to higher latitudes, the paucity of observations of bleaching on these equatorial reefs precludes such an analysis. The methodology of the ENSO-Neutral Percentile based method is more directly designed to compare thermal stress in equatorial environments with higher latitudes than the MMM model. Combined with the evidence of equivalent if not superior prediction at locations where bleaching observations have been made suggest that this model is better suited to be used in comparing thermal tolerances of equatorial versus higher latitude corals.

A3.3 Supplementary figures and tables

Figure A3.1: Distribution of Brier Score (BS) for each percentile of weekly SSTs over the ENSO neutral calibration period (1984-5, 1990, 1993, 1996) used to calculate bleaching thresholds for reef sites reported in Donner *et al.*, (2017). The percentile used to set the thermal threshold at each site was varied across a range of 90.00th to 99.99th at increments of 0.01. The minimum BS, and therefore the maximum predictive power occurred at the 97.55th percentile.

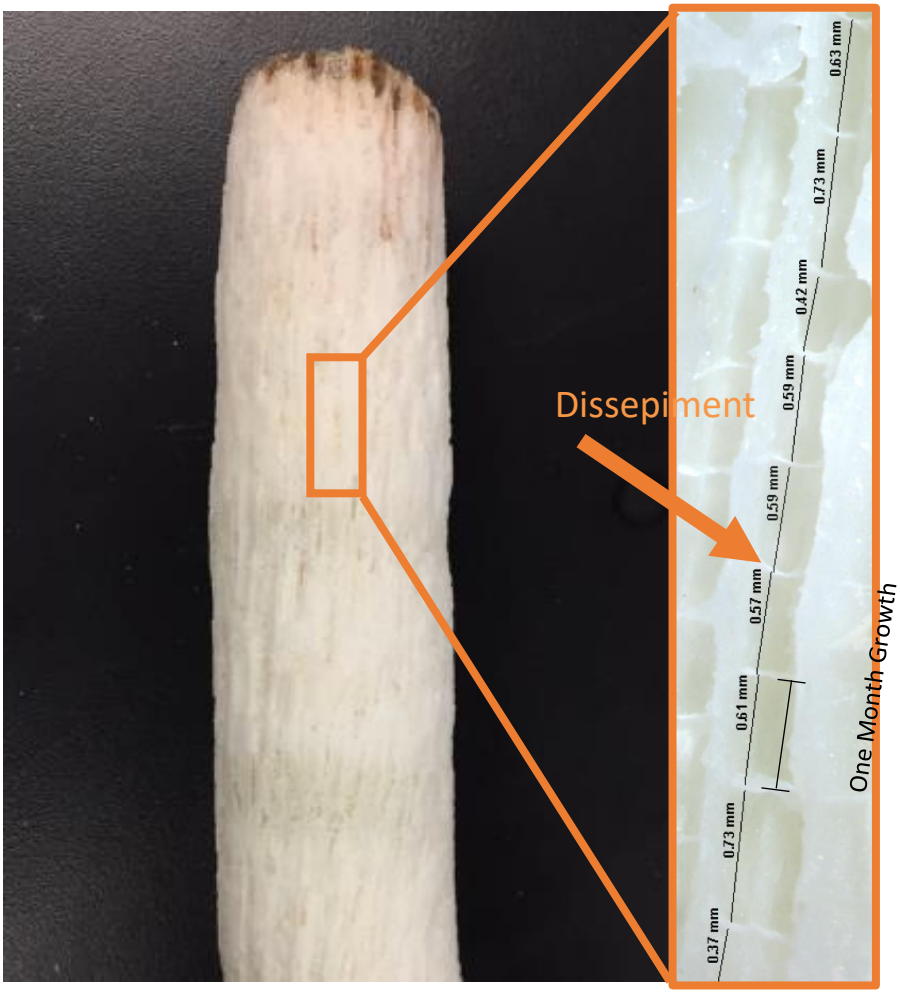

Figure A3.2: Microscope image of *Montastrea* coral core in which annual banding was difficult to interpret in CT imaging. Monthly dissepiments used to verify annual growth banding shown in right panel. SPOT Microscope software was used to measure distances between dissepimental sheets, representing monthly growth.

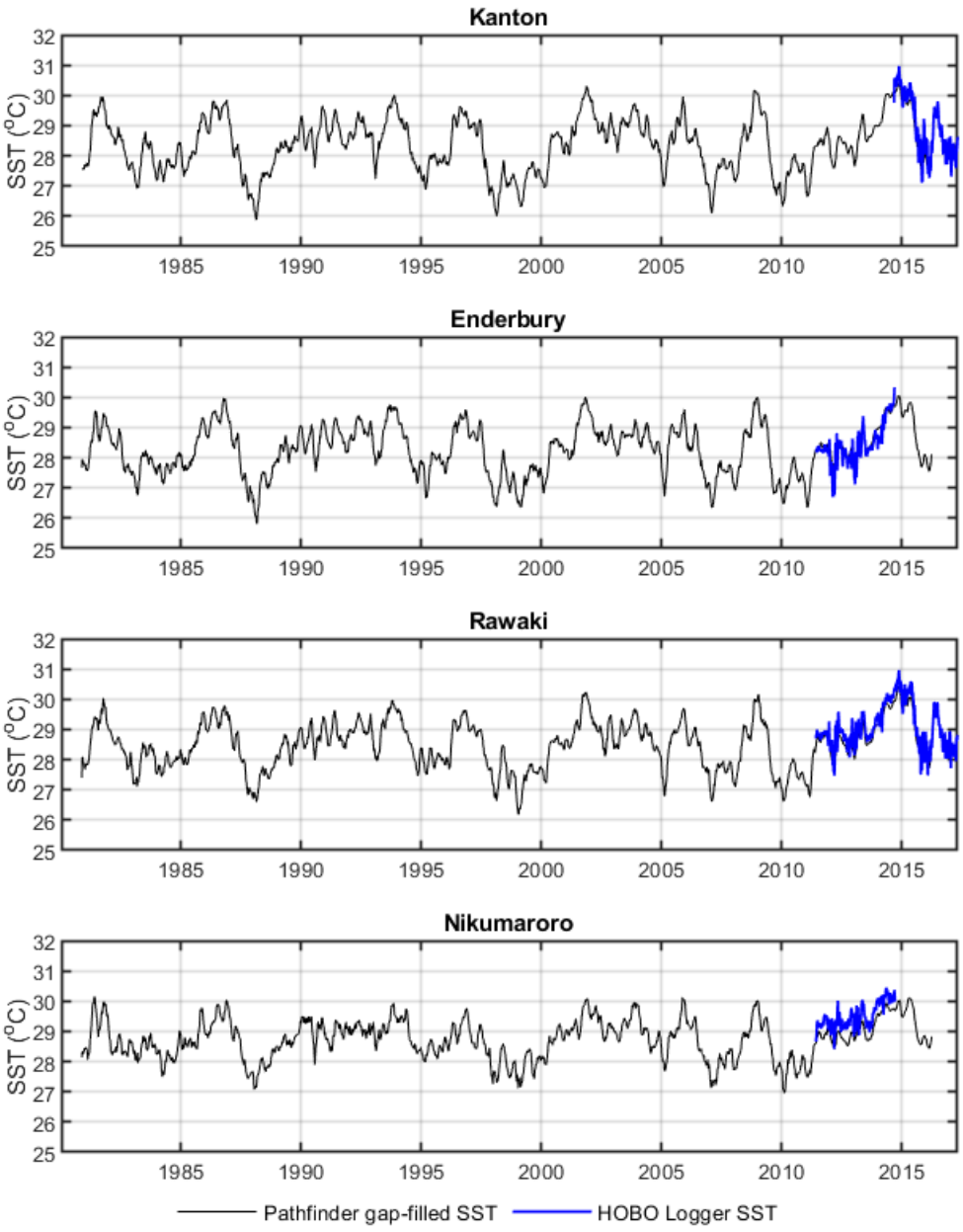

Figure A3.3: Weekly averaged Hobo logger temperatures at Kanton, Enderbury, Rawaki, and Nikumaroro compared with weekly averaged gap-filled pathfinder SST data. All locations are within 0.25 °C on average, suggesting reef temperatures are closely represented by the open ocean SST.

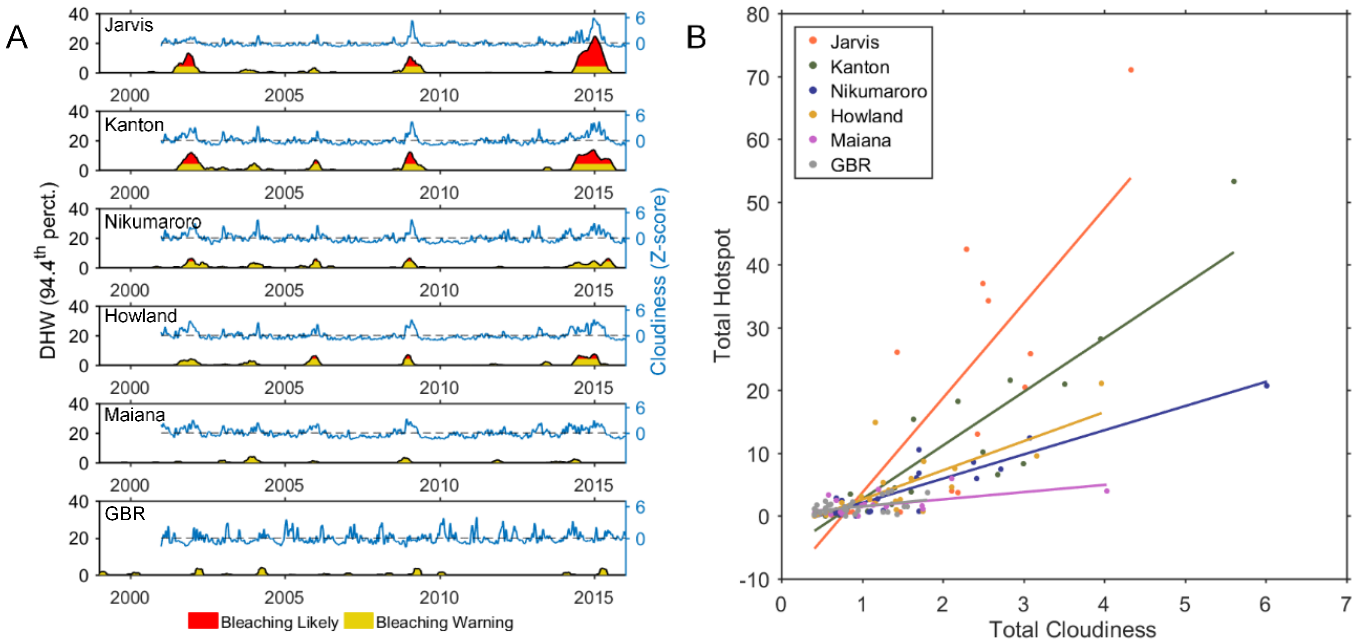

Figure A3.4 A: Degree heating weeks calculated using the ENSO-neutral percentile-based method compared with Cloud Fraction calculated from weekly OLR. During El Niño events, cloudiness increases significantly in the Central Pacific. **B:** Total Hotspot for each thermal stress event at each island compared with total cloudiness over the associated time period. Jarvis Island, despite having the highest thermal tolerance ($b_{½}$), shows the lowest amount of cloudiness per Hotspot while the GBR and Maiana show the highest suggesting cloudiness does not increase the relative thermal tolerance between reef communities in this study.

Table A3.1: Comparison of predictive power of bleaching predictions made using the ENSO-Neutral model versus the traditional MMM model of calculating bleaching thresholds.

Method	Bleaching Alert Level (ºC·weeks)	Type 1 prediction Error (%)	Type 2 prediction Error (%)	Correct Predictions (%)	ETS (-⅓ to 1) (0 desired)
MMM (NOAA)	4	12.4	3.8	83.7	0.059
ENSO-Neutral %	4	7.4	4.1	88.5	0.083

Predictions were assessed using the bleaching observations dataset of Donner et al., (2017).

Table A3.2: Coral Cores used in the stress band-observed bleaching incidence calibration

Location	Core ID	Lat	Lon	Depth	Date Collected	length (cm)
Palau	166	7.3259	134.4945	5	9/20/2011	38
Palau	167	7.3259	134.4945	9	9/20/2011	36
Palau	168	7.3259	134.4945	10	9/20/2011	38
Palau	169	7.3259	134.4945	20	9/20/2011	33
Palau	178	7.1526	134.1334	4	4/13/2011	33
Palau	210	7.2688	134.5222	13	9/22/2011	10
Palau	211	7.2697	134.5496	1.3	9/23/2011	38
Palau	213	7.1347	134.1349	11	9/21/2011	10
Palau	214	7.2688	134.5222	7	9/22/2011	33
Palau	216	7.1347	134.1349	6	9/21/2011	9
Palau	217	7.1347	134.1349	8	9/21/2011	35
Palau	218	7.1347	134.1349	12	9/21/2011	31
Palau	219	7.1347	134.1349	8	9/21/2011	10
Palau	220	7.1347	134.1349	8	9/21/2011	32
Palau	221	7.2688	134.5222	18	9/22/2011	33
Palau	222	7.1347	134.1349	12	9/21/2011	12
Palau	223	7.1347	134.1349	5	9/21/2011	11
Palau	224	7.1347	134.1349	10	9/21/2011	37
Palau	225	7.1347	134.1349	10	9/21/2011	36
Palau	229	7.2688	134.5222	8	9/22/2011	37
Palau	230	7.2688	134.5222	9	9/22/2011	30
Palau	231	7.2688	134.5222	5	9/22/2011	36
Palau	232	7.2688	134.5222	10	9/22/2011	9
Palau	233	7.2688	134.5222	6	9/22/2011	9
Palau	234	7.2688	134.5222	11	9/22/2011	12
Palau	235	7.2688	134.5222	6	9/22/2011	7
Palau	237	7.2697	134.5496	1.9	9/23/2011	36
Palau	239	7.2697	134.5496	1.5	9/23/2011	37
Palau	240	7.2697	134.5496	5	9/23/2011	9
Palau	243	7.2697	134.5496	5	9/23/2011	10
Palau	244	7.2697	134.5496	4	9/23/2011	32
Palau	266	7.3235	134.4943	6	4/7/2012	35
Palau	267	7.3235	134.4943	22	4/7/2012	37
Palau	268	7.3235	134.4943	19	4/7/2012	37
Palau	269	7.3235	134.4943	19	4/7/2012	37
Palau	270	7.3235	134.4943	19	4/7/2012	38
Palau	271	7.3095	134.4768	4	4/6/2008	37
Palau	272	7.3095	134.4768	5	4/6/2008	33
Palau	275	7.3095	134.4768	15	4/5/2012	34

Palau	276	7.3095	134.4768	15	4/5/2012	37
Palau	277	7.3095	134.4768	10	4/5/2012	37
Palau	279	7.2726	134.5495	4	4/5/2012	46.5
Palau	325	7.2675	134.5215	5	3/31/2012	57
Palau	772	7.4349	134.3570	6	10/30/2013	31
Palau	773	7.4349	134.3570	6	10/30/2013	37.5
Palau	774	7.4349	134.3570	6	10/30/2013	37
Palau	775	7.4349	134.3570	6	10/30/2013	37
Palau	776	7.4349	134.3570	6	10/30/2013	16.5
Palau	777	7.4349	134.3570	6	10/30/2013	11.5
Palau	778	7.4349	134.3570	6	10/30/2013	11.5
Palau	779	7.4349	134.3570	6	10/30/2013	12
Palau	780	7.4349	134.3570	6	10/30/2013	37
Palau	781	7.4349	134.3570	6	10/30/2013	31
Palau	782	7.1619	134.3502	15	11/1/2013	37
Palau	783	7.1619	134.3502	24	11/1/2013	33
Palau	784	7.1619	134.3502	16	11/1/2013	34
Palau	785	7.1619	134.3502	25	11/1/2013	35.5
Palau	786	7.1619	134.3502	16	11/1/2013	36.5
Palau	787	7.1619	134.3502	16	11/1/2013	35.5
Palau	788	7.1619	134.3502	18	11/1/2013	17
Palau	789	7.1619	134.3502	18	11/1/2013	26
Palau	790	7.1619	134.3502	18	11/1/2013	34
Palau	791	7.1619	134.3502	18	11/1/2013	35
Palau	812	7.2763	134.4270	4	11/2/2013	37
Palau	813	7.2763	134.4270	4	11/2/2013	27
Palau	814	7.2763	134.4270	4	11/2/2013	27
Palau	815	7.2763	134.4270	5	11/2/2013	30
Palau	816	7.2763	134.4270	7	11/2/2013	37
Palau	817	7.2763	134.4270	10	11/2/2013	37
Palau	818	7.2763	134.4270	12	11/2/2013	37
Palau	819	7.2763	134.4270	12	11/2/2013	37
Palau	820	7.2763	134.4270	13	11/2/2013	23
Palau	821	7.2763	134.4270	8	11/2/2013	37
Palau	854	7.3380	134.4643	8	11/9/2013	31
Palau	855	7.3380	134.4643	19	11/9/2013	36
Palau	856	7.3380	134.4643	22	11/9/2013	37
Palau	857	7.3380	134.4643	7	11/9/2013	37
Palau	858	7.3380	134.4643	5	11/9/2013	34
Palau	859	7.3380	134.4643	6	11/9/2013	38
Palau	860	7.3380	134.4643	6	11/9/2013	36
Palau	861	7.3380	134.4643	6	11/9/2013	25
Palau	862	7.3380	134.4643	8	11/9/2013	28
Palau	863	7.3380	134.4643	5	11/9/2013	35

Palau	958	7.8217	134.5625	3	8/24/2014	27
Palau	959	7.8217	134.5625	3	8/24/2014	23
Palau	960	7.8217	134.5625	3	8/24/2014	31
Palau	961	7.8217	134.5625	3	8/24/2014	38
Palau	962	7.8217	134.5625	3	8/24/2014	41
Palau	963	7.8217	134.5625	3	8/24/2014	37
Palau	964	7.8217	134.5625	3	8/24/2014	37
Palau	970	7.3170	134.2197	23	1/24/2015	35
Palau	971	7.3170	134.2197	23	1/24/2015	36
Palau	972	7.3170	134.2197	23	1/24/2015	32
Palau	973	7.3170	134.2197	22	1/24/2015	37
Palau	974	7.3170	134.2197	22	1/24/2015	38
Palau	975	7.3170	134.2197	21	1/24/2015	34
Palau	976	7.3170	134.2197	20	1/24/2015	31
Palau	977	7.3170	134.2197	20	1/24/2015	37
Palau	978	7.3170	134.2197	26	1/24/2015	29
Palau	I	7.3259	134.4945	4	9/20/2011	20
Palau	O	7.3259	134.4945	5	9/20/2011	10
Dongsha Atoll	756	20.6990	116.9016	5	6/18/2013	62
Dongsha Atoll	757	20.6990	116.9016	5	6/18/2013	24
Dongsha Atoll	759	20.6990	116.9016	4	6/18/2013	51
Dongsha Atoll	760	20.6990	116.9016	3	6/18/2013	58
Dongsha Atoll	761	20.6990	116.9016	4	6/18/2013	24
Dongsha Atoll	762	20.6980	116.8911	3	6/18/2013	71
Dongsha Atoll	763	20.6980	116.8911	3	6/18/2013	28
Dongsha Atoll	764	20.6980	116.8911	3	6/18/2013	29
Dongsha Atoll	765	20.6980	116.8911	3	6/18/2013	26
Dongsha Atoll	884	20.6993	116.9022	1	5/26/2014	19
Dongsha Atoll	886	20.6993	116.9022	1	5/26/2014	28
Dongsha Atoll	887	20.6993	116.9022	1	5/26/2014	21
Dongsha Atoll	888	20.6993	116.9022	1	5/26/2014	37
Dongsha Atoll	889	20.6993	116.9022	1	5/26/2014	28
Dongsha Atoll	890	20.6993	116.9022	1	5/26/2014	36
Dongsha Atoll	891	20.6993	116.9022	1	5/26/2014	24
Dongsha Atoll	892	20.6993	116.9022	1	5/26/2014	31
Dongsha Atoll	893	20.6993	116.9022	1	5/26/2014	28
Dongsha Atoll	901	20.6993	116.9022	1	6/4/2014	38
Dongsha Atoll	904	20.6993	116.9022	1	6/4/2014	34
Dongsha Atoll	918	20.6990	116.9022	1	6/20/2014	36
Dongsha Atoll	919	20.6990	116.9022	1	6/20/2014	35
Dongsha Atoll	1271	20.6993	116.9024	3	6/24/2017	36
Dongsha Atoll	1272	20.6993	116.9024	3	6/24/2017	33
Dongsha Atoll	1273	20.6993	116.9024	3	6/24/2017	22
Dongsha Atoll	890 D	20.6993	116.9024	3	6/24/2017	33

Dongsha Atoll	1275	20.6993	116.9024	3	6/26/2017	8
Dongsha Atoll	1276	20.6993	116.9024	3	6/26/2017	35
Dongsha Atoll	1277	20.6993	116.9024	3	6/26/2017	35
Dongsha Atoll	1278	20.6993	116.9024	3	6/26/2017	37
Dongsha Atoll	1279	20.6993	116.9024	3	6/26/2017	37
Dongsha Atoll	1280	20.6993	116.9024	3	6/26/2017	35
Dongsha Atoll	1268	20.6996	116.9069	2	7/2/2017	34
Dongsha Atoll	1282	20.6996	116.9069	2	7/2/2017	25
Dongsha Atoll	1283	20.6996	116.9069	2	7/2/2017	24
Dongsha Atoll	1284	20.6996	116.9069	2	7/2/2017	37
Dongsha Atoll	1285	20.6996	116.9069	2	7/2/2017	33
Dongsha Atoll	1287	20.6996	116.9069	2	7/2/2017	21
Dongsha Atoll	1288	20.6996	116.9069	2	7/2/2017	35
Dongsha Atoll	1289	20.6996	116.9069	2	7/2/2017	36
Martinique	719	14.4574	-60.9209	15	12/11/2013	101
Martinique	727	14.6483	-61.1515	28	12/10/2013	58
Martinique	728	14.4574	-60.9209	15	12/11/2013	67
Martinique	729	14.4574	-60.9209	15	12/11/2013	86
Martinique	731	14.4574	-60.9209	15	12/11/2013	96
Martinique	733	14.4574	-60.9209	15	12/11/2013	61
Martinique	734	14.4574	-60.9209	15	12/11/2013	111
Martinique	735	14.4563	-60.9257	20	12/12/2013	41
Martinique	737	14.4563	-60.9257	16	12/12/2013	42
Martinique	738	14.4563	-60.9257	15	12/12/2013	105
Martinique	739	14.4563	-60.9257	18	12/12/2013	70
Martinique	740	14.4563	-60.9257	18	12/12/2013	60
Barbados	742	13.0975	-59.6266	23	12/14/2013	43
Barbados	743	13.0975	-59.6266	23	12/14/2013	64
Barbados	732	13.1139	-59.6349	25	12/15/2013	60
Barbados	736	13.1139	-59.6349	25	12/15/2013	65
Barbados	741	13.1135	-59.6347	25	12/15/2013	71
Barbados	744	13.1139	-59.6349	22	12/15/2013	96
Barbados	745	13.1135	-59.6347	19	12/15/2013	67
Barbados	746	13.1135	-59.6347	16	12/15/2013	62
Curacao	747	12.0823	-68.8915	20	12/20/2013	74
Curacao	748	12.0823	-68.8915	18	12/20/2013	111
Curacao	876	12.0823	-68.8915	20	12/20/2013	61
Curacao	877	12.0804	-68.8893	9	12/21/2013	65
Curacao	878	12.0804	-68.8893	7	12/21/2013	67
Curacao	879	12.2021	-69.0829	12	12/22/2013	60
Curacao	880	12.2023	-69.0833	12	12/22/2013	45
Curacao	881	12.1872	-69.0623	16	12/22/2013	84
Curacao	882	12.2021	-69.0829	13	12/22/2013	52
Curacao	883	12.1872	-69.0623	15	12/22/2013	66

Curacao	885	12.2023	-69.0833	12	12/22/2013	66
Jarvis	481	-0.3710	-159.9839	17	9/14/2012	102
Jarvis	490	-0.3696	-160.0083	24	9/16/2012	83
Jarvis	494	-0.3692	-160.0083	39	9/15/2012	45
Jarvis	499	-0.3715	-159.9823	20	9/14/2012	98
Jarvis	500	-0.3715	-159.9823	17	9/14/2012	68
Jarvis	1200	-0.3714	-159.9825	20	11/14/2015	8.75
Jarvis	1201	-0.3714	-159.9825	20	11/14/2015	9
Jarvis	1202	-0.3714	-159.9825	20	11/14/2015	8
Jarvis	1203	-0.3714	-159.9825	20	11/14/2015	6.5
Jarvis	1204	-0.3714	-159.9825	20	11/14/2015	8
Jarvis	1206	-0.3690	-160.0081	36	11/15/2015	5.5
Jarvis	1207	-0.3690	-160.0081	32	11/15/2015	8.5
Jarvis	1208	-0.3690	-160.0081	36	11/15/2015	6.5
Jarvis	1209	-0.3690	-160.0081	26	11/15/2015	8.5
Jarvis	1210	-0.3690	-160.0081	25	11/15/2015	7.5
Jarvis	1212	-0.3690	-160.0081	13	11/15/2015	10.2
Jarvis	1213	-0.3687	-160.0078	17	11/15/2015	7
Jarvis	1214	-0.3690	-160.0081	25	11/15/2015	9.8
Jarvis	1215	-0.3690	-160.0081	14	11/15/2015	9
Jarvis	1217	-0.3711	-159.9837	20	5/24/2016	164
Jarvis	JAR1-5	-0.3690	-160.0082	55	4/4/2010	28
Jarvis	JAR3-7	-0.3691	-160.0082	42	4/4/2010	35
Jarvis	JAR5-9	-0.3763	-160.0139	23	4/4/2010	33
Jarvis	JAR6-10	-0.3761	-160.0139	45	4/4/2010	33
Jarvis	JAR-H-017	-0.3695	-160.0084	36	5/6/2012	74
Jarvis	JAR-H-018	-0.3691	-159.9831	11	5/6/2012	196
Jarvis	JAR-P-016	-0.3739	-159.9834	15	5/5/2012	62
Kanton	1025	-2.84599	-171.63937	4.5	9/5/2015	31
Kanton	1032	-2.80543	-171.72057	48	9/6/2015	42
Kanton	1033	-2.80641	-171.70673	15	9/6/2015	106
Kanton	1037	-2.84597	-171.63932	5	9/7/2015	28
Kanton	1038	-2.84597	-171.63932	5	9/7/2015	31
Kanton	1039	-2.84597	-171.63932	5	9/7/2015	40
Kanton	1040	-2.83136	-171.66009	5	9/7/2015	30.5
Kanton	1041	-2.83136	-171.66009	5	9/7/2015	22
Kanton	1043	-2.79282	-171.72250	39	9/7/2015	107.5
Enderbury	1080	-3.11266	-171.09329	39	9/9/2015	56
Enderbury	1081	-3.11266	-171.09329	45	9/9/2015	50
Enderbury	1084	-3.11260	-171.09326	39	9/9/2015	39
Enderbury	1089	-3.11272	-171.09329	39	9/10/2015	40
Enderbury	1092	-3.11274	-171.09325	39	9/10/2015	58.5
Enderbury	1094	-3.1111	-171.0937	36	9/11/2015	69
Enderbury	1102	-3.11106	-171.0939	36	9/11/2015	51

Nikumororo	1176	-4.65047	-174.543	37	9/25/2015	38
Nikumororo	1177	-4.65067	-174.5429	29	9/25/2015	73
Nikumororo	1178	-4.65067	-174.5429	28	9/25/2015	74
Nikumororo	1179	-4.65039	-174.5431	41	9/25/2015	28
Nikumororo	1180	-4.65039	-174.5431	38	9/25/2015	33
Nikumororo	1181	-4.6503	-174.5428	37	9/26/2015	44
Nikumororo	1182	-4.65031	-174.5428	37	9/26/2015	38
Nikumororo	1183	-4.65033	-174.5433	37	9/27/2015	33
Nikumororo	1184	-4.65057	-174.5431	37	9/27/2015	39
Nikumororo	1185	-4.6504	-174.5434	37	9/27/2015	24
Rawaki	1132	-3.72019	-170.7176	39	9/13/2015	50
Rawaki	1137	-3.72019	-170.7176	39	9/13/2015	89.5
Rawaki	1142	-3.72019	-170.7176	33	9/13/2015	61
Rawaki	1151	-3.71849	-170.7183	39	9/14/2015	70
Rawaki	1152	-3.71849	-170.7183	38	9/14/2015	70
Rawaki	1153	-3.71849	-170.7183	39	9/14/2015	34
Rawaki	1154	-3.71849	-170.7183	41	9/14/2015	28
Rawaki	1155	-3.71838	-170.7183	41	9/14/2015	36
Rawaki	1156	-3.71838	-170.7183	39	9/14/2015	22.5
Rawaki	1157	-3.71838	-170.7183	38	9/14/2015	37
Rawaki	1160	-3.72019	-170.7176	33	9/15/2015	43
Howland	501	0.8090	-176.6219	16	9/22/2012	20
Howland	502	0.8104	-176.6224	38	9/23/2012	30
Howland	503	0.8094	-176.6221	22	9/22/2012	18.5
Howland	504	0.8105	-176.6225	19	9/23/2012	24
Howland	505	0.8105	-176.6225	27	9/23/2012	74
Howland	506	0.8090	-176.6219	22	9/22/2012	86
Howland	509	0.8094	-176.6221	22	9/22/2012	20
Howland	511	0.8090	-176.6219	17	9/22/2012	18
Howland	HOW-001	0.7990	-176.6202	19	3/13/2012	35
Howland	HOW-002	0.7987	-176.6201	34	3/14/2012	26
Howland	HOW-003	0.8003	-176.6208	33	3/14/2012	94

Table A3.3: Coral Cores used in the reconstruction of thermal tolerances

Location	Core ID	Lat (N)	Lon (E)	Depth	Date Collected	length (cm)
Enderbury	428	-3.1177	-171.0931	34	6/11/2012	13
Enderbury	429	-3.1177	-171.0931	34	6/11/2012	10.4
Enderbury	430	-3.1177	-171.0931	35	6/11/2012	10.8
Enderbury	432	-3.1125	-171.0933	36	6/13/2012	201
Enderbury	1080	-3.1127	-171.0933	39	9/9/2015	56
Enderbury	1081	-3.1127	-171.0933	45	9/9/2015	50
Enderbury	1084	-3.1126	-171.0933	39	9/9/2015	39
Enderbury	1089	-3.1127	-171.0933	39	9/10/2015	40
Enderbury	1092	-3.1127	-171.0933	39	9/10/2015	58.5
Enderbury	1094	-3.1111	-171.0937	36	9/11/2015	69
Enderbury	1102	-3.1111	-171.0939	36	9/11/2015	51
Howland	501	0.8090	-176.6219	16	9/22/2012	20
Howland	502	0.8104	-176.6224	38	9/23/2012	30
Howland	503	0.8094	-176.6221	22	9/22/2012	18.5
Howland	504	0.8105	-176.6225	19	9/23/2012	24
Howland	505	0.8105	-176.6225	27	9/23/2012	74
Howland	506	0.8090	-176.6219	22	9/22/2012	86
Howland	509	0.8094	-176.6221	22	9/22/2012	20
Howland	511	0.8090	-176.6219	17	9/22/2012	18
Howland	HOW-001	0.7990	-176.6202	19	3/13/2012	35
Howland	HOW-002	0.7987	-176.6201	34	3/14/2012	26
Howland	HOW-003	0.8003	-176.6208	33	3/14/2012	94
Jarvis	481	-0.3710	-159.9839	17	9/14/2012	102
Jarvis	490	-0.3696	-160.0083	24	9/16/2012	83
Jarvis	494	-0.3692	-160.0083	39	9/15/2012	45
Jarvis	499	-0.3715	-159.9823	20	9/14/2012	98
Jarvis	500	-0.3715	-159.9823	17	9/14/2012	68
Jarvis	1200	-0.3714	-159.9825	20	11/14/2015	8.75
Jarvis	1201	-0.3714	-159.9825	20	11/14/2015	9
Jarvis	1202	-0.3714	-159.9825	20	11/14/2015	8
Jarvis	1203	-0.3714	-159.9825	20	11/14/2015	6.5
Jarvis	1204	-0.3714	-159.9825	20	11/14/2015	8
Jarvis	1206	-0.3690	-160.0081	36	11/15/2015	5.5
Jarvis	1207	-0.3690	-160.0081	32	11/15/2015	8.5
Jarvis	1208	-0.3690	-160.0081	36	11/15/2015	6.5
Jarvis	1209	-0.3690	-160.0081	26	11/15/2015	8.5
Jarvis	1210	-0.3690	-160.0081	25	11/15/2015	7.5
Jarvis	1212	-0.3690	-160.0081	13	11/15/2015	10.2
Jarvis	1213	-0.3687	-160.0078	17	11/15/2015	7

Jarvis	1214	-0.3690	-160.0081	25	11/15/2015	9.8
Jarvis	1215	-0.3690	-160.0081	14	11/15/2015	9
Jarvis	1217	-0.3711	-159.9837	20	5/24/2016	164
Jarvis	JAR1-5	-0.3690	-160.0082	55	4/4/2010	28
Jarvis	JAR3-7	-0.3691	-160.0082	42	4/4/2010	35
Jarvis	JAR5-9	-0.3763	-160.0139	23	4/4/2010	33
Jarvis	JAR6-10	-0.3761	-160.0139	45	4/4/2010	33
Jarvis	JAR-H-017	-0.3695	-160.0084	36	5/6/2012	74
Jarvis	JAR-H-018	-0.3691	-159.9831	11	5/6/2012	196
Jarvis	JAR-P-016	-0.3739	-159.9834	15	5/5/2012	62
Kanton	407	-2.8064	-171.7067	12	6/9/2012	20.6
Kanton	408	-2.8064	-171.7067	3	6/9/2012	15.6
Kanton	409	-2.8064	-171.7067	3	6/9/2012	13
Kanton	410	-2.8064	-171.7067	3	6/9/2012	17.8
Kanton	411	-2.8064	-171.7067	3	6/9/2012	14.8
Kanton	413	-2.8064	-171.7067	20	6/9/2012	29.4
Kanton	415	-2.8056	-171.7206	28	6/9/2012	12.6
Kanton	416	-2.8056	-171.7206	36	6/9/2012	63
Kanton	417	-2.8056	-171.7206	27	6/9/2012	12.2
Kanton	1032	-2.8054	-171.7206	48	9/6/2015	42
Kanton	1033	-2.8064	-171.7067	15	9/6/2015	106
Kanton	1043	-2.7928	-171.7225	39	9/7/2015	107.5
Maiana	453	0.9535	172.9552	7	9/30/2012	103.5
Maiana	454	0.9537	172.9547	6	9/30/2012	105
Maiana	455	0.9664	173.0742	20	10/2/2012	106
Maiana	456	0.9664	173.0742	33	10/2/2012	17.5
Maiana	457	0.9664	173.0742	31	10/2/2012	16
Maiana	458	0.9664	173.0742	29	10/2/2012	15
Maiana	459	0.9664	173.0742	30	10/2/2012	20
Maiana	460	0.9664	173.0742	32	10/2/2012	17
Maiana	510	1.0071	172.9827	13	9/29/2012	105
Maiana	513	1.0074	172.9825	14	9/29/2012	94
Maiana	514	1.0071	172.9827	9	9/29/2012	13
Maiana	515	1.0071	172.9827	12	9/29/2012	12
Maiana	518	1.0071	172.9827	10	9/29/2012	11
Maiana	520	1.0069	172.9829	6	9/29/2012	42
Maiana	521	1.0071	172.9827	13	9/29/2012	18
Maiana	523	1.0071	172.9827	9	9/29/2012	15.5
Nikumaroro	441	-4.6502	-174.5428	41	6/17/2012	16
Nikumaroro	443	-4.6502	-174.5428	41	6/17/2012	22.2
Nikumaroro	444	-4.6502	-174.5428	45	6/17/2012	23.4
Nikumaroro	445	-4.6502	-174.5428	45	6/17/2012	28.6
Nikumaroro	446	-4.6502	-174.5428	45	6/17/2012	146
Nikumaroro	447	-4.6502	-174.5428	22	6/18/2012	13.2

Nikumaroro	448	-4.6502	-174.5428	24	6/18/2012	10.8
Nikumaroro	449	-4.6502	-174.5428	20	6/18/2012	15.4
Nikumaroro	450	-4.6502	-174.5428	28	6/18/2012	15
Nikumaroro	451	-4.6502	-174.5428	25	6/18/2012	10.6
Nikumororo	1176	-4.6505	-174.5430	37	9/25/2015	38
Nikumororo	1177	-4.6507	-174.5429	29	9/25/2015	73
Nikumororo	1178	-4.6507	-174.5429	28	9/25/2015	74
Nikumororo	1180	-4.6504	-174.5431	38	9/25/2015	33
Nikumororo	1181	-4.6503	-174.5428	37	9/26/2015	44
Nikumororo	1182	-4.6503	-174.5428	37	9/26/2015	38
Nikumororo	1184	-4.6506	-174.5431	37	9/27/2015	39
Nikumororo	1185	-4.6504	-174.5434	37	9/27/2015	24
Rawaki	434	-3.7218	-170.7169	45	6/14/2012	29
Rawaki	435	-3.7218	-170.7169	45	6/14/2012	16.6
Rawaki	437	-3.7218	-170.7169	45	6/14/2012	14.6
Rawaki	439	-3.7218	-170.7169	45	6/14/2012	120
Rawaki	1132	-3.7202	-170.7176	39	9/13/2015	50
Rawaki	1137	-3.7202	-170.7176	39	9/13/2015	89.5
Rawaki	1142	-3.7202	-170.7176	34	9/13/2015	61
Rawaki	1151	-3.7185	-170.7183	39	9/14/2015	70
Rawaki	1152	-3.7185	-170.7183	38	9/14/2015	70
Rawaki	1153	-3.7185	-170.7183	39	9/14/2015	34
Rawaki	1154	-3.7185	-170.7183	41	9/14/2015	28
Rawaki	1155	-3.7184	-170.7183	41	9/14/2015	36
Rawaki	1156	-3.7184	-170.7183	39	9/14/2015	22.5
Rawaki	1157	-3.7184	-170.7183	38	9/14/2015	37
Kingman	KIN-H-021	6.40235	-162.38513	30	5/13/2012	134
Kingman	KIN-H-022	6.39025	-162.36037	22	5/14/2012	106
Kingman	KIN01-14	6.42032	-162.37946	37	4/18/2010	37
Kingman	KIN02-15	6.42017	-162.37932	33	4/18/2010	37
Kingman	KIN03-16	6.42062	-162.37934	34	4/18/2010	37
Kingman	KIN04-17	6.40214	-162.38533	34	4/18/2010	37
Kingman	KIN05-18	6.40221	-162.38557	37	4/18/2010	34
Kingman	KIN-P-019	6.39243	-162.34229	16	5/13/2012	95
Kingman	KIN-P-020	6.39225	-162.34227	21	5/13/2012	41
Kingman	3-1	6.390	-162.360	20	10/1/2010	42
Kingman	3-2	6.390	-162.360	20	10/1/2010	44
Kingman	3-3	6.390	-162.360	20	10/1/2010	58
Kingman	2-3	6.386	-162.356	20	10/1/2010	66

Table A3.4: Measurements of observed bleaching incidence and stress band counts from calibration sites.

Reef	Site Name	Year	Total cores	Cores with stress band	Percent Bleaching Observed (± 1σ)	Reference
Palau	Siaes	1998	9	6	75 ± 7	*Bruno et al., 2001*
Palau	Short Drop Off	1998	11	7	66 ± 12	*Bruno et al., 2001*
Palau	Ngerdiluches	1998	6	3	47 ± 4	*Bruno et al., 2001*
Palau	Mecherchar	1998	10	5	46 ± 5	*Bruno et al., 2001*
Palau	Risong	1998	12	3	32 ± 5	*Bruno et al., 2001*
Palau	Ngerdiluches	2010	10	3	33 ± 3	*van Woesik et al., 2012*
Palau	Short Drop Off	2010	19	4	29 ± 15	*van Woesik et al., 2012*
Palau	Ngerchelong	2010	7	2	27 ± 6	*van Woesik et al., 2012*
Palau	Siaes	2010	9	2	25 ± 0	*van Woesik et al., 2012*
Palau	Nikko Bay	2010	11	3	20 ± 15	*van Woesik et al., 2012*
Palau	Risong	2010	15	3	19 ± 3	*van Woesik et al., 2012*
Palau	Taoch	2010	10	2	16 ± 2	*van Woesik et al., 2012*
Palau	Mecherchar	2010	10	2	14 ± 6	*van Woesik et al., 2012*
Jarvis	Jarvis	2015	17	15	94 ± 2	*Vargas-Ángel et al., 2011*
Jarvis	Jarvis	2010	24	3	3 ± 1	*Vargas-Ángel et al., 2011*
Kanton	Kanton	2015	9	2	13 ± 5	*This Study*
Enderbury	Enderbury	2015	7	2	21 ± 7	*This Study*
Rawaki	Rawaki	2015	10	1	6 ± 3	*This Study*
Nikumaroro	Nikumaroro	2015	10	1	6 ± 2	*This Study*
Howland	Howland	2010	11	6	44 ± 10	*Vargas-Ángel et al., 2011*
Barbados	Barbados	2005	8	5	71 ± 11	*Eakin et al., 2010*
Curacao	Curacao	2010	11	5	30 ± 11	*Waitt institution, 2017*
Curacao	Curacao	2005	11	1	14 ± -	*Bouchon et al., 2014*
Curacao	Curacao	1998	11	3	31 ± -	*Bouchon et al., 2014*
Martinique	Martinique	2005	12	7	51 ± 22	*Eakin et al., 2010*
Martinique	Martinique	1998	12	5	59 ± 2	*Bouchon et al., 2014*
Dongsha Atoll	Dongsha E5	2015	10	6	66 ± 16	*De Carlo et al., 2017*
Dongsha Atoll	Donghsa E3	2015	8	3	31 ± 22	*De Carlo et al., 2017*

Table A3.5: Proportion of stress bands measured in *Porites spp.* skeletal cores at eight reefs from 1982 to 2016.

	Stress Band Proportion (%) and number of cores (n)							
	Jarvis[1]	**Kanton**	**Enderbury**	**Rawaki**	**Nikumaroro**	**Howland**	**Maiana**	**Kingman[2]**
Lat, Lon (N, E)	-0.37 -160.00	-2.80 -171.64	-3.13 -171.08	-3.72 -170.71	-4.68 -174.52	0.81 -176.62	0.96 173.00	6.40 162.35
2015/6	88(17)	n.d	n.d	n.d	n.d	n.d	n.d	n.d
2009/10	14(14)	50(14)	64(11)	43(14)	47(17)	55(11)	40(15)	0(13)
2006/7	0(14)	0(11)	0(10)	0(14)	13(15)	64(11)	0(13)	0(13)
2004/5	0(14)	0(10)	0(10)	0(13)	0(14)	0(11)	83(12)	0(13)
2002/3	43(14)	80(10)	67(9)	54(13)	77(13)	80(10)	13(8)	0(13)
1997/8	79(14)	*43(7)*	11(9)	8(13)	18(11)	10(10)	0(8)	0(12)
1994/5	0(14)	*50(6)*	25(8)	22(9)	40(10)	88(8)	0(8)	0(11)
1991/2	50(12)	*0(4)*	*0(6)*	0(9)	*0(5)*	0(8)	*50(6)*	0(8)
1987/8	45(11)	*67(3)*	*67(6)*	*3(6)*	*50(4)*	14(7)	*50(6)*	0*(5)*
1982/3	64(11)	*0(2)*	*0(5)*	*0(5)*	*0(4)*	14(7)	*0(5)*	0*(5)*

[1]Stress bands at Jarvis were previously published in (Barkley et al. 2018).

[2]Four cores analyzed from Kingman were previously analyzed and published in (Carilli et al. 2017).

n.d. refers to time periods not covered by cores. Italicized are years when error on reconstructed community bleaching estimates exceeded 35%, and were therefore left out of the thermal tolerance analysis.

Table A3.6: Reconstructed bleaching incidence between 1982 and 2016.

Site	Location (Decimal Deg) (N, E)		Reconstructed Bleaching (% ± 2σ)									
			2015/6	2009/10	2006/7	2004/5	2002/3	1997/8	1994/5	1991/2	1987/8	1982/3
Jarvis[1]	-0.37	-160.00	94.5 ± 1.8	15.3 ± 14.2	0.0 ± 0.0	0.0 ± 0.0	44.8 ± 22.3	79.9 ± 21.2	0.0 ± 0.0	52.0 ± 27.1	47.4 ± 30.6	65.4 ± 28.7
Kanton	-2.80	-171.64	n.d.	52.0 ± 27.1	0.0 ± 0.0	0.0 ± 0.0	81.2 ± 24.3	44.8 ± 38.1	52.0 ± 41.0	0.0 ± 0.0	68.4 ± 53.1	0.0 ± 0.0
Enderbury	-3.13	-171.08	n.d.	65.4 ± 28.7	0.0 ± 0.0	0.0 ± 0.0	68.4 ± 30.8	13.4 ± 24.9	26.5 ± 32.0	0.0 ± 0.0	68.7 ± 37.6	0.0 ± 0.0
Rawaki	-3.72	-170.71	n.d.	44.8 ± 27.1	0.0 ± 0.0	0.0 ± 0.0	55.7 ± 27.8	8.3 ± 15.8	23.4 ± 29.0	0.0 ± 0.0	3.2 ± 15.0	0.0 ± 0.0
Nikumaroro	-4.68	-174.52	n.d.	49.0 ± 24.7	14.3 ± 18.7	0.0 ± 0.0	78.3 ± 22.6	19.4 ± 24.6	41.9 ± 31.8	0.0 ± 0.0	52.0 ± 41.0	0.0 ± 0.0
Howland	0.81	-176.62	n.d.	56.4 ± 30.1	65.4 ± 28.7	0.0 ± 0.0	81.2 ± 24.3	10.7 ± 20.3	88.3 ± 22.1	15.0 ± 27.8	15.0 ± 27.8	0.0 ± 0.0
Maiana	0.96	173.00	n.d.	41.9 ± 26.1	0.0 ± 0.0	84.4 ± 20.6	13.4 ± 24.9	0.0 ± 0.0	0.0 ± 0.0	52.0 ± 35.6	52.0 ± 35.6	0.0 ± 0.0

[1]2015 in Jarvis is reported as the observed bleaching measurement published in (Barkley et al. 2018).

n.d. refers to time periods not covered by core. Note: Kingman reef is not listed as no stress bands were observed.

Table A3.7: Average *in situ* measurements of seawater chemistry at study sites during ENSO neutral years.

Island	Salinity (PSU)	TA (µmol kg^{-1})	DIC (µmol kg^{-1})	Ω_{Ar}	$NO_2 + NO_3$ (µM)	NH_4 (µM)	SiO_4 (µM)	PO_4 (µM)	Reference
Jarvis	35.34 ± 0.15	2320.4 ± 2.6	2038.3 ± 24.8	3.40 ± 0.18	5.44 ± 0.91	n.d.	n.d.	n.d.	Barkley et al. (in Press)
Kanton	35.52 ± 0.13	2340.9 ± 1.7	2012.0 ± 6.5	3.77 ± 0.07	3.15 ± 0.26	0.48 ± 0.33	0.32 ± 0.07	1.79 ± 0.09	This study
Kanton Lagoon	38.07 ± 0.54	2259.4 ± 12.0	1910.0 ± 21.8	3.81 ± 0.12	0.16 ± 0.14	0.36 ± 0.31	2.58 ± 0.14	0.04 ± 0.03	This study
Enderbury	35.62 ± 0.23	2338.8 ± 2.9	2005.6 ± 8.2	3.81 ± 0.11	3.21 ± 0.30	0.39 ± 0.33	0.28 ± 0.06	1.78 ± 0.24	This study
Rawaki	35.50 ± 0.04	2337.8 ± 4.8	2006.3 ± 10.0	3.80 ± 0.07	3.44 ± 0.13	0.37 ± 0.24	0.24 ± 0.14	1.94 ± 0.09	This study
Nikumaroro	35.54 ± 0.02	2336.4 ± 8.3	1991.0 ± 14.5	3.95 ± 0.12	2.12 ± 0.17	0.53 ± 0.20	0.27 ± 0.08	1.43 ± 0.11	This study
Niku Lagoon	36.43 ± 0.44	2226 ± 48.7	1856 ± 91.1	4.13 ± 0.80	0.67 ± 0.57	0.89 ± 0.34	1.61 ± 0.15	0.07 ± 0.03	This study
Howland	35.20 ± 0.02	2312.4 ± 3.5	2002.8 ± 8.9	3.53 ± 0.06	2.06 ± -	n.d.	2.57 ± -	0.39 ± -	Oliver et al. (2015), WOA v2 (2013)[1]
Maiana	35.04 0.20	2243.6 ± 53.1	1946.7 ± 29.3	3.44 ± 0.37	0.48 ± 0.43	1.13 ± 1.32	1.96 ± 0.32	0.16 ± 0.06	-
Dongsha Reef Flat	33.54 ± 0.49	2127.8 ± 99.9	1852.0 ± 189.9	3.19 ± 0.97	n.d.	n.d.	n.d.	n.d.	DeCarlo et al. (2017b)
Palau Barrier	33.74 ± 0.19	2183.5 ± 17.9	1864.7 ± 20.1	3.66 ± 0.04	0.15 ± 0.13	0.28 ± 0.11	2.23 ± 0.64	0.10 ± 0.14	Barkely et al. (2015)
Palau Rock Islands[2]	32.96 ± 0.48	2050.2 ± 62.8	1831.3 ± 39.9	2.60 ± 0.26	0.28 ± 0.08	0.43 ± 0.31	2.91 ± 1.09	0.06 ± 0.01	Barkely et al. (2015)

[1]Salinity, TA, and DIC values were averaged over measurements made in 2012 (Oliver et al. 2015); Nitrate, silicate, and phosphate measurements were taken from annual average climatological values in the World Ocean Atlas 2013 v2.

[2]Rock Island seawater chemistry values are averages of values reported for Nikko Bay, Risong Bay, and Mecherchar.

Table A3.8: Tissue thicknesses during ENSO neutral and El Niño years for each reef

	Enso Neutral		El Niño		
Site	Tissue (ocean) (mm)	Tissue (interior)[1] (mm)	Tissue (ocean) (mm)	Tissue (interior) (mm)	**Reference**
Jarvis	8.3 ± 0.4	n/a	4.8 ± 0.4	n/a	Barkley et al. (2018)
Kanton	9.47 ± 1.47	6.17 ± 2.11	3.90 ± 1.84	4.34 ± 0.62	This study
Enderbury	10.54 ± 2.52	n/a	5.06 ± 0.87	n/a	This study
Rawaki	7.52 ± 0.12	n/a	4.49 ± 1.07	n/a	This study
Nikumaroro	8.26 ± 1.35	n/a	6.72 ± 1.08	n/a	This study
Howland	6.06 ± 0.85	n/a	n.d.	n/a	This study
Maiana	5.27 ± 0.65	n/a	n.d.	n/a	This study
Dongsha	n.d.	5.82 ± 0.58	n.d.	n/a	This study
GBR	5.3 ± 1.3	n/a	n.d.	n/a	Lough et al. (2000)
Palau Barrier	4.68 ± 0.99	3.88 ± 0.93	n.d.	n.d.	This study

[1]For Kanton Atoll, interior refers to corals collected inside the atoll lagoon. In Palau interior refers to the rock island bays. In Donghsa, this refers to the reef flat.

A3.4 References

Barkley HC, Cohen AL, Brainard RE, Mollica NR, Rivera HE, Drenkard EJ, Young CW, Vargas-Ángel B, Lohmann GP, Decarlo TM, Alpert AE, Lino KC, Oliver TA, Pietro KR, Luu VH (2018) Repeat bleaching of a central Pacific coral reef over the past six decades (1960-2016). Nat Biol Commun

Carilli JE, Hartmann AC, Heron SF, Pandolfi JM, Cobb K, Sayani H, Dunbar R, Sandin SA (2017) Porites coral response to an oceanographic and human impact gradient in the Line Islands. Limnol Oceanogr 62:2850–2863

Donner SD, Rickbeil GJM, Heron SF (2017) A new, high-resolution global mass coral bleaching database. PLoS One 12:1–17

Oliver T, Young C, Jeanette C, Pomeroy N (2015) Dissolved inorganic carbon, total alkalinity, temperature, salinity and other variables collected from profile and discrete sample observations using CTD, Niskin bottle, and other instruments.

Appendix A4 – Supplementary text, figures, and data for chapter 4

A4.1 Laser Data Reduction

When materials are analyzed via LA-ICPMS, it is common to set the associated mass spectrometer to continuously collect element counts for long periods of time while the laser ablates aliquots of various samples and standards. This results in data in the format of long time series of counts of each analyte detected by the mass spectrometer with two dominant features – peaks during which an analyte is being ablated, and periods of very low counts (noise) between ablations. The processing and statistical analysis involved in converting this raw data to the form presented in many studies has unfortunately not been consistent as the field has developed, and no 'best practices' have been established, although there have been some recent efforts (i.e. Branson et al. 2019). Here we draw from these efforts and attempt to lay out our data reduction routine as explicitly as possible to both elucidate our own methods and also provide a tool to the community tailored towards coral LA-ICPMS.

A4.1.1 Baseline Subtraction

After importing the raw ICPMS data, we subtract baseline noise from the time series of each analyte by identifying periods between ablations during the run. This is nominally set to time periods when the ICPMS detected fewer than 3000 total counts for longer than 10 seconds. These values may be adjusted to best fit the specific ICPMS setup and sampling interval. We then reduce these intervals to single points centered within the interval and at the median analyte value over the interval. We then apply a Piecewise Cubic Hermite Interpolating Polynomial between the noise points and subtract the corresponding fit from each analyte.

A4.1.2 Peak Identification

Once baseline corrected, peaks are identified via a guess-and-check routine. In short, standard position and interval are specified, and peaks in the run are then automatically identified based on a select analyte or the sum total of analytes (total beam). For our analysis we used ^{43}Ca

counts above 3×10^4 due to its abundance in all samples. We then implemented a user interface to verify and adjust peak labeling.

A4.1.3 Peak Quality Analysis

After sample and standard peaks have been successfully identified, peaks are checked for quality. First, a threshold length of 20 seconds was required. Our ablation time for each spot was 50 seconds, meaning peaks under 20 seconds are likely a result of faulty ablation or encountering non-coral material. After this we remove the first and last 5 seconds of each peak to account for differences in travel time of each analyte to the detector. The routine then then performs a cluster analysis on a subset of analytes (here we used Sr, U, and Ca) to identify periods of covariation between these elements. This technique was adapted from algorithms used in the LAtools package (Branson et al. 2019), and is designed to filter out anomalous intervals (i.e. minor foreign bodies in ablation material). We chose this method because it had the most success in matching qualitative visual checks of good vs. bad regions of sample peaks.

It should be noted at this point that while analyte peaks are generally asymmetric and trend linearly down as ablation both passes out of laser focus and down hole effects increase, analyte ratios in our analyses appear to be minimally affected, and present flat peaks (Fig. A4.2C). We therefore do not make any down hole correction, and from here on only work with element ratio data. We then take the median and MAD of each analyte ratio of interest (here Sr/Ca and U/Ca) over the sampling interval as the point-estimate of each analyte for a given sample.

A4.1.4 Standard Conversion

Once the point estimates of each element ratio for all samples and standards in a run are calculated, a standard correction is applied to convert from detection counts to molar ratios. Here we use a single-standard correction (coral standard JCP-1), however the code may be adapted easily to calibrate on a standard curve. For our work we used a powder standard, which resulted in higher noise in the analyzed element ratios compared to glass standards, and so to robustly correct the data using a single standard we perform a montecarlo simulation. We generate standard element ratios 1e5 times from a normal distribution with the mean and standard deviation of detections made during each standard ablation, and fit a Piecewise Cubic Hermite Interpolating Polynomial during each simulation, which are then averaged for the final correction. This is applied to both sample points and any secondary standards, which can be evaluated at this point.

A4.1.5 Coordinate Mapping and binning

At this point, the data has been reduced to a familiar (i.e. tabular) form. However, it has not been referenced to the positioning of each spot ablated and remains simply as an ordered list. The rest of the routine is designed to spatially orient each ablation point to the X, Y, and Z coordinates within the laser stage.

A4.1.6 Laser spot sorting and attribution

To reference each sample to the corresponding coordinates, they must be imported (i.e. from an excel or ascii file). If multiple coral thin sections or other subjects were analyzed during the same run, it can be helpful to have a screenshot or image of the laser stage, which can be loaded in to a user interface at this point, and compared with a mapping of the imported coordinates. The gui allows the user to then select and attribute different groupings of points to the various subjects in the stage.

A4.1.7 Track alignment

In our work, we used multiple coral thick sections to mount a section of core, and our analysis track continued from one section to another. The routine facilitates combining these into a single track by allowing the user to identify groupings of points that should be combined into a single referenced datasheet, and aligns the coordinates of these points to the major axis along which they are distributed (Fig. A4.2).

A4.1.8 Sr-U Calculation

Sr-U is calculated via a boxcar depth binning using 2 mm bins with a 1 mm overlap. Processed laser spot data is binned accordingly along the rotated depth axis (A4.1.7). Sr/Ca and U/Ca element ratios from spots within a given bin are regressed (Linear least squares), and outliers that are either 2σ from the U/Ca mean or have a residual 2σ greater than the mean are removed. The Sr-U is then calculated as the Sr/Ca at which the regression line passes a U/Ca value of 1.05 μmol/mol, the average observed within our cores (This value is arbitrary, but must be consistent across analyses, and minimizes error when chosen near the mean of U/Ca measurements (Decarlo et al. 2016)) (Fig. A4.3). To remove potential bias from outlying data, this process is iterated n = 10e5 times while bootstrap resampling each point from a normal distribution with mean and standard deviation corresponding to the mean and standard deviation of each analyte ratio during the ablation of that spot. The reported Sr-U is the average over this simulation.

A4.2 Supplementary figures and tables

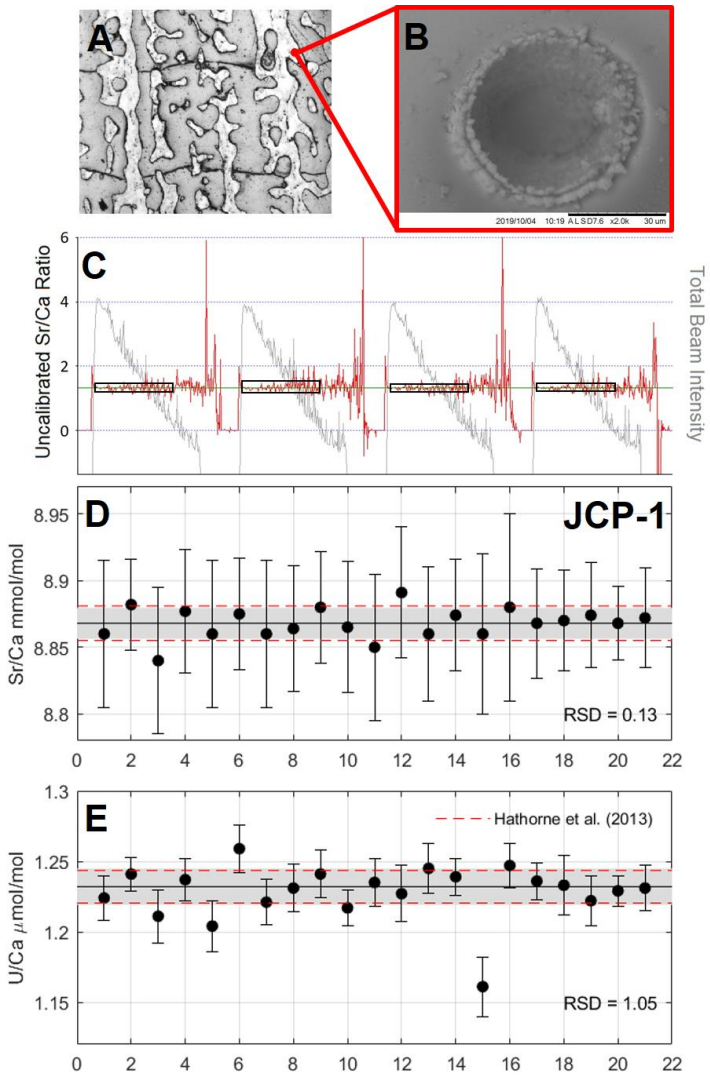

Figure A4.1 Quality check on laser ablation ICPMS measurements of Sr/Ca and U/Ca in coral aragonite. **A:** Ablation spots are strategically placed along the coral ultra-structure to avoid epoxy and compromised skeletal areas. **B:** Laser ablation pits are circular with no signs of melt during ablation and shallow enough to not puncture into the epoxy. **C:** Sample collection profile of four coral laser spots. Red is the measured Sr/Ca counts ratio collected as a function of time. Critically, measured element ratios remain roughly constant despite the decreasing beam intensity (grey). Black boxes show the analyzed section of each peak after cropping high variability regions using the cluster analysis (A4.1.3). **D and E:** Example plots of primary standard JCP-1 through a

6-hour run. Grey shading = standard deviation about the mean (black line). Dashed red lines in **D** and **E** are the median within-lab standard deviation of an inter-lab comparison study analyzing Sr/Ca (21 labs) and U/Ca (8 labs) in JCP-1 using solution analyses (Hathorne et al. 2013). Error bars represent 1σ. During the run shown, one outlying U/Ca measurement was made which we attribute to inhomogeneities in the powder standard.

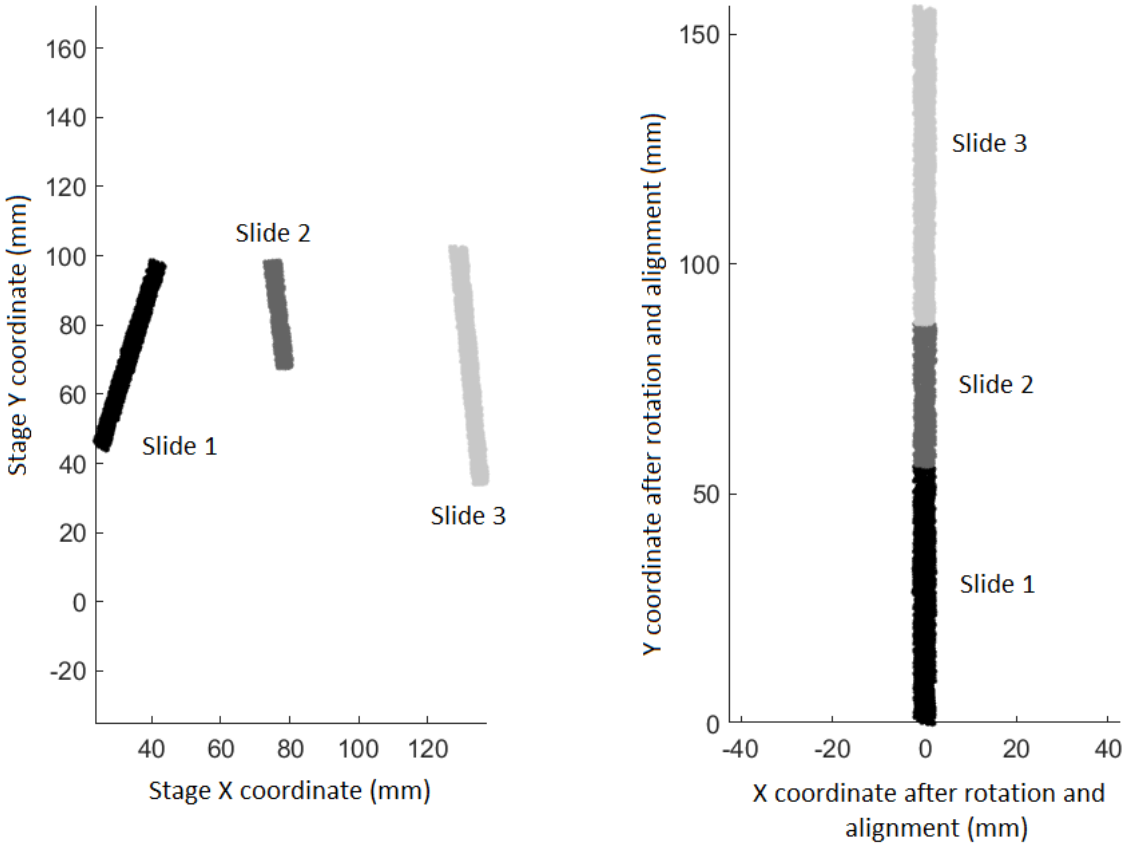

Figure A4.2 Example result of the alignment and rotation algorithms described in A4.1.7. Sample tracks, made up of hundreds of laser spots, are shown in black, dark grey, and light grey, corresponding to three different coral slides. After user input designates each track to be merged, a major axis fitting algorithm determines the down core direction, rotates the sample points in that track to align the Y stage coordinate with distance down core, and stacks each track in the order designated. This allows tracks from multiple thin sections to be oriented along polyp growth axes.

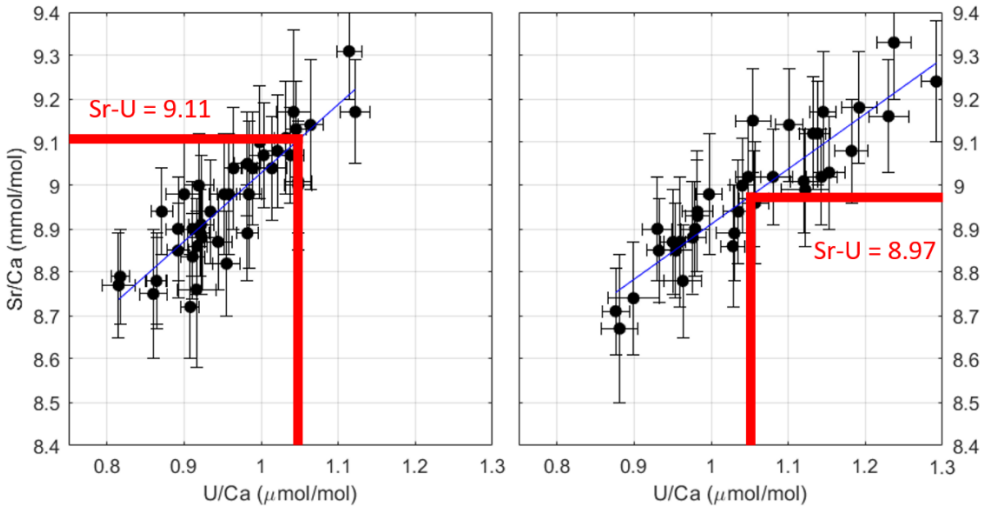

Figure A4.3. Calculating Sr-U. ~25 Sr/Ca data points collected from coral skeleton that fall within a 2 mm depth bin are regressed against paired U/Ca data points. The Sr-U value for each month is the Sr/Ca value at a U/Ca value of 1.05µmol/mol (red lines in each plot). The paired Sr/Ca and U/Ca values at left indicate a Sr-U value of 9.11 and thus a cooler temperature than the paired Sr/Ca and U/Ca data points at right, which indicate an Sr-U value of 8.97. Each regression is simulated n = 10e5 times by resampling the laser data from a normal distribution corresponding to the error bars shown.

Table A4.1 Sr-U, Sr/Ca, and U/Ca ratios generated from coral Jarvis 1222.

Depth (mm)	Year	Sr-U	Sr-U Error (1SD)	Sr/Ca (mmol/mol)	Sr/Ca Error (1SD) (mmol/mol)	U/Ca (μmol/mol)	U/Ca Error (1SD) (μmol/mol)
1	2016.891	9.008	0.034	9.005	0.019	1.034	0.013
2	2016.872	9.062	0.035	9.064	0.020	1.056	0.014
3	2016.786	9.066	0.035	9.078	0.020	1.067	0.014
4	2016.68	9.029	0.037	9.007	0.022	1.018	0.014
5	2016.642	9.008	0.037	8.970	0.020	0.973	0.015
6	2016.623	8.978	0.033	8.973	0.019	1.011	0.018
7	2016.594	9.010	0.039	9.015	0.022	1.061	0.015
8	2016.518	9.029	0.036	9.029	0.020	1.032	0.013
9	2016.451	9.054	0.034	9.051	0.018	1.055	0.013
10	2016.432	9.070	0.038	9.077	0.020	1.075	0.012
11	2016.393	8.994	0.038	8.997	0.021	1.066	0.013
12	2016.298	8.916	0.028	8.912	0.017	1.052	0.015
13	2016.212	8.904	0.030	8.892	0.019	1.028	0.015
14	2016.145	8.869	0.035	8.858	0.017	1.006	0.013
15	2016.087	8.828	0.043	8.806	0.016	0.952	0.014
16	2016.03	8.839	0.060	8.787	0.017	0.913	0.011
17	2015.953	8.825	0.061	8.769	0.019	0.922	0.011
18	2015.915	8.769	0.061	8.753	0.019	0.938	0.012
19	2015.896	8.780	0.044	8.764	0.018	0.968	0.014
20	2015.877	8.800	0.043	8.779	0.016	0.963	0.013
21	2015.8	8.848	0.049	8.822	0.016	0.951	0.011
22	2015.723	8.821	0.041	8.804	0.019	0.991	0.015
23	2015.704	8.833	0.038	8.822	0.019	1.011	0.016
24	2015.618	8.876	0.035	8.860	0.015	0.979	0.013
25	2015.532	8.865	0.059	8.851	0.018	0.954	0.010
26	2015.474	8.891	0.049	8.869	0.022	0.982	0.014
27	2015.397	8.891	0.044	8.880	0.021	0.995	0.013
28	2015.359	8.915	0.050	8.897	0.018	0.961	0.012
29	2015.34	8.922	0.055	8.895	0.019	0.940	0.013
30	2015.321	8.910	0.045	8.885	0.020	0.961	0.017
31	2015.282	8.914	0.052	8.904	0.028	1.002	0.020
32	2015.225	8.931	0.049	8.929	0.025	1.006	0.018
33	2015.119	8.954	0.042	8.938	0.023	0.998	0.019
34	2015.014	8.929	0.036	8.897	0.022	0.998	0.018
35	2014.975	8.911	0.036	8.889	0.021	0.991	0.016
36	2014.956	8.906	0.042	8.897	0.020	0.985	0.014

37	2014.927	8.923	0.038	8.909	0.022	1.011	0.017
38	2014.851	8.950	0.037	8.963	0.024	1.072	0.019
39	2014.784	8.943	0.037	8.960	0.025	1.078	0.018
40	2014.764	8.934	0.039	8.939	0.025	1.065	0.016
41	2014.726	8.971	0.039	8.985	0.020	1.078	0.014
42	2014.621	8.972	0.027	8.981	0.015	1.058	0.015
43	2014.534	8.944	0.028	8.936	0.018	1.034	0.017
44	2014.515	8.936	0.030	8.927	0.019	1.028	0.017
45	2014.458	8.946	0.031	8.941	0.019	1.027	0.016
46	2014.381	8.946	0.026	8.928	0.020	1.024	0.020
47	2014.333	8.955	0.028	8.953	0.019	1.036	0.019
48	2014.285	8.978	0.027	8.963	0.017	1.019	0.014
49	2014.199	9.001	0.029	8.976	0.018	1.010	0.014
50	2014.132	8.972	0.032	8.956	0.018	1.005	0.015
51	2014.112	8.970	0.039	8.953	0.023	1.018	0.017
52	2014.055	8.992	0.042	8.974	0.027	1.014	0.018
53	2013.997	8.970	0.039	8.937	0.024	0.990	0.016
54	2013.978	8.960	0.037	8.945	0.025	1.022	0.019
55	2013.94	8.995	0.038	8.998	0.026	1.075	0.021
56	2013.873	9.019	0.033	9.020	0.023	1.062	0.018
57	2013.777	9.037	0.035	9.041	0.020	1.065	0.015
58	2013.681	9.033	0.039	9.034	0.021	1.077	0.016
59	2013.614	8.968	0.039	8.971	0.020	1.076	0.016
60	2013.575	8.935	0.044	8.945	0.022	1.059	0.020
61	2013.556	9.120	0.028	9.162	0.023	1.117	0.020
62	2013.537	9.078	0.033	9.109	0.026	1.092	0.022
63	2013.451	9.019	0.029	9.019	0.018	1.045	0.016
64	2013.345	9.026	0.029	9.038	0.020	1.060	0.014
65	2013.307	9.095	0.034	9.120	0.025	1.087	0.018
66	2013.288	9.062	0.032	9.085	0.025	1.074	0.020
67	2013.23	9.046	0.026	9.089	0.024	1.108	0.022
68	2013.163	9.071	0.027	9.129	0.022	1.127	0.019
69	2013.115	9.082	0.027	9.152	0.023	1.138	0.020
70	2013.058	9.102	0.030	9.168	0.022	1.150	0.019
71	2012.99	9.061	0.030	9.099	0.021	1.099	0.016
72	2012.943	9.082	0.039	9.106	0.024	1.082	0.015
73	2012.923	9.095	0.036	9.104	0.025	1.064	0.016
74	2012.885	9.048	0.025	9.060	0.017	1.072	0.016
75	2012.828	9.016	0.029	9.055	0.022	1.108	0.020
76	2012.723	9.009	0.029	9.039	0.023	1.098	0.019
77	2012.617	9.022	0.038	9.057	0.029	1.084	0.017

78	2012.579	9.078	0.051	9.117	0.037	1.084	0.018
79	2012.56	9.126	0.061	9.181	0.038	1.111	0.019
80	2012.541	9.030	0.036	9.049	0.028	1.066	0.019
81	2012.445	9.014	0.027	9.019	0.020	1.055	0.017
82	2012.35	9.049	0.027	9.071	0.022	1.088	0.019
83	2012.331	9.075	0.024	9.089	0.021	1.077	0.017
84	2012.311	9.066	0.038	9.089	0.018	1.112	0.016
85	2012.264	9.032	0.041	9.078	0.020	1.139	0.017
86	2012.206	9.070	0.037	9.128	0.021	1.152	0.016
87	2012.158	9.086	0.029	9.129	0.023	1.127	0.022
88	2012.053	9.109	0.041	9.144	0.025	1.118	0.021
89	2011.967	9.024	0.049	9.063	0.032	1.092	0.018
90	2011.948	8.957	0.043	8.965	0.031	1.065	0.019
91	2011.929	9.006	0.036	9.035	0.022	1.094	0.017
92	2011.842	9.034	0.025	9.050	0.019	1.070	0.019
93	2011.756	9.020	0.025	9.043	0.019	1.096	0.020
94	2011.737	9.011	0.026	9.065	0.019	1.151	0.019
95	2011.708	9.032	0.040	9.094	0.021	1.169	0.020
96	2011.641	9.039	0.032	9.078	0.025	1.117	0.025
97	2011.584	9.054	0.027	9.110	0.025	1.127	0.026
98	2011.545	9.035	0.041	9.101	0.023	1.162	0.020
99	2011.449	8.999	0.039	9.067	0.026	1.143	0.018
100	2011.344	9.024	0.033	9.086	0.028	1.122	0.019
101	2011.296	9.097	0.039	9.163	0.025	1.136	0.018
102	2011.277	9.132	0.034	9.199	0.024	1.137	0.018
103	2011.258	9.124	0.039	9.208	0.026	1.157	0.022
104	2011.21	9.089	0.044	9.180	0.027	1.168	0.021
105	2011.152	9.092	0.038	9.148	0.023	1.136	0.019
106	2011.104	9.122	0.035	9.175	0.022	1.127	0.019
107	2010.999	9.130	0.033	9.194	0.022	1.139	0.018
108	2010.912	9.106	0.029	9.139	0.022	1.099	0.018
109	2010.893	9.100	0.026	9.099	0.022	1.054	0.017
110	2010.874	9.118	0.029	9.133	0.020	1.072	0.015
111	2010.778	9.135	0.031	9.152	0.020	1.083	0.016
112	2010.673	9.092	0.029	9.092	0.022	1.052	0.017
113	2010.625	9.032	0.029	9.013	0.021	1.026	0.014
114	2010.586	9.015	0.032	9.006	0.022	1.036	0.014
115	2010.567	9.010	0.031	9.001	0.019	1.034	0.014
116	2010.49	9.029	0.028	9.069	0.024	1.115	0.025
117	2010.395	9.003	0.035	9.077	0.028	1.160	0.027
118	2010.337	8.981	0.029	9.015	0.023	1.101	0.020

119	2010.299	8.986	0.028	9.016	0.017	1.106	0.016
120	2010.241	8.985	0.025	9.016	0.017	1.116	0.017
121	2010.164	8.992	0.032	9.022	0.022	1.095	0.018
122	2010.126	9.024	0.030	9.068	0.022	1.117	0.021
123	2010.107	9.048	0.027	9.107	0.018	1.169	0.023
124	2010.088	9.024	0.031	9.073	0.021	1.144	0.021
125	2010.001	9.009	0.036	9.047	0.025	1.117	0.019
126	2009.896	9.011	0.033	9.020	0.022	1.085	0.016
127	2009.858	9.025	0.028	9.023	0.019	1.060	0.017
128	2009.838	9.034	0.029	9.049	0.022	1.075	0.019
129	2009.81	9.019	0.033	9.034	0.024	1.082	0.018
130	2009.771	8.921	0.035	8.918	0.026	1.046	0.016
131	2009.666	8.964	0.038	8.999	0.033	1.090	0.020
132	2009.57	9.107	0.029	9.144	0.020	1.129	0.021
133	2009.551	9.064	0.033	9.089	0.026	1.104	0.024
134	2009.532	8.993	0.032	8.990	0.032	1.046	0.027
135	2009.445	8.986	0.038	8.956	0.028	1.012	0.018
136	2009.34	9.023	0.035	9.023	0.025	1.057	0.015
137	2009.282	9.080	0.037	9.144	0.025	1.155	0.021
138	2009.225	9.085	0.033	9.184	0.026	1.195	0.024
139	2009.167	9.097	0.032	9.164	0.030	1.146	0.028
140	2009.11	9.111	0.037	9.177	0.027	1.156	0.027
141	2009.062	9.132	0.049	9.213	0.025	1.206	0.026
142	2009.023	9.146	0.038	9.197	0.021	1.161	0.023
143	2008.966	9.121	0.031	9.158	0.020	1.122	0.019
144	2008.899	9.080	0.031	9.116	0.027	1.101	0.020
145	2008.842	9.054	0.031	9.087	0.027	1.101	0.023
146	2008.794	9.008	0.033	9.051	0.028	1.111	0.025
147	2008.765	8.996	0.035	9.017	0.029	1.075	0.022
148	2008.746	9.007	0.033	9.014	0.025	1.061	0.019
149	2008.66	9.058	0.033	9.073	0.024	1.073	0.019
150	2008.574	9.094	0.031	9.122	0.023	1.081	0.019
151	2008.555	9.084	0.033	9.095	0.033	1.066	0.026

Table A4.2 Sr-U, Sr/Ca, and U/Ca ratios generated from coral Niku 1344.

Depth (mm)	Year	Sr-U	Sr-U Error (1SD)	Sr/Ca (mmol/mol)	Sr/Ca Error (1SD) (mmol/mol)	U/Ca (μmol/mol)	U/Ca Error (1SD) (μmol/mol)
1	2018.198	8.866	0.077	8.764	0.025	0.889	0.016
2	2018.111	8.905	0.085	8.830	0.029	0.915	0.017
3	2018.015	8.939	0.068	8.862	0.024	0.924	0.016
4	2017.92	8.851	0.092	8.756	0.026	0.893	0.015
5	2017.824	8.844	0.099	8.768	0.028	0.907	0.014
6	2017.757	8.898	0.073	8.830	0.025	0.940	0.013
7	2017.632	8.896	0.064	8.835	0.024	0.948	0.013
8	2017.507	8.900	0.068	8.862	0.023	0.945	0.014
9	2017.45	8.910	0.098	8.847	0.029	0.933	0.014
10	2017.364	8.825	0.102	8.764	0.030	0.930	0.016
11	2017.239	8.813	0.066	8.766	0.022	0.943	0.014
12	2017.172	8.767	0.100	8.738	0.024	0.926	0.011
13	2017.105	8.779	0.086	8.724	0.028	0.921	0.017
14	2016.98	8.864	0.058	8.784	0.024	0.917	0.019
15	2016.856	8.931	0.059	8.810	0.029	0.920	0.018
16	2016.799	8.841	0.087	8.790	0.025	0.920	0.015
17	2016.741	8.857	0.060	8.826	0.019	0.948	0.014
18	2016.626	8.865	0.035	8.856	0.017	1.005	0.019
19	2016.502	8.840	0.043	8.822	0.021	0.981	0.020
20	2016.397	8.867	0.032	8.836	0.022	0.997	0.021
21	2016.301	8.872	0.026	8.851	0.019	1.006	0.021
22	2016.235	8.887	0.038	8.848	0.018	0.965	0.015
23	2016.177	8.878	0.050	8.791	0.026	0.930	0.017
24	2016.062	8.844	0.086	8.705	0.028	0.882	0.015
25	2015.938	8.794	0.155	8.757	0.027	0.903	0.009
26	2015.842	8.883	0.105	8.818	0.024	0.921	0.010
27	2015.775	8.894	0.080	8.810	0.030	0.937	0.016
28	2015.679	8.838	0.069	8.754	0.031	0.938	0.019
29	2015.555	8.842	0.053	8.769	0.024	0.935	0.017
30	2015.487	8.867	0.065	8.792	0.022	0.921	0.013
31	2015.43	8.849	0.085	8.791	0.022	0.933	0.009
32	2015.315	8.823	0.062	8.757	0.023	0.928	0.015
33	2015.219	8.777	0.068	8.702	0.022	0.909	0.015
34	2015.123	8.838	0.075	8.734	0.029	0.924	0.016
35	2015.027	8.878	0.053	8.823	0.028	0.975	0.019
36	2014.96	8.860	0.046	8.839	0.022	0.982	0.019

37	2014.836	8.855	0.074	8.800	0.022	0.939	0.013
38	2014.74	8.841	0.089	8.755	0.028	0.925	0.013
39	2014.682	8.906	0.086	8.799	0.032	0.933	0.014
40	2014.567	8.900	0.061	8.834	0.021	0.942	0.011
41	2014.452	8.868	0.051	8.794	0.019	0.934	0.011
42	2014.356	8.853	0.048	8.794	0.020	0.943	0.013
43	2014.28	8.849	0.057	8.821	0.021	0.957	0.015
44	2014.203	8.858	0.065	8.816	0.025	0.952	0.016
45	2014.078	8.884	0.082	8.800	0.030	0.940	0.014
46	2013.963	8.870	0.094	8.774	0.029	0.924	0.013
47	2013.906	8.896	0.065	8.825	0.022	0.928	0.012
48	2013.848	8.881	0.053	8.836	0.017	0.931	0.012
49	2013.724	8.892	0.044	8.824	0.022	0.953	0.014
50	2013.599	8.930	0.048	8.856	0.025	0.965	0.014
51	2013.532	8.933	0.067	8.848	0.027	0.937	0.015
52	2013.465	8.924	0.056	8.819	0.024	0.920	0.016
53	2013.34	8.864	0.062	8.793	0.021	0.931	0.013
54	2013.254	8.850	0.061	8.801	0.021	0.951	0.013
55	2013.168	8.919	0.071	8.887	0.030	0.981	0.017
56	2013.053	8.930	0.070	8.875	0.038	0.975	0.025
57	2012.985	8.848	0.045	8.812	0.023	0.978	0.020
58	2012.909	8.860	0.055	8.835	0.018	0.953	0.014
59	2012.785	8.885	0.085	8.792	0.025	0.911	0.013
60	2012.689	8.810	0.108	8.707	0.024	0.883	0.011
61	2012.593	8.866	0.085	8.771	0.024	0.911	0.011
62	2012.469	8.843	0.058	8.770	0.020	0.918	0.013
63	2012.412	8.802	0.079	8.733	0.018	0.903	0.011
64	2012.354	8.949	0.071	8.854	0.028	0.933	0.014
65	2012.23	8.928	0.050	8.870	0.020	0.953	0.012
66	2012.135	8.907	0.051	8.845	0.020	0.944	0.012
67	2012.039	8.918	0.068	8.831	0.028	0.943	0.015
68	2011.943	8.900	0.055	8.825	0.032	0.955	0.021
69	2011.847	8.924	0.049	8.840	0.026	0.941	0.017
70	2011.761	8.857	0.040	8.828	0.018	0.979	0.016
71	2011.704	8.859	0.044	8.840	0.020	0.982	0.017
72	2011.608	8.866	0.062	8.808	0.022	0.930	0.015
73	2011.512	8.866	0.056	8.794	0.021	0.931	0.013
74	2011.416	8.909	0.057	8.861	0.020	0.955	0.010
75	2011.32	8.922	0.049	8.878	0.024	0.965	0.015
76	2011.224	8.935	0.038	8.890	0.026	0.983	0.019
77	2011.1	8.941	0.038	8.885	0.021	0.962	0.014

78	2010.985	8.921	0.045	8.844	0.021	0.941	0.014
79	2010.898	8.882	0.062	8.804	0.023	0.932	0.014
80	2010.831	8.880	0.048	8.827	0.018	0.950	0.012
81	2010.764	8.883	0.057	8.829	0.019	0.934	0.013
82	2010.668	8.922	0.074	8.832	0.023	0.916	0.013
83	2010.572	8.933	0.064	8.844	0.024	0.938	0.013
84	2010.486	8.879	0.094	8.757	0.029	0.914	0.012
85	2010.371	8.861	0.067	8.752	0.025	0.921	0.013
86	2010.246	8.885	0.043	8.836	0.021	0.968	0.014
87	2010.151	8.913	0.048	8.895	0.018	0.994	0.011
88	2010.055	8.922	0.055	8.876	0.020	0.957	0.012
89	2009.988	8.938	0.088	8.863	0.032	0.934	0.018
90	2009.892	8.822	0.066	8.770	0.019	0.932	0.011
91	2009.767	8.839	0.068	8.798	0.021	0.947	0.010
92	2009.71	8.909	0.066	8.802	0.028	0.927	0.014
93	2009.623	8.891	0.064	8.774	0.027	0.915	0.014
94	2009.528	8.929	0.062	8.865	0.021	0.936	0.011
95	2009.46	8.922	0.052	8.892	0.018	0.968	0.010
96	2009.336	8.906	0.032	8.866	0.017	0.984	0.012
97	2009.24	8.904	0.033	8.842	0.022	0.968	0.015
98	2009.144	8.926	0.044	8.863	0.024	0.969	0.014
99	2009.019	8.924	0.053	8.881	0.021	0.956	0.013
100	2008.962	8.870	0.076	8.831	0.016	0.889	0.011
101	2008.905	8.927	0.080	8.852	0.017	0.880	0.010
102	2008.78	8.951	0.049	8.890	0.021	0.933	0.016
103	2008.685	8.936	0.062	8.859	0.026	0.947	0.015
104	2008.589	8.946	0.069	8.850	0.031	0.940	0.014
105	2008.465	8.965	0.075	8.862	0.031	0.940	0.013
106	2008.398	8.970	0.082	8.866	0.029	0.918	0.014
107	2008.302	8.957	0.056	8.869	0.023	0.926	0.014
108	2008.216	8.926	0.050	8.860	0.023	0.942	0.015
109	2008.159	8.934	0.054	8.879	0.021	0.953	0.013
110	2008.035	8.944	0.045	8.912	0.017	0.970	0.010
111	2007.939	8.954	0.033	8.923	0.019	0.996	0.015
112	2007.843	8.951	0.038	8.918	0.024	0.996	0.017
113	2007.718	8.979	0.046	8.916	0.030	0.984	0.016
114	2007.623	9.029	0.039	8.979	0.033	1.004	0.018
115	2007.565	9.034	0.030	8.992	0.025	1.006	0.016
116	2007.508	9.007	0.028	8.969	0.022	0.998	0.017
117	2007.412	8.974	0.038	8.921	0.023	0.988	0.015
118	2007.316	8.914	0.043	8.836	0.024	0.961	0.014

119	2007.191	8.860	0.038	8.806	0.020	0.960	0.014
120	2007.067	8.909	0.060	8.864	0.024	0.966	0.012
121	2006.999	9.006	0.067	8.956	0.025	0.955	0.013
122	2006.942	8.998	0.049	8.925	0.023	0.930	0.018
123	2006.856	8.908	0.040	8.842	0.018	0.921	0.018

A4.3 References

Branson O, Fehrenbacher JS, Vetter L, Sadekov AY, Eggins SM, Spero HJ (2019) LAtools: A data analysis package for the reproducible reduction of LA-ICPMS data. Chem Geol 504:83–95

Decarlo TM, Gaetani GA, Cohen AL, Foster GL, Alpert AE, Stewart JA (2016) Coral Sr-U thermometry. Paleoceanography 626–638

Hathorne EC, Gagnon A, Felis T, Adkins J, Asami R, Boer W, Caillon N, Case D, Cobb KM, Douville E, Demenocal P, Eisenhauer A, Garbe-Schönberg D, Geibert W, Goldstein S, Hughen K, Inoue M, Kawahata H, Kölling M, Cornec FL, Linsley BK, McGregor H V., Montagna P, Nurhati IS, Quinn TM, Raddatz J, Rebaubier H, Robinson L, Sadekov A, Sherrell R, Sinclair D, Tudhope AW, Wei G, Wong H, Wu HC, You CF (2013) Interlaboratory study for coral Sr/Ca and other element/Ca ratio measurements. Geochemistry, Geophys Geosystems 14:3730–3750

Appendix A5 – Supplementary text, figures, and data for chapter 5

A5.1 Supplementary figures and tables

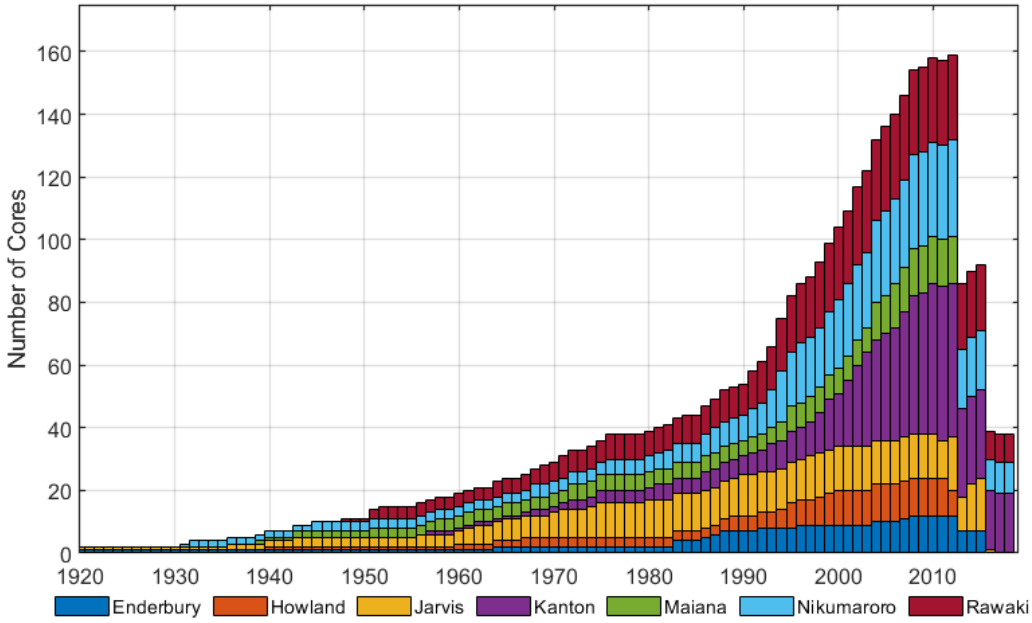

Figure A5.1. Number of cores, by island, used in the regional bleaching estimate. Cores were collected during 2012 (all sites), 2015 (Jarvis, Kanton, Nikumaroro, Rawaki, Enderbury), and 2018 (Kanton, Nikumaroro, Rawaki). Cores collected in all locations except Jarvis were sampled prior to bleaching, and are thus not included in the regional estimate for the 2015 event.

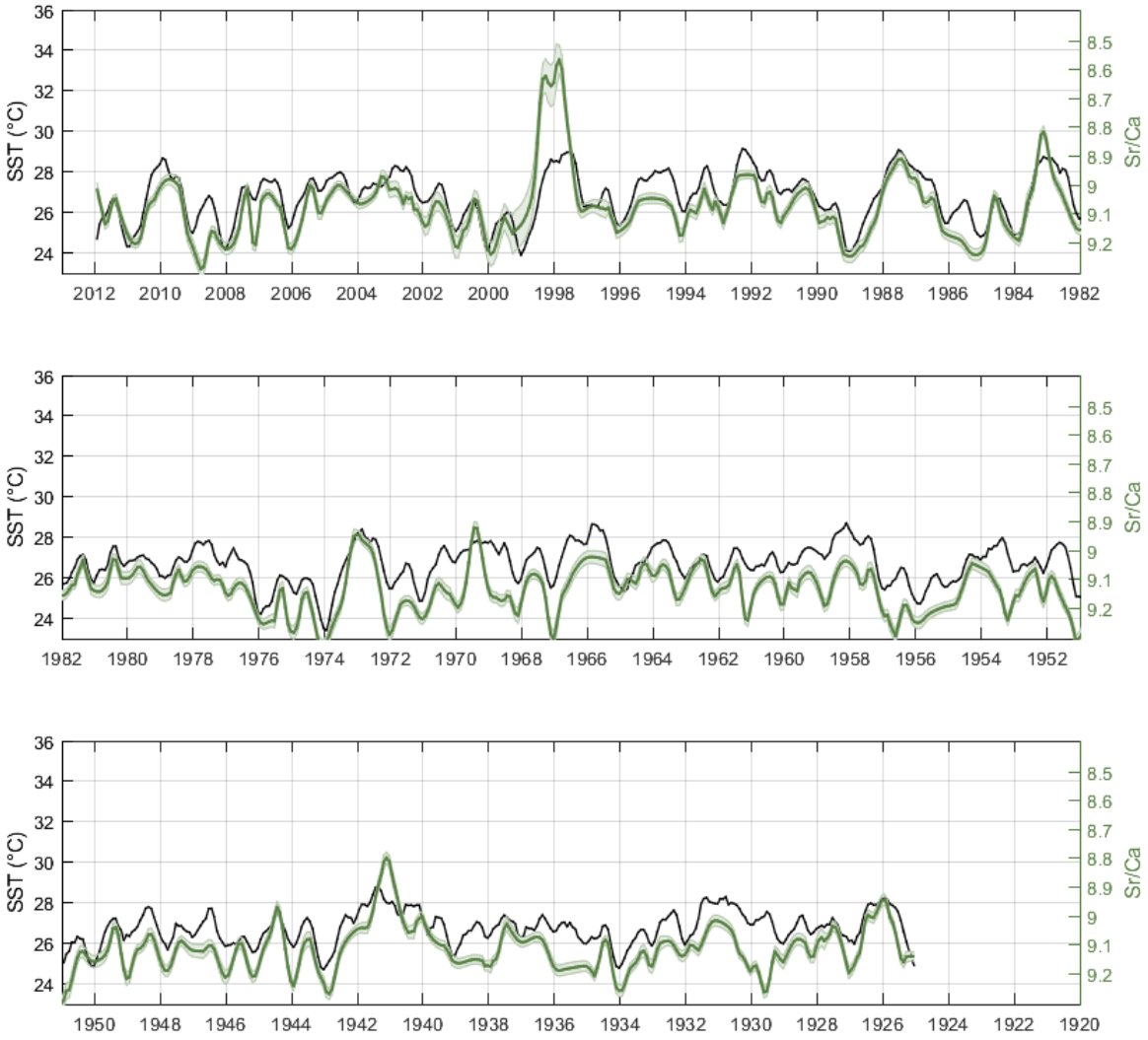

Figure A5.2. Monthly Sr/Ca reconstruction of SST at Jarvis island (from core J018). The Sr/Ca (green) has been aligned with the SST axis using the internal 10-year calibration (see section 5.3.5, table 5.1). The Sr/Ca and the adjusted HadISST (black) has been binned in the same manner as the Sr-U.

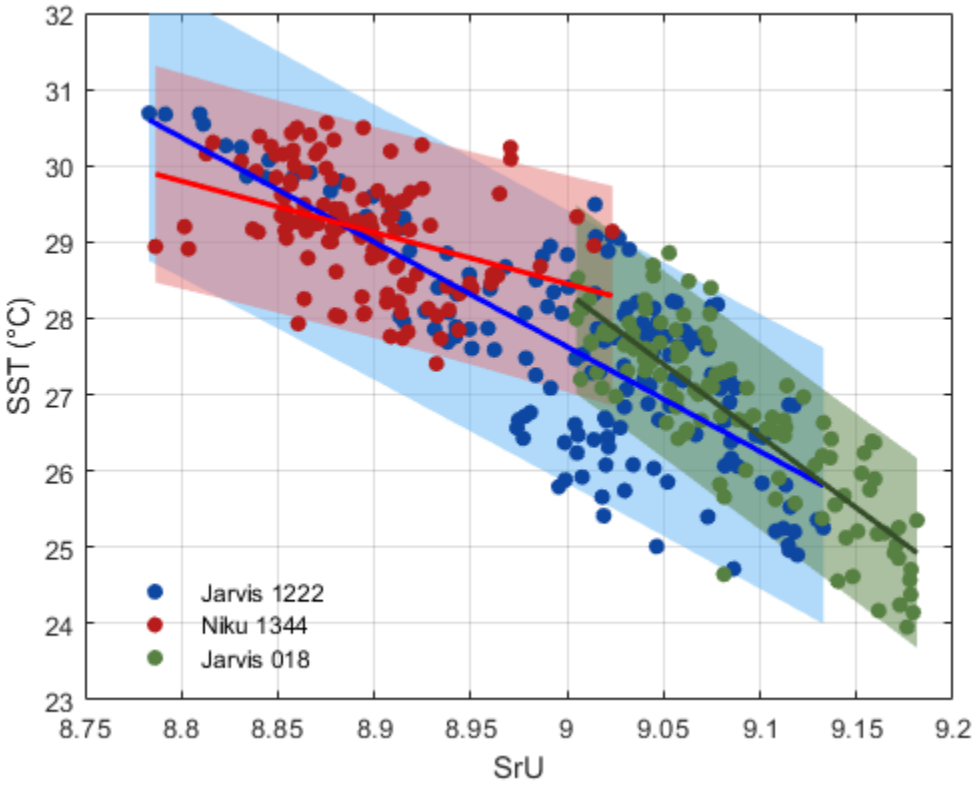

Figure A5.3. Individual calibration curves for each of the three corals and their respective prediction envelops ($p < 0.05$). While the prediction bounds of each individual regression overlap near completely, there is a difference in slope between the three relationships; in particular, J018 is significantly steeper (-18.83±2.16) than N1344 (-6.73±2.98). We attribute this difference to the limited and nearly non-overlapping Sr-U domain and the underrepresentation of the 2010 MHW in core J018 (discussed in section 5.2.3).

Table A5.1 Tabulated stress bands from all cores used in the regional bleaching estimate. Bleaching years are labeled by the latest year during which the bleaching occurred (often bleaching occurs during December-February in the CEP).

Reef	Core ID	latitude (Deg N)	longitude (Deg E)	length (cm)	Start year	End year	2016	2010	2007	2005	2003	1998	1995	1992	1987	1983	1977	1973	1969	1966	1964	1958	1953	1947	1941	1931	1919
Enderbury	426	-3.118	-171.093	18.8	2012	2006																					
Enderbury	428	-3.118	-171.093	13	2012	1995		X			X																
Enderbury	429	-3.118	-171.093	10.4	2012	2007		X																			
Enderbury	430	-3.118	-171.093	10.8	2012	2003		X																			
Enderbury	432	-3.113	-171.093	201	2012	1890					X				X				X		X		X				X
Enderbury	1080	-3.113	-171.093	56	2015	1982							X		X												
Enderbury	1081	-3.113	-171.093	50	2015	1982		X			X					X											
Enderbury	1084	-3.113	-171.093	39	2015	1991						X															
Enderbury	1089	-3.113	-171.093	40	2015	1987		X			X																
Enderbury	1092	-3.113	-171.093	58.5	2015	1986		X							X												
Enderbury	1094	-3.111	-171.094	69	2015	1963					X				X		X		X	X							
Enderbury	1102	-3.111	-171.094	51	2015	1985		X			X		X														
Howland	501	0.809	-176.622	20	2012	1994		X			X																
Howland	502	0.810	-176.622	30	2012	1993			X																		
Howland	503	0.809	-176.622	18.5	2012	1997		X	X																		
Howland	504	0.809	-176.622	24	2012	1988			X		X		X														
Howland	505	0.810	-176.622	74	2012	1959		X	X		X		X	X		X		X		X							
Howland	506	0.809	-176.622	86	2012	1939					X		X			X		X		X		X			X		
Howland	509	0.809	-176.622	20	2012	1998		X			X																
Howland	511	0.809	-176.622	18	2012	2003																					
Howland	H003	0.800	-176.621	94	2011	1966		X	X		X	X	X		X												
Howland	H004	0.809	-176.622	63	2011	1999		X			X																
Howland	P-001	0.799	-176.620	35	2011	1987		X	X		X		X	X	X												
Howland	P-002	0.799	-176.620	26	2011	1994			X		X		X														
Jarvis	481	-0.371	-159.984	102	2012	1942					X					X				X							

Jarvis	490	-0.370	-160.008	83	2012	1935											X					X				
Jarvis	494	-0.369	-160.008	45	2012	1969						X				X										
Jarvis	497	-0.369	-160.008	100	2012	1960						X		X	X	X		X		X						
Jarvis	499	-0.371	-159.982	98	2012	1970					X	X		X	X	X	X									
Jarvis	500	-0.371	-159.982	68	2012	1964					X	X		X	X	X		X		X						
Jarvis	1200	-0.371	-159.982	8.75	2015	2010	X																			
Jarvis	1201	-0.371	-159.982	9.0	2015	2010	X																			
Jarvis	1202	-0.371	-159.982	8.0	2015	2011	X																			
Jarvis	1203	-0.371	-159.982	6.5	2015	2012	X																			
Jarvis	1204	-0.371	-159.982	8.0	2015	2011																				
Jarvis	1205	-0.371	-159.982	9.0	2015	2011	X																			
Jarvis	1206	-0.369	-160.008	5.5	2015	2013	X																			
Jarvis	1207	-0.369	-160.008	8.5	2015	2011	X																			
Jarvis	1208	-0.369	-160.008	6.5	2015	2012	X																			
Jarvis	1209	-0.369	-160.008	8.5	2015	2011	X																			
Jarvis	1210	-0.369	-160.008	7.5	2015	2012																				
Jarvis	1211	-0.369	-160.008	8.0	2015	2014	X																			
Jarvis	1212	-0.369	-160.008	10.2	2015	2013	X																			
Jarvis	1213	-0.369	-160.008	7.0	2015	2014	X																			
Jarvis	1214	-0.369	-160.008	9.8	2015	2013	X																			
Jarvis	1215	-0.369	-160.008	9.0	2015	2013	X																			
Jarvis	1217	-0.371	-159.984	164	2016	1979	X					X		X												
Jarvis	J5	-0.369	-160.008	28	2010	1996		X			X	X														
Jarvis	J7	-0.369	-160.008	35	2010	1989						X		X												
Jarvis	J9	-0.376	-160.014	33	2010	1974					X	X		X	X											
Jarvis	J10	-0.376	-160.014	33	2010	1973		X			X	X														
Jarvis	J017	-0.370	-160.008	74	2012	1955										X				X						
Jarvis	J018	-0.369	-159.983	196	2012	1913						X			X			X							X	
Jarvis	J016	-0.374	-159.983	62	2012	1961						X				X				X						
Kanton	402	-2.846	-171.639	12	2012	2004		X																		

Kanton	404	-2.846	-171.639	48	2012	2003		X																		
Kanton	405	-2.846	-171.639	18.6	2012	2001					X															
Kanton	406	-2.846	-171.639	25.8	2012	1998		X			X															
Kanton	407	-2.806	-171.707	20.6	2012	1994					X		X													
Kanton	408	-2.806	-171.707	15.6	2012	2002																				
Kanton	409	-2.806	-171.707	13	2012	2002																				
Kanton	410	-2.806	-171.707	17.8	2012	2006		X			X															
Kanton	411	-2.806	-171.707	14.8	2012	1996		X																		
Kanton	413	-2.806	-171.707	29.4	2012	1997					X															
Kanton	414	-2.806	-171.721	10	2012	2007																				
Kanton	415	-2.806	-171.721	12.6	2012	2001		X			X															
Kanton	416	-2.806	-171.721	10	2012	2009		X																		
Kanton	417	-2.806	-171.721	12.2	2012	2002		X			X															
Kanton	418	-2.806	-171.721	9.4	2012	2006																				
Kanton	419	-2.806	-171.721	9.4	2012	2001					X															
Kanton	420	-2.828	-171.664	18.6	2012	2002																				
Kanton	421	-2.828	-171.664	30.4	2012	1999					X															
Kanton	422	-2.828	-171.664	18.8	2012	2000																				
Kanton	423	-2.828	-171.664	30.2	2012	1998																				
Kanton	424	-2.828	-171.664	29.8	2012	2000																				
Kanton	425	-2.828	-171.664	22.8	2012	2001		X																		
Kanton	1025	-2.846	-171.639	31	2015	2007		X																		
Kanton	1032	-2.805	-171.721	42	2015	1992		X			X		X													
Kanton	1033	-2.806	-171.707	106	2015	1956		X			X				X	X		X				X				
Kanton	1037	-2.846	-171.639	28	2015	2005		X ?																		
Kanton	1038	-2.846	-171.639	31	2015	2012																				
Kanton	1039	-2.846	-171.639	40	2015	2003																				
Kanton	1040	-2.831	-171.660	30.5	2015	2000		X	X		X															
Kanton	1041	-2.831	-171.660	22	2015	2004																				

Kanton	1043	-2.793	-171.723	107.5	2015	1967	X	X			X		X		X				X								
Kanton	1309	2.830	171.672	28	2018	2010	X																				
Kanton	1311	2.830	171.672	36	2018	1998																					
Kanton	1312	2.830	171.672	22	2018	2009	X																				
Kanton	1313	2.830	171.672	22	2018	2008	X																				
Kanton	1317	2.830	171.672	27	2018	2007	X	X																			
Kanton	1319	2.831	171.660	37	2018	2000	X	X	X		X																
Kanton	1320	2.831	171.660	27	2018	2007	X	X																			
Kanton	1323	2.831	171.660	28.5	2018	2005	X	X																			
Kanton	1324	2.831	171.660	19	2018	2009	X																				
Kanton	1326	2.836	171.700	25.5	2018	1997	X																				
Kanton	1327	2.836	171.700	58	2018	1974	X				X																
Kanton	1328	2.836	171.700	53	2018	1990	X				X		X														
Kanton	1330	2.836	171.700	32.5	2018	1980	X				X		X		X												
Kanton	1337	2.836	171.700	39	2018	1992		X																			
Kanton	1338	2.836	171.700	34	2018	2001	X	X			X																
Kanton	1339	2.836	171.700	28	2018	2006																					
Kanton	1340	2.836	171.700	33	2018	2006	X	X																			
Kanton	1341	2.836	171.700	69	2018	1971	X	X			X				X	X											
Kanton	1318 B	2.831	171.668	57	2018	1985	X	X			X																
Maiana	453	0.953	172.955	103.5	2012	1957		X		X					X	X				X		X					
Maiana	454	0.954	172.955	105	2012	1971		X																			
Maiana	455	0.966	173.074	106	2012	1938				X				X	X	X				X			X	X			
Maiana	457	0.966	173.074	16	2012	2003				X																	
Maiana	458	0.966	173.074	15	2012	1994		X		X																	
Maiana	459	0.966	173.074	20	2012	2003		X		X																	
Maiana	460	0.966	173.074	17	2012	2005																					
Maiana	510	1.007	172.983	105	2012	1950				X	X							X									
Maiana	513	1.007	172.983	94	2012	1942									X					X			X	X			

Maiana	514	1.007	172.983	13	2012	2003		X		X																	
Maiana	515	1.007	172.983	12	2012	2005		X																			
Maiana	518	1.007	172.983	11	2012	2007																					
Maiana	520	1.007	172.983	42	2012	1993				X																	
Maiana	521	1.007	172.983	18	2012	1994				X																	
Maiana	523	1.007	172.983	15.5	2012	2003				X																	
Nikumaroro	441	-4.650	-174.543	16	2012	2004																					
Nikumaroro	442	-4.650	-174.543	12.4	2012	2007																					
Nikumaroro	443	-4.650	-174.543	22.2	2012	1999					X																
Nikumaroro	444	-4.650	-174.543	23.4	2012	1999																					
Nikumaroro	445	-4.650	-174.543	28.6	2012	1993		X	X		X																
Nikumaroro	446	-4.650	-174.543	146	2012	1931			X		X	X			X	X		X		X			X		X		
Nikumaroro	447	-4.667	-174.517	13.2	2012	2003																					
Nikumaroro	448	-4.667	-174.517	10.8	2012	2007		X																			
Nikumaroro	449	-4.667	-174.517	15.4	2012	1998		X			X																
Nikumaroro	450	-4.667	-174.517	15	2012	2006		X																			
Nikumaroro	451	-4.667	-174.517	10.6	2012	2011																					
Nikumaroro	452	-4.667	-174.517	14	2012	2003		X																			
Nikumaroro	1343	4.651	174.543	114	2018	1930	X					X	X		X	X	X	X			X			X		X	
Nikumaroro	1344	4.651	174.543	113	2018	1944	X	X			X	X			X				X								
Nikumaroro	1345	4.650	174.543	28.5	2018	1992	X				X		X														
Nikumaroro	1346	4.650	174.543	37	2018	1994	X				X																
Nikumaroro	1347	4.650	174.543	37	2018	1993	X					X	X														
Nikumaroro	1348	4.650	174.543	37	2018	1991	X	X	X		X	X		X													
Nikumaroro	1349	4.650	174.543	37	2018	1993	X					X	X														
Nikumaroro	1350	4.650	174.543	37	2018	2000	X		X		X																
Nikumaroro	1383	4.650	174.543	36	2018	1995	X				X	X															
Nikumaroro	1182b	4.650	174.543	36	2018	1992	X				X	X	X														
Nikumaroro	1176	-4.650	-174.543	38	2015	1985					X		X	X	x												
Nikumaroro	1177	-4.651	-174.543	73	2015	1975	X	X					X		X	X											

Nikumaroro	1178	-4.651	-174.543	74	2015	1967					X				X				X								
Nikumaroro	1179	-4.650	-174.543	28	2015	2001		X			X	X															
Nikumaroro	1180	-4.650	-174.543	33	2015	1993						X															
Nikumaroro	1181	-4.650	-174.543	44	2015	1986		X			X		X		X												
Nikumaroro	1182	-4.650	-174.543	38	2015	1990					X																
Nikumaroro	1184	-4.651	-174.543	39	2015	1981		X			X		X		X	X											
Nikumaroro	1185	-4.650	-174.543	24	2015	1995					X																
Rawaki	433	-3.722	-170.717	15	2012	2001					X																
Rawaki	434	-3.722	-170.717	19	2012	1998		X			X																
Rawaki	435	-3.722	-170.717	16.6	2012	1997					X																
Rawaki	436	-3.722	-170.717	20.4	2012	1999		X			X																
Rawaki	437	-3.722	-170.717	14.6	2012	2004																					
Rawaki	439	-3.722	-170.717	120	2012	1951					X						X				X	X					
Rawaki	1132	-3.720	-170.718	50	2015	1975		X							X	X											
Rawaki	1137	-3.720	-170.718	89.5	2015	1950							X														
Rawaki	1142	-3.720	-170.718	61	2015	1983		X			X	X			X												
Rawaki	1151	-3.718	-170.718	70	2015	1963	X								X			X		X							
Rawaki	1152	-3.718	-170.718	70	2015	1968		X			X		X		X	X		X	X								
Rawaki	1153	-3.718	-170.718	34	2015	1993	X				X																
Rawaki	1154	-3.718	-170.718	28	2015	1993		X			X																
Rawaki	1155	-3.718	-170.718	36	2015	1992		X																			
Rawaki	1156	-3.718	-170.718	22.5	2015	1997																					
Rawaki	1157	-3.718	-170.718	37	2015	1994	X																				
Rawaki	1160	-3.720	-170.718	43	2015	1990		X			X	X	X														
Rawaki	1308	-3.722	-170.717	120	2018	1947	X	X					X			X					X						
Rawaki	1310	-3.722	-170.717	108	2018	1950	X	X									X										
Rawaki	1314	-3.722	-170.717	32	2018	1990	X				X			X													
Rawaki	1315	-3.722	-170.717	37	2018	1987	X	X						X	X												
Rawaki	1316	-3.722	-170.717	34	2018	1993	X					X	X														
Rawaki	1321	-3.722	-170.717	21	2018	2002	X	X	X		X																

Rawaki	1322	-3.722	-170.717	37	2018	1991	X				X	X	X														
Rawaki	1329	-3.722	-170.717	37	2018	1995	X	X			X																
Rawaki	1336	-3.722	-170.717	37	2018	2001	X				X																
Rawaki	1137	-3.720	-170.718	89.5	2015	1970		X	X						X	X		X									

Table A5.2 U-Th dating results from MIT McGee lab, November 2019.

Core ID	^{238}U (ng/g)[a]	(2σ)	^{232}Th (pg/g)[a]	(2σ)	$\delta^{234}U$ (per mil)[b]	(2σ)	($^{230}Th/^{238}U$) activity	(2σ)	$^{230}Th/^{232}Th$ ppm atomic	(2σ)	Age (yr) (uncorrected)[c]	(2σ)	Age (yr) (corrected)[d]	(2σ)	$\delta^{234}U$ initial (per mil)[e]	(2σ)	Year CE (corrected)	(2σ)
JAR-H-018	2287	46	36	1	145	2	9.27E-04	8.40E-06	930	15	88	1	88	1	145	2	1931	1

[a]Reported errors for ^{238}U and ^{232}Th concentrations are estimated to be ±1% due to uncertainties in spike concentration; analytical uncertainties are smaller.
[b]$\delta^{234}U = ([^{234}U/^{238}U]_{activity} - 1) \times 1000$.
[c]$[^{230}Th/^{238}U]_{activity} = 1 - e^{-\lambda 230 T} + (\delta^{234}U_{measured}/1000)[\lambda_{230}/(\lambda_{230} - \lambda_{234})](1 - e^{-(\lambda 230 - \lambda 234) T})$, where T is the age. "Uncorrected" indicates that no correction has been made for initial ^{230}Th.
[d]Ages are corrected for detrital ^{230}Th assuming an initial $^{230}Th/^{232}Th$ of $(4.4 \pm 2.2) \times 10^{-6}$.
[e]$\delta^{234}U_{initial}$ corrected was calculated based on ^{230}Th age (T), i.e., $\delta^{234}U_{initial} = \delta^{234}U_{measured} X e^{\lambda 234 * T}$, and T is corrected age.
Decay constants for ^{230}Th and ^{234}U are from (Cheng et al. 2013); decay constant for ^{238}U is 1.55125×10^{-10} yr^{-1} (Jaffey et al. 1971).

Table A5.3 Sr-U, Sr/Ca, and U/Ca ratios generated from coral Jarvis 018. Values have been interpolated to monthly resolution (See methods).

Year	Sr-U	Sr-U Error (1SD)	Sr/Ca (mmol/mol)	Sr/Ca Error (1SD) (mmol/mol)	U/Ca (μmol/mol)	U/Ca Error (1SD) (μmol/mol)
2011.934	9.081	0.056	9.012	0.020	0.931	0.011
2011.851	9.050	0.038	9.030	0.017	0.977	0.012
2011.768	9.113	0.028	9.122	0.016	1.075	0.012
2011.684	9.115	0.036	9.130	0.017	1.092	0.009
2011.601	9.127	0.036	9.153	0.017	1.097	0.009
2011.518	9.087	0.025	9.093	0.016	1.070	0.011
2011.434	9.025	0.027	9.011	0.014	1.006	0.010
2011.351	9.058	0.026	9.049	0.016	1.038	0.010
2011.268	9.071	0.024	9.081	0.019	1.069	0.013
2011.184	9.108	0.025	9.115	0.018	1.064	0.012
2011.101	9.145	0.024	9.144	0.016	1.056	0.012
2011.018	9.168	0.024	9.168	0.015	1.048	0.010
2010.934	9.172	0.027	9.190	0.016	1.093	0.013
2010.851	9.178	0.027	9.200	0.016	1.105	0.014
2010.768	9.184	0.027	9.207	0.015	1.111	0.015
2010.684	9.183	0.028	9.205	0.015	1.111	0.015
2010.601	9.168	0.031	9.189	0.016	1.106	0.016
2010.518	9.143	0.033	9.160	0.017	1.095	0.016
2010.434	9.075	0.029	9.078	0.017	1.048	0.015
2010.351	9.072	0.028	9.055	0.017	1.020	0.013
2010.268	9.073	0.030	9.076	0.017	1.041	0.014
2010.184	9.077	0.033	9.048	0.020	0.995	0.016
2010.101	9.073	0.036	9.028	0.019	0.978	0.015
2010.018	9.064	0.039	9.009	0.019	0.963	0.014
2009.935	9.052	0.042	8.994	0.018	0.953	0.012
2009.851	9.043	0.044	8.983	0.018	0.947	0.011
2009.768	9.039	0.045	8.979	0.018	0.945	0.011
2009.685	9.039	0.046	8.980	0.019	0.947	0.011
2009.601	9.042	0.046	8.984	0.022	0.955	0.012
2009.518	9.048	0.046	8.991	0.026	0.967	0.013
2009.435	9.055	0.047	9.002	0.030	0.984	0.014
2009.351	9.066	0.047	9.017	0.031	1.005	0.015
2009.268	9.131	0.047	9.129	0.032	1.055	0.014

2009.185	9.140	0.049	9.168	0.031	1.092	0.015
2009.101	9.145	0.051	9.193	0.028	1.122	0.015
2009.018	9.148	0.054	9.214	0.027	1.152	0.016
2008.935	9.151	0.057	9.239	0.026	1.189	0.017
2008.851	9.153	0.060	9.270	0.027	1.236	0.018
2008.768	9.154	0.063	9.297	0.027	1.278	0.020
2008.685	9.155	0.064	9.308	0.027	1.297	0.021
2008.601	9.100	0.052	9.245	0.025	1.264	0.020
2008.518	9.083	0.039	9.177	0.022	1.206	0.018
2008.435	9.097	0.032	9.138	0.017	1.138	0.015
2008.351	9.139	0.029	9.165	0.018	1.095	0.015
2008.268	9.161	0.029	9.188	0.019	1.089	0.015
2008.185	9.171	0.030	9.204	0.020	1.098	0.015
2008.101	9.177	0.032	9.216	0.020	1.111	0.016
2008.018	9.181	0.034	9.223	0.020	1.123	0.016
2007.935	9.180	0.036	9.223	0.020	1.128	0.016
2007.852	9.173	0.038	9.217	0.020	1.132	0.016
2007.768	9.162	0.040	9.205	0.020	1.134	0.016
2007.685	9.147	0.041	9.188	0.020	1.135	0.015
2007.602	9.121	0.031	9.143	0.017	1.103	0.014
2007.518	9.099	0.033	9.121	0.018	1.104	0.018
2007.435	9.000	0.032	8.995	0.022	1.048	0.015
2007.352	9.006	0.032	8.997	0.020	1.027	0.013
2007.268	9.049	0.034	9.055	0.021	1.046	0.013
2007.185	9.177	0.043	9.241	0.024	1.141	0.015
2007.102	9.248	0.058	9.301	0.022	1.203	0.016
2007.018	9.053	0.032	9.079	0.018	1.099	0.016
2006.935	9.041	0.029	9.054	0.017	1.074	0.015
2006.852	9.033	0.026	9.038	0.016	1.057	0.013
2006.768	9.029	0.025	9.029	0.015	1.046	0.011
2006.685	9.028	0.025	9.027	0.015	1.040	0.011
2006.602	9.037	0.025	9.035	0.015	1.036	0.010
2006.518	9.057	0.025	9.054	0.015	1.032	0.010
2006.435	9.077	0.026	9.072	0.015	1.030	0.010
2006.352	9.087	0.027	9.081	0.015	1.029	0.010
2006.268	9.062	0.030	9.078	0.018	1.073	0.012
2006.185	9.161	0.040	9.205	0.019	1.131	0.012
2006.102	9.173	0.038	9.222	0.018	1.142	0.013
2006.019	9.178	0.036	9.227	0.018	1.146	0.014
2005.935	9.164	0.034	9.216	0.018	1.145	0.014
2005.852	9.136	0.032	9.190	0.018	1.141	0.015

2005.769	9.110	0.031	9.159	0.018	1.136	0.015
2005.685	9.094	0.035	9.124	0.019	1.109	0.015
2005.602	9.074	0.038	9.080	0.020	1.069	0.015
2005.519	9.036	0.028	9.031	0.017	1.034	0.010
2005.435	9.011	0.030	8.984	0.017	1.007	0.010
2005.352	9.011	0.027	8.992	0.015	1.009	0.010
2005.269	9.042	0.031	9.061	0.024	1.073	0.015
2005.185	9.078	0.032	9.113	0.024	1.095	0.015
2005.102	9.079	0.030	9.112	0.021	1.093	0.013
2005.019	9.051	0.025	9.068	0.015	1.073	0.011
2004.935	9.042	0.025	9.050	0.015	1.062	0.011
2004.852	9.035	0.026	9.038	0.016	1.053	0.011
2004.769	9.025	0.026	9.025	0.016	1.045	0.011
2004.685	9.011	0.025	9.009	0.015	1.039	0.011
2004.602	9.001	0.024	8.997	0.014	1.033	0.010
2004.519	9.002	0.025	8.998	0.014	1.024	0.010
2004.435	9.018	0.031	9.011	0.016	1.011	0.011
2004.352	9.036	0.032	9.021	0.016	1.002	0.011
2004.269	9.051	0.032	9.030	0.015	0.997	0.011
2004.185	9.059	0.029	9.043	0.015	1.011	0.011
2004.102	9.063	0.025	9.055	0.015	1.033	0.012
2004.019	9.062	0.025	9.063	0.016	1.050	0.012
2003.936	9.062	0.026	9.067	0.017	1.059	0.013
2003.852	9.061	0.024	9.066	0.016	1.057	0.013
2003.769	9.059	0.022	9.062	0.015	1.051	0.012
2003.686	9.057	0.022	9.057	0.014	1.045	0.012
2003.602	9.054	0.023	9.050	0.015	1.038	0.012
2003.519	9.049	0.025	9.041	0.015	1.030	0.011
2003.436	9.042	0.028	9.029	0.016	1.021	0.011
2003.352	9.030	0.031	9.009	0.018	1.009	0.011
2003.269	9.003	0.037	8.965	0.020	0.990	0.011
2003.186	8.987	0.041	8.939	0.022	0.980	0.012
2003.102	9.046	0.041	9.016	0.025	1.001	0.012
2003.019	9.013	0.045	9.018	0.026	1.042	0.012
2002.936	9.008	0.045	9.016	0.026	1.051	0.012
2002.852	9.005	0.043	9.011	0.026	1.056	0.013
2002.769	9.004	0.042	9.009	0.025	1.058	0.013
2002.686	9.026	0.038	9.030	0.023	1.057	0.013
2002.602	9.067	0.032	9.071	0.020	1.054	0.013
2002.519	9.089	0.029	9.093	0.018	1.049	0.013
2002.436	8.966	0.030	8.957	0.019	1.031	0.014

2002.352	9.079	0.034	9.094	0.019	1.072	0.012
2002.269	9.075	0.028	9.077	0.016	1.051	0.009
2002.186	9.088	0.040	9.082	0.022	1.037	0.010
2002.102	9.103	0.035	9.097	0.021	1.042	0.011
2002.019	9.133	0.042	9.126	0.023	1.039	0.010
2001.936	9.172	0.065	9.161	0.031	1.021	0.010
2001.853	9.159	0.064	9.143	0.032	1.011	0.010
2001.769	9.132	0.063	9.105	0.032	1.002	0.011
2001.686	9.104	0.062	9.067	0.032	0.995	0.012
2001.603	9.092	0.060	9.050	0.032	0.993	0.013
2001.519	9.095	0.056	9.055	0.031	0.997	0.013
2001.436	9.101	0.050	9.069	0.029	1.007	0.013
2001.353	9.112	0.045	9.089	0.027	1.020	0.013
2001.269	9.124	0.042	9.111	0.027	1.031	0.014
2001.186	9.148	0.056	9.142	0.034	1.040	0.015
2001.103	9.180	0.071	9.179	0.042	1.049	0.015
2001.019	9.214	0.075	9.219	0.040	1.059	0.014
2000.936	9.235	0.076	9.242	0.036	1.065	0.012
2000.853	9.190	0.062	9.189	0.030	1.050	0.013
2000.769	9.146	0.048	9.137	0.026	1.036	0.013
2000.686	9.152	0.051	9.149	0.027	1.052	0.013
2000.603	9.158	0.056	9.161	0.029	1.068	0.012
2000.519	9.064	0.062	9.068	0.032	1.067	0.011
2000.436	8.995	0.061	9.031	0.030	1.128	0.017
2000.353	9.007	0.064	9.047	0.030	1.154	0.017
2000.269	9.035	0.073	9.088	0.032	1.176	0.018
2000.186	9.072	0.083	9.140	0.034	1.193	0.018
2000.103	9.110	0.094	9.193	0.037	1.205	0.018
2000.019	9.138	0.102	9.233	0.039	1.213	0.018
1999.936	9.150	0.106	9.250	0.041	1.216	0.018
1999.853	9.140	0.105	9.238	0.042	1.211	0.018
1999.770	9.115	0.105	9.209	0.043	1.199	0.018
1999.686	9.082	0.104	9.172	0.043	1.184	0.018
1999.603	9.049	0.103	9.134	0.044	1.168	0.017
1999.520	9.024	0.102	9.105	0.045	1.156	0.017
1999.436	9.014	0.102	9.094	0.047	1.152	0.016
1999.353	9.150	0.139	9.187	0.049	1.161	0.012
1999.270	9.161	0.121	9.166	0.068	1.068	0.017
1999.186	9.187	0.118	9.157	0.069	1.029	0.018
1999.103	9.222	0.116	9.150	0.070	1.003	0.018
1999.020	9.240	0.115	9.141	0.070	0.986	0.018

1998.936	9.239	0.118	9.126	0.071	0.973	0.018
1998.853	9.237	0.124	9.106	0.072	0.964	0.017
1998.770	9.234	0.132	9.080	0.073	0.957	0.016
1998.686	9.230	0.141	9.046	0.074	0.948	0.015
1998.603	9.224	0.149	9.003	0.074	0.936	0.015
1998.520	9.113	0.157	8.875	0.069	0.913	0.015
1998.436	8.914	0.165	8.688	0.059	0.884	0.014
1998.353	8.807	0.174	8.592	0.054	0.865	0.014
1998.270	8.835	0.185	8.617	0.059	0.859	0.016
1998.186	8.895	0.197	8.657	0.068	0.854	0.019
1998.103	8.965	0.207	8.663	0.072	0.842	0.019
1998.020	9.066	0.218	8.650	0.074	0.815	0.019
1997.937	9.120	0.223	8.625	0.074	0.799	0.018
1997.853	8.812	0.175	8.480	0.050	0.805	0.015
1997.770	8.838	0.173	8.591	0.049	0.846	0.014
1997.687	8.900	0.109	8.722	0.041	0.880	0.016
1997.603	8.873	0.061	8.791	0.025	0.940	0.013
1997.520	8.892	0.072	8.859	0.028	0.984	0.010
1997.437	8.962	0.053	8.944	0.030	1.017	0.013
1997.353	9.013	0.044	9.027	0.030	1.062	0.016
1997.270	9.041	0.041	9.088	0.027	1.107	0.018
1997.187	9.083	0.034	9.096	0.022	1.066	0.016
1997.103	9.092	0.031	9.091	0.021	1.042	0.015
1997.020	9.097	0.030	9.081	0.021	1.024	0.014
1996.937	9.099	0.029	9.075	0.021	1.017	0.013
1996.853	9.096	0.031	9.074	0.021	1.019	0.013
1996.770	9.089	0.036	9.073	0.023	1.025	0.014
1996.687	9.082	0.041	9.072	0.025	1.033	0.014
1996.603	9.078	0.046	9.083	0.027	1.056	0.014
1996.520	9.062	0.048	9.084	0.029	1.086	0.014
1996.437	9.029	0.049	9.075	0.031	1.108	0.014
1996.353	9.077	0.029	9.095	0.017	1.097	0.015
1996.270	9.063	0.023	9.067	0.017	1.046	0.014
1996.187	9.126	0.037	9.168	0.019	1.118	0.012
1996.103	9.130	0.036	9.166	0.020	1.111	0.013
1996.020	9.132	0.034	9.161	0.020	1.096	0.013
1995.937	9.134	0.032	9.154	0.020	1.084	0.014
1995.854	9.132	0.032	9.147	0.020	1.083	0.014
1995.770	9.122	0.032	9.138	0.019	1.091	0.014
1995.687	9.105	0.032	9.125	0.017	1.100	0.014
1995.604	9.084	0.032	9.107	0.017	1.105	0.013

1995.520	9.053	0.027	9.062	0.017	1.071	0.012
1995.437	9.045	0.027	9.056	0.017	1.072	0.012
1995.354	9.040	0.027	9.052	0.017	1.073	0.012
1995.270	9.036	0.028	9.049	0.017	1.075	0.012
1995.187	9.033	0.029	9.047	0.018	1.077	0.012
1995.104	9.032	0.029	9.046	0.018	1.079	0.013
1995.020	9.032	0.030	9.046	0.018	1.080	0.013
1994.937	9.033	0.029	9.047	0.018	1.082	0.012
1994.854	9.034	0.029	9.048	0.017	1.082	0.012
1994.770	9.036	0.029	9.049	0.016	1.083	0.012
1994.687	9.038	0.028	9.052	0.016	1.085	0.012
1994.604	9.041	0.028	9.055	0.015	1.087	0.011
1994.520	9.047	0.028	9.064	0.014	1.092	0.011
1994.437	9.055	0.027	9.081	0.013	1.109	0.011
1994.354	9.052	0.037	9.075	0.016	1.144	0.014
1994.270	9.067	0.070	9.145	0.025	1.213	0.016
1994.187	9.103	0.079	9.181	0.024	1.222	0.015
1994.104	9.129	0.082	9.196	0.023	1.225	0.012
1994.020	9.092	0.062	9.144	0.018	1.197	0.011
1993.937	9.045	0.041	9.086	0.014	1.163	0.011
1993.854	9.033	0.046	9.078	0.020	1.153	0.018
1993.771	9.063	0.044	9.097	0.022	1.109	0.013
1993.687	9.074	0.043	9.102	0.022	1.097	0.012
1993.604	9.074	0.044	9.095	0.022	1.100	0.014
1993.521	9.007	0.042	9.032	0.022	1.098	0.015
1993.437	8.986	0.039	9.006	0.023	1.084	0.015
1993.354	9.001	0.036	9.003	0.023	1.049	0.016
1993.271	9.091	0.027	9.105	0.019	1.067	0.015
1993.187	9.076	0.032	9.090	0.020	1.074	0.012
1993.104	9.049	0.037	9.059	0.020	1.066	0.011
1993.021	9.025	0.038	9.025	0.020	1.039	0.011
1992.937	9.137	0.040	9.140	0.022	1.058	0.010
1992.854	9.135	0.036	9.139	0.022	1.057	0.012
1992.771	9.114	0.031	9.116	0.020	1.046	0.013
1992.687	9.070	0.027	9.053	0.017	1.020	0.013
1992.604	9.072	0.027	9.060	0.017	1.028	0.013
1992.521	9.004	0.034	8.986	0.019	1.019	0.011
1992.437	8.984	0.025	8.968	0.017	1.026	0.013
1992.354	8.977	0.025	8.966	0.015	1.026	0.013
1992.271	8.972	0.025	8.965	0.014	1.026	0.013
1992.187	8.969	0.025	8.964	0.014	1.025	0.012

1992.104	8.969	0.025	8.964	0.013	1.025	0.011
1992.021	8.970	0.025	8.965	0.014	1.025	0.011
1991.937	8.973	0.025	8.966	0.014	1.024	0.011
1991.854	8.978	0.026	8.967	0.014	1.024	0.010
1991.771	9.039	0.029	9.016	0.017	1.014	0.011
1991.688	9.092	0.025	9.105	0.016	1.070	0.013
1991.604	9.056	0.029	9.053	0.018	1.047	0.012
1991.521	9.018	0.036	9.025	0.020	1.061	0.013
1991.438	8.997	0.043	9.012	0.023	1.081	0.013
1991.354	9.019	0.049	9.035	0.025	1.094	0.014
1991.271	9.066	0.053	9.085	0.025	1.101	0.014
1991.188	9.145	0.032	9.164	0.017	1.103	0.014
1991.104	9.095	0.032	9.124	0.018	1.110	0.015
1991.021	9.086	0.032	9.107	0.018	1.099	0.014
1990.938	9.082	0.031	9.095	0.018	1.077	0.013
1990.854	9.076	0.031	9.083	0.018	1.061	0.012
1990.771	9.061	0.033	9.064	0.019	1.056	0.012
1990.688	9.042	0.035	9.043	0.021	1.052	0.012
1990.604	9.030	0.037	9.029	0.022	1.049	0.013
1990.521	9.027	0.034	9.024	0.020	1.045	0.010
1990.438	9.022	0.033	9.017	0.019	1.041	0.009
1990.354	9.010	0.033	9.006	0.020	1.039	0.010
1990.271	9.013	0.034	9.007	0.021	1.034	0.010
1990.188	9.045	0.037	9.031	0.022	1.023	0.010
1990.104	9.082	0.040	9.061	0.023	1.016	0.010
1990.021	9.125	0.036	9.096	0.022	1.019	0.011
1989.938	9.154	0.032	9.133	0.020	1.026	0.011
1989.855	9.159	0.038	9.162	0.022	1.059	0.012
1989.771	9.087	0.034	9.084	0.021	1.044	0.012
1989.688	9.121	0.034	9.124	0.021	1.053	0.012
1989.605	9.122	0.036	9.128	0.021	1.062	0.012
1989.521	9.092	0.040	9.098	0.021	1.067	0.011
1989.438	9.096	0.038	9.106	0.021	1.071	0.012
1989.355	9.118	0.040	9.148	0.021	1.098	0.014
1989.271	9.170	0.049	9.232	0.023	1.159	0.016
1989.188	9.188	0.049	9.240	0.023	1.153	0.016
1989.105	9.202	0.048	9.245	0.023	1.140	0.015
1989.021	9.211	0.047	9.248	0.023	1.126	0.015
1988.938	9.214	0.046	9.248	0.022	1.116	0.014
1988.855	9.213	0.045	9.242	0.022	1.110	0.014
1988.771	9.207	0.045	9.227	0.022	1.105	0.014

1988.688	9.198	0.044	9.212	0.021	1.101	0.013
1988.605	9.187	0.044	9.205	0.021	1.100	0.013
1988.521	9.160	0.053	9.213	0.020	1.191	0.017
1988.438	9.121	0.040	9.165	0.022	1.134	0.018
1988.355	9.112	0.035	9.137	0.020	1.100	0.014
1988.271	9.115	0.031	9.144	0.019	1.098	0.014
1988.188	9.104	0.031	9.117	0.020	1.073	0.014
1988.105	9.078	0.032	9.066	0.021	1.036	0.014
1988.021	9.050	0.033	9.028	0.022	1.028	0.014
1987.938	9.013	0.033	8.997	0.021	1.027	0.014
1987.855	8.983	0.033	8.973	0.020	1.027	0.014
1987.772	8.968	0.033	8.959	0.018	1.025	0.013
1987.688	8.957	0.034	8.946	0.018	1.020	0.012
1987.605	8.942	0.038	8.925	0.018	1.006	0.011
1987.522	8.930	0.045	8.905	0.019	0.988	0.010
1987.438	8.932	0.049	8.904	0.020	0.982	0.010
1987.355	8.952	0.051	8.920	0.021	0.979	0.010
1987.272	8.979	0.052	8.940	0.022	0.978	0.010
1987.188	9.011	0.044	8.973	0.020	0.979	0.011
1987.105	9.045	0.036	8.996	0.019	0.979	0.012
1987.022	9.071	0.050	8.961	0.025	0.940	0.012
1986.938	9.111	0.053	8.971	0.026	0.919	0.013
1986.855	9.057	0.024	9.038	0.018	1.014	0.016
1986.772	9.058	0.024	9.054	0.016	1.044	0.014
1986.688	9.078	0.024	9.080	0.017	1.052	0.015
1986.605	9.052	0.029	9.053	0.018	1.047	0.011
1986.522	9.055	0.036	9.036	0.020	1.016	0.011
1986.438	9.064	0.043	9.044	0.026	1.024	0.013
1986.355	9.071	0.037	9.073	0.022	1.052	0.012
1986.272	9.144	0.034	9.147	0.020	1.046	0.012
1986.188	9.147	0.034	9.161	0.019	1.060	0.013
1986.105	9.148	0.034	9.168	0.018	1.087	0.014
1986.022	9.147	0.035	9.173	0.018	1.108	0.016
1985.938	9.145	0.035	9.177	0.018	1.125	0.017
1985.855	9.140	0.036	9.180	0.018	1.142	0.017
1985.772	9.135	0.037	9.183	0.019	1.158	0.018
1985.689	9.131	0.039	9.187	0.019	1.173	0.019
1985.605	9.129	0.041	9.192	0.019	1.187	0.019
1985.522	9.132	0.043	9.203	0.020	1.202	0.019
1985.439	9.138	0.047	9.220	0.020	1.217	0.018
1985.355	9.144	0.050	9.235	0.020	1.230	0.017

1985.272	9.147	0.052	9.242	0.020	1.235	0.017
1985.189	9.148	0.052	9.242	0.020	1.229	0.015
1985.105	9.149	0.051	9.242	0.020	1.216	0.014
1985.022	9.148	0.049	9.240	0.020	1.200	0.014
1984.939	9.146	0.042	9.228	0.020	1.176	0.014
1984.855	9.140	0.036	9.205	0.021	1.146	0.015
1984.772	9.117	0.035	9.157	0.021	1.110	0.014
1984.689	9.048	0.036	9.058	0.021	1.074	0.013
1984.605	8.999	0.027	9.003	0.018	1.065	0.012
1984.522	9.054	0.037	9.052	0.021	1.051	0.011
1984.439	9.093	0.037	9.096	0.020	1.055	0.012
1984.355	9.112	0.038	9.123	0.020	1.066	0.013
1984.272	9.125	0.039	9.142	0.018	1.094	0.013
1984.189	9.134	0.040	9.157	0.017	1.129	0.013
1984.105	9.139	0.041	9.169	0.016	1.155	0.013
1984.022	9.139	0.042	9.178	0.016	1.159	0.013
1983.939	9.138	0.044	9.187	0.017	1.159	0.013
1983.856	9.136	0.046	9.194	0.020	1.159	0.014
1983.772	9.133	0.048	9.196	0.023	1.159	0.015
1983.689	9.048	0.051	9.116	0.032	1.137	0.019
1983.606	8.972	0.050	9.052	0.033	1.145	0.021
1983.522	8.937	0.042	9.026	0.026	1.189	0.021
1983.439	8.965	0.038	9.029	0.023	1.172	0.020
1983.356	8.958	0.038	8.997	0.023	1.120	0.016
1983.272	8.891	0.040	8.875	0.025	1.028	0.010
1983.189	8.848	0.039	8.825	0.018	0.994	0.009
1983.106	8.866	0.052	8.786	0.019	0.929	0.010
1983.022	8.888	0.038	8.836	0.019	0.973	0.011
1982.939	8.925	0.032	8.903	0.019	1.021	0.011
1982.856	8.960	0.030	8.958	0.018	1.052	0.011
1982.772	8.979	0.030	8.983	0.019	1.060	0.011
1982.689	8.994	0.031	8.999	0.019	1.064	0.011
1982.606	9.007	0.032	9.015	0.020	1.068	0.011
1982.522	9.020	0.033	9.036	0.020	1.079	0.012
1982.439	9.031	0.035	9.063	0.019	1.101	0.012
1982.356	9.046	0.037	9.087	0.019	1.124	0.012
1982.272	9.074	0.040	9.107	0.018	1.141	0.013
1982.189	9.121	0.034	9.139	0.016	1.113	0.013
1982.106	9.133	0.034	9.151	0.016	1.110	0.012
1982.022	9.138	0.034	9.158	0.016	1.108	0.011
1981.939	9.138	0.035	9.158	0.016	1.111	0.011

1981.856	9.129	0.038	9.150	0.016	1.124	0.011
1981.773	9.115	0.040	9.137	0.016	1.138	0.011
1981.689	9.095	0.038	9.121	0.016	1.138	0.012
1981.606	9.074	0.030	9.104	0.016	1.120	0.014
1981.523	9.122	0.030	9.129	0.017	1.055	0.012
1981.439	9.014	0.032	9.014	0.018	1.045	0.011
1981.356	9.038	0.031	9.037	0.019	1.056	0.012
1981.273	9.058	0.029	9.052	0.019	1.040	0.012
1981.189	9.102	0.033	9.124	0.020	1.086	0.014
1981.106	9.110	0.035	9.133	0.020	1.095	0.014
1981.023	9.115	0.037	9.140	0.020	1.101	0.014
1980.939	9.118	0.038	9.143	0.020	1.105	0.014
1980.856	9.119	0.039	9.144	0.021	1.106	0.014
1980.773	9.114	0.039	9.141	0.022	1.105	0.015
1980.689	9.101	0.039	9.131	0.024	1.103	0.016
1980.606	9.082	0.039	9.113	0.025	1.098	0.018
1980.523	9.057	0.038	9.088	0.026	1.090	0.018
1980.439	9.002	0.033	8.996	0.019	1.035	0.013
1980.356	9.016	0.033	9.010	0.018	1.021	0.012
1980.273	9.057	0.036	9.093	0.022	1.107	0.017
1980.189	9.063	0.036	9.095	0.022	1.106	0.017
1980.106	9.067	0.036	9.096	0.022	1.105	0.016
1980.023	9.069	0.036	9.097	0.022	1.104	0.016
1979.939	9.070	0.037	9.097	0.022	1.104	0.015
1979.856	9.062	0.038	9.089	0.022	1.103	0.015
1979.773	9.045	0.041	9.072	0.023	1.103	0.015
1979.690	9.028	0.043	9.055	0.023	1.103	0.015
1979.606	9.020	0.044	9.047	0.024	1.103	0.015
1979.523	9.054	0.040	9.071	0.021	1.094	0.012
1979.440	9.077	0.038	9.093	0.020	1.093	0.011
1979.356	9.085	0.038	9.107	0.019	1.103	0.011
1979.273	9.093	0.038	9.118	0.018	1.109	0.012
1979.190	9.102	0.037	9.129	0.019	1.110	0.012
1979.106	9.111	0.037	9.140	0.019	1.111	0.013
1979.023	9.120	0.037	9.150	0.020	1.111	0.013
1978.940	9.125	0.037	9.155	0.020	1.111	0.013
1978.856	9.126	0.036	9.156	0.020	1.111	0.013
1978.773	9.125	0.036	9.153	0.020	1.107	0.013
1978.690	9.122	0.036	9.148	0.021	1.101	0.013
1978.606	9.117	0.035	9.140	0.021	1.092	0.013
1978.523	9.042	0.034	9.044	0.019	1.065	0.011

1978.440	9.049	0.034	9.064	0.018	1.088	0.011
1978.356	9.064	0.034	9.093	0.017	1.111	0.011
1978.273	9.087	0.034	9.110	0.018	1.096	0.012
1978.190	9.104	0.033	9.119	0.019	1.078	0.013
1978.106	9.074	0.039	9.084	0.021	1.075	0.013
1978.023	9.035	0.039	9.069	0.020	1.128	0.016
1977.940	9.015	0.036	9.057	0.018	1.147	0.017
1977.856	9.012	0.035	9.055	0.018	1.149	0.017
1977.773	9.016	0.035	9.056	0.018	1.141	0.016
1977.690	9.023	0.035	9.059	0.018	1.130	0.014
1977.607	9.032	0.034	9.062	0.018	1.120	0.013
1977.523	9.051	0.033	9.077	0.018	1.113	0.012
1977.440	9.077	0.031	9.100	0.017	1.107	0.011
1977.357	9.094	0.029	9.112	0.016	1.095	0.011
1977.273	9.099	0.027	9.101	0.017	1.051	0.011
1977.190	9.083	0.028	9.088	0.016	1.061	0.012
1977.107	9.101	0.035	9.119	0.015	1.123	0.012
1977.023	9.074	0.049	9.147	0.017	1.242	0.016
1976.940	9.099	0.047	9.172	0.018	1.234	0.018
1976.857	9.081	0.043	9.150	0.019	1.191	0.016
1976.773	9.075	0.042	9.129	0.019	1.166	0.015
1976.690	9.075	0.042	9.117	0.018	1.157	0.014
1976.607	9.077	0.041	9.112	0.019	1.144	0.015
1976.523	9.079	0.041	9.110	0.019	1.137	0.015
1976.440	9.086	0.041	9.118	0.019	1.142	0.015
1976.357	9.098	0.041	9.138	0.019	1.154	0.016
1976.273	9.112	0.041	9.160	0.018	1.166	0.016
1976.190	9.132	0.043	9.184	0.018	1.179	0.015
1976.107	9.158	0.045	9.212	0.018	1.195	0.015
1976.023	9.184	0.048	9.239	0.018	1.210	0.015
1975.940	9.200	0.050	9.256	0.017	1.220	0.015
1975.857	9.202	0.051	9.257	0.018	1.220	0.015
1975.774	9.193	0.052	9.253	0.019	1.215	0.015
1975.690	9.180	0.052	9.246	0.020	1.209	0.015
1975.607	9.165	0.052	9.241	0.022	1.204	0.016
1975.524	9.153	0.051	9.243	0.023	1.207	0.017
1975.440	9.137	0.046	9.249	0.025	1.218	0.018
1975.357	9.056	0.037	9.059	0.023	1.046	0.014
1975.274	9.066	0.041	9.109	0.023	1.124	0.017
1975.190	9.140	0.058	9.226	0.020	1.257	0.017
1975.107	9.150	0.069	9.262	0.021	1.293	0.016

1975.024	9.155	0.077	9.285	0.022	1.315	0.015
1974.940	9.156	0.080	9.293	0.023	1.322	0.015
1974.857	9.130	0.074	9.277	0.024	1.310	0.017
1974.774	9.082	0.059	9.237	0.026	1.275	0.020
1974.690	9.056	0.045	9.183	0.027	1.225	0.022
1974.607	9.067	0.032	9.090	0.016	1.111	0.012
1974.524	9.154	0.037	9.173	0.018	1.113	0.012
1974.440	9.132	0.050	9.172	0.022	1.142	0.014
1974.357	9.132	0.055	9.194	0.021	1.178	0.013
1974.274	9.237	0.049	9.292	0.019	1.173	0.013
1974.190	9.256	0.046	9.313	0.017	1.181	0.013
1974.107	9.266	0.044	9.326	0.017	1.195	0.014
1974.024	9.270	0.043	9.330	0.017	1.202	0.015
1973.940	9.245	0.043	9.319	0.018	1.202	0.016
1973.857	9.199	0.044	9.295	0.022	1.202	0.018
1973.774	9.175	0.044	9.266	0.023	1.201	0.019
1973.691	9.187	0.041	9.233	0.021	1.152	0.016
1973.607	9.175	0.041	9.227	0.020	1.139	0.013
1973.524	9.145	0.042	9.197	0.020	1.152	0.013
1973.441	9.118	0.040	9.166	0.019	1.147	0.013
1973.357	9.089	0.038	9.127	0.018	1.134	0.013
1973.274	9.032	0.035	9.045	0.021	1.088	0.014
1973.191	8.994	0.032	8.973	0.024	1.016	0.016
1973.107	9.034	0.049	8.954	0.025	0.945	0.014
1973.024	8.975	0.050	8.926	0.017	0.952	0.008
1972.941	8.969	0.035	8.954	0.014	0.990	0.008
1972.857	8.972	0.030	8.964	0.014	1.006	0.010
1972.774	8.978	0.029	8.973	0.015	1.017	0.011
1972.691	8.985	0.030	8.980	0.017	1.024	0.012
1972.607	8.994	0.032	8.989	0.018	1.030	0.013
1972.524	9.007	0.034	9.002	0.019	1.038	0.013
1972.441	9.052	0.037	9.040	0.021	1.047	0.013
1972.357	9.120	0.040	9.103	0.022	1.058	0.013
1972.274	9.154	0.046	9.159	0.023	1.079	0.012
1972.191	9.133	0.058	9.197	0.020	1.201	0.014
1972.107	9.162	0.069	9.312	0.026	1.274	0.017
1972.024	9.173	0.067	9.290	0.024	1.294	0.021
1971.941	9.174	0.059	9.274	0.022	1.294	0.022
1971.857	9.168	0.045	9.266	0.020	1.273	0.022
1971.774	9.130	0.050	9.200	0.020	1.197	0.015
1971.691	9.138	0.044	9.186	0.016	1.197	0.015

1971.608	9.126	0.045	9.178	0.017	1.207	0.016
1971.524	9.108	0.046	9.172	0.017	1.222	0.016
1971.441	9.108	0.048	9.172	0.017	1.220	0.016
1971.358	9.132	0.051	9.180	0.018	1.194	0.015
1971.274	9.158	0.052	9.191	0.019	1.172	0.014
1971.191	9.183	0.051	9.214	0.019	1.164	0.014
1971.108	9.205	0.049	9.240	0.019	1.158	0.013
1971.024	9.206	0.047	9.242	0.019	1.163	0.014
1970.941	9.191	0.046	9.231	0.017	1.191	0.015
1970.858	9.170	0.045	9.213	0.016	1.209	0.016
1970.774	9.136	0.043	9.185	0.018	1.185	0.016
1970.691	9.103	0.043	9.150	0.019	1.169	0.016
1970.608	9.074	0.046	9.111	0.020	1.163	0.016
1970.524	9.057	0.048	9.107	0.021	1.169	0.017
1970.441	9.045	0.050	9.124	0.023	1.204	0.019
1970.358	9.040	0.051	9.140	0.024	1.227	0.020
1970.274	9.047	0.049	9.147	0.024	1.221	0.020
1970.191	9.066	0.043	9.152	0.023	1.203	0.019
1970.108	9.119	0.037	9.154	0.017	1.149	0.014
1970.024	9.127	0.053	9.198	0.017	1.218	0.012
1969.941	9.113	0.048	9.203	0.019	1.232	0.015
1969.858	9.093	0.043	9.191	0.020	1.226	0.018
1969.774	9.067	0.038	9.162	0.022	1.212	0.020
1969.691	9.038	0.035	9.124	0.022	1.192	0.021
1969.608	8.997	0.033	9.050	0.022	1.137	0.020
1969.525	8.951	0.031	8.952	0.021	1.057	0.018
1969.441	8.924	0.029	8.903	0.020	1.016	0.016
1969.358	8.918	0.027	8.909	0.020	1.026	0.014
1969.275	8.953	0.028	8.956	0.019	1.048	0.013
1969.191	9.018	0.030	9.034	0.018	1.076	0.012
1969.108	9.068	0.033	9.089	0.018	1.096	0.013
1969.025	9.115	0.039	9.134	0.019	1.111	0.014
1968.941	9.140	0.043	9.160	0.019	1.127	0.016
1968.858	9.142	0.043	9.169	0.019	1.150	0.018
1968.775	9.115	0.036	9.157	0.018	1.166	0.020
1968.691	9.092	0.034	9.163	0.018	1.204	0.021
1968.608	9.080	0.036	9.192	0.020	1.261	0.022
1968.525	9.067	0.033	9.168	0.019	1.240	0.021
1968.441	9.066	0.033	9.154	0.019	1.210	0.019
1968.358	9.077	0.037	9.150	0.019	1.176	0.016
1968.275	9.112	0.040	9.174	0.020	1.162	0.016

1968.191	9.173	0.043	9.245	0.024	1.156	0.017
1968.108	9.154	0.056	9.233	0.026	1.166	0.016
1968.025	9.138	0.055	9.199	0.019	1.223	0.015
1967.941	9.103	0.034	9.130	0.018	1.110	0.014
1967.858	9.088	0.033	9.106	0.018	1.097	0.014
1967.775	9.076	0.032	9.089	0.018	1.090	0.013
1967.692	9.070	0.032	9.080	0.017	1.085	0.013
1967.608	9.071	0.031	9.080	0.017	1.080	0.012
1967.525	9.080	0.030	9.085	0.016	1.075	0.011
1967.442	9.094	0.028	9.094	0.015	1.072	0.011
1967.358	9.105	0.028	9.108	0.015	1.070	0.011
1967.275	9.111	0.033	9.138	0.018	1.100	0.015
1967.192	9.148	0.046	9.239	0.023	1.189	0.018
1967.108	9.180	0.056	9.318	0.026	1.257	0.019
1967.025	9.168	0.056	9.313	0.029	1.247	0.020
1966.942	9.143	0.056	9.296	0.030	1.228	0.020
1966.858	9.106	0.051	9.183	0.021	1.205	0.016
1966.775	9.097	0.048	9.149	0.020	1.173	0.016
1966.692	9.095	0.051	9.143	0.020	1.169	0.015
1966.608	9.083	0.051	9.129	0.022	1.160	0.015
1966.525	9.052	0.049	9.097	0.024	1.140	0.016
1966.442	9.047	0.047	9.080	0.023	1.122	0.016
1966.358	9.043	0.045	9.065	0.023	1.102	0.015
1966.275	9.040	0.043	9.051	0.023	1.082	0.015
1966.192	9.037	0.041	9.039	0.022	1.063	0.014
1966.108	9.036	0.040	9.030	0.022	1.047	0.013
1966.025	9.035	0.039	9.024	0.022	1.035	0.013
1965.942	9.034	0.038	9.022	0.022	1.029	0.012
1965.858	9.035	0.039	9.022	0.022	1.027	0.012
1965.775	9.036	0.040	9.023	0.022	1.026	0.013
1965.692	9.038	0.041	9.024	0.023	1.024	0.013
1965.609	9.042	0.042	9.026	0.024	1.023	0.013
1965.525	9.046	0.043	9.029	0.024	1.022	0.013
1965.442	9.052	0.044	9.032	0.025	1.022	0.013
1965.359	9.059	0.045	9.037	0.025	1.022	0.014
1965.275	9.084	0.043	9.110	0.024	1.092	0.014
1965.192	9.107	0.044	9.134	0.024	1.101	0.013
1965.109	9.127	0.047	9.150	0.023	1.106	0.012
1965.025	9.135	0.049	9.155	0.022	1.108	0.012
1964.942	9.128	0.048	9.144	0.022	1.110	0.012
1964.859	9.108	0.047	9.119	0.021	1.110	0.013

1964.775	9.085	0.046	9.097	0.020	1.112	0.013
1964.692	9.050	0.046	9.082	0.019	1.134	0.012
1964.609	9.088	0.056	9.117	0.020	1.144	0.010
1964.525	9.098	0.060	9.125	0.021	1.145	0.010
1964.442	9.076	0.061	9.102	0.023	1.141	0.011
1964.359	9.040	0.057	9.062	0.023	1.127	0.014
1964.275	9.000	0.043	9.016	0.022	1.105	0.016
1964.192	9.029	0.032	9.059	0.019	1.110	0.016
1964.109	9.030	0.045	9.070	0.021	1.130	0.014
1964.025	9.024	0.052	9.080	0.024	1.156	0.015
1963.942	9.065	0.039	9.108	0.018	1.154	0.015
1963.859	9.053	0.032	9.077	0.016	1.108	0.012
1963.775	9.041	0.029	9.045	0.016	1.061	0.010
1963.692	9.042	0.029	9.047	0.018	1.059	0.011
1963.609	9.047	0.030	9.053	0.021	1.058	0.013
1963.526	9.055	0.030	9.062	0.022	1.062	0.014
1963.442	9.073	0.030	9.089	0.022	1.076	0.015
1963.359	9.140	0.032	9.159	0.019	1.075	0.012
1963.276	9.160	0.042	9.183	0.021	1.105	0.014
1963.192	9.143	0.052	9.171	0.021	1.144	0.014
1963.109	9.119	0.059	9.153	0.021	1.175	0.014
1963.026	9.095	0.065	9.132	0.022	1.198	0.015
1962.942	9.055	0.061	9.108	0.021	1.210	0.017
1962.859	9.013	0.042	9.082	0.019	1.216	0.020
1962.776	9.027	0.038	9.058	0.020	1.121	0.017
1962.692	9.045	0.037	9.052	0.020	1.072	0.014
1962.609	9.045	0.033	9.042	0.019	1.061	0.011
1962.526	9.028	0.027	9.028	0.015	1.061	0.010
1962.442	9.019	0.038	9.024	0.020	1.059	0.010
1962.359	9.048	0.044	9.059	0.022	1.081	0.012
1962.276	9.098	0.042	9.111	0.021	1.089	0.013
1962.192	9.145	0.034	9.155	0.017	1.089	0.013
1962.109	9.149	0.034	9.162	0.017	1.093	0.013
1962.026	9.143	0.035	9.156	0.017	1.098	0.013
1961.942	9.115	0.040	9.125	0.017	1.106	0.011
1961.859	9.115	0.045	9.124	0.018	1.114	0.011
1961.776	9.134	0.050	9.143	0.020	1.121	0.011
1961.693	9.119	0.053	9.119	0.019	1.123	0.010
1961.609	9.067	0.037	9.102	0.017	1.133	0.012
1961.526	9.041	0.029	9.075	0.017	1.105	0.013
1961.443	9.021	0.033	9.014	0.018	1.034	0.010

1961.359	9.037	0.036	9.060	0.024	1.076	0.014
1961.276	9.104	0.043	9.163	0.024	1.143	0.015
1961.193	9.218	0.055	9.278	0.019	1.198	0.014
1961.109	9.213	0.049	9.265	0.020	1.165	0.014
1961.026	9.145	0.031	9.183	0.018	1.125	0.015
1960.943	9.125	0.029	9.149	0.017	1.103	0.014
1960.859	9.117	0.029	9.130	0.016	1.085	0.013
1960.776	9.112	0.029	9.116	0.015	1.065	0.011
1960.693	9.108	0.029	9.106	0.015	1.052	0.010
1960.609	9.102	0.030	9.098	0.015	1.045	0.010
1960.526	9.095	0.031	9.091	0.016	1.040	0.009
1960.443	9.092	0.032	9.088	0.017	1.038	0.009
1960.359	9.098	0.034	9.093	0.019	1.040	0.010
1960.276	9.112	0.035	9.107	0.020	1.048	0.011
1960.193	9.142	0.037	9.148	0.021	1.068	0.012
1960.109	9.184	0.039	9.220	0.022	1.111	0.014
1960.026	9.145	0.042	9.190	0.020	1.132	0.013
1959.943	9.108	0.040	9.148	0.019	1.130	0.014
1959.859	9.083	0.034	9.107	0.019	1.104	0.015
1959.776	9.064	0.034	9.080	0.019	1.081	0.014
1959.693	9.137	0.047	9.201	0.019	1.177	0.013
1959.610	9.085	0.044	9.122	0.022	1.117	0.012
1959.526	9.072	0.037	9.098	0.023	1.086	0.013
1959.443	9.058	0.036	9.089	0.023	1.089	0.015
1959.360	9.039	0.040	9.083	0.022	1.127	0.017
1959.276	9.007	0.045	9.069	0.023	1.156	0.017
1959.193	9.013	0.045	9.075	0.023	1.155	0.017
1959.110	9.027	0.044	9.089	0.023	1.155	0.017
1959.026	9.045	0.043	9.108	0.023	1.155	0.016
1958.943	9.066	0.043	9.129	0.023	1.157	0.016
1958.860	9.096	0.043	9.164	0.022	1.169	0.015
1958.776	9.126	0.044	9.198	0.021	1.183	0.015
1958.693	9.140	0.046	9.213	0.020	1.190	0.014
1958.610	9.082	0.054	9.146	0.025	1.157	0.014
1958.526	9.058	0.053	9.113	0.025	1.143	0.014
1958.443	9.038	0.051	9.084	0.024	1.131	0.013
1958.360	9.023	0.048	9.060	0.022	1.121	0.012
1958.276	9.013	0.046	9.044	0.021	1.115	0.012
1958.193	9.008	0.044	9.035	0.020	1.111	0.011
1958.110	9.007	0.044	9.035	0.020	1.111	0.011
1958.026	9.012	0.044	9.039	0.019	1.115	0.011

1957.943	9.020	0.044	9.048	0.019	1.120	0.011
1957.860	9.034	0.045	9.061	0.019	1.125	0.011
1957.776	9.052	0.045	9.079	0.019	1.129	0.012
1957.693	9.075	0.045	9.101	0.019	1.131	0.012
1957.610	9.151	0.041	9.164	0.020	1.100	0.013
1957.527	9.092	0.044	9.090	0.024	1.044	0.011
1957.443	9.064	0.043	9.063	0.024	1.049	0.012
1957.360	9.052	0.040	9.052	0.024	1.059	0.013
1957.277	9.074	0.038	9.081	0.022	1.070	0.012
1957.193	9.109	0.036	9.131	0.020	1.087	0.012
1957.110	9.134	0.038	9.177	0.021	1.119	0.012
1957.027	9.172	0.044	9.214	0.020	1.139	0.012
1956.943	9.181	0.048	9.232	0.019	1.171	0.013
1956.860	9.177	0.051	9.238	0.019	1.220	0.017
1956.777	9.091	0.070	9.199	0.025	1.252	0.017
1956.693	9.214	0.086	9.329	0.021	1.326	0.015
1956.610	9.179	0.075	9.304	0.022	1.301	0.016
1956.527	9.125	0.056	9.256	0.024	1.252	0.018
1956.443	9.116	0.048	9.219	0.024	1.209	0.018
1956.360	9.121	0.043	9.184	0.021	1.164	0.015
1956.277	9.130	0.041	9.167	0.019	1.142	0.013
1956.193	9.164	0.042	9.219	0.017	1.181	0.014
1956.110	9.197	0.046	9.242	0.018	1.171	0.013
1956.027	9.210	0.053	9.249	0.018	1.171	0.013
1955.943	9.216	0.065	9.252	0.020	1.189	0.013
1955.860	9.217	0.071	9.253	0.021	1.201	0.013
1955.777	9.209	0.062	9.242	0.020	1.177	0.013
1955.693	9.196	0.052	9.228	0.019	1.153	0.012
1955.610	9.188	0.049	9.221	0.018	1.154	0.012
1955.527	9.180	0.047	9.215	0.017	1.155	0.012
1955.444	9.172	0.045	9.210	0.017	1.156	0.012
1955.360	9.166	0.044	9.206	0.016	1.158	0.012
1955.277	9.162	0.043	9.202	0.016	1.159	0.012
1955.194	9.160	0.042	9.198	0.016	1.159	0.012
1955.110	9.161	0.041	9.195	0.016	1.157	0.012
1955.027	9.161	0.040	9.193	0.016	1.153	0.012
1954.944	9.162	0.040	9.191	0.017	1.145	0.013
1954.860	9.163	0.039	9.189	0.017	1.135	0.013
1954.777	9.163	0.038	9.185	0.018	1.122	0.013
1954.694	9.164	0.037	9.180	0.019	1.107	0.014
1954.610	9.136	0.035	9.136	0.022	1.060	0.013

1954.527	9.102	0.036	9.109	0.021	1.070	0.012
1954.444	9.074	0.044	9.097	0.018	1.139	0.013
1954.360	9.047	0.032	9.043	0.018	1.046	0.011
1954.277	9.049	0.033	9.045	0.019	1.046	0.011
1954.194	9.053	0.034	9.048	0.019	1.047	0.010
1954.110	9.057	0.036	9.053	0.020	1.049	0.010
1954.027	9.060	0.037	9.058	0.020	1.051	0.010
1953.944	9.062	0.037	9.063	0.020	1.057	0.010
1953.860	9.063	0.037	9.067	0.019	1.069	0.010
1953.777	9.064	0.037	9.074	0.019	1.083	0.010
1953.694	9.066	0.037	9.083	0.018	1.096	0.010
1953.611	9.094	0.036	9.115	0.017	1.109	0.010
1953.527	9.102	0.038	9.123	0.017	1.109	0.010
1953.444	9.110	0.038	9.134	0.017	1.112	0.011
1953.361	9.124	0.037	9.156	0.018	1.130	0.015
1953.277	9.169	0.046	9.220	0.018	1.182	0.015
1953.194	9.243	0.051	9.273	0.018	1.182	0.013
1953.111	9.207	0.040	9.229	0.016	1.132	0.011
1953.027	9.114	0.042	9.132	0.017	1.129	0.011
1952.944	9.156	0.040	9.172	0.020	1.098	0.012
1952.861	9.148	0.039	9.162	0.021	1.083	0.012
1952.777	9.128	0.037	9.139	0.021	1.071	0.012
1952.694	9.104	0.036	9.112	0.021	1.063	0.012
1952.611	9.084	0.035	9.093	0.021	1.060	0.012
1952.527	9.068	0.034	9.081	0.021	1.061	0.012
1952.444	9.052	0.033	9.071	0.020	1.066	0.012
1952.361	9.040	0.032	9.063	0.020	1.076	0.013
1952.277	9.035	0.032	9.060	0.020	1.089	0.013
1952.194	9.102	0.053	9.175	0.024	1.159	0.013
1952.111	9.155	0.044	9.220	0.021	1.175	0.017
1952.027	9.080	0.043	9.134	0.024	1.152	0.019
1951.944	9.069	0.040	9.095	0.021	1.117	0.016
1951.861	9.066	0.038	9.078	0.019	1.093	0.013
1951.777	9.086	0.039	9.096	0.019	1.089	0.011
1951.694	9.116	0.041	9.126	0.019	1.088	0.010
1951.611	9.132	0.040	9.154	0.021	1.097	0.014
1951.528	9.146	0.037	9.175	0.021	1.109	0.015
1951.444	9.161	0.033	9.190	0.018	1.122	0.015
1951.361	9.191	0.037	9.217	0.015	1.154	0.014
1951.278	9.194	0.041	9.231	0.018	1.150	0.014
1951.194	9.203	0.046	9.263	0.021	1.162	0.015

1951.111	9.237	0.054	9.325	0.023	1.213	0.018
1951.028	9.306	0.085	9.360	0.021	1.240	0.012
1950.944	9.181	0.045	9.232	0.027	1.117	0.016
1950.861	9.236	0.068	9.285	0.028	1.159	0.016
1950.778	9.212	0.062	9.264	0.027	1.148	0.015
1950.694	9.166	0.053	9.221	0.026	1.130	0.014
1950.611	9.128	0.047	9.181	0.024	1.124	0.014
1950.528	9.091	0.043	9.137	0.022	1.123	0.013
1950.444	9.073	0.040	9.115	0.021	1.122	0.013
1950.361	9.080	0.038	9.121	0.021	1.118	0.013
1950.278	9.095	0.035	9.134	0.021	1.114	0.014
1950.194	9.111	0.033	9.148	0.021	1.109	0.014
1950.111	9.123	0.032	9.158	0.021	1.104	0.015
1950.028	9.124	0.032	9.160	0.021	1.102	0.015
1949.944	9.121	0.032	9.157	0.021	1.099	0.015
1949.861	9.116	0.033	9.153	0.021	1.097	0.015
1949.778	9.110	0.033	9.147	0.021	1.095	0.015
1949.694	9.104	0.033	9.139	0.021	1.094	0.015
1949.611	9.096	0.033	9.124	0.018	1.111	0.013
1949.528	9.078	0.032	9.096	0.018	1.088	0.013
1949.445	9.044	0.031	9.045	0.018	1.050	0.012
1949.361	9.005	0.029	8.988	0.018	1.017	0.012
1949.278	9.058	0.038	9.084	0.022	1.100	0.017
1949.195	9.085	0.041	9.123	0.019	1.133	0.014
1949.111	9.128	0.046	9.183	0.020	1.156	0.014
1949.028	9.177	0.053	9.253	0.023	1.173	0.014
1948.945	9.149	0.053	9.216	0.021	1.181	0.013
1948.861	9.113	0.044	9.165	0.019	1.148	0.012
1948.778	9.092	0.037	9.131	0.017	1.126	0.011
1948.695	9.081	0.033	9.109	0.016	1.117	0.012
1948.611	9.080	0.034	9.109	0.016	1.127	0.012
1948.528	9.081	0.041	9.119	0.018	1.159	0.014
1948.445	9.039	0.047	9.078	0.019	1.149	0.012
1948.361	9.016	0.043	9.061	0.020	1.140	0.014
1948.278	9.006	0.039	9.054	0.021	1.135	0.016
1948.195	9.026	0.042	9.076	0.022	1.134	0.015
1948.111	9.066	0.047	9.116	0.024	1.134	0.015
1948.028	9.099	0.048	9.146	0.024	1.133	0.014
1947.945	9.132	0.047	9.175	0.022	1.133	0.012
1947.861	9.156	0.045	9.196	0.020	1.132	0.011
1947.778	9.157	0.044	9.196	0.020	1.131	0.011

1947.695	9.136	0.043	9.178	0.021	1.126	0.012
1947.611	9.108	0.042	9.151	0.022	1.121	0.013
1947.528	9.078	0.039	9.116	0.021	1.118	0.013
1947.445	9.053	0.035	9.080	0.017	1.116	0.011
1947.362	9.056	0.037	9.084	0.017	1.118	0.012
1947.278	9.063	0.040	9.094	0.018	1.124	0.013
1947.195	9.072	0.044	9.105	0.020	1.132	0.014
1947.112	9.079	0.047	9.115	0.021	1.141	0.015
1947.028	9.082	0.050	9.120	0.022	1.149	0.016
1946.945	9.079	0.051	9.121	0.023	1.157	0.016
1946.862	9.071	0.053	9.122	0.023	1.167	0.016
1946.778	9.061	0.054	9.122	0.023	1.176	0.017
1946.695	9.050	0.054	9.123	0.024	1.183	0.017
1946.612	9.040	0.055	9.123	0.024	1.186	0.017
1946.528	9.028	0.046	9.095	0.021	1.181	0.017
1946.445	9.043	0.037	9.093	0.019	1.164	0.018
1946.362	9.101	0.034	9.121	0.018	1.127	0.021
1946.278	9.108	0.035	9.132	0.020	1.095	0.016
1946.195	9.124	0.043	9.173	0.023	1.129	0.017
1946.112	9.145	0.050	9.208	0.025	1.163	0.018
1946.028	9.170	0.045	9.214	0.024	1.140	0.016
1945.945	9.185	0.038	9.216	0.021	1.103	0.014
1945.862	9.172	0.034	9.191	0.019	1.067	0.013
1945.778	9.147	0.031	9.145	0.017	1.037	0.012
1945.695	9.125	0.031	9.115	0.017	1.032	0.011
1945.612	9.103	0.033	9.091	0.019	1.032	0.012
1945.529	9.093	0.036	9.080	0.020	1.033	0.012
1945.445	9.110	0.040	9.115	0.021	1.069	0.013
1945.362	9.138	0.044	9.165	0.022	1.115	0.014
1945.279	9.162	0.048	9.196	0.021	1.137	0.013
1945.195	9.183	0.051	9.218	0.020	1.151	0.012
1945.112	9.181	0.049	9.216	0.018	1.151	0.012
1945.029	9.153	0.040	9.188	0.017	1.136	0.011
1944.945	9.115	0.031	9.141	0.017	1.108	0.012
1944.862	9.102	0.030	9.113	0.017	1.080	0.012
1944.779	9.093	0.030	9.092	0.018	1.055	0.011
1944.695	9.084	0.031	9.075	0.019	1.037	0.011
1944.612	9.073	0.035	9.057	0.020	1.020	0.011
1944.529	9.039	0.037	9.011	0.020	0.999	0.011
1944.445	8.981	0.039	8.943	0.020	0.980	0.011
1944.362	8.983	0.032	8.955	0.021	1.010	0.013

1944.279	9.057	0.030	9.068	0.020	1.062	0.012
1944.195	9.088	0.031	9.103	0.018	1.084	0.012
1944.112	9.132	0.039	9.175	0.019	1.135	0.012
1944.029	9.205	0.059	9.253	0.016	1.214	0.011
1943.945	9.192	0.064	9.249	0.017	1.232	0.012
1943.862	9.158	0.061	9.227	0.018	1.223	0.013
1943.779	9.091	0.045	9.158	0.022	1.164	0.014
1943.695	9.067	0.042	9.116	0.024	1.124	0.015
1943.612	9.058	0.043	9.088	0.025	1.098	0.013
1943.529	9.055	0.043	9.076	0.026	1.078	0.013
1943.446	9.063	0.043	9.079	0.025	1.062	0.013
1943.362	9.084	0.043	9.086	0.024	1.053	0.013
1943.279	9.152	0.035	9.177	0.018	1.109	0.012
1943.196	9.174	0.036	9.212	0.017	1.144	0.014
1943.112	9.149	0.034	9.187	0.017	1.131	0.014
1943.029	9.147	0.046	9.239	0.021	1.193	0.015
1942.946	9.177	0.057	9.268	0.020	1.225	0.014
1942.862	9.208	0.064	9.281	0.019	1.239	0.013
1942.779	9.193	0.062	9.261	0.020	1.227	0.014
1942.696	9.161	0.059	9.220	0.020	1.201	0.014
1942.612	9.105	0.043	9.157	0.020	1.152	0.015
1942.529	9.084	0.037	9.127	0.020	1.133	0.015
1942.446	9.070	0.033	9.105	0.018	1.120	0.014
1942.362	9.060	0.030	9.089	0.016	1.111	0.014
1942.279	9.053	0.029	9.076	0.015	1.103	0.013
1942.196	9.046	0.030	9.064	0.015	1.095	0.013
1942.112	9.042	0.031	9.055	0.016	1.088	0.012
1942.029	9.037	0.032	9.047	0.016	1.083	0.011
1941.946	9.032	0.033	9.042	0.017	1.079	0.011
1941.862	9.023	0.033	9.039	0.018	1.078	0.010
1941.779	9.025	0.033	9.041	0.019	1.074	0.011
1941.696	9.039	0.031	9.046	0.019	1.065	0.012
1941.612	9.037	0.031	9.033	0.018	1.053	0.012
1941.529	8.980	0.028	8.978	0.016	1.046	0.010
1941.446	8.936	0.028	8.938	0.015	1.034	0.009
1941.363	8.918	0.036	8.884	0.017	0.987	0.010
1941.279	8.896	0.045	8.856	0.021	0.969	0.013
1941.196	8.883	0.052	8.836	0.024	0.958	0.013
1941.113	8.819	0.064	8.747	0.020	0.916	0.010
1941.029	8.864	0.048	8.813	0.021	0.957	0.011
1940.946	8.909	0.045	8.872	0.024	0.991	0.012

1940.863	8.908	0.044	8.882	0.022	0.998	0.011
1940.779	8.953	0.038	8.940	0.021	1.015	0.011
1940.696	8.993	0.037	8.989	0.020	1.033	0.011
1940.613	9.016	0.037	9.020	0.020	1.052	0.011
1940.529	9.033	0.037	9.043	0.020	1.061	0.012
1940.446	9.049	0.037	9.060	0.021	1.062	0.014
1940.363	9.058	0.037	9.069	0.022	1.063	0.015
1940.279	9.053	0.040	9.035	0.026	1.015	0.014
1940.196	9.039	0.024	9.053	0.015	1.082	0.016
1940.113	8.978	0.030	8.969	0.017	1.025	0.011
1940.029	9.008	0.029	9.003	0.017	1.046	0.011
1939.946	9.028	0.028	9.029	0.017	1.053	0.011
1939.863	9.046	0.028	9.052	0.017	1.057	0.011
1939.779	9.061	0.027	9.071	0.016	1.060	0.011
1939.696	9.070	0.027	9.083	0.016	1.064	0.011
1939.613	9.076	0.027	9.091	0.016	1.067	0.011
1939.530	9.080	0.026	9.098	0.016	1.071	0.012
1939.446	9.083	0.026	9.102	0.017	1.074	0.013
1939.363	9.088	0.026	9.104	0.017	1.076	0.013
1939.280	9.094	0.028	9.103	0.019	1.064	0.014
1939.196	9.122	0.033	9.142	0.019	1.081	0.013
1939.113	9.131	0.033	9.154	0.019	1.091	0.013
1939.030	9.137	0.032	9.162	0.018	1.100	0.013
1938.946	9.140	0.032	9.165	0.017	1.106	0.013
1938.863	9.137	0.032	9.164	0.017	1.112	0.013
1938.780	9.132	0.032	9.161	0.016	1.117	0.013
1938.696	9.125	0.032	9.158	0.016	1.121	0.012
1938.613	9.118	0.032	9.154	0.016	1.125	0.012
1938.530	9.113	0.032	9.152	0.016	1.128	0.012
1938.446	9.110	0.032	9.151	0.016	1.129	0.012
1938.363	9.111	0.032	9.151	0.016	1.130	0.011
1938.280	9.112	0.032	9.152	0.016	1.130	0.011
1938.196	9.114	0.032	9.154	0.016	1.131	0.011
1938.113	9.118	0.033	9.158	0.016	1.132	0.011
1938.030	9.168	0.036	9.209	0.017	1.145	0.014
1937.946	9.115	0.037	9.147	0.021	1.102	0.012
1937.863	9.147	0.037	9.171	0.017	1.118	0.012
1937.780	9.124	0.041	9.151	0.018	1.132	0.012
1937.696	9.093	0.042	9.125	0.019	1.132	0.011
1937.613	9.058	0.042	9.096	0.021	1.112	0.012
1937.530	9.002	0.036	9.009	0.024	1.064	0.014

1937.447	9.034	0.036	9.028	0.025	1.040	0.013
1937.363	9.051	0.036	9.044	0.024	1.041	0.013
1937.280	9.066	0.034	9.060	0.022	1.044	0.013
1937.197	9.079	0.031	9.074	0.020	1.048	0.013
1937.113	9.087	0.029	9.086	0.018	1.052	0.013
1937.030	9.092	0.027	9.092	0.016	1.054	0.013
1936.947	9.092	0.027	9.092	0.016	1.054	0.013
1936.863	9.091	0.027	9.089	0.016	1.053	0.013
1936.780	9.089	0.027	9.084	0.016	1.050	0.013
1936.697	9.086	0.027	9.078	0.016	1.047	0.013
1936.613	9.082	0.027	9.073	0.017	1.044	0.013
1936.530	9.078	0.027	9.072	0.017	1.044	0.014
1936.447	9.070	0.029	9.074	0.018	1.058	0.014
1936.363	9.065	0.033	9.079	0.019	1.083	0.014
1936.280	9.069	0.038	9.097	0.019	1.114	0.014
1936.197	9.082	0.044	9.125	0.020	1.148	0.013
1936.113	9.098	0.047	9.152	0.020	1.163	0.012
1936.030	9.133	0.042	9.177	0.019	1.139	0.012
1935.947	9.160	0.036	9.191	0.019	1.115	0.012
1935.863	9.152	0.036	9.190	0.019	1.123	0.013
1935.780	9.136	0.035	9.188	0.019	1.143	0.014
1935.697	9.117	0.035	9.185	0.019	1.164	0.016
1935.613	9.104	0.035	9.183	0.020	1.179	0.017
1935.530	9.102	0.035	9.181	0.020	1.181	0.017
1935.447	9.104	0.035	9.180	0.019	1.179	0.017
1935.364	9.106	0.035	9.178	0.019	1.174	0.017
1935.280	9.110	0.035	9.176	0.019	1.168	0.017
1935.197	9.115	0.035	9.175	0.018	1.162	0.016
1935.114	9.120	0.035	9.174	0.018	1.155	0.016
1935.030	9.126	0.035	9.173	0.018	1.150	0.015
1934.947	9.134	0.035	9.176	0.018	1.146	0.015
1934.864	9.150	0.035	9.191	0.017	1.144	0.014
1934.780	9.167	0.035	9.211	0.017	1.141	0.013
1934.697	9.175	0.034	9.220	0.017	1.135	0.013
1934.614	9.090	0.023	9.110	0.016	1.084	0.014
1934.530	9.090	0.022	9.098	0.015	1.066	0.012
1934.447	9.077	0.023	9.073	0.015	1.057	0.012
1934.364	9.080	0.029	9.080	0.019	1.058	0.013
1934.280	9.116	0.037	9.131	0.019	1.080	0.013
1934.197	9.210	0.045	9.244	0.018	1.143	0.012
1934.114	9.217	0.059	9.247	0.019	1.153	0.010

1934.030	9.224	0.058	9.256	0.020	1.151	0.010
1933.947	9.232	0.044	9.274	0.020	1.134	0.011
1933.864	9.211	0.037	9.246	0.020	1.119	0.013
1933.780	9.173	0.032	9.198	0.018	1.108	0.014
1933.697	9.152	0.032	9.179	0.018	1.108	0.014
1933.614	9.141	0.032	9.172	0.018	1.119	0.015
1933.530	9.130	0.033	9.166	0.018	1.129	0.016
1933.447	9.113	0.032	9.151	0.018	1.127	0.016
1933.364	9.087	0.030	9.125	0.020	1.113	0.015
1933.281	9.057	0.035	9.103	0.023	1.108	0.017
1933.197	9.088	0.041	9.135	0.023	1.111	0.014
1933.114	9.127	0.046	9.175	0.023	1.127	0.015
1933.031	9.151	0.049	9.199	0.023	1.141	0.016
1932.947	9.121	0.045	9.152	0.024	1.110	0.017
1932.864	9.086	0.039	9.101	0.025	1.079	0.017
1932.781	9.077	0.035	9.094	0.023	1.080	0.016
1932.697	9.071	0.031	9.090	0.021	1.081	0.015
1932.614	9.067	0.028	9.087	0.018	1.083	0.013
1932.531	9.065	0.026	9.085	0.015	1.085	0.012
1932.447	9.066	0.026	9.087	0.015	1.088	0.011
1932.364	9.073	0.029	9.100	0.016	1.092	0.011
1932.281	9.085	0.032	9.119	0.017	1.097	0.011
1932.197	9.099	0.035	9.137	0.018	1.101	0.011
1932.114	9.111	0.037	9.144	0.019	1.103	0.011
1932.031	9.124	0.034	9.138	0.020	1.081	0.012
1931.947	9.122	0.032	9.123	0.020	1.052	0.012
1931.864	9.105	0.032	9.099	0.019	1.028	0.011
1931.781	9.097	0.032	9.080	0.017	1.016	0.009
1931.697	9.143	0.034	9.130	0.019	1.026	0.010
1931.614	9.136	0.035	9.123	0.019	1.024	0.010
1931.531	9.119	0.036	9.104	0.019	1.020	0.010
1931.448	9.097	0.037	9.079	0.019	1.013	0.010
1931.364	9.073	0.037	9.053	0.019	1.007	0.010
1931.281	9.053	0.038	9.030	0.019	1.002	0.010
1931.198	9.040	0.038	9.016	0.019	0.998	0.010
1931.114	9.039	0.038	9.015	0.019	0.998	0.010
1931.031	9.040	0.038	9.016	0.019	0.998	0.010
1930.948	9.044	0.037	9.020	0.019	0.999	0.010
1930.864	9.049	0.036	9.024	0.019	1.001	0.010
1930.781	9.055	0.035	9.031	0.019	1.003	0.011
1930.698	9.063	0.034	9.038	0.019	1.007	0.011

1930.614	9.071	0.033	9.048	0.019	1.010	0.011
1930.531	9.082	0.032	9.062	0.019	1.019	0.011
1930.448	9.103	0.031	9.096	0.019	1.039	0.010
1930.364	9.152	0.030	9.151	0.016	1.051	0.011
1930.281	9.148	0.027	9.145	0.015	1.045	0.012
1930.198	9.116	0.023	9.126	0.013	1.073	0.012
1930.114	9.162	0.028	9.190	0.015	1.124	0.013
1930.031	9.180	0.030	9.212	0.013	1.148	0.013
1929.948	9.133	0.031	9.172	0.016	1.127	0.012
1929.864	9.121	0.027	9.147	0.016	1.097	0.012
1929.781	9.177	0.049	9.198	0.016	1.157	0.010
1929.698	9.198	0.045	9.238	0.018	1.158	0.012
1929.614	9.184	0.051	9.259	0.021	1.208	0.016
1929.531	9.245	0.045	9.295	0.017	1.196	0.015
1929.448	9.186	0.039	9.227	0.019	1.120	0.011
1929.365	9.125	0.033	9.138	0.018	1.083	0.011
1929.281	9.107	0.030	9.119	0.019	1.071	0.012
1929.198	9.122	0.032	9.114	0.022	1.044	0.014
1929.115	9.175	0.038	9.177	0.023	1.045	0.014
1929.031	9.158	0.039	9.162	0.023	1.051	0.015
1928.948	9.139	0.038	9.142	0.023	1.052	0.015
1928.865	9.120	0.036	9.121	0.022	1.052	0.015
1928.781	9.102	0.034	9.100	0.022	1.051	0.015
1928.698	9.088	0.031	9.085	0.021	1.050	0.015
1928.615	9.083	0.030	9.078	0.021	1.049	0.015
1928.531	9.084	0.031	9.080	0.021	1.050	0.015
1928.448	9.086	0.033	9.084	0.021	1.053	0.013
1928.365	9.089	0.035	9.092	0.021	1.056	0.012
1928.281	9.096	0.036	9.103	0.021	1.057	0.012
1928.198	9.175	0.030	9.176	0.018	1.053	0.011
1928.115	9.148	0.034	9.147	0.022	1.049	0.012
1928.031	9.104	0.040	9.098	0.028	1.045	0.014
1927.948	9.087	0.041	9.080	0.029	1.044	0.014
1927.865	9.078	0.040	9.073	0.029	1.045	0.014
1927.781	9.075	0.039	9.070	0.029	1.045	0.014
1927.698	9.098	0.029	9.117	0.015	1.109	0.012
1927.615	9.034	0.022	9.044	0.015	1.073	0.014
1927.531	9.048	0.031	9.030	0.017	1.013	0.012
1927.448	9.065	0.033	9.032	0.019	1.000	0.012
1927.365	9.082	0.031	9.053	0.020	1.011	0.012
1927.282	9.099	0.028	9.085	0.020	1.028	0.013

1927.198	9.116	0.026	9.118	0.020	1.048	0.014
1927.115	9.137	0.028	9.159	0.020	1.083	0.015
1927.032	9.158	0.032	9.205	0.020	1.128	0.015
1926.948	9.167	0.034	9.227	0.020	1.150	0.016
1926.865	9.104	0.032	9.123	0.018	1.095	0.011
1926.782	9.129	0.031	9.157	0.016	1.109	0.011
1926.698	9.119	0.032	9.151	0.017	1.111	0.012
1926.615	9.049	0.033	9.075	0.021	1.092	0.015
1926.532	8.999	0.031	8.990	0.019	1.027	0.014
1926.448	9.001	0.028	8.983	0.018	1.011	0.014
1926.365	9.036	0.027	9.019	0.018	1.022	0.015
1926.282	9.029	0.026	9.009	0.019	1.018	0.015
1926.198	9.017	0.025	8.991	0.019	1.008	0.015
1926.115	9.007	0.027	8.968	0.019	0.992	0.015
1926.032	8.998	0.029	8.944	0.019	0.972	0.014
1925.948	8.993	0.030	8.932	0.019	0.962	0.014
1925.865	8.996	0.026	8.953	0.019	0.986	0.013
1925.782	9.005	0.022	8.997	0.018	1.030	0.013
1925.698	9.044	0.023	9.060	0.015	1.075	0.012
1925.615	8.996	0.022	9.009	0.016	1.060	0.015
1925.532	9.029	0.036	9.101	0.016	1.203	0.015
1925.448	9.101	0.056	9.194	0.019	1.237	0.015
1925.365	9.108	0.031	9.145	0.019	1.122	0.017
1925.282	9.115	0.031	9.141	0.019	1.123	0.017
1925.199	9.123	0.036	9.139	0.017	1.129	0.017
1925.115	9.131	0.050	9.139	0.016	1.145	0.015
1925.032	9.139	0.076	9.141	0.014	1.175	0.011

A5.2 References

Cheng H, Edwards RL, Shen C, Polyak VJ, Asmerom Y, Woodhead J, Hellstrom J, Wang Y, Kong X, Spötl C, Wang X, Alexander EC (2013) Improvements in ^{230}Th dating , ^{230}Th and ^{234}U half-life values , and U – Th isotopic measurements by multi-collector inductively coupled plasma mass spectrometry. Earth Planet Sci Lett 371–372:82–91

Jaffey AH, Flynn KF, Glendenin LE, Bentley WC, Essling AM (1971) Precision Measurement of Half-Lives and Specific Activities of ^{235}U and ^{238}U. Phys Rev C 4: